Department of Bioproducts and Biosystems

Utilization of cellulosic building blocks in material design

Tiia-Maria Tenhunen

Aalto University

DOCTORAL DISSERTATIONS

Tiia-Maria Tenhunen

Utilization of cellulosic building blocks in material design

Aalto University

2018

Aalto University publication series
DOCTORAL DISSERTATIONS 94/2018
VTT SCIENCE 175

Utilization of cellulosic building blocks in material design

Tiia-Maria Tenhunen

A doctoral dissertation completed for the degree of Doctor of Science (Technology) to be defended, with the permission of the Aalto University School of Chemical Engineering, at a public examination held at the auditorium U1 (Aalto University Undergraduate Centre, Otakaari 1) on 25th of May 2018 at 12.

Aalto University
School of Chemical Engineering
Department of Bioproducts and Biosystems

Supervising professor
Prof. Monika Österberg, Aalto University, Finland

Thesis advisor
Dr. Tekla Tammelin, VTT Technical Research Centre of Finland Ltd, Finland

Preliminary examiners
Prof. Monica Ek, KTH Royal Institute of Technology, Sweden
Prof. Laurent Heux, CEntre de Recherches sur les MAcromolécules Végétales, France

Opponent
Prof. Kristin Syverud, Norwegian University of Science and Technology, Norway

Aalto University publication series
DOCTORAL DISSERTATIONS 94/2018

VTT SCIENCE 175

ISBN 978-952-60-7994-3 (printed)
ISBN 978-952-60-7995-0 (pdf)
ISSN 1799-4934 (printed)
ISSN 1799-4942 (pdf)
http://urn.fi/URN:ISBN:978-952-60-7995-0

ISBN 978-951-38-8636-3 (printed)
ISBN 978-951-38-8635-6 (pdf)
ISSN 2242-119X (printed)
ISSN 2242-1203 (pdf)
http://urn.fi/URN:ISBN:978-951-38-8635-6

Unigrafia Oy
Helsinki 2018

Finland

441 697
Printed matter

Aalto University

Abstract

Aalto University, P.O. Box 11000, FI-00076 Aalto www.aalto.fi

Author
Tiia-Maria Tenhunen

Name of the doctoral dissertation
Utilization of cellulosic building blocks in material design

Publisher School of Chemical Engineering

Unit Department of Bioproducts and Biosystems

Series Aalto University publication series DOCTORAL DISSERTATIONS 94/2018

Field of research Bioproduct technology

Manuscript submitted 26 January 2018 **Date of the defence** 25 May 2018

Permission to publish granted (date) 24 April 2018 **Language** English

☐ **Monograph** ☒ **Article dissertation** ☐ **Essay dissertation**

Abstract

In this thesis, three cellulosic building blocks: pulp fibres, cellulose nanofibrils (CNF) and polymeric cellulose were applied in the development of 1D-, 2D- and 3D-structures. For their efficient utilization in material and application design, systematic analysis of the materials and their interactions were conducted using complementary analytical tools.

Cellulose pulp fibres were used as building blocks for 1D fibre yarn production, CNF was used for 2D films and polymeric cellulose for 3D modification and functionalization of cellulosic textiles. Pulp fibres were converted into yarns without dissolution and regeneration using a deep eutectic solvent (DES) acting as a rheology modifier and dispersing agent, and therefore, enabling the spinning of yarn. The intrinsic properties of cellulose I crystalline structure were retained in the final structure. In order to understand the effect of DES on cellulose fibres and to improve the macroscale properties of the final product, the changes in pulp fibre composition and morphology due to DES were examined. As a result, electrostatically bound residuals of DES were revealed, which had an effect on charge of the fibres, and therefore, also affecting the properties of the fibre yarn. In 2D CNF films the effect of xylan, which is a major hemicellulose in hardwood, on the stability and properties of CNF films was examined. The effect of xylan on surface interactions was linked to macroscale film properties. It was discovered, that removal of xylan affected the microscale stability and water uptake behaviour. However, the film properties in larger scale, such as barrier properties, remained intact. 3D modifications of textiles were conducted using 3D-printing and two cellulose derivatives, cellulose acetate and acetoxypropyl cellulose. Macroscale properties, such as the adhesion, of the materials were analysed. The obtained results were linked to the strength of material interactions during adsorption. As an outcome, promising material combinations for textile applications were determined and several application prototypes for textile modification and functionalization were demonstrated.

Overall, the work demonstrates the significance of understanding the macroscale material properties and the surface interactions of the chosen cellulosic building blocks with other substances in the development of new cellulosic materials and applications.

Keywords cellulose, pulp fibre filament, CNF film, 3D-printing, cellulose derivatives

ISBN (printed) 978-952-60-7994-3 **ISBN (pdf)** 978-952-60-7995-0

ISSN (printed) 1799-4934 **ISSN (pdf)** 1799-4942

Location of publisher Helsinki **Location of printing** Helsinki **Year** 2018

Pages 156 **urn** http://urn.fi/URN:ISBN:978-952-60-7995-0

Tekijä
Tiia-Maria Tenhunen

Väitöskirjan nimi
Selluloosapohjaiset materiaalit sovellussuunnittelun rakennuspalikoina

Julkaisija Kemian tekniikan korkeakoulu

Yksikkö Biotuotteiden ja biotekniikan laitos

Sarja Aalto University publication series DOCTORAL DISSERTATIONS 94/2018

Tutkimusala Biotuotetekniikka

Käsikirjoituksen pvm 26.01.2018 **Väitöspäivä** 25.05.2018

Julkaisuluvan myöntämispäivä 24.04.2018 **Kieli** Englanti

☐ **Monografia** ☒ **Artikkeliväitöskirja** ☐ **Esseeväitöskirja**

Tiivistelmä

Tässä työssä tutkittiin selluloosapohjaisten materiaalien hyödyntämistä materiaalisuunnittelun ja sovelluskehityksen rakennuspalikoina. Työssä hyödynnettiin sellukuituja, nanoselluloosaa sekä polymeeristä selluloosaa perinteisestä käytöstä poikkeavien sovellusten 1D-, 2D- ja 3D-rakenteissa. Lopputuotteen optimoimiseksi materiaalien ominaisuuksia sekä vuorovaikutuksia karakterisoitiin systemaattisesti toisiaan täydentävillä analysointimenetelmillä.

Kokonaisia sellukuituja käytettiin rakennuspalikoina uudenlaisen kuitulangan valmistuksessa, kun taas nanoselluloosa mahdollisti muovinkaltaiset kaksiulotteiset kalvorakenteet. Kemiallisesti muokattuja selluloosajohdannaisia (selluloosa-asetaattia ja asetyloitua hydroksipropyyliselluloosaa) voitiin geelimäisinä materiaaleina käyttää 3D-tulostuksessa. Langan valmistuksessa, kuitujen liuotuksen ja saostuksen sijaan, koliinikloridista ja ureasta muodostetun syväeutektisen nesteen ominaisuuksia hyödynnettiin kuitujen dispergoinnissa sekä reologian muokkauksessa kehruuseen soveltuvaksi. Täten saatiin myös säilytettyä selluloosa I kidemuoto sekä sen ominaisuudet lopputuotteessa. Lisäksi tarkasteltiin syväeutektisen nesteen vaikutusta sellukuitujen morfologiaan ja koostumukseen. Tarkastelun tuloksena huomattiin syväeutektisessa nesteessä käytetyn koliiniklorinin sitoutuvan elektrostaattisesti kuituihin vaikuttaen niiden varaukseen ja siten myös vaikuttaen lopputuotteena olevan kuitulangan ominaisuuksiin.

Kaksiulotteisissa kalvoissa käytettiin nanomittakaavaan jauhettua lehtipuuselluloosaa, joka sisältää merkittävän määrän hemiselluloosia, erityisesti ksylaania. Ksylaanin vaikutusta kalvon muodostumisen aikaisissa pintavuorovaikutuksissa sekä lopullisen kalvon ominaisuuksissa tutkittiin. Todettiin, että vaikka ksylaanilla on vaikutusta materiaalin pintaominaisuuksiin ja vedenottokykyyn molekyylitasolla, ei sen poistaminen vaikuta valmiin nanosellukalvon ominaisuuksiin. Selluloosajohdannaisten materiaalivuorovaikutuksia tutkittiin molekyylitasolla seuraamalla adsorptiota selluloosamallipintaan sekä makrotasolla mittaamalla adheesio-ominaisuuksia. Tuloksia hyödynnettiin 3D-tulostettavien tekstiilisovellusten suunnittelussa ja niiden perusteella valmistettiin useita prototyyppejä.

Kaiken kaikkiaan, saatuja tuloksia voidaan hyödyntää selluloosamateriaalien ominaisuuksien ja vuorovaikutusten laajempaan ymmärtämiseen sekä uusien sovellusten kehittämiseen. Tulokset selventävät molekyylitason vuorovaikutusten merkitystä lopputuotteen makrotason ominaisuuksiin selluloosapohjaisia materiaaleja käytettäessä.

Avainsanat selluloosa, sellukuitu, kuitulanka, nanoselluloosakalvo, 3D-tulostus, selluloosajohdannaiset

ISBN (painettu) 978-952-60-7994-3 **ISBN (pdf)** 978-952-60-7995-0

ISSN (painettu) 1799-4934 **ISSN (pdf)** 1799-4942

Julkaisupaikka Helsinki **Painopaikka** Helsinki **Vuosi** 2018

Sivumäärä 156 **urn** http://urn.fi/URN:ISBN:978-952-60-7995-0

Preface

This dissertation was carried out at the VTT Technical Research Centre of Finland Ltd during 2014-2018. The work was part of the Naseva2 and Design Driven Value Chains in the World of Cellulose (DWoC and DWoC2.0) projects supported by Tekes.

First and foremost, I would like to thank my advisor and mentor, Dr. Tekla Tammelin, who gave me the opportunity to start working with cellulosic materials by including me to her projects and guiding me through the jungle-like journey of academic research and writing. Thank you for your valuable support, shared knowledge, and especially, the critical feedback. In addition, it has been a pleasure to work and travel with you.

I am also grateful for my supervising professor Monika Österberg for giving me the chance to do the doctoral thesis at Aalto University and for all the advice and feedback along the way. Additionally, I would like to thank Dr. Hannes Orelma for his continuous help with everything. Thank you for always being there and answering my never-ending questions. You are probably the most even-tempered person I know. Overall, it has been an interesting and educating journey and I am extremely glad I did it.

I would also like to thank all the co-authors, DWoC project manager Kirsi Kataja, as well as our technical staff Vuokko Liukkonen, Mari Leino, Ulla Salonen and Katja Pettersson. My gratitude goes also to my current and former managers, Dr. Heli Kangas, Pia Qvintus, Dr. Jani Lehto and Dr. Annaleena Kokko for enabling and supporting the work required to complete this dissertation.

Furthermore, this endeavour would have been less fun without my colleagues and lunchmates Marie Gestranius, Dr. Minna Hakalahti, Dr. Katri Kontturi and Ville Rissanen. During my many years at VTT, I have also had an amazing time and pleasure to work with many of my former and current teammates and colleagues, such as our active recreational committee members Laura Kela, Panu Lahtinen, Otto-Ville Kaukoniemi and Vesa Kunnari, as well as, the VTT Young Professionals' board, especially Colm Mc Caffrey, Visa Vallivaara and Dr. Caitlin Huotilainen.

I also happen to have the most amazing group of friends. I am thankful for the friends that have stayed by my side from the childhood and I am grateful for having met so many wonderful people in my adult life. Thank you for celebrating also this achievement with me. You truly make my life worth living.

Finally, I would like to express my deepest gratitude to my parents, äiti and iskä. You have always supported me and believed that I could do whatever I set my mind to. I hope you can be proud of me (and yourselves) today. I can never thank you enough <3

Espoo, 17th of April 2018

List of publications

This thesis is based on the following original publications which are referred to in the text as I–IV. The publications are reproduced with kind permission from the publishers.

I Tenhunen Tiia-Maria; Hakalahti Minna; Kouko Jarmo; Salminen Arto; Härkäsalmi Tiina; Pere Jaakko; Harlin Ali; Hänninen Tuomas (2016). Method for Forming Pulp Fibre Yarns Developed by a Design-driven Process, BioResources 11(1), 2492-2503

II Tenhunen Tiia-Maria; Lewandowska Anna E.; Orelma Hannes; Johansson Leena-Sisko; Virtanen Tommi; Harlin Ali; Österberg Monika; Eichhorn Stephen J.; Tammelin Tekla (2018) Understanding the interactions of cellulose fibres and deep eutectic solvent of choline chloride and urea. Cellulose 25, 137-150

III Tenhunen Tiia-Maria; Peresin, Maria Soledad; Penttilä Paavo A.; Pere Jaakko; Serimaa, Ritva; Tammelin Tekla (2014) Significance of xylan on the stability and water interactions of cellulosic nanofibrils. Reactive and Functional Polymers 85, 157-166

IV Tenhunen Tiia-Maria; Moslemian Oldouz; Kammiovirta Kari; Harlin Ali; Kääriäinen Pirjo; Österberg Monika; Tammelin Tekla; Orelma Hannes (2018) Surface tailoring and design-driven prototyping of fabrics with 3D-printing: An all-cellulose approach, Materials & Design 140, 409-419

Author's contributions

Paper I: Method for Forming Pulp Fibre Yarns Developed by a Design-driven Process

TMT was responsible, together with MH, for the development of the process and the materials as well as the production of the fibre yarns and performing FTIR spectroscopy. JK conducted the tensile tests and AS the NMR spectroscopy. TMT analysed the results, together with co-authors, and wrote the manuscript under supervision of TH.

Paper II: Understanding the interactions of cellulose fibres and deep eutectic solvent of choline chloride and urea

TMT was responsible for the experimental design, preparation of the materials, FTIR spectroscopy and methylene blue adsorption measurements. She participated in AFM imaging, analysing the results and wrote the main part of the manuscript under supervision of TT. Raman spectroscopy and the analysis were conducted by AL, NMR spectroscopy by TV and XPS by LSJ.

Paper III: Significance of xylan on the stability and water interactions of cellulosic nanofibrils

TMT was responsible for the experimental work for the stability studies, performing the Turbiscan and QCM-D measurements and writing the first draft of the manuscript. Experimental design was conducted and the results were analysed together with the co-authors. PP performed the WAXS analysis.

Paper IV: Surface tailoring and design-driven prototyping of fabrics with 3D-printing: the all-cellulose approach

TMT was responsible for the experimental design, material compatibility for 3D printing, QCM-D measurements, peeling tests and writing the main part of the manuscript under the supervision of TT and HO. Materials were prepared by KK and a design perspective was contributed by OM. Results were analysed together with the co-authors.

Contents

List of abbreviations and symbols

1D	one-dimensional (such as filament)
2D	two-dimensional (such as paper)
3D	three-dimensional (such as furniture)
ABS	acrylonitrile butadiene styrene
AGU	D-anhydroglucopyranose unit
APC	acetoxypropyl cellulose/acetylated hydroxypropyl cellulose
ATR	attenuated total reflection
C	carbon
CA	cellulose acetate
ChCl	choline chloride
CMC	carboxymethyl cellulose
CMF	cellulose microfibrils
CNC	cellulose nanocrystals
CNF	cellulose nanofibrils
DES	deep eutectic solvent
DRIFT	diffuse reflectance infrared
DVS	dynamic vapour sorption
EFC	elemental chlorine free
EFP	enzymatically fibrillated pulp
FDM	fused deposition modelling
FTIR	Fourier transform infrared spectroscopy
H	hydrogen

HPAEC	high performance anion exchange chromatography
HPC	hydroxypropyl cellulose
MS	molecular substitution
N	nitrogen
NaOH	sodium hydroxide
NMR	nuclear magnetic resonance spectroscopy
O	oxygen
OTR	oxygen transmission rate
PAA	polyacrylic acid
PLA	polylactic acid
ppm	parts per million
PVAm	polyvinyl amine
QCM-D	quartz crystal microbalance with dissipation monitoring
RH	relative humidity
SEM	scanning electron microscope
TEMPO	2,2,6,6-tetramethyl-piperidinyl-1-oxyl
TMSC	trimethylsilyl cellulose
XPS	x-ray photoelectron spectroscopy

1. Introduction

After decades of developing petroleum-based plastics that would last forever, we are now facing enormous ecological issues with landfills piling up and micro plastics threatening the marine life. Today, topics like sustainability, eco-efficiency, and green chemistry are guiding technological development. The materials should be biobased, recyclable and biodegrade after use. The awareness of ecological issues in many countries has made them enact legislation in order to diminish the use of unsustainable plastics and promote recycling. This has led to the increased development of biobased and biodegradable polymers worldwide. Cellulose is the most abundant biopolymer in the world, and also incredibly versatile, which makes it a great candidate as the multipurpose material of the future.

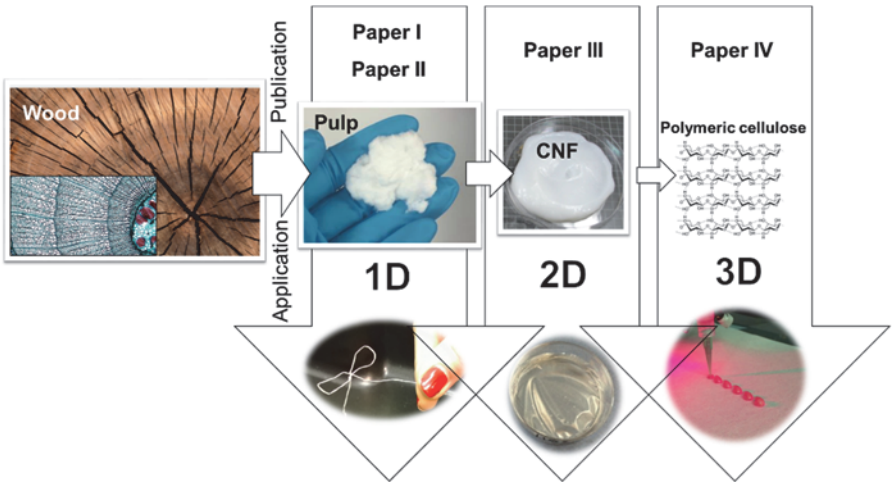

Figure 1 Outline of the doctoral thesis

In this thesis the objective was to utilize the inherent properties of cellulosic building blocks, from macrofibres to polymeric cellulose, in material development and design

and to understand the fundamental properties of the materials, their role in molecular level interaction at interfaces, as well as in macroscale applications, and the demands for research methodology for each material. Outline of the work is presented in Figure 1.

The thesis begins with a background presenting the materials, their properties and the current state-of-the-art regarding the applications. In the results, **Paper I** presents a new production method for producing 1D textile fibre yarns utilizing the largest building block, the pulp fibres, which are traditionally used in bulk paper and cardboard applications. Cellulose based textiles, on the other hand, have been made using long fibres of cotton or by dissolving and regenerating wood based pulp. However, due to the unsustainability of cotton production and the chemicals used in traditional dissolution processes, the direct utilization of pulp fibres would be attractive. This would also enable the utilization of cellulose I structure and other beneficial natural properties of the wood fibre. Due to the challenge presented by the short fibre length that prevents traditional yarn spinning, a new type of cellulose fibre yarn manufacturing process was developed. The presented pulp fibre yarns are manufactured using a deep eutectic solvent (DES) composed of choline chloride and urea and a dry-wet spinning method. DES was used as a dispersing agent and medium for the yarn forming process and washed away prior to drying. It was also shown in **Paper I** how fibre yarns could be made waterproof using a small amount of polyacrylic acid as a crosslinking polymer. A patent has been applied for the method (Hakalahti et al. 2015). In **Paper II** the interactions between this particular DES and pulp fibres were studied in detail. The influence of DES on fibre morphology, chemical compositions and derivatisation, was examined as well as the effect of residual DES on the fibre yarns. It was discovered that extensive washing is required in order to remove electrostatically bound residuals of choline chloride. The knowledge acquired in **Paper II** could be utilized in the improvement of the fibre yarn properties.

In **Paper III**, the effect of xylan on stability in dilute cellulose nanofibril (CNF) dispersions and the properties of 2D CNF films were studied. CNF is an excellent material for manufacturing biobased and biodegradable films due to its unique properties such as high strength, stiffness and its ability to form transparent or translucent films upon drying using water based systems. These properties also make it a great candidate for industrial scale film production methods. One of the special properties, also crucial in film formation, is its gel forming ability in low concentrations (Pääkko et al. 2007). However, wood based CNF, particularly from hardwood, has a high weight percentage of glucuronoxylan (xylan), which has a big influence on the surface chemistry and on the properties and behaviour of CNF in various applications (Arola et al. 2013; Eronen et al. 2011; Iwamoto et al. 2008; Penttilä et al. 2013). Therefore, in order to effectively utilize CNF as a building block in 2D film applications, it is crucial to unravel the effect of xylan on the stability, formation and properties of CNF films. Moreover, there is an increasing interest in utilizing xylan in other high added value products and several pre-treatments have been developed in order to recover hemicelluloses in biorefinaries (Tunc and Van Heiningen 2008). As a result, the significance of xylan for the stability in dispersions, films and

during film formation was chosen for investigation in **Paper III.** It was discovered that xylan affects the stability at the molecular level and affects the water uptake ability of nanoscale films. However, the effects were diminished in macroscale films. These results enhance the effective utilization both of hardwood CNF as well as the hemicelluloses.

In **Paper IV**, the potential of utilizing 3D printable cellulosic materials for surface tailoring and functionalizing cellulosic fabrics was studied. Combining 3D printable cellulose based materials with cellulose fabrics enables the development of all-cellulose garments. The two cellulose derivatives, cellulose acetate (CA) and acetoxypropyl cellulose (APC), chosen as building blocks were both acetylated and in dissolved form, but had completely different properties due to differences in their molecular structures. Cellulose acetate, which is commercially available and widely used, forms rigid structures while acetoxypropyl cellulose forms soft/flexible structures, which could both be useful in textile applications. Visually, CA is transparent and APC a slightly cloudy white paste, but they can both be dyed as shown in **Paper IV.** Additionally, the use of these materials was demonstrated for 3D textile modification and functionalization by several prototypes. 3D printing technology also enables customization and diminishes production waste. The results provide new application possibilities for textiles and might furthermore simplify their recycling process due to an all-cellulose approach.

2. Background

2.1 Cellulosic building blocks

In this thesis, the versatility of cellulose is investigated and discussed as the utilization and characterization of three cellulosic building blocks, the wood fibres, the nanofibrils and the polymer are presented as well as their bottom up utilization in designing 1D-, 2D- and 3D-applications.

2.1.1 Wood fibres

Even though all wood is basically composed of cellulose, lignin, hemicelluloses and various extractives, it is a very heterogeneous material due to different species and tissue-dependent variations. In general, wood species can be divided into two groups: softwood (or gymnosperms) and hardwood (or angiosperms). (Dufresne 2012; Kargarzadeh et al. 2017). In this thesis, long fibres of softwood were used as pulp and short fibres of hardwood were further processed into CNF.

Plant fibres, nature's own biocomposite structures, are tough and water-insoluble layered structures. They are typically 1 to 59 mm long and approximately 10 to 50 µm wide hollow tubes where cell walls surround the lumen (Figure 2), which contribute to the water uptake. Microfibrils are arranged in the cell walls with different orientations depending on the layer. The middle lamella does not have a special structure and in the thin primary cell wall the microfibrils are randomly arranged. S_1, S_2 and S_3 are called the secondary wall and there the microfibrils are closely packed. S_1 is a relatively thin layer consisting of 4-6 lamellae, the S_2 layer is thick (30-150 lamellae) and the S_3 layer is thin again (up to 6 lamellae). The correct orientations of the microfibrils in each layer are currently under debate and new characterization methods, to determine them, are being developed. (Casdorff et al. 2017; Reza et al. 2014; Tsoumis 1991)

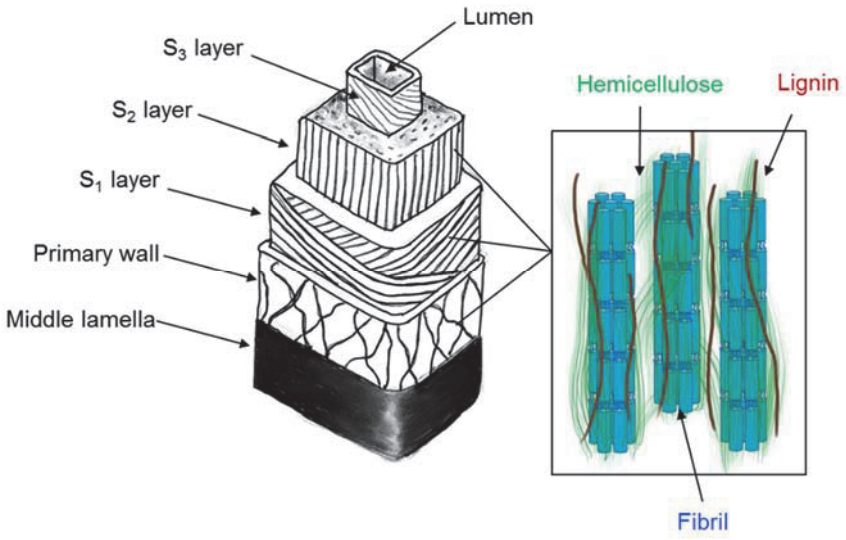

Figure 2 Simplified schematic presentation of the wood fibre structure

Hemicelluloses are also found as support material in the cell walls. They are heteropolysaccharides composed of a variety of monosaccharides such as xyloglucans, xylans, mannans and glucomannans. In wood, the amount of hemicelluloses is usually around 20-30 wt%, however, the content, composition and structure differs depending on the wood species. In softwood the main hemicellulose is galactoglucomannan and in hardwood glucuronoxylan. Birch kraft pulp, used in **Paper III**, contains approximately 23 wt% of glucuronoxylan (O-acetyl-4-O-methylglucurono-β-D-xylan). It is partially loosely bound on the fibril surfaces and has a large contribution to the material properties. For example, in nanocellulose production, the presence of hemicelluloses aids the mechanical fibrillation. (Fengel and Wegener 1984; Iwamoto et al. 2008; Penttilä et al. 2013; Sjöström 1993).

Lignins are a group of complex aromatic polymers resulting from oxidative combinatorial coupling of 4-hydroxyphenylpropanoids (Ralph et al. 2004). Lignins have been, in this thesis, removed by bleaching from the materials used and thus will not be discussed further.

2.1.2 Nanoscaled cellulose

The plant cell wall is composed of cellulose nano- and microfibrils, which can be disintegrated using a top-down process involving mechanical and chemical methods. According to the IUPAC definition, materials are considered to be nanosized when at least one dimension is in the size range of 1 nm - 100 nm. Therefore, the term CNF can be used for a variety of cellulose materials produced with different fibrillation protocols.

Microfibrillation was first reported by Turbak et al. (1983). Micro- and nanofibrillated celluloses are produced top-down by disintegrating pulp fibres using mechanical processing such as grinders or high pressure (*e.g.* microfluidization). The material produced using mechanical grinding is still rather coarse (diameter 10-100 nm, length 0.5-50 µm) as the microfibrils are formed of elemental nanofibril aggregates. By using chemical pre-treatments, aggregates can be deconstructed into smaller units by effectively weakening the interfibrillar hydrogen bonds prior to mechanical processing, for example, by utilizing 2,2,6,6-tetramethyl-piperidinyl-1-oxyl radical (TEMPO) region selective oxidation (Saito et al. 2006), carboxymethylation (Wågberg et al. 1987) or enzymatic hydrolysis (Pääkko et al. 2007) as a pre-treatment. Nanofibrils are composed of crystalline regions and, less ordered, amorphous regions. Debates, of how these regions are intermixed have been on-going for decades, but the so-called fringed fibrillar model, where there is less structured arrangement of non-uniform crystalline segments with presumably very small amorphous parts (4-5 anhydroglucose units in length), is nowadays widely accepted. (Hearle 1958; Nishiyama et al. 2003a; TAPPI 2011)

Cellulose nanocrystals (CNCs) were first reported on in the 1950s (Rånby 1951). Nanocrystals are formed using acid hydrolysis (*e.g.* H_2SO_4 or HCl) that, according to current knowledge, removes (hydrolyses) the amorphous regions of the cellulose microfibrils leaving only the rod-like particles (diameter 3-10 nm, L/D >5) (Kargarzadeh et al. 2017; Mariano et al. 2014; Moon et al. 2011; TAPPI 2011).

In order to study these materials, microscopic tools can be applied. A scanning electron microscope (SEM) can be utilized to examine dimensions from millimetre to micrometre scale whereas dimensions at the nanometre scale can be revealed using an atomic force microscope (AFM) or cryogenic transmission electric microscope (cryo-TEM). Photographs and microscopic images of the micro and nanoscale cellulosic materials can be found in Figure 3.

The aforementioned CNFs have a large surface area, high aspect ratio and high swellability. They generally form strong hydrogels in low solids content (1-3 wt%) and have excellent film formation ability (Mautner et al. 2018). However, recent developments regarding a production technique for high consistency (20-40 wt%) enzymatically fibrillated pulp (EFP) material introduced a new nanocellulosic material (Hiltunen et al. 2015). The material is produced using specific cellulase enzymes and fibre-fibre friction during mixing at low water content and it resembles more a paste than a gel.

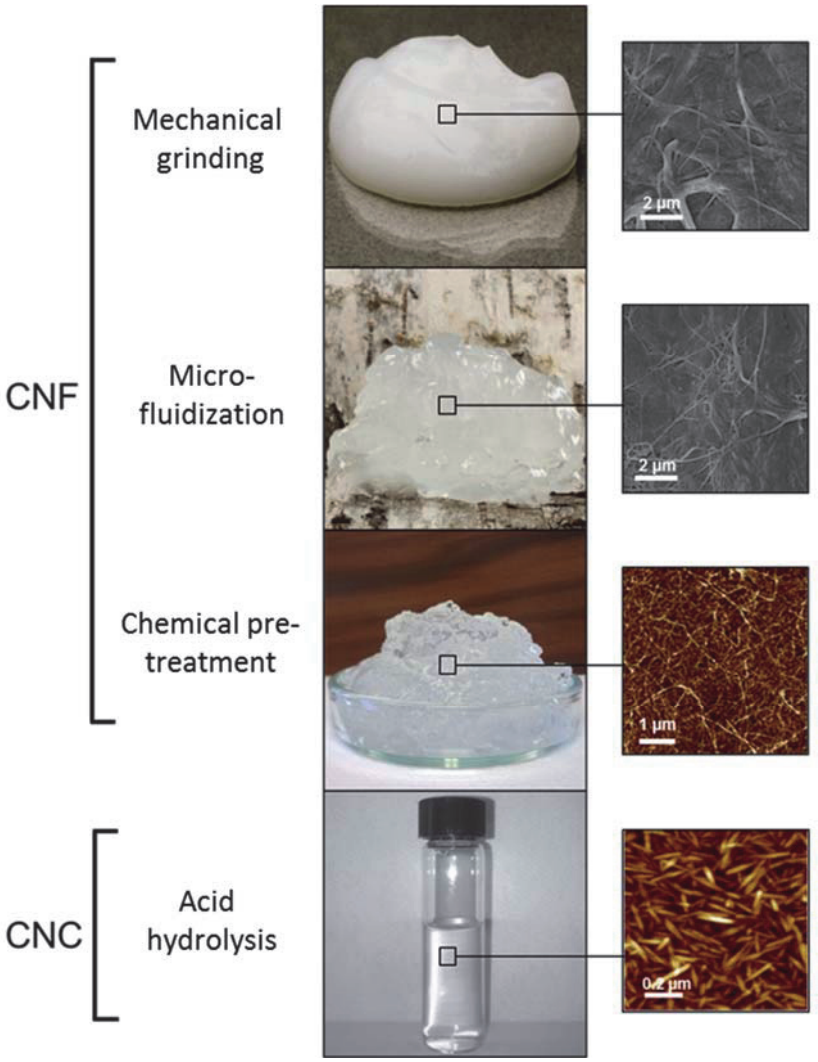

Figure 3 Cellulose micro- and nanofibrils and nanocrystals

There have been many published and demonstrated applications for CNF, however, so far only a few are commercial. Despite that, CNF is today produced by several companies worldwide. For instance, Sappi has a pilot-scale plant for CNF production in the Netherlands and Nippon Paper in Japan started large-scale production of TEMPO-oxidized CNF in 2017. (Nippon Paper Group 2017; Sappi 2017)

2.1.3 Cellulose polymer

Cellulose polymer is the molecular building block and the main structural component of woods and plants of the earth. Anselme Payen, a French professor, was the first to discover it in 1838 by noticing the difference in compositions of lignified and non-lignified plant matters (Payen 1838).

The structure of cellulose is relatively simple in the field of polysaccharides, however, its simple structure makes the chemical reactions rather complex and is responsible for the unique macroscopic properties of the polymer. Cellulose is a linear homopolymer composed of glucose monomers called D-anhydroglucopyranose units (AGUs) linked together by β-(1 →4)-glycosidic bonds (Figure 4). Every other monomer is rotated 180 degrees with respect to its neighbours. There are around 10000 AGUs in native wood polymer and three hydroxyl groups in each AGU (C2, C3 and C6), which are capable of typical chemical reactions for primary and secondary alcohols. The length of cellulose chains varies and the number of repeating glucose units is presented as degree of polymerization (DP). (Klemm et al. 1998; Roman 2009; Sjöström 1993)

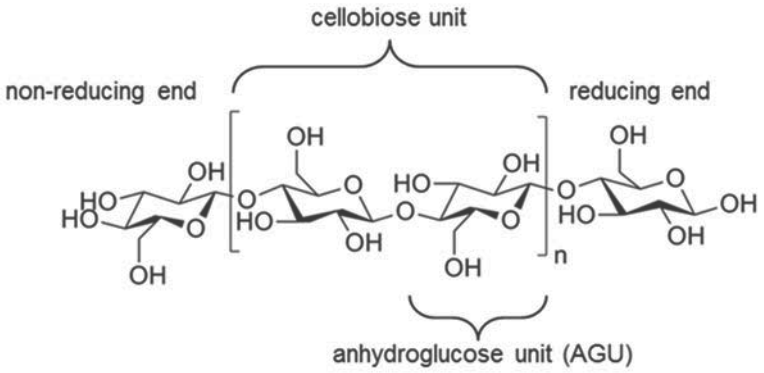

Figure 4 Molecular structure of cellulose

Cellulose polymers in native wood are packed in a semi ordered structure. The relatively rigid polymer chains are connected with intramolecular hydrogen bonds and assembled in sheet structures via intermolecular bonding. The sheets are connected via van der Waals forces. (Gross and Chu 2010)

According to current knowledge, there are three different cellulose crystalline structures (cellulose I, II, and III). Cellulose I is native cellulose, and can be divided into I_α and I_β. They both coexist in nature but I_α is dominant in bacteria and algae and I_β in higher plants. The structures of cellulose I_α and I_β differ in their molecular conformation, hydrogen bonding network and packing. The crystalline structure of cellulose I_α is triclinic and I_β is monoclinic. Cellulose II is formed irreversibly from cellulose I either by dissolution and regeneration or by alkali treatment. Regeneration alters the hydrogen bonding patterns (from parallel to anti-parallel) affecting

also the material properties. Cellulose III can be prepared reversibly, using various chemical treatments, from cellulose I (parallel chains III_I) or II (anti-parallel chains III_{II}). Previously, a cellulose IV form was also suggested, but it has been shown that it is only a slightly disordered form of cellulose I_β. (Atalla and Vanderhart 1984; Newman 2008; Nishiyama et al. 2002, 2003b; Wada et al. 2004)

Cellulose processing and modifying often involves dissolution. However, cellulose is not an easily dissolving polymer due to the rigidity of the chains, crystallinity, amphiphilicity and the high molecular weight, therefore, it is soluble only in selected solvents (Medronho et al. 2012; Nishiyama 2014; Olsson and Westman 2013). Solvents that are capable of dissolving cellulose are divided into derivatizing and non-derivatizing (or direct) solvents, depending whether they form covalent modifications on the cellulose backbone or interact only physically (Heinze 2016). A rather large number of non-derivatizing cellulose solvents are known today such as aqueous alkali (*e.g.* NaOH) solutions (Isogai and Atalla 1998), amine oxides (Chanzy 1980; Rosenau et al. 2001), ionic liquids (Swatloski et al. 2002), organic solvents with inorganic salts (DMAc/LiCl) (McCormick and Callais 1987), inorganic metal complexes (Saalwächter et al. 2000), molten inorganic salts (Fischer et al. 2003), and DMSO/ TBAF (Köhler and Heinze 2007). Cellulose derivatization is discussed in the next section. Cellulose solubility is, in general, a very complex topic with several disputed theories and is discussed elsewhere in detail (Olsson and Westman 2013), therefore there is no further discussion here regarding the subject.

2.1.4 Cellulose derivatives

Cellulose derivatives are manmade biopolymers and also the world's first synthetic polymers ever developed. The first cellulose derivative, cellulose nitrate was discovered by Braconnot (1833). It was the first cellulose derivative produced industrially as a textile material called artificial silk and it is still manufactured for applications such as explosives and lacquers for nail polishes. From the mid-19th century to this day, a large number of cellulose derivatives have been developed and many of them are also currently used. (Edgar et al. 2001; Klemm et al. 1998)

In cellulose derivatization, the hydrogens in the hydroxyl groups are substituted with functional groups typically by esterification, etherification or oxidation (Figure 5) (Kang et al. 2013; Klemm et al. 1998). These substituents can alter the properties of cellulose drastically and enable the formation of bioplastics. Degree of substitution (DS) expresses the number of cellulose hydroxyl groups per one repeating unit that is substituted during the reaction and it can range from 0 to 3. However, complete functionalization rarely occurs. (Klemm et al. 1998)

Probably the most important industrial scale derivatization application for cellulose is the viscose process (cellulose xanthogenate), where a mixture of copper(II) hydroxide and aqueous ammonia is used for cellulose dissolution (Cross et al. 1894). The dissolved polymer can be spun into fibres and precipitated in dilute sulphuric acid.

Esterification: R = H, NO_2, SO_3, H2PO2 etc.
Etherification: R= H, alkyl, hydroxyalkyl, sulfoalkyl, silyl, etc. groups

Figure 5 Synthesis of cellulose esters and ethers (redrawn from Kang et al 2013)

Cellulose acetate is the cellulose derivative with the second largest industrial production. It was discovered by Schützenberger in the 1860s and was the first cellulose ester of an organic acid. Today cellulose acetate is manufactured from cotton or wood pulp using acetic anhydride as the esterifying agent and sulphuric acid as the catalyst. Some of its many applications include: cigarette filters, films and eyeglass frames. Cellulose acetate is biodegradable, however, the degradation rate and method depends on the DS; the higher the DS the slower the degradation. Deacetylation of the polymer needs to be first accomplished by enzymes, hydrolysis or by photochemical degradation, followed by rather rapid enzymatic hydrolysis of the cellulose backbone. (Klemm et al. 1998; Puls et al. 2011)

Acetoxypropyl cellulose (APC) is synthetized from hydroxypropyl cellulose using acetylation. Hydroxypropyl cellulose is a commercial, water-soluble polymer that is used, for example, in the medical industry for tablets and as a thickening agent (Kargarzadeh et al. 2017). APC, on the other hand, is not a very commonly used cellulose derivative, but some research was conducted in the 80s on its liquid crystalline properties (Laivins and Gray 1985; Tseng et al. 1981) and, more recently, it has been used for electrospinning (Canejo et al. 2008) and in thin films (Filip et al. 2006; Godinho et al. 2009; Maji et al. 2013). In this thesis, APC was utilized for 3D printing due to its favourable mechanical and physical properties, as it is a soft and flexible polymer (amorphous solid). CA, on the other hand is a hard and rigid material.

2.2 Cellulosic building blocks in materials design

2.2.1 1D stuctures from cellulosic materials

Long cellulosic fibres from cotton or flax can be spun into a 1D yarn structure using a simple process. However, in order to transform wood based cellulosic materials into yarns and filaments, dissolution and regeneration of cellulose solutions has been traditionally required, and as a result, man-made cellulosic materials, such as

viscose, modal or lyocell, are obtained (Woodings 2001). These materials are currently widely used in textiles.

In order to retain the inherent properties of wood fibres, an alternative approaches, where dissolution and regeneration is not used, have recently gained a lot of attention. One approach is the utilization of CNF in fibre spinning where several methods for wet-spinning (Håkansson et al. 2014; Iwamoto et al. 2008; Lundahl et al. 2016; Walther et al. 2011) and dry-spinning (Ghasemi et al. 2017; Hooshmand et al. 2015; Shen et al. 2016) have been developed. Additionally, monofilaments from enzymatically fibrillated pulp (EFP) have also been reported (Spoljaric et al. 2017). However, all the CNF and EFP filaments are still only produced at laboratory scale due to challenges in process upscaling and water stability issues (Lundahl et al. 2017). Another approach is to manufacture yarns utilizing pulp fibres as building blocks. Due to short wood fibre, the formation of filament or yarn from pulp fibres is not as simple as with the long fibres of cotton or flax, and therefore the development of new spinning methods is required. Salmela et al. (2013) have demonstrated a yarn manufacturing method using aqueous pulp suspension with alginate as a gelling agent with a subsequent dewatering step, and in this thesis a waterless process utilizing deep eutectic solvent (DES) as a medium for dry-wet spinning for fibre yarn is presented.

Figure 6 Pulp fibre filaments from DES process (photo: Eeva Suorlahti)

By using the very basic bleached pulp, less processing steps are required. Wood pulp is also considered more environmentally friendly than cotton, due to cotton's high consumption of water and arable land (Hämmerle 2011). Despite the fact that the resulted fibre yarns are not as strong as cotton or filaments made using traditional methods, they are water-stable and strong enough to have potential application areas, for example, in textiles, disposable textiles or composite structures as demonstrated in **Paper IV**.

2.2.2 2D structures from cellulosic materials

Paper and board, the most common 2D applications of cellulose, are produced from wood fibres. Prior to production, pulp fibres are dispersed using industrial processes for mechanical (*e.g.* thermomechanical pulp (TMP)) and chemical pulps (*e.g.* Kraft). Also, various types of films from cellulose derivatives have been developed (Cao et al. 2010; Li et al. 2012; Zhang et al. 2001), cellophane being the most common application. However, the recent advances in the nanofibrillation process, such as improvement in energy efficiency due to cheap and effective pre-treatments and up-scalable production methods, have inspired many new CNF film applications (Pääkko et al. 2007; Saito et al. 2007).

CNF films are typically prepared from dilute dispersions (Tammelin et al. 2013). Solvent (often water) is removed by evaporation or vacuum filtration and additional pressing could be applied. Fibrils are held together by strong hydrogen bonds and the films are often translucent since thin fibrils do not scatter light. (Benítez et al. 2013; Nogi et al. 2009; Österberg et al. 2013). The inherent film forming ability, intrinsic mechanical properties due to high crystallinity, high surface area and nanoscale dimensions of CNF make it an excellent material for various film applications (Benítez et al. 2013; Nogi et al. 2009; Tammelin and Vartiainen 2014; Österberg et al. 2013)

CNF films exhibit good barrier properties due to densely packed fibrils. Oxygen permeability at low relative humidities is often much lower compared to other biomaterials and at a similar level to conventional synthetic films. CNF films can also be used as coatings to improve oxygen and oil barrier properties. (Aulin et al. 2010; Syverud and Stenius 2009; Österberg et al. 2013)

In this thesis, 2D films from CNF with different hemicellulose (xylan) contents were produced and the effect of xylan was investigated. Since the hemicelluloses cover the microfibrils, they have a large effect on the material properties. Hemicelluloses have been noticed to prevent hornification of the fibres, induce swelling, decrease the aggregation behaviour of cellulose, decrease the average crystallinity and affect the dimensions of the microfibrils (Duchesne et al. 2001; Köhnke et al. 2010; Oksanen et al. 1997; Uhlin et al. 1995; Wan et al. 2010; Whitney et al. 1998; Young and Rowland 1933). In papermaking, hemicelluloses, particularly xylan, have been used to improve paper strength by contributing to hydrogen bonding and increasing flexibility (Helmerius et al. 2010; Schönberg et al. 2001), however, high amounts of hemicelluloses tend to decrease the tear strength (Hannuksela et al. 2004; Schönberg et al. 2001) and hinder filler retention due to higher charge (Lyytikäinen 2017). In CNF films, xylan decreases fibril aggregation by increasing repulsion between fibril surfaces (Paananen et al. 2003), however, the role of xylan for CNF film strength properties is somewhat unclear since both addition (Lucenius et al. 2014) and removal (Arola et al. 2013) of xylan have been observed to improve strength. If TEMPO oxidation is used as a pre-treatment for CNF, large amounts of xylan have been observed to hinder the reactivity of cellulose towards oxidation (Pääkkönen et al. 2016). For the production of dissolving pulp, low hemicellulose content is a requirement (Borrega et al. 2013). Removal of xylan from pulp would

also be attractive, due to its potential to be exploited as a value added product elsewhere (Lyytikäinen 2017).

Ultrathin model films

Ultrathin films of CNF and cellulose derivatives can be used to reveal surface interactions. Thin film studies enable thorough investigation of the materials and interactions at molecular level eliminating the bulk effect. Native cellulose I (with hemicelluloses) can be studied using a dilute CNF dispersion and cellulose II (or amorphous cellulose if spin coating is used) using a cellulose derivative Trimethylsilyl cellulose (TMSC) with regeneration to pure cellulose. (Hoeger et al. 2014; Holmberg et al. 1997; Tammelin et al. 2006)

Model films are deposited on a flat surface and consist of a very thin layer of one or more chemically well-defined compounds. These model films can be made, for example, using spin coating or dipping procedures such as Langmuir-Blodgett or Langmuir-Schaefer (Langmuir and Schaefer 1938). The surface sensitive methodology used today to study these films is quite extensive. Some of the most commonly utilized characterization methods are Quartz Crystal Microbalance with Dissipation monitoring (QCM-D), X-ray Photoelectron Spectroscopy (XPS) and Atomic Force Microscopy (AFM), which have all also been used in this thesis. Typical phenomena studied using cellulose model films are adsorption, interaction and swelling (Kontturi et al. 2006; Tammelin et al. 2006; Wågberg et al. 2010; Österberg and Valle-Delgado 2017). In addition to research purposes, ultrathin CNF films have been demonstrated as a biobased coating for implants to prevent corrosion (Wilson et al. 2017).

In Paper III, the water interactions of spin coated cellulose model films from CNF were studied and in **Paper IV** the material compatibility of 3D printed cellulose derivatives with pure cellulose II were investigated using QCM-D.

2.2.3 3D printed structures from cellulosic materials

Wood has traditionally been used for manufacturing large 3D objects such as buildings and furniture utilizing timber, plywood and wood chips as building blocks. However, 3D structures can also be formed from other cellulosic materials such as CNF or cellulose derivatives utilizing new manufacturing methods such as 3D or bioprinting.

3D printing belongs to the novel additive manufacturing methods that build a product from successive materials layers. It has immense potential to be utilized with new materials and in various manufacturing industries since moulds are not needed and waste is minimized. 3D printing also enables the mass customization of products on-demand. (Berman 2012; Peng et al. 2015)

There are a few previous publications combining cellulose with 3D printing. Cellulose dissolved in ionic liquid and nanocellulose based ink for biomedical applications such as tissue engineering and regenerative medicine have been previously reported by Markstedt et al. (2014, 2015, 2017). Moreover, 3D printable nanocellulose-alginate hydrogel was recently reported as having a potential application in

wound dressing (Leppiniemi et al. 2017). Cellulosic objects have been printed using cellulose acetate (Pattinson and Hart 2017) and Z corporation has used short cellulose fibres as one component in their commercial powder for 3D powder printing (Pfister et al. 2004). Furthermore, wood chips with gypsum as a binder have been utilized to manufacture 3D objects (Henke and Treml 2013). However, in the textile world there were no previous records of combining cellulosic materials with cellulosic textiles using 3D printing. Materials from non-renewable sources are commonly used in the textile and fashion industries as fabrics (nylon, polyester) as well as in add-ons to garments in fashion such as buttons, prints, and labelling. By mixing different materials in garments, the recycling becomes more complex and non-cellulosic materials need to be removed from cellulosic textiles prior to post-consumer recycling (Blackburn 2009). If these materials could be exchanged for cellulose and applied directly by a 3D printing process, recycling could be simplified, the need for manual labour decreased and the high internal affinity of cellulosic materials utilized. Additionally, the versatility of cellulosic materials enables printing of both hard and soft structuring, which creates endless possibilities for textile applications.

Therefore, in this thesis, polymeric cellulose and cellulose derivatives were used as building blocks for 3D applications. To be precise, CA, APC and cellulose dissolved in ionic liquid were utilized for textile modification using 3D printing. The approach was to develop all-cellulose garment applications by utilizing cellulose as both a textile and a printing material.

3. Experimental

The work done in this dissertation focused on utilizing cellulose in its different forms as building blocks for 1D-, 2D- and 3D-applications and studying the properties and interactions of these materials from molecular level to macroscale utilizing complimentary methods. Even though, the used materials are all cellulose based, their material properties are completely different due to chemical modifications or differences in size. Therefore, quite a number of different analysis methods were needed.

The main analytical methods used in this thesis represent the methods that are the most versatile and give the most information about the materials properties or the interactions. For chemical composition and structure Fourier transform infrared spectroscopy (FTIR) (**Papers I** and **IV**), ^{13}C CP MAS NMR spectroscopy (liquid and solid-state) (**Papers I, II** and **IV**) and X-Ray photoelectron spectroscopy (XPS) (**Paper II**) were applied. For surface interactions and to reveal phenomena at interfaces a quartz crystal microbalance with dissipation monitoring (QCM-D) (**Papers III and IV**), and turbidity measurement (**Paper III**) were used and for physical performance tensile testing (**Paper I**) and adhesion measurements (**Paper IV**) were conducted.

3.1 Cellulosic materials

3.1.1 Pulp fibres as raw materials and for 1D yarn manufacturing

Never-dried, bleached pine pulp was used for 1D yarns in **Papers I and II** and elemental chlorine free (ECF) bleached birch kraft pulp for 2D films in **Paper III**. Pulps were supplied by Finnish pulp mills and, for **Papers II** and **III**, pulps were ion-exchanged to the sodium form in order to control the pulp properties and in **Paper III** to improve fibrillation. The ion-exchange was based on a slightly modified version of a method originally described by Swerin et al. (1990) with some additions (Lahtinen et al. 2014)

Pulp samples with decreasing xylan content in **Paper III** were prepared by xylanase hydrolysis with purified Trichoderma reesei Xyl II (pI9) using variable times: 3, 24 and 68 hours in deionized water at 45 ºC. Enzymatic action was terminated by soaking the pulps in water at 90 ºC for 15 min.

3.1.2 Nanofibrillated cellulose for 2D films application

The pulps with variable xylan contents studied in **Paper III** were nanofibrillated by first pre-refining the pulp using Voith laboratory scale refiner (LR-1, Voith) to avoid clogging during fibrillation. Pre-refined pulps were then diluted to 1.8 wt% consistency with deionized water and dispersed using Dispermat (VMA Getsman Gmbh) at 3400 rpm for 60 minutes. Fibrillation was conducted with several successive passes using a high-pressure fluidizer (Microfluidizer EH110, Microfluidicies Corp.) through two differently sized chamber pairs. The first chamber pair was used

for the first pass with diameters of 400 µm and 200 µm at a pressure of 1350 bars. The rest, 17 passes, were done through a chamber pair with diameters of 400 µm and 100 µm at a pressure of 1850 bars until the resulting material was homogenous, viscous and gel-like. The samples were stored at +4 ºC until use.

3.1.3 Cellulose derivatives for 3D printing

The cellulose derivatives (Figure 7) used for 3D printing in **Paper IV** were cellulose acetate (CA, DS_{Ac} of 3, M_w ~60000) and acetoxypropyl cellulose (APC) synthetized from hydroxypropylcellulose (HPC, DS_{HP} of 4-5, M_w ~80000, average M_n ~10000, powder, 20 mesh particle size). Both chemicals were obtained from Sigma Aldrich (USA).

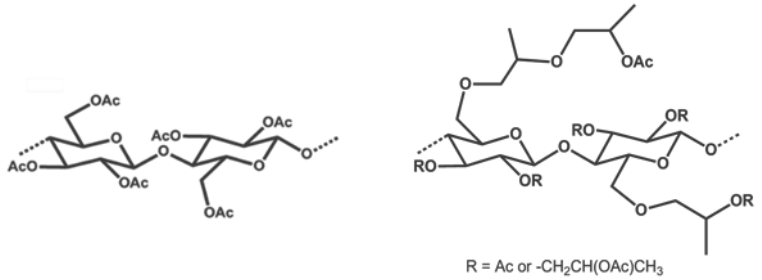

Figure 7 Cellulose acetate (left) and acetoxypropyl cellulose (APC) (right)

Synthesis of APC was conducted via esterification as previously published by Tseng et al. (1981) with slight modifications. A detailed description can be found in **Paper IV**. The molar substitution of hydroxypropyl cellulose was MS_{HP} 4.3 and the degree of substitution for acetylation was DS_{Ac} 3.0. Chemicals used in the synthesis (N,N-dimethylacetamide, pyridine and acetic anhydride) were obtained from Sigma Aldrich (USA).

The printable cellulosic materials used in **Paper IV** were prepared by dissolving CA in acetic acid (concentration 30 wt%) and APC in acetone (concentration of 80 wt%).

IL dissolved cellulose for demonstrator purposes was done by dissolving cellulose cotton linters in [emim]OAc in 10 wt% concentration using the previously reported procedure (Kosan et al. 2008). All printable cellulosic materials were stored in sealed containers at room temperature prior to 3D printing.

3.1.4 Cellulosic fabrics for 3D printing

Cellulose fabrics (Figure 8) used in the 3D printing studies in **Paper IV** were uncoated and undyed woven cotton (plain weave, 100 % cotton, 150 g/m^2, Iisalmen kangastukku, Finland), knitted cotton (single knit, 100 % cotton, 155 g/m^2, Orneule,

Finland) and woven viscose (Bamboo Plain Ivory (BB12), plain weave, 100 % viscose, 140 g/m^2, Whaleys Bradford Ltd., UK).

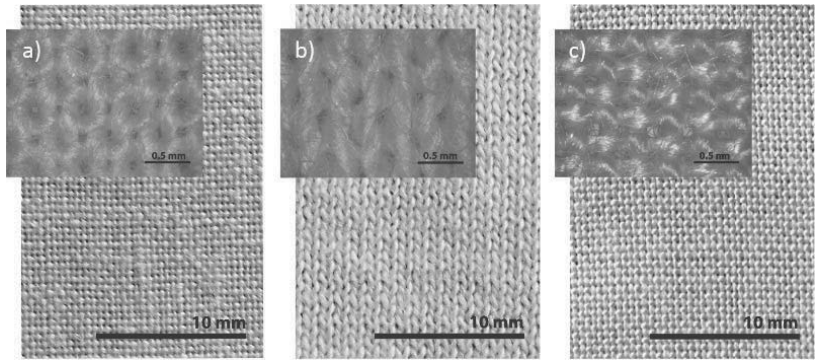

Figure 8 Photographs and microscopic inserts of cellulose fabrics used as the substrates for printed structures. a) Woven cotton, b) knitted cotton and c) woven viscose fabric. Inserts show microscopy images of the yarn looping of the used textiles.

3.2 Other chemicals and materials

Choline chloride (Sigma Aldrich, USA) and urea (Sigma Aldrich, USA) were mixed together with heat (100 °C) in molar ratio 1:2 according to Abbott et al. (2003) in order to produce a clear and homogenous deep eutectic solvent (DES) used in **Paper I-II**. Polyacrylic acid (PAA, Sigma Aldrich, USA) was used in **Paper I**.

In **Paper IV**, the chemicals used in the synthesis of APC were *N,N*-dimethylacetamide, pyridine and acetic anhydride (obtained from Sigma Aldrich, USA) and the materials for tailoring fabric surfaces were 1-ethyl-3-methylimidazolium acetate ([EMIM][OAc]) (IoLiTec, Germany), cellulose cotton linters (Milouban, Israel), thermochromic pigment paste (Zenit, Sweden), reflective beads (commercial high index standard beads, particle size of 180-600 microns, white/clear) (Cole Safety International, USA), black colourant (commercial food grade paste colorant), and conductive yarn (BEKAERT's Bekinox VN12/1*275/100Z steel yarn, Belgium). All other chemicals used were analytical grade and water MilliQ unless otherwise stated.

3.3 Methods

3.3.1 Spectroscopic methods to reveal chemical composition

3.3.1.1 FTIR Spectroscopy

Fourier Transform Infrared (FTIR) spectroscopy utilizes the interaction of mid-infrared light (from 4000 to 400 wavenumbers) with materials. In general, IR spectra can

determine the molecules present in the studied sample and their concentration. There are several different IR spectrometer types available but the most commonly used is FTIR. This is also commonly used in cellulose research. The theory behind FTIR is that it measures the absorbance of infrared light that corresponds to the resonant frequencies of specific bonds or groups. (Smith 2011)

The advantages of FTIR are that it can be used with many types of samples (including solids, liquids, gases, semi-solids, polymers, powders, organics and inorganics, biological materials and mixtures). FTIR gives a lot of information about the sample, it is simple and fast and the amount of material needed is very small. It has a long history in paper research as a tool for qualitative analysis, quantification of individual components and contaminant identification. In current cellulose research, it can also be used to determine wood constituents or chemical changes taking place. However, the interpretation of complex materials, such as pulp, is often challenging due to large number of signals in the fingerprint region marking variable polysaccharides, such as hemicelluloses. (Friese and Banerjee 1995; Pandey 1999; Smith 2011)

Over the years, FTIR has included several different sampling techniques; *e.g.* attenuated total reflection (ATR) and diffuse reflectance infrared (DRIFT) spectroscopy. With the non-destructive DRIFT method the quality of the spectra has improved and measurement time decreased (Fan et al. 2016; Pandey 1999).

FTIR spectrometer with ATR diamond (Thermo Scientific™ Nicolet™ iS™50 FTIR Spectrometer, United States) was used to determine the chemical components and study chemical bonds in bulk materials. In **Paper I** it was used to study the possible crosslinking of PAA to cellulose pulp and determine the purity of DES after recycling and in **Paper IV** to determine the purity of the materials by analysing the chemical composition of the fabrics, CA and APC and the regenerated cellulose from IL. All spectra were obtained from 32 scans with a resolution of 4 cm^{-1} and transmission mode from 350 to 4000 cm^{-1}.

3.3.1.2 Raman Spectroscopy

Raman spectroscopy is a non-destructive analysis method based on monochromatic light interacting with the sample. Intense laser beams are used in the UV-visible region to irradiate the sample and the scattered light is observed in a direction perpendicular to the incident beam. The interaction results in a shift in energy that gives information about the vibrational and/or rotational modes in the system. In Raman, the scattered light consists of two types of scattering: Rayleigh scattering and Raman scattering. The former is strong and has the same frequency as the incident beam and the latter is very weak, about 10^{-5} of the incident beam. (Edwards et al. 1997; Ferraro et al. 2002; Moon et al. 2014)

Raman spectroscopy is related to the aforementioned infrared spectroscopy as they both operate in the same range; however, Raman is sensitive to non-polar bonds whereas IR is sensitive to polar bonds. (Solala 2015)

Raman spectroscopy was used to study the structural properties of pulp fibres in bulk in **Paper II**. Measurements were conducted using a Renishaw RM-1000 System equipped with a thermoelectrically cooled CCD detector. A Leica microscope with a 50× objective lens was used to focus the laser on the samples. A laser with 785 nm wavelength was used to excite and record the Raman scattering with 10 s exposure time and ten accumulations. In the experiment, the fibres were oriented parallel and perpendicular to the polarization configuration of the laser light. Raman spectra of pulp fibres were normalized to the intensity of a band located at ~897 cm^{-1} in order to remove amorphous contributions from the region of 250-700 cm^{-1}. (Agarwal et al. 2010)

3.3.1.3 Solid and liquid state 13C NMR Spectroscopy

Nucleus magnetic resonance (NMR) is a spectroscopic technique that utilizes the magnetic properties of the atomic nucleus. Certain nuclei resonate at a characteristic (radio) frequency when placed in a magnetic field. The small variations on that frequency reveal detailed information about the molecular structure of the characterized material. Here, the ^{13}C nucleus was used, which is a common nucleus observed in both liquid and solid state spectroscopy (Conte et al. 1997; Jacobsen 2007)

Due to its ability to provide information about the chemical environment as well as ultrastructural details solid-state NMR spectroscopy is often used in lignocellulosic research. The first cellulose NMR studies were conducted by Atalla and Vanderhart et al. (Atalla 1999; Atalla and Vanderhart 1984; Earl and VanderHart 1981; VanderHart and Atalla 1984)

Solid state ^{13}C cross polarisation magic angle spinning (CP MAS) NMR spectrometers (Agilent 600 NMR spectrometer (I) and Bruker AVANCE-III 400 MHz, Bruker BioSpin, Germany (II)) were used in **Paper I-II** to measure spectra from an untreated reference pulp sample and a pulp sample kept in ChCl/urea overnight to determine the possible residuals from DES treatment. Agilent 600 NMR 20,000 scans were accumulated with a MAS rate of 10 kHz using a 1.1 ms contact time and a 3.0 s relaxation delay between successive scans. In Brucker AVANCE, 10,000 scans were collected for each sample using 8 kHz spinning frequency, 2 ms contact time, and 5 s delay between pulses.

Liquid state ^{13}C NMR spectroscopy was used in **Paper II** to determine the spectra for ChCl and urea in order to compare them to additional signals found in DES treated pulp and in **Paper IV** to compare the spectra of HPC and APC in order to determine a successful esterification reaction. 30 mg of ChCl and urea were dissolved in DMSO-d6t and APC was dissolved in acetone-d6 with concentration 100 mg ml^{-1} and 8 mg ml^{-1} and Cr(acac)3 was added for enhanced relaxation. Magnetic flux density was in both cases 11.7 T. and a 13C spectrum was acquired with a BB(F)O double resonance probe head at 22 °C, using a 30 degree pulse and a waltz16 proton decoupling sequence. A total of 1200 scans were collected for ChCl

and urea and 20,000 scans for APC with a 1.5 s relaxation delay between successive scans. Referencing was conducted using the lock frequency and Bruker TopSpin 3.5 software was used to process the spectrum.

3.3.1.4 X-Ray photoelectron spectroscopy

X-Ray photoelectron spectroscopy (XPS) is a widely used, surface sensitive analysis method that is based on the photoelectric effect discovered by Hertz in the late 19th century (Hertz 1887) and further elaborated by Einstein (1905). For lignocellulosic materials the method was first applied in the 70s (Dorris and Gray 1978). When a sample is irradiated with X-rays, a photoelectron emission is triggered. The measured kinetic energy of the photoelectron is directly proportional to the binding energy of the electron to a nucleus. The binding energy is element-specific, which enables the determination of the element. Since the photoelectrons can travel only very short distances and lose energy due to collisions, the method is highly surface sensitive and the measurements have to be performed in ultrahigh vacuum conditions (pressure below 9-10 mbar). For cellulose samples the analysis depth is approximately 10 nm.

XPS was used to analyse the surface elemental compositions and chemical states in **Paper II** using an AXIS Ultra electron spectrometer (Kratos Analytical Ltd, UK.) with monochromatic A1 Kα irradiation at 100 W and effective charge neutralization with slow thermal electrons. Johansson and Campbell (2004) have been previously published the set-up and acquisition parameters. Prior to the measurements, the samples were placed in a pre-chamber overnight. Low-resolution wide spectra, and additionally for some samples, high resolution spectra of the carbon (C 1s) region were collected. Three parallel measurements were made from each sample. As an in situ reference, a sample of ash free 100 % cellulose filter paper, stored under dust free ambient conditions, was analysed. (Johansson and Campbell 2004). Due to ultrahigh vacuum or X-rays no degradation of the samples was observed during the measurements.

3.3.1.5 UV-VIS spectroscopy

UV-VIS spectroscopy was used to study the changes in charge using the adsorption of methylene blue on cellulose fibres in Paper II. The adsorption has been previously published by Ho et al. (2011), and it was applied with some modifications. The method was based on the (electrostatic) adsorption of the cationic dye to the anionic sites of cellulose. The adsorption level was measured using the intensity level of the supernatant (Palit and Moulik 2000). Cationic methylene blue dye solution was prepared by mixing 0.0161 g of methylene blue with MilliQ-water (100 ml) at room temperature. 0.016 g of dry pulp was mixed with 1 ml of dye solution and 39 g of MilliQ-water. Continuous shaking was applied for 24 hours at room temperature using a Stuart orbital shaker (SSL1, UK) at a speed of 160 rpm. Subsequently, the dispersion was centrifuged for 30 minutes at 10000 rpm and a few millilitres of supernatant

was collected for the absorbance measurement, which was then placed in a 1 cm polystyrene cuvette and measured using a UV-VIS spectrophotometer (UV/VIS/NIR Lambda 900, Perkin Elmer, USA). Two parallel measurements were conducted and the maximum absorbance for methylene blue at 664 nm were compared.

3.3.2 Microscopic techniques to reveal morphology

3.3.2.1 AFM

Atomic force microscopy (AFM) (Nanoscope IIIa multimode AFM, Digital Instrument, Santa Barbara, CA) was used to characterize the changes in pulp surface morphology in **Paper I** and analyse the spin coated CNF thin films on QCM-D crystals in **Paper III**. The topography images were scanned in tapping mode in air using a 10279EVLR scanner and silicon cantilevers (NCHV-A, Bruker, Camarillo, CA in **Paper I** and IMasch, Tallinn, Estonia in **Paper III**) with resonant frequencies of 320-360 kHz. No image processing apart from flattening was made. At least three images were taken per sample.

3.3.2.2 SEM

Scanning electron microscopy (SEM) (Merlin® FE-SEM, Carl Zeiss NTS GmbH, Germany) was used to examine the changes in the morphology of pulp taking place during solvent exchange (water removal) and DES treatment in **Paper II,** as well as the morphology of the fibre yarns in **Paper I**. Samples were prepared on double-sided carbon adhesive discs attached to aluminium specimen stubs. The samples were first sputter-coated (Agar™ Auto Sputter Coater, England) with platinum (Pt) to improve specimen conductivity and the imaging was conducted using 3.0 keV electron energy and 30 pA probe current. The pixel resolution was 2048 × 1536.

SEM imaging for CNF samples in **Paper III** was performed using LEO DSM 982 Gemini FEG-SEM (Noran Instruments Inc. Middleton, USA). Prior to the imaging, the nanofibril samples were solvent exchanged to acetone and the removal of acetone was carried out by the critical point drying method (CPD, Bal-Tec CPD 030 Critical Point Dryer) using CO2 as the transition liquid. CNF samples were, in this case, also sputter coated with platinum and examination was conducted using an acceleration voltage of 2.0 keV.

3.3.3 Overall chemical composition

Elemental analysis (C, H, N, S) of the pulp samples in **Paper II** was done with a FLASH 2000 series analyser (Thermo Scientific, USA). In order to remove excess moisture, the samples were dried at 105 °C overnight. The calculated elemental compositions of the samples were based on the carbon, nitrogen, and oxygen composition of an anhydroglucose unit ($C_6H_{10}O_6$).

Carbohydrate composition (rhamnose, arabinose, galactose, glucose, xylose, and mannose) of the pulp samples was determined in **Papers II-III** by hydrolysing the samples. The resulting monosaccharide contents were determined by high performance anion exchange chromatography (HPAEC) with pulse amperometric detection (Dionex ICS-5000 equipped with CarboPac PA20 column) according to an NREL standard (NREL Standard 2008; Sluiter et al. 2012; Willför et al. 2009)

3.3.4 Surface interactions by QCM-D

Quartz crystal microbalance with dissipation monitoring was used to study water vapour uptake with a humidity module (QHM401) of CNF thin film **in Paper III** and for the interaction assessment between cellulose derivatives and cellulose model surface in **Paper IV**.

The QCM-D technique is an acoustic method based on oscillation of a piezoelectric quartz crystal that is sensitive to changes in mass and viscoelastic properties of a film deposited on a crystal surface due to solvent or adsorbed material. These changes can be monitored in solid/liquid and solid/gas interfaces. (Höök et al. 1998; Rodahl and Kasemo 1996).

The piezoelectric quartz crystal oscillates at its resonance frequency, f_0. The frequency depends on the total oscillating mass affecting the crystal and it increases or decreases with mass changes on the crystal surface. The amount of adsorbed material can be calculated using the Sauerbrey equation (Eq. 1) (Sauerbrey 1959). If the mass of adsorbed materials is evenly distributed, rigid and small, the shift in frequency $\Delta f = f - f_0$ is related to the adsorbed mass, Δm, per unit surface.

$$\Delta m = -\frac{C\Delta f}{n} \qquad (1)$$

where *C* is a constant that describes the sensitivity of the device to changes in mass and *n* is the overtone number (*n* = 1, 3, 5, 7) and. The adsorption of studied material to a thin film on crystal surface can be monitored on-line (Rodahl et al. 1995).

If the film on the sensor surface is not fully elastic or rigidly attached, frictional losses occur that lead to damping of oscillation with a decay rate of amplitude, which is dependent on the viscoelastic properties of the material. The change in dissipation ($\Delta D = D - D_0$) measures qualitatively the rigidity of the film on the sensor surface and it is calculated using dissipation, D, defined by Eq. (1).

$$D = \frac{E_{diss}}{2\pi E_{stor}} \qquad (2)$$

where E_{diss} is the total dissipated energy during one oscillation cycle and E_{stor} is the total energy stored in oscillation. The film can be considered fully elastic and rigid when $\Delta D \leq 1 \times 10^{-1}$ and there is no spreading of the overtones. By measuring

simultaneously several overtones of frequency and dissipation responses, it becomes possible to determine the elastic or viscoelastic nature of the layer on the sensor.

CNF thin films (**Paper III**) were prepared by spin coating (at 3000 rpm for 10 min) 50 µl of dilute CNF dispersion in water (~0.05-0.1 wt%). Prior to spin coating the dispersion was treated with ultrasonic micro tip (Branson Digital Sonifier) and the sensor crystals were cleaned for 15 min using UV/ozone treatment and subsequent immersion in polyvinyl amine (PVAm) solution. PVAm was used to improve the adhesion to the sensor surface and nanofibrils (Ahola et al. 2008). Spin coating was conducted to apply the CNF film on to the crystal surface. After spin coating, the CNF layer was rinsed with MilliQ water and dried gently with N_2 (g). Final drying and heat-treatment was conducted in an oven at 80 ºC for 30 min to remove water and further enhance adhesion.

QCM-D and a humidity module were used to determine the areal mass of the spin coated CNF layer. Areal mass was calculated by measuring the difference in frequency response of the sensor before and after CNF deposition in air (at 23 ºC) with an air flow of 0.1 ml/min after approximately 25 min stabilization of the signal. The collected frequency data, from the before and after measurements, was stitched together using QTools-software, and the areal mass was calculated using Eq. 1 (Peresin et al. 2012).

The coated CNF sensors were stored, prior to the measurement, in a desiccator and protected from light. Before commencing the measurement, the sensors were allowed to stabilize overnight at RH 11 % inside the QCM-D humidity module. By monitoring the frequency and dissipation changes as a function of time while exposing the CNF films to different RHs, changes in water vapour uptake and viscoelastic properties could be observed. Different RHs were applied by circulating saturated salt solutions (Table 1) through the humidity chamber using a peristaltic pump (High Precision Multichannel Dispenser, Ismatec, Germany) at a flow rate of 100 ml/min for 30 minutes at 23 ºC. The typical result of varying humidity using CNF thin film is presented in Figure 29.

Table 1 Saturated salt solutions used in water vapour uptake monitored with QCM-D with their respective relative humidity (Greenspan 1977).

Salt solution	Relative humidity (%)
LiCl	11
$MgCl_2$	33
$Mg(NO_3)_2$	53
NaCl	75
$K2SO_4$	97
Pure milliQ H_2O	100

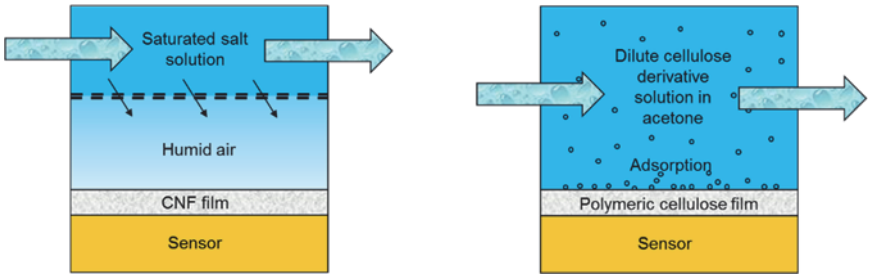

Figure 9 Schematic representation of the humidity chamber (left) and adsorption chamber (right)

In **Paper IV**, QCM-D was used for the evaluation of adsorption and the strength of interactions of cellulosic materials. Trimethylsilyl cellulose (TMSC) was used for thin film preparation. It was synthetized from high purity cellulose powder from spruce (Sigma Aldrich, USA) using the method described by Österberg and Claesson (2000). Cellulose thin films were prepared on gold coated QCM-D sensor crystals. The crystals were first cleaned using UV/ozone treatment for 30 min and then spin coated with toluene using a speed of 3000 rpm for 15 s to purify the crystal surface. 10 mg ml^{-1} of TMSC in toluene was then spin coated onto the crystal surface with a speed of 4000 rpm for 60 s. Finally, the coated crystals were dried in an oven at 60 °C for at least 10 min for proper adhesion. Desilylation was carried out in 10 % HCl vapour in vacuum for 5 minutes. Prior to the QCM-D measurements, the regenerated (pure) cellulose surfaces were kept in MilliQ-water overnight and gently dried with nitrogen gas before being placed in the QCM-D chamber.

Adsorption was monitored while dilute dispersions (0.5 mg ml^{-1}) of CA or APC in acetone were allowed to flow over the cellulose surface. Dispersions were pumped at a flow rate of 0.1 ml min^{-1} at 22 °C. A schematic representation of the systems can be found in Figure 9.

The QCM-D sensor crystals used in this study were AT-cut quartz crystal coated with silicon dioxide (SiO_2) (**Paper III**) and gold (**Paper IV**) with fundamental resonance frequency of (f_0) 5 MHz and the sensitivity constant of $C \approx 0.177$ mg m^{-2} Hz^{-1}. Sensor crystals were obtained from Q-Sense, (Gothenburg, Sweden)

3.3.5 Stability by turbidity

The stability of the dilute CNF dispersions (**Paper III**) was observed using a turbidity analyser Turbiscan LAB (Formulaction SA, L'Union, France) by measuring transmission and backscattering. CNF dispersions (0.05 wt%) with varying electrolyte concentrations (0.1 M, 0.01 M and 0.001 M NaCl) were prepared using homogenizer (Heidolph, SilentCrusher M, Type 18 F/M, Germany) during 1 min at 12000 rpm. The dispersions were analysed, using a scanning mode, in a cylindrical glass cell,

where the optical reading head scanned the length of the sample cell from bottom up to 55mm, acquiring transmission and backscattering data every 40 µm (Figure 10). Scanning was performed every 5 minutes for 2 hours and the transmitted and backscattering data was plotted as curves.

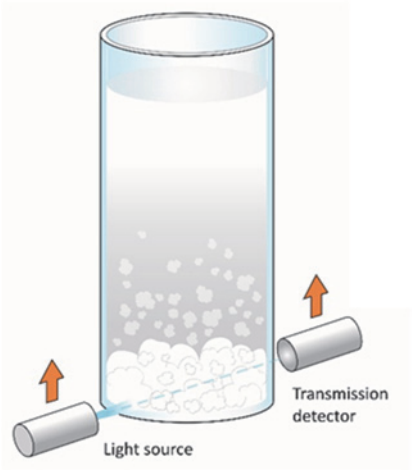

Figure 10 Schematic presentation of turbidity measurement.

3.3.6 Physical performance

3.3.6.1 Tensile testing of 1D fibre yarns

The mechanical properties of fibre yarns in **Paper I** were tested using C-Impact fast strain rate tensile tester (assembled at VTT). The span length of the sample was 50 mm and the strain rate was 1 mm/s (2 %/s). The accuracy of displacement and force measurements was better than 6 µm and 15 mN, respectively.

Dry samples were stored at 23 °C in 50 % relative humidity for at least 24 h prior to tensile testing. In order to measure wet strength, fibre yarns were immersed in water for 24 h. Tenacity (cN/tex) values were calculated by dividing ultimate breaking force of the fibre yarns by the linear density (tex). The weight of the samples was measured at 50 % RH and 23 °C.

3.3.6.2 The oxygen transmission rate of 2D films

The oxygen transmission rate (OTR) through CNF films in **Paper III** was determined according to the standard ASTM F1927 using an Ox-Tran 2/20 oxygen transmission rate tester (Mocon, Modern Controls Inc., USA). The tests were carried out by varying relative humidity between 0 % RH and 90 % RH using 100 % oxygen as test gas at 23 ºC.

3.3.6.3 Adhesion of 3D printed structures through peeling and washability

The adhesion of printed structures to cellulose fabrics was investigated by utilizing a Lloyd universal material tester LS5 (Lloyd Instruments Ltd., UK) with a 100 N load cell. The system measures the tensile force as a function of material extension that correlates with the load needed to peel the printed structure from fabric (Figure 11). The preload of the experiment was 0.5 N (preload speed 1 mm/min) and the separation speed was kept at a constant 5 mm/min. All measurements were carried out in standard conditions at 23 °C with 65 % humidity and samples were stored for 24 hours in standard conditions prior to mechanical testing and three measurements were taken of each sample points.

Printed structures for the peeling resistance measurements were prepared by printing half of the structure on fabric and the other half of the structure on a plastic tape in order to prevent the adhesion to the fabric and enable the peeling test. Two successive layers were printed. During testing, the other end of the structure was mounted between upper jaws of the material tester and the fabric between the lower jaws. The dimensions of the test strips were 10 mm × 40 mm and the adhered print on the fabric was 20 mm long.

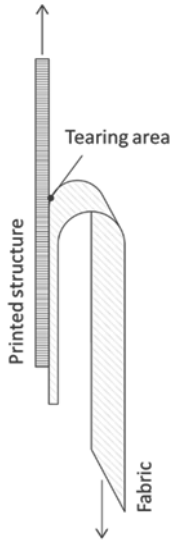

Figure 11 Schematic image of peeling test: printed structure and fabric are attached between clamps and pulled apart at an angle of 180°

The washability test was applied to investigate the durability of the printed structures on cellulose fabrics. The test was carried out using standard SFS-EN ISO 6330 (Domestic washing and drying procedures for textile testing) with standard washing powder (IEC-A Reference Detergent 60456 without phosphate) at 40 °C water temperature for 48 min. Two layer structures of dimensions 10 mm × 10 mm were

printed on fabrics. Five washing cycles were conducted and after each wash cycle, the printed structures were dried on a flat surface in air and examined visually with both the naked eye and a microscope.

3.3.6.4 Capillary viscometry

A capillary viscometer was used to determine viscosity average molecular weights of the untreated pulp sample and pulp sample after ChCl/urea in **Paper I** according to ISO 5351 (2004). Prior to measurement, samples were washed and filtered using distilled water and dried in a vacuum at 40 °C.

3.3.6.5 Dynamic gravimetric water vapour sorption

A dynamic gravimetric water vapour sorption instrument (DVS, Surface Measurement Systems, UK) was used for the freeze-dried CNF powders in **Paper III** to determine water vapour sorption isotherms with different xylan content at 20 °C. The samples were measured in different RHs and the change in mass measured and the results were plotted as a curve.

3.3.7 Manufacturing methods for cellulosic materials

3.3.7.1 1D: Fibre yarn spinning

Preparation of dopes for fibre yarn extrusion was done by dispersing pulp in ChCl/urea overnight at 100 °C with stirring. Subsequently, the dispersions were cooled down to room temperature and mixed in a SpeedMixer (FlackTek Inc., UK) in a vacuum at 800 rpm for 2 min and then at 1500 rpm for 8 min. Variable amounts of PAA (0 %, 5 %, 10 %, and 25 %) were added to the suspensions (4.5 wt%) and mixed with the SpeedMixer. Dry-wet fibre spinning was conducted via extrusion into ethanol with a small air gap (Figure 12). The system used was a laboratory-scale device that was assembled at VTT. During extrusion a constant speed (~1.4 ml/min) and a 5 ml syringe with a tapered tip with a nozzle diameter of 0.63 mm were used. DES was removed from the fibre yarns by soaking them in ethanol for at least 10 min and the fibre yarns were dried in ambient conditions. In order to improve strength properties, the fibre yarns were dipped in MilliQ water for 5 s and placed in an oven at 140 °C for 30 min.

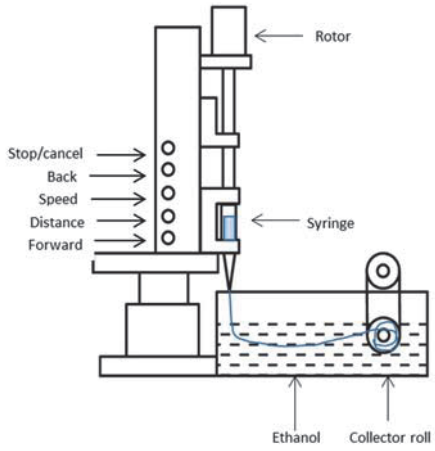

Figure 12 Schematic representation of the fibre yarn spinning system

3.3.7.2 2D: Film formation by solvent casting

2D films were prepared using solvent casting in **Paper III**. Due to the exceptional film forming ability of CNF, the preparation of 2D CNF films with variable xylan contents in **Paper III** was done using the solvent casting method and 0.4 wt% CNF dispersions. The dispersion was poured on a plastic petri dish and allowed to dry at room temperature for several days. As a result, films of ~30 µm thickness were obtained (Figure 13).

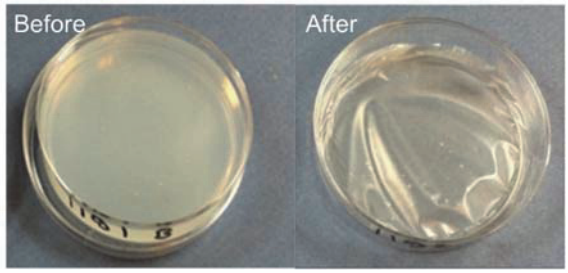

Figure 13 Solvent casting of CNF film before (left) and after (right) drying

3.3.7.3 3D printing and prototyping

In **Paper IV**, the modification of fabric surfaces was conducted using a commercial direct-write 3D printer (3Dn-300, nScrypt Inc., USA). The 3D printer system used was based on an extrusion technique for paste-like materials with suitable viscosity range between 1-1,000,000 cps. The system utilizes a simple syringe pump system with disposable 2.5 ml syringes and tapered tips. The nozzle size of the tip used

was 0.84 mm (Nordson EFD, USA). The printing speed used for materials was 5 mm/s and printing pressure for CA was 41.5 psi and for APC 20.5 psi due to its lower viscosity. Fabrics were attached on plastic films using adhesive tape during printing and drying.

4. Results and discussion

The main results of this thesis are summarized in the following section, which has been divided into three parts depending on the dimensional level of the application made using cellulosic materials as building blocks (see Figure 1). In the first part, pulp fibres were used as building blocks for a novel fibre yarn application. The development, the properties and the interactions between the chosen solvent are discussed (**Paper I-II**). In the second part, the crucial aspects of stability induced by cellulose nanofibrils in the making of cellulose film were examined (**Paper III**). In the third part, polymeric cellulose was used as a building block for 3D printing. In this part, a novel concept of modifying and functionalizing cellulose-based textiles is presented (**Paper IV**). More detailed results and analysis are provided in the attached **Papers I-IV**.

4.1 Pulp as a building block for 1D cellulose fibre yarn

Due to the challenge presented by the short fibre lengths that prevents traditional yarn spinning, a new type of cellulose fibre yarn manufacturing process was developed. The process does not use harsh chemicals and the end result would withstand water. This new 1D cellulosic material could be suitable in textile applications, bio-composites, and in decorative items.

4.1.1 Utilizing DES in fibre yarn manufacturing

The utilization of deep eutectic solvent (DES) composed of choline chloride and urea for fibre yarn formation was investigated in **Paper I**. Furthermore, the effect of DES on cellulose was studied in detail in **Paper II** in order to determine the influence of DES on pulp fibre chemical composition and morphology, and consequently, to improve the process and the end product.

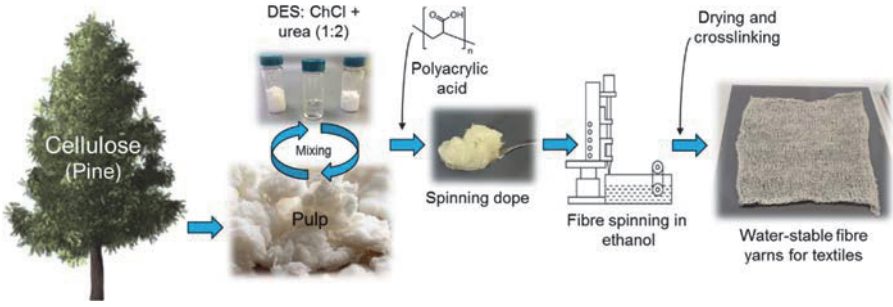

Figure 14 Schematic image of the pulp fibre yarn manufacturing process

DES is a mixture of two or more components that combined have a decreased melting point. The first publications related to this subject were by Abbott et al. (2003), by mixing choline chloride and urea with heating and stirring. In this mixture choline chloride acts as hydrogen bond acceptor and urea as hydrogen bond donor. ChCl (also known as 2-hydroxyethyltrimethyl ammonium chloride or vitamin B4) is a cheap and biodegradable salt that is, in general, considered as “green” (Nockemann et al. 2007; Radošević et al. 2015). Although, its benignity or low toxicity is still the subject of debate (Nockemann et al. 2007; Radošević et al. 2015; Wen et al. 2015), it has been approved to be used as a feed additive in all animal species by the European Food Safety Authority (EFSA FEEDAP Panel 2011). DES composed of choline chloride and urea (also known as reline) is readily biodegradable and a non-toxic material (less toxic that ChCl itself to some organisms) (Wen et al. 2015). It has similar physicochemical properties to ionic liquids, but negligible ability to dissolve cellulose. It has been utilized in several cellulose applications, for example to induce nanofibrillation or introduce functional groups; however, the interaction mechanisms have been unknown (Abbott et al. 2006; Sirviö et al. 2015; Willberg-Keyriläinen et al. 2017).

Due to the versatility and distinct properties of DES, composed of choline chloride and urea, it was also tested for yarn production directly from pulp. As a result, it was discovered that this particular DES was suitable for the process due to its ability to disperse pulp fibres, form a spinnable gel and be removed using ethanol without breaking the fibre yarn structure. Prior to DES treatment pulp fibres were solvent exchanged to acetone to prevent hornification. A schematic image of the process is presented in Figure 14. Improved water stability and overall strength was achieved by heat initiated esterification by crosslinking fibres with PAA during drying at 140 °C (Spoljaric et al. 2013). In order to determine the optimal pulp-PAA ratio, four samples with different ratios were made (Pulp-PAA 100 %:0 %, 95 %:5 %, 90 %:10 % and 75 %:25 %). The amount of DES in the mixture remained constant at 96 wt%. The amount of PAA did not have an effect on the linear densities of the fibre yarns, which measured between 21 and 24 tex.

4.1.2 From native cellulose I to 1D fibre yarn

The morphology and mechanical properties of the 1D pulp fibre yarns were studied in **Paper I** by measuring the tenacity and analysing the SEM images. The SEM images (Figure 15) were taken to observe the fibre orientation in dry yarns. Parallel fibre orientation has a positive effect on the strength properties. According to the SEM images, most of the pulp fibres were well aligned along the fibre yarn axis, however, due to removal of DES prior to drying the fibre yarns were observed to be relatively porous.

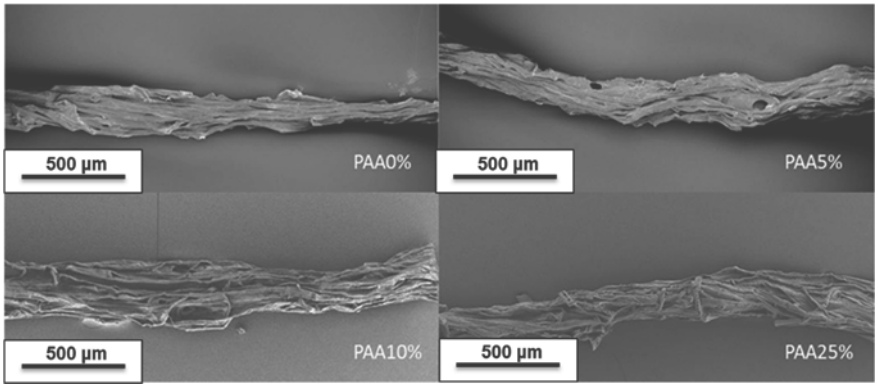

Figure 15 SEM images of pulp fibre yarns

Tenacity and the effect of PAA on the mechanical properties of fibre yarns were analysed using a mechanical tensile tester. Water stability could only be measured in fibre yarns with PAA, due to disintegration of the yarns without it during wetting. In pure pulp fibre yarns, the hydrogen bonds play the main role in keeping the fibres together and water is able to break those bonds between the fibres (Fernandes Diniz et al. 2004).

It was observed (Figure 16) that the maximum tenacity was reached when the Pulp-PAA ratio was 90 % of pulp and 10 % of PAA. The best wet reinforcement was also attained in fibre yarns when the amount of PAA was 10 % or more, however, in dry yarns the tenacity decreased when PAA content was over 10 %. The same effect was seen in fracture strain results, which could be an indication of PAA hindering the bonding. The wet strength values of the pulp fibre yarns with PAA were roughly 1/3 of the dry strength values, which indicates that, in addition to crosslinking by PAA, hydrogen bonding between fibres also played an important role in dry state. The maximum value attained with 10 % of PAA was around 9 cN/tex. As a reference, the tenacities of cotton and viscose measured were 16.2 cN/tex and 15 cN/tex, respectively.

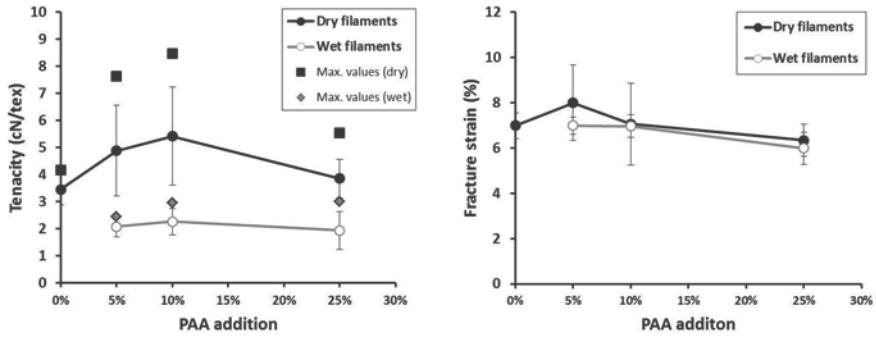

Figure 16 Average and measured maximum tenacity values (left) and fracture strain (right) in variable PAA concentrations.

Porosity and defects affected the mechanical strength values of the fibre yarns negatively, which can be observed from the long error bars. Porosity decreases the fibre-fibre contact area, which is crucial for strength (Lindström et al. 2005). Simple twisting, plying, cabling (Häyrinen 1973) or improving the interfibre bonding by using more fibrillated fibres could improve the mechanical properties.

4.1.3 Effect of DES treatment on the morphology of pulp

In order to study the effects of DES on pulp, the morphological, structural and chemical changes were studied using complementary spectroscopic and microscopic tools. The changes can occur in the fibre surface or in the bulk, therefore both analysis methods were used. Additionally, chemical composition was analysed before and after DES treatment. Even though DES composed of choline chloride and urea is considered a relatively mild treatment on fibres, even the smallest changes in surface chemistry or the presence of solvent residuals could be important for the material properties or the future utilization of the process.

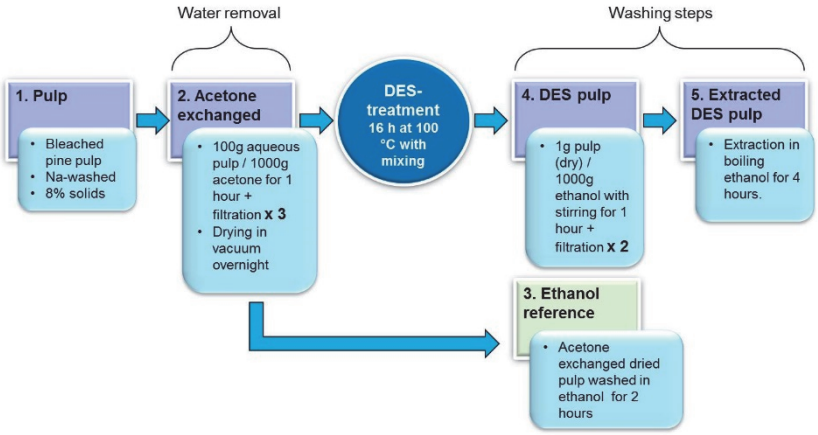

Figure 17 Schematic image of the process and the samples in order to study the changes of the DES treatment.

For the experiments the process for fibre yarn manufacturing was used, excluding the PAA addition, and five pulp samples were taken from different stages of the process. However, it was observed that the washing procedure used was not sufficient to remove DES and consequently an additional washing step was added. Moreover, a reference sample was added to demonstrate the effects of the process without the DES treatment. Samples were dried prior to analysis. A schematic image of the studied samples and the treatment process is presented in Figure 17.

Changes in pulp morphology were assessed visually using SEM imaging and AFM and by calculating the degree of polymerisation. In the SEM images (Figure 18), the morphological changes were looked for, however, in heterogeneous systems, such as natural fibres, visual assessment is often cumbersome. Hence, it is difficult to make reliable conclusions. Through careful inspection, a minor increase in fibrillation during the processing could be observed. However, it should be noted that the drying of the fibres also plays a role, which can cause increased fibrillation and cracking (Suchy et al. 2009).

AFM was used for a more detailed surface examination in order to compare the surface morphology of DES treated samples to cellulose samples after mercerization to determine if DES has any dissolution ability on the fibre. Merceration using NaOH causes the formation of an irregular layer on the fibre surface and removes fibrillary structures (Eronen et al. 2009). However, no change in the morphology of the fibres was found after DES treatments (**Paper III)**. Therefore, it cannot be said that DES treatment would induce physical changes in fibre surfaces. Similar findings have been reported by Sirviö et al. (2015).

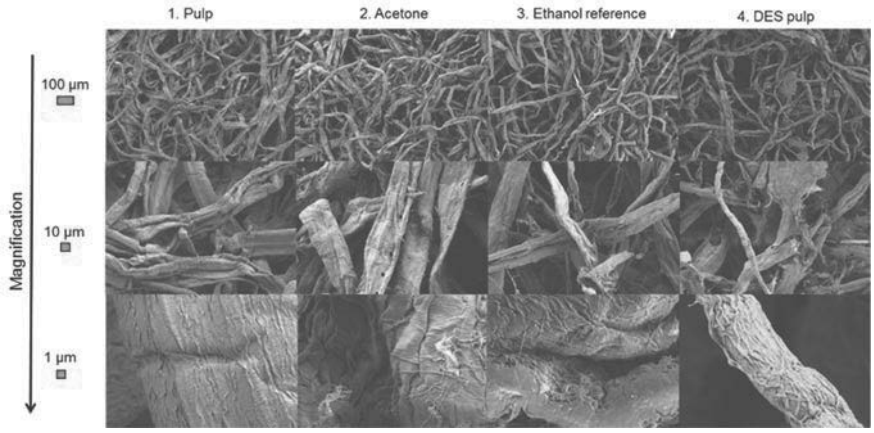

Figure 18 SEM micrographs with magnifications of ×100, ×500 and ×5000 for bleached pine pulp samples when exposed to different treatment stages.

4.1.4 Effect of DES treatment on the chemical composition of pulp

The chemical composition of the pulp samples was analysed in order to determine the dissolution of any component of the fibre or external chemicals.

Even though the cellulose structure remained intact, dissolution of hemicelluloses might have occurred. Therefore, the hemicelluloses were studied by analysing the monosaccharide contents (Table 2). In the case of dissolution by DES, the analysis would show a significant change in monosaccharides, however, the changes observed here were negligible or very small and fall below the measuring accuracy of the method, which varies within 6-8 %. Furthermore, if a considerable amount of hemicelluloses had dissolved, this should also have been seen as decrease in the degree of polymerisation (DP), approximated from the intrinsic viscosity measurement (da Silva Perez and van Heiningen 2002, ISO 5351 2004). However, only a minor decrease was detected from 1226 (± 0.5 %) to 1194 (± 0.8 %), which could have been induced by stirring.

The hypothesis of hemicellulose dissolution was based on the observations of Sirviö et al. (2015) who utilized DES as a pre-treatment for nanofibrillation. Since nanofibrillation was reported to improve due to DES treatment (Sirviö et al. 2015; Suopajärvi et al. 2017), significant dissolution of hemicelluloses is not probable as that would hinder the fibrillation process (Hauru et al. 2013; Iwamoto et al. 2008). But since minor changes were observed regarding xylose, mannose and arabinose, dissolution of those monosaccharides cannot be completely excluded.

Table 2 Neutral sugars of pulp samples

	Monosaccharides (mg/100 mg)					
	Rhamnose	Arabinose	Galactose	Glucose	Xylose	Mannose
1. Pulp	<0.1 ± 0.00	0.63 ± 0.03	0.22 ± 0.01	85.07 ± 0.73	7.5 ± 0.12	6.23 ± 0.15
2. Acetone	<0.1 ± 0.00	0.63 ± 0.02	0.22 ± 0.01	83.68 ± 0.41	7.4 ± 0.13	6.21 ± 0.12
3. Ethanol reference	<0.1 ± 0.00	0.63 ± 0.02	0.22 ± 0.01	85.28 ± 0.91	7.47 ± 0.07	6.28 ± 0.09
4. DES pulp	<0.1 ± 0.00	0.54 ± 0.04	0.20 ± 0.01	83.19 ± 0.11	6.96 ± 0.12	5.86 ± 0.13

Since cellulose and hemicelluloses are composed of only carbon, hydrogen and oxygen. All other elements found in the pulp fibre samples are from external sources. Therefore, elemental analysis is a good method of determining if any chemical reactions with external materials have occurred by analysing the changes in chemical composition.

In the studied pulp samples, small amounts of nitrogen (N) could be detected in the DES treated samples. Nitrogen content varied, depending on the batch, from 0.46 % to 1.59 %, indicating residuals due to an inadequate washing step instead of a chemical reaction. Therefore, an additional washing procedure was introduced (extraction for 4 hours in boiling ethanol) to study how strongly nitrogen was attached to cellulose. As a result, a significant decrease in the nitrogen content was observed (to 0.16 %), but it could not be removed completely.

Since both choline chloride and urea contain nitrogen the samples were further examined with spectroscopic tools in order to determine the origin of the nitrogen.

4.1.5 Changes in structural characteristics of pulp by spectroscopy

Spectroscopic tools can be used as complementary methods to study both the surface of the material as well as the bulk. XPS can detect chemical composition on the surface whereas NMR and Raman can be used to study the bulk of the material.

Two pulp samples were used to study the changes in the fibre surfaces due to DES treatment: 1. Pulp, as a reference without any treatment, and 4. DES Pulp. Moreover, a sample of pure cellulose (XPS reference sample) (Johansson and Campbell 2004), was used as a reference. XPS spectra of the samples with high resolution carbon and zoom-up at 460-300 eV are presented in Figure 19. Both of the samples were found to be very similar to the reference sample with the typical cellulose C 1s signature consisting of carbons with one or two bonds to oxygen at 286.7 eV and 288.1 eV (Beamson and Briggs 1993). That indicates that the samples were not contaminated or that the DES treatment did not chemically alter cellulose. However, a barely detectable peak for nitrogen N 1s can be observed at 400 eV. In order to determine its origin, further examination was conducted for the region of a

possible chloride peak (Cl 2p at 199 eV). Even though the signal was below quantification limit, small traces could be observed from 4. DES pulp sample, which indicated that the traces originated from choline chloride.

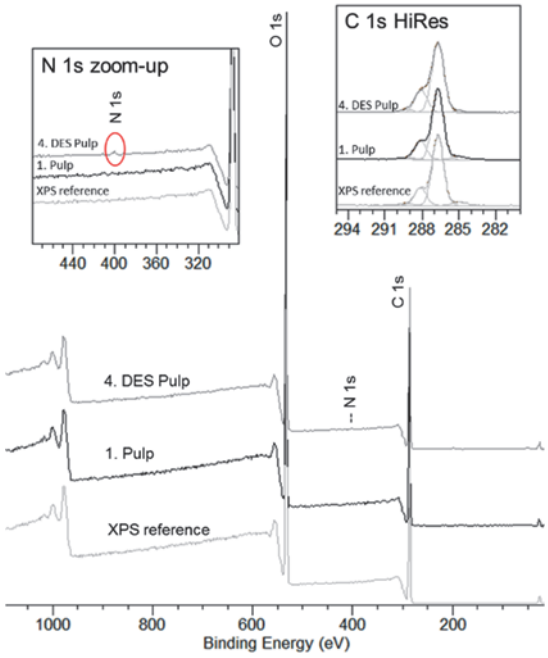

Figure 19 Typical low resolution wide spectra of in situ XPS reference for cellulose, 1. Pulp sample and 4. DES pulp samples showing signals due to emission of O 1s, N 1s and C 1s. Insets present the magnification of N 1s region and the C 1s HiRes regions.

In order to confirm the origin of the nitrogen, spectra of both materials, urea and choline chloride, were measured using liquid state NMR. The signal for urea was located at 161.1 ppm and resonances for ChCl were determined in signals corresponding to $HO\text{-}CH_2\text{-}CH_2\text{-}N$- (67.2 ppm), $HO\text{-}CH_2$- (55.2 ppm), and $\text{-}CH_2\text{-}N\text{-}(CH_3)_3$ (53.5 ppm) moieties, which were comparable to previously published values (Ardenkjaer-Larsen et al. 2003; Lobo et al. 2012).

Solid state NMR was used to determine the chemical composition of pulp samples (Figure 20). Sample 1. Pulp was used as a reference and sample 4. DES pulp as the treated sample. Two additional signals were identified in the latter spectra, which were comparable to the choline chloride moieties. Additional signals in the urea region were not detected, which confirmed the origin as choline chloride. Raman spectroscopy was employed to further analyse the bonding mechanism to cellulose.

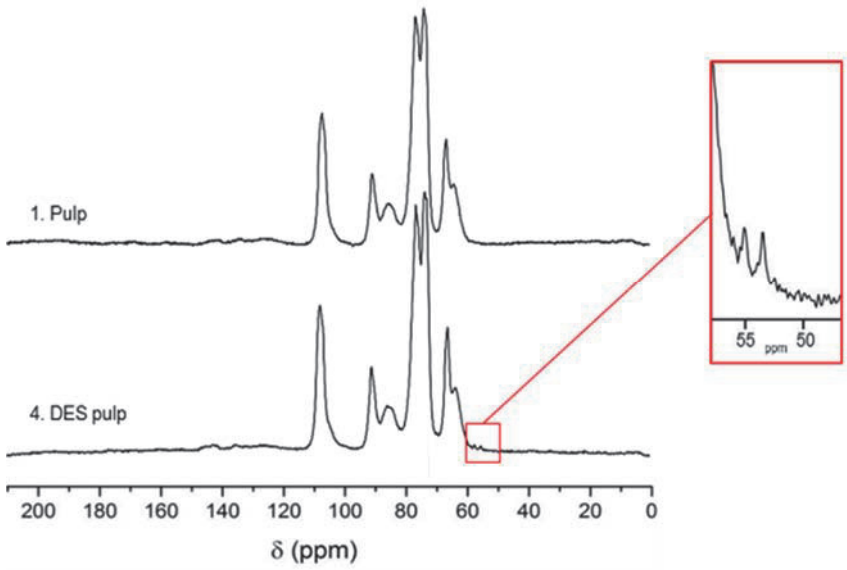

Figure 20 Typical solid state NMR spectra of 1. Pulp (reference) and 4. DES pulp (after mild washing) samples.

In addition to spectra of choline chloride and urea (Figure 21), all the pulp samples were used to study the changes in pulp samples using Raman spectroscopy. Raman bands emanating from the vibrational modes of atoms in cellulose chains are sensitive to the orientation of the fibres with respect to the polarisation configuration of the laser light (Lewandowska et al. 2015; Wiley and Atalla 1987). Here, the Raman spectra illustrate the changes in the intensity of the Raman bands as a function of the orientation of the fibres (parallel and perpendicular) to the polarisation configuration of the laser light. Samples without DES treatment are presented in Figure 22 where typical Raman spectra of cellulose could be observed (Wiley and Atalla 1987).

There were no differences between these samples, which supports the previous finding that no structural changes occurred during solvent exchange or the washing steps. Four bands for choline chloride were located. The strongest was at ~719 cm^{-1}, which was assigned to the "totally" symmetric stretching vibration of four C-N bonds (υ_1) and less strong bands at ~865 cm^{-1}, ~954 cm^{-1} (medium) and at ~768 cm^{-1} (weak) (Akutsu 1981).

The strongest urea band was located at ~1010 cm^{-1} (assigned to the symmetric stretching vibration of the C-N bonds) (Keuleers et al. 1999). In 4. DES pulp sample an additional band can be observed at ~715 cm^{-1}, which matches the strongest choline band. This also suggests that there is no chemical reaction between the -OH groups of cellulose and DES components.

Furthermore, a higher intensity is shown when the fibre is oriented perpendicularly, which suggests that the positively charged choline groups are electrostatically interacting with the anionic groups of cellulose and their $^{+}$N-C-C-O backbones 'poke out' from the cellulose chain perpendicularly. The effect of the residuals on the charge was examined using methylene blue adsorption and UV-VIS spectroscopy.

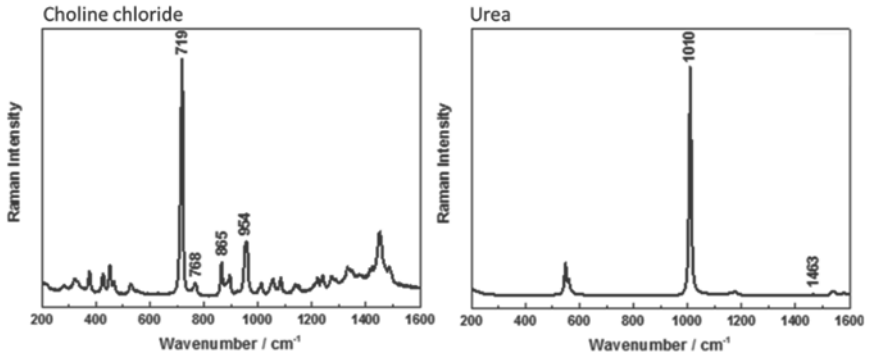

Figure 21 Typical Raman spectra of choline chloride and urea

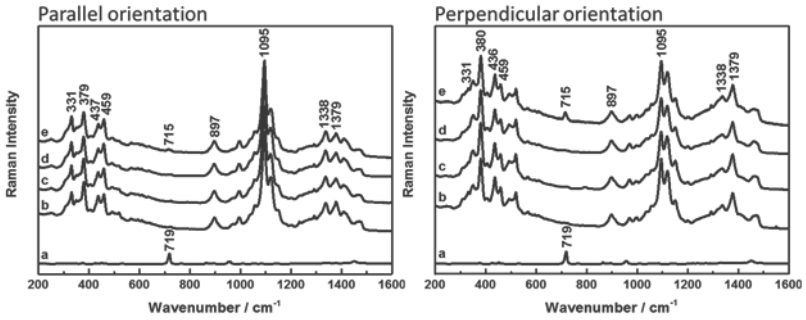

Figure 22 Typical Raman spectra of a) ChCl and samples b) 1. Pulp, c) 2. Acetone, d) 3. Ethanol reference and e) 4. DES pulp measured in parallel and perpendicular orientation of the fibres to the polarisation configuration of the laser light.

According to the methylene blue adsorption experiment and UV-VIS spectroscopy the positively charged choline groups decreased the charge, as significantly more methylene blue was adsorbed into the reference pulp (3.) compared to DES treated pulp (4.). Extensive washing is required to remove the residuals, which also partially restores the charge (Figure 23). In theory, complete removal of solvent residues should restore the original charge, however, this was not observed. Low charge of pulp fibres has been observed to have a negative effect on the interfibre bonding

and therefore also decrease the mechanical strength of the fibre yarns (Rohm et al. 2014; Zhao et al. 2016). By increasing the charge, attractive Coulomb interaction between the fibre surfaces could enhance the strength of the bond. Therefore a complete removal of DES would be preferred in order to utilize the material in textiles and composites.

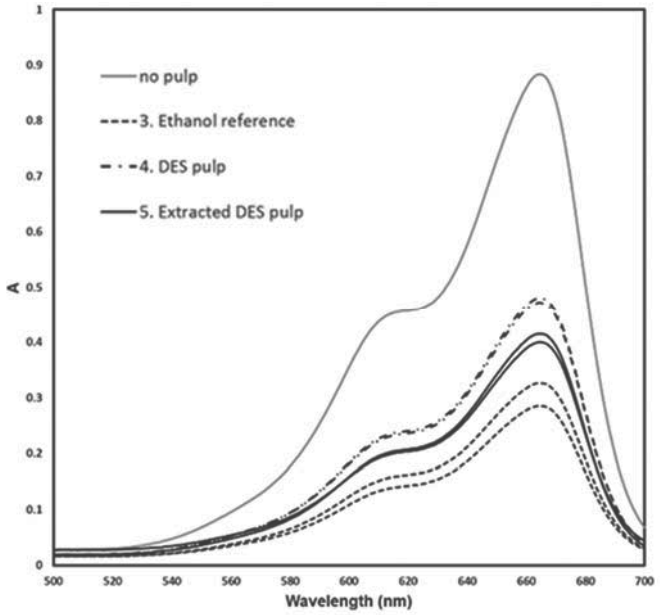

Figure 23 Typical absorption spectra for methylene blue solution supernatant solution after fibre adsorption to 3. Ethanol reference pulp, 4. DES pulp and 5. Extracted DES pulp samples. (Two parallel measurements)

4.1.6 Recyclability of DES in the process

Recyclability of the process chemicals in DES fibre yarn production would not only decrease the environmental impact of the process, but make the process economically more attractive. The recycling possibility of DES was also examined in **Paper I** by evaporating the ethanol used for removal of DES after spinning and comparing what was recovered with fresh DES using FTIR (Figure 24). No changes in the spectra were observed, which indicates that the recovered DES was chemically identical to the freshly prepared DES. These observations support the previous studies of successful recycling of DES composed ChCl and urea (Azizi and Gholibeglo 2012; Lobo et al. 2012; Singh et al. 2011).

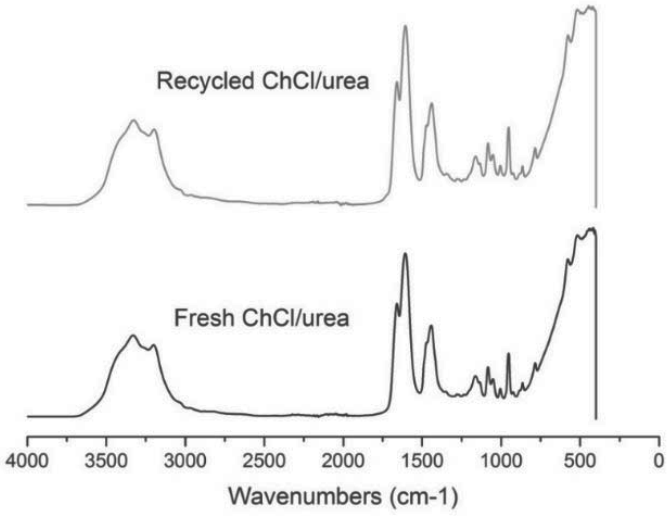

Figure 24 FTIR spectra of recovered and fresh DES

4.2 2D films from CNF

4.2.1 Effects of decreasing xylan content on the pulp

Paper III discussed the effect of xylan on the behaviour of nanofibrillated birch kraft pulp cellulose and investigated the influence of CNF xylan content on fibril morphology, charge and stability as well as on film formation ability. A schematic image of the study is presented in Figure 25.

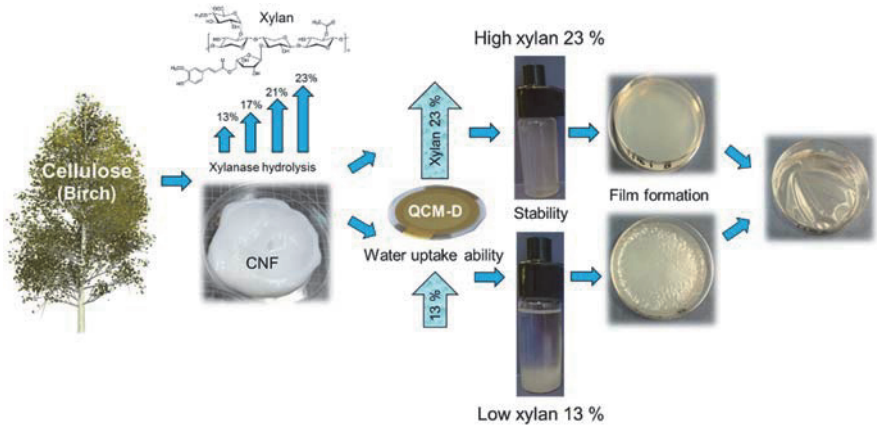

Figure 25 Schematic representation of the study linking 2D film properties to the molecular level stability and water interactions

For the study, four bleached birch pulp samples were modified by enzymatic hydrolysis using purified Trichoderma reesei xylanase II. This method has been previously presented by Rauvanto et al. (2006). The pulps and their carbohydrate compositions, with four levels of glucuronoxylan as monosaccharides and acidic oligomers, are presented in Table 3. Additionally, the anionic charge of the samples was determined using conductometric titration according to the standard SCAN CM 65:02 (Table 3). The charge decreased correspondingly as a function of the xylan content, which supports the previous research regarding the effect of charged hemicellulose on fibril surfaces affecting the charge of CNF (Fall et al. 2011)

Table 3 Carbohydrate composition and charge of the pulps used for production of nanocellulose samples

Pulp sample	**Neutral sugars and acidic oligomers, mg/100 mg**				**Anionic charge, mmol/kg**
	Glucose	Xylose	Methyl glucuronic acid	HexA oligomers	
High xylan	73.0	23.0	0.154	0.086	39
Medium xylan 1	79.1	21.0	0.126	0.064	19
Medium xylan 2	80.7	16.8	0.092	0.041	15
Low xylan	88.5	13.3	0.078	0.020	13

The pH and conductivity of the suspension remained constant, which means all the investigated changes in the stability, film formation ability and water adsorption properties are related to changes in xylan content. The prepared pulps were then

further fibrillated until the comparable fibril dimensions were achieved. As a result four gel like CNF samples were attained with solid contents of ~1.8 %. These CNFs were then diluted into dispersions in order to study the effect of xylan in dispersion stability.

4.2.2 Stability of dispersion

Since films are made using a solvent casting method, to understand the stability and the properties of the films the dispersion stability requires assessment. For this, the high xylan content sample (23 wt% of xylan) and low xylan content sample (13.3 wt% of xylan) were diluted into 0.05 wt% in order to clarify the interactions within the individual nanofibres and the effect on the stability without the contribution of the CNF network.

The measurements were done using Turbiscan and the results are presented in Figure 26. In order to analyse the Turbiscan measurements, the higher and less noisy the transmission curve is the more stable is the CNF dispersion. Variations along the curve indicate disturbance in stability, in this case, either agglomeration or sedimentation. Measurements were done from bottom to top. In Figure 26 clear differences in stabilities can be observed after 20 minutes of measurement. Dilute dispersion with high xylan content CNF is highly stable, whereas, in the sample with low xylan content the dispersions have flocculated and larger agglomerates are settling.

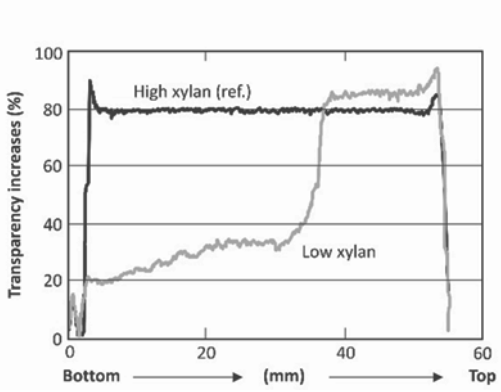

Figure 26 Transmission profiles of dilute dispersions of high and low xylan CNF samples. Measuring is conducted from bottom to top *t*= 20 min.

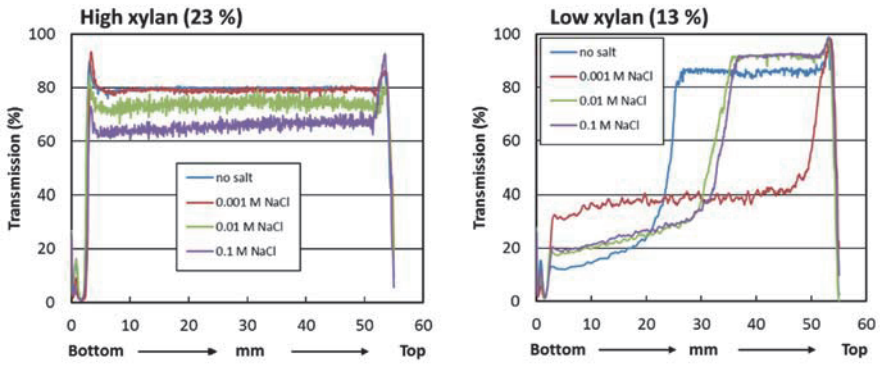

Figure 27 Transmission profiles of high xylan content CNF and low xylan content CNF. t = 2h

To further study the mechanisms contributing to stability, variable electrolyte (NaCl) concentrations (0 M, 0.001 M, 0.01 M and 0.1 M) were added to the dispersions. Results after 2 hours are shown in Figure 27, where despite increasing ionic strength disturbing the system, dispersion with high xylan content remains stable. A minor increase in noise and decrease in general transmission level can be observed, but salt addition did not lead to sedimentation. However, with low xylan content the system is unstable even without the salt addition.

The results indicate that even though the electric double layer forces are somewhat disturbed by increasing electrolyte concentration with high xylan content samples, the steric forces dominate due to the xylan located in fibril surfaces. Mobile polymeric chains, such as xylan on fibril surfaces, can stabilize the system through electrosteric interactions (Nigmatullin et al. 2004). Moreover, the effect of electrolyte concentration on xylan behaviour has previously been shown to be rather weak (Tammelin et al. 2009), even though it was been observed to affect the xylan conformation by contracting in high ionic strength (Österberg et al. 2001). This could be expected to affect the steric repulsion by lowering it, however, due to the relatively high amount of xylan on the fibril surfaces (although in compact conformation), dominating steric forces are introduced to the system preventing agglomeration and sedimentation. A similar tendency was later reported by Tanaka et al. (2016)

In the low xylan sample, the charge of CNF with low xylan content is lower and therefore the electrostatic repulsion is also weaker and the system agglomerates. A clear interface between supernatant and the agglomerating suspension was observed during agglomeration and the rate of settling decreased over time. It is known that CNF forms an entangled and gel-like network already in low concentrations (Pääkko et al. 2007), when this concentration is achieved the settling of unstable dispersion is hindered. This hindered settling (Holdich 2002) can be observed in Figure 28 after ~40 minutes. Since the removal of xylan had such a severe effect on dispersion stability, its effect on film formation and interaction with water was further studied using both nanoscaled model and macroscale films.

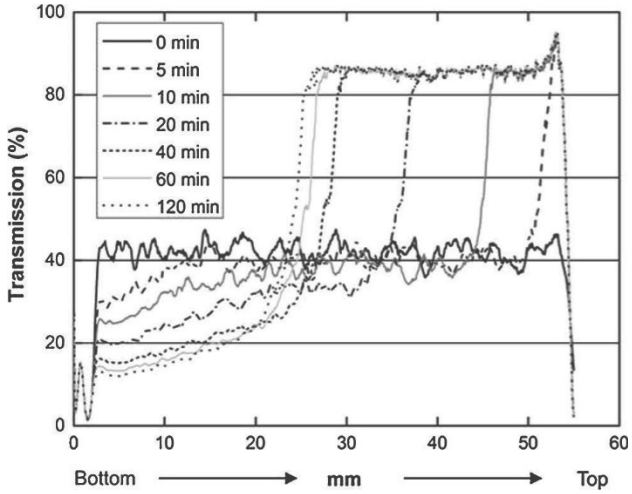

Figure 28 Transmission profiles of low xylan content CNF during two hour measurement

4.2.2.1 Nanoscale CNF films

Films in two different scales (nanoscale and macroscale) were studied to gain better understanding of the factors affecting the film formation and its properties. Due to the high amount of hygroscopic hydroxyl groups of CNF as well as the carboxylic groups of xylan on the fibril surfaces the change in xylan content would presumably influence the water interactions of the CNF (Fall et al. 2011). Therefore water interactions were studied using surface sensitive QCM-D (nanoscale) and with dynamic vapour sorption (macroscale).

Thin films of nanocellulose with variable xylan content were deposited on silicon coated quartz crystal using spin coating. Several layers were spun in order to achieve areal mass of 11-15 mg/m^2. It was observed that films with low xylan content required more layers, which could indicate lower dispersion stability.

The films were analysed using QCM-D equipped with a humidity module, which gives essential information on the material behaviour in the presence of water at molecular level and on the surface. The changes in frequency and dissipation were monitored while the humidity was increased in the chamber.

In Figure 29, the samples with the highest (~23 wt%) and lowest (~13 wt%) xylan contents were compared and the changes in frequency and dissipation were monitored while gradually increasing the relative humidity from RH 11 % to RH 97 %. At first both thin film samples had a very similar response to the humidity change, however minor differences in dissipation took place when the humidity level reaches RH 97 %. Changes in dissipation indicate altered layer properties, which in this case could originate from swelling of the fibres. However, since the films are rather thin

(areal mass ~ 15 mg/m^2), the attained response for changes in moisture content is due to the behaviour of individual fibrils instead of a response of evenly distributed fibrillar network. In thicker layers (~170 mg/m^2) the dissipation change has been shown to be higher (up to 4.5×10^{-6}) caused by softening of the layer (Tammelin and Vartiainen 2014). Since both CNF layers with different xylan contents showed a similar response to the changes in RH, swelling of xylan was not observed (Uetani and Yano 2012).

An additional observation made for the water vapour uptake measurement for thin films was that a full stabilization of the sample in QCM-D chamber requires an overnight in relative humidity of 11 % prior to the measurement, despite storing in a desiccator. After approximately 13 hours in RH 11 %, the frequency curves levelled off and reached equilibrium.

Water vapour uptake is summarized in Figure 30, where bound water by milligrams of CNF was calculated using the Sauerbrey equation from data collected from the 3rd overtone. A thin film with high xylan content appears to be able to uptake more water molecules compared to a thin film with low xylan content. However the differences are relatively minor and could be considered significant only when surface behaviour is dictating the material performance.

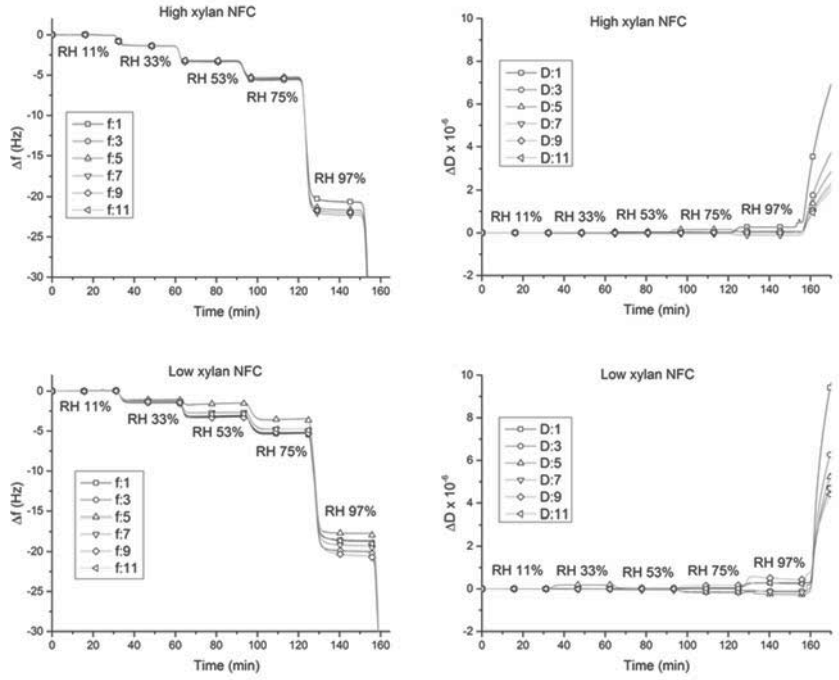

Figure 29 Water vapour uptake monitored using QCM-D equipped with the humidity module. Change in frequency (left) and dissipation (right) as a function of time for

high xylan CNF (areal mass of 11 mg/m^2) (top) and low xylan CNF (areal mass 14.5 mg/m^2) (bottom) at different levels of humidity. (f_0 = 5 MHz, n = 1, 3, 5, 7, 9, 11)

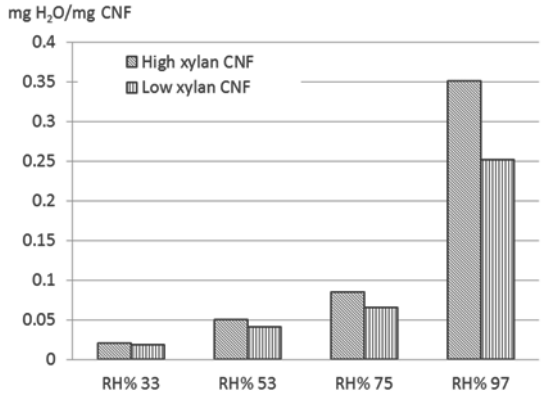

Figure 30 Water vapour uptake data in milligrams of water bound by milligrams of CNF using Sauerbrey equation (3rd overtone).

4.2.3 Macroscale effects in bulk on film properties and barrier performance due to changes in xylan content

In order to study the water vapour uptake behaviour and film properties in macroscale (bulk), dynamic vapour sorption (DVS) and oxygen transmission rate (OTR) were measured in increasing relative humidity.

During film formation (Figure 31), it was observed that the transparency and visual properties of the drying samples varied depending on the xylan content. Clear flocculation could be seen in a low xylan sample. However, the flocculation tendency did not cause clear differences between samples in DVS and OTR tests. The measured DVS curve (Figure 32a) represents the shape of typical hydrophilic material and no significant differences between samples with different xylan contents could be observed. Similar behaviour has also been seen in previous studies (Arola et al. 2013; Belbekhouche et al. 2011). The measured OTR values in Figure 32b show no trend of decreased oxygen barrier properties in measured relative humidity. In addition, the values are close to the trendline of previous measurements of unmodified birch kraft pulp measurements. Solvent cast CNF films are even and dense enough to maintain the oxygen transmission properties at all xylan content levels.

Therefore, from the study in **Paper III,** the conclusion can be made that the effect of xylan needs to be taken into account where molecular level stability is concerned since is acts as electrosteric stabilizer. In addition, xylan might have a small effect on the water uptake properties. However, these effects diminish in bulk. Xylan decreases the flocculation tendency and improves transparency, but the water adsorption and barrier properties of the CNF film remain intact despite the removal of xylan.

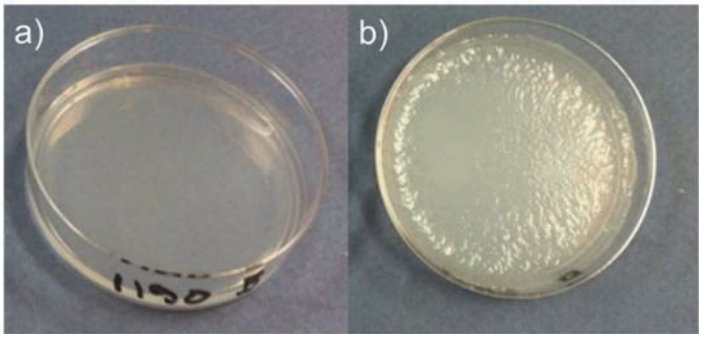

Figure 31 Film formation during drying with high xylan sample (~23 % xylan) and low xylan sample (~11 % xylan).

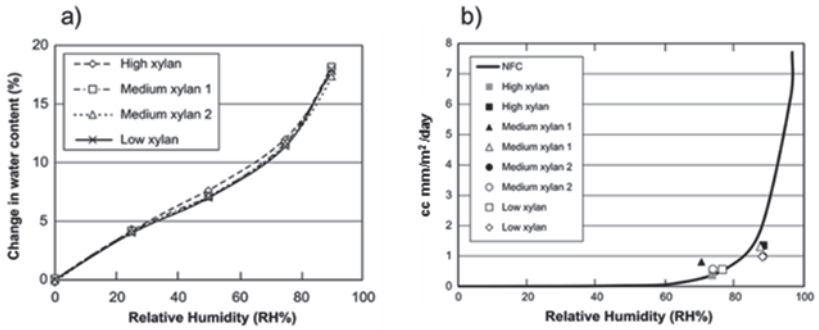

Figure 32 a) Dynamic vapour sorption and b) oxygen transmission rate as a function of relative humidity measured from the samples with variable xylan content. Trendline of oxygen barrier behaviour of unmodified birch kraft pulp CNF as a comparison.

4.3 Cellulose based polymers as building blocks for 3D printable structures

In **Paper IV**, the potential of utilizing 3D printable cellulosic materials for surface tailoring and functionalizing cellulosic fabrics was studied. Combining 3D printable cellulose based materials with cellulose fabrics also enables the development of all-cellulose garments. A schematic image of the process is presented in Figure 33.

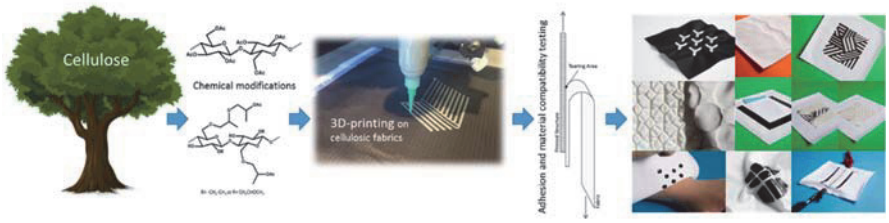

Figure 33 Schematic image of textile modification using cellulose derivatives and 3D printing.

To study the interaction and adhesion properties of two cellulose derivatives, cellulose acetate (CA) and acetoxypropyl cellulose (APC) on cellulose, the adsorption was studied first at molecular level using surface sensitive QCM-D and after printing on cellulosic fabrics, cotton and viscose, the adhesion was examined using peeling and washing tests. Both woven and knitted cotton textile fabrics were chosen in order to determine the effect of the structure of fabric on adhesion.

3D printing of the materials was conducted using a commercial direct-write 3D printer, CA dissolved in acetic acid (concentration 30 wt%) and APC dissolved in acetone (concentration 80 wt%). Even though both materials are soluble in acetone and acetic acid, different solvents were used due to their evaporation rates. The fast evaporation rate of acetone was too rapid for CA, which resulted in poor processability and clogging of the nozzle during extrusion, thus acetic acid was used. Compared to CA, APC was a less viscose material and solvent evaporated very slowly therefore acetone was used as a solvent. In general, high solids content and high viscosity were considered as desired qualities in direct-write printing on textiles, due to their lower shrinkage and good 3D formation. However, too high a viscosity leads to problems in extrusion and adhesion and therefore an optimization between printability, shrinkage, and adhesion properties is required for the desired result.

4.3.1 Adsorption by QCM-D

The interactions and adsorption of the materials on pure cellulose model films were studied in **Paper IV** using QCM-D. Adsorbed mass and adsorption rate were observed by monitoring changes in frequency and dissipation as a function of time while pumping dilute (0.5 mg ml^{-1}) CA and APC dispersions through a spin coated cellulose model film. The change in frequency and the change in dissipation as a function of time are presented in Figure 34a-b from which the compatibility and strength of interaction can be qualitatively studied.

The cellulose surface was first allowed to stabilize in acetone for approximately 10 minutes. Pure acetone was subsequently replaced by a dilute dispersion of either CA or APC in acetone and adsorption was monitored for 60 minutes, followed by washing step with pure acetone. Both cellulose derivatives induced a clear negative

change in frequency and a positive change in dissipation (in Figure 34a-b). However the change in CA was faster and more pronounced compared to that in APC. CA adsorbs on cellulose yielding a frequency and dissipation change of -39 Hz and 6.5 × 10^{-6}, respectively. A similar adsorption rate could be observed with water vapour on hygroscopic CNF films (Tammelin et al. 2015). Whereas with APC the change was -10 Hz and 3 × 10^{-6}. Moreover, equilibrium was not completely reached after 60 minutes with APC.

According to the results, both cellulose derivatives possess a positive attraction towards cellulose, though the affinity of APC was clearly lower due to the lower adsorption rate and amount. The rinsing step with pure acetone did not significantly affect the adsorbed layer of either of the derivatives, which indicates either removal of a negligible amount of material or reorganization of the adlayer conformation rather than remarkable desorption (Kargl et al. 2012). This denotes relatively strong attachment of both of the derivatives on the cellulose surface.

Acetone had not been used previously in literature as a solvent for adsorption experiments by QCM-D. However, the data was comparable to the adsorption data conducted in water when chitosan or carboxymethyl cellulose (CMC) were used as adsorbed polymers (Myllytie et al. 2009; Orelma et al. 2012), indicating that acetone works rather well as medium.

The viscoelastic properties of the adsorbed CA and APC layers can be compared by plotting the change in dissipation versus change in frequency. The steeper the curve, the more dissipative the layer is and the more energy is bound per unit (Tammelin et al. 2006). $\Delta D/\Delta f$ ratios are presented in Figure 34c, where both derivatives display a similar curve suggesting that they both possess similar viscoelastic properties and the structural changes do not have significant influence on the physical properties of a wet layer. To acquire more information about the adhesion properties at macroscopic scale, mechanical testing after printing was conducted via peeling and washability tests.

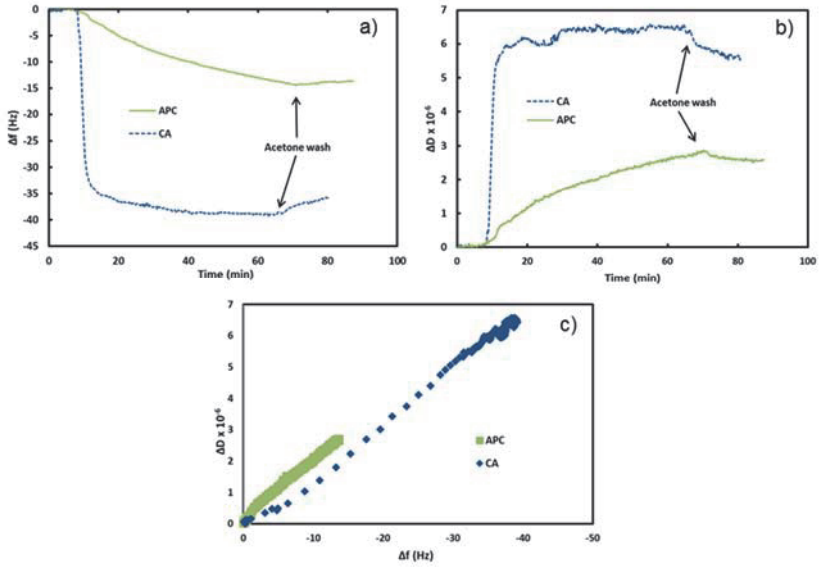

Figure 34 a) The change in the frequency and b) dissipation on the adsorption of dilute CA and APC dispersions on pure cellulose surfaces followed by rinsing with acetone. c) Change in dissipation factor as a function of the change in frequency for adsorption. f_0 = 5 MHz, n = 5

4.3.2 Adhesion by peeling and washability

In addition to the affinity and compatibility of the materials, firm adhesion on fabrics requires materials to penetrate and spread on the yarn surfaces (Gustafsson 2012; Melnikova et al. 2014; Pei et al. 2015). The strength of adhesion was tested in **Paper IV** using mechanical T-peel test and durability and washability using EN ISO 6330, which is a widely used standard to determine visible changes in the appearance of the textile after a number of washing cycles (Faulde et al. 2012; Ulbrich et al. 2014).

In peeling tests the force required to peel the printed structure was measured from a 10 mm wide strip along the attached part of 20 mm using a separation speed of 5 mm/min. The results were converted to N/100 mm width for qualitative comparison. The force-extension curves are presented in Figure 35. The first slope of the curve comprises the elongation of the fabric, which was much longer with a knitted structure. The curve for CA on viscose does not represent the peeling force but the strength of the viscose material since the fabric tore instead of peeling. The average peeling forces from 3 parallel measurements were calculated and are presented in Table 4.

The results for CA on woven and knitted cotton were in a similar range, however, the better values on knitted cotton could be due to the more complex fabric structure

in the z-direction enabling more surface area for improved adhesion. For APC average peeling forces are considerably lower compared to CA and no significant differences between materials were observed.

Sanatgar et al (2017) observed average peeling forces of 40-120 N/100 mm and 5-70 N/100 mm, respectively for FDM printed thermoplastic nylon and polylactic acid (PLA) on polyamide fabric. Due to the small differences in experiment setups, the qualitative comparison of the results indicated that the average values for CA could be considered excellent and for APC relatively poor. In addition, Pei et al. (2015) have studied FDM printable polymers (ABS and PLA) on fabrics where the best results regarding adhesion were attained when natural or natural blend fabrics were used.

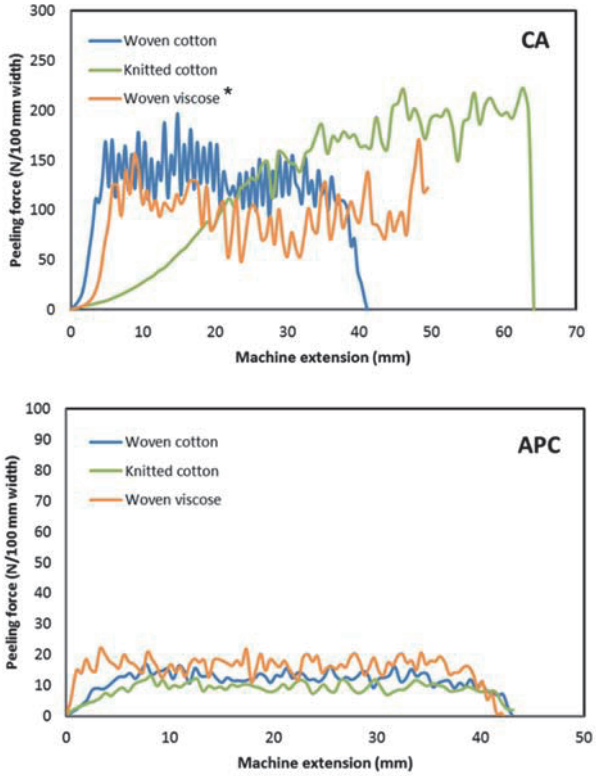

Figure 35 The peeling force as a function of machine extension for CA (upper) and the peeling force as a function of machine extension for APC (lower) *fabric tore instead of peeling.

Table 4 Average peeling force converted to N/100 mm width (speed 5mm/min) with standard deviations. 3 measurements. *fabric tore instead of peeling.

Average peeling force (N/100 mm width)	Woven cotton	Knitted cotton	Woven viscose
CA	124.8 ± 2.0	193.0 ± 19.2	(90.8* ± 1.7)
APC	12.2 ± 1.7	15.1 ± 10.0	15.0 ± 4.3

Washability results supported the results of the peeling tests. The samples were washed 5 times using detergent. CA was somewhat detached from the corners during the first wash, but remained attached during all 5 washing cycles without further changes and APC prints were detached and dissolved during the first cycle. The choice of fabric did not affect the result. HPC (MS_{HP} ~4), which was used as a raw material for APC, is water soluble in cold water when MS_{HP} >3 (Klemm et al. 1998). However, APC is insoluble in water, but amphiphilic, and hence might react with the detergent (Tseng et al. 1981). It could be speculated that by lowering the MS_{Hp} of HPC, the water solubility could be altered and that could also affect the sensitivity of APC. However, the adhesion properties of APC on cellulose would still require improvement in order to be utilized in consumer products.

4.4 From materials to prototypes

4.4.1 1D - Fibre yarn in applications

The fibre yarns developed in **Paper I** have potential in various applications. Due to its strength properties it could be utilized, for example, in semi-permanent textile structures, nonwoven structures and all-cellulose composites.

The prototypes made from fibre yarns were all-cellulose composite structures with CNF as the continuous phase and DES fibre yarns as the reinforcement. Additionally, a hand knitted water stable cloth was made (Figure 36) demonstrating the potential use also in consumer textiles. However, in order to enable machine knitting, the strength properties would require improvement.

Figure 36 Knitted sample from pulp fibre yarn

4.4.2 2D - CNF Films

In **Paper III** the laboratory scale films were solvent cast, however, the development of CNF film production has currently proceeded to pilot scale (Vartiainen et al. 2013) (Figure 37). Due to the mechanical performance, sustainability, extreme smoothness and optical properties and upscaled production methods of CNF films, a wide variety of applications have been developed. CNF films have been demonstrated as transparent (or translucent) and flexible substrates for organic electronics and diagnostics (Benítez et al. 2013; Hassinen et al. 2016), membranes for flexible batteries (Fu et al. 2016) and for water purification (Hakalahti et al. 2016; Karim et al. 2017; Mautner et al. 2015; Yang et al. 2014). Even though, the potential of CNF films has been already acknowledged in scientific literature for years, and a myriad of patents and applications have been developed, the technologies are yet to be commercialized.

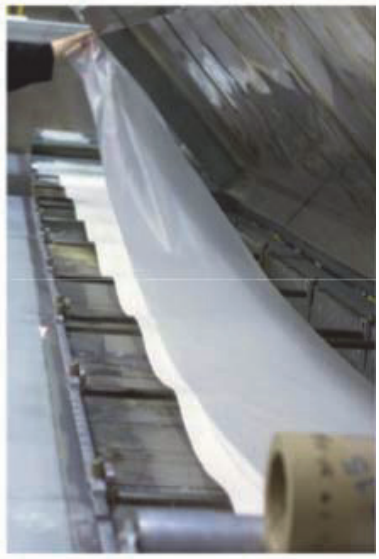

Figure 37 Roll to roll CNF film at VTT's SutCo pilot line (Kangas 2014)

4.4.3 3D - Surface modification and functionalization of cellulosic fabrics using polymeric cellulose

3D printing creates endless possibilities to functionalize and modify textiles. Textiles can be mass manufactured and post-customized by 3D printing according to the needs or applications. Wood based materials are from renewable sources, environmentally safe and often also hypoallergenic (Duchemin et al. 2009; Li and Frey 2010). In addition, cellulosic materials for the modifications on cellulosic textiles can simplify post-consumer recycling.

In **Paper IV** iterative prototyping was used for the material explorations and application development resulting in several porotypes. In iterative prototyping the qualities and capabilities of the materials are explored (Stappers 2006). The same printing method and cellulose derivatives (CA and APC) were used as in the experiments reported in **Paper V,** to study the usability of the materials in textile modification. In addition, utilization of cellulose dissolved in ionic liquid (IL), [emim]OAc was demonstrated.

Two sets of prototypes were designed and made: functional and decorative. In functional prototypes, flexible and rigid structuring as well as refracting and thermoresponsive structuring were demonstrated. In decorative structuring printable smocking was created using regenerated cellulose from IL solution. In functional structuring the ability to attach active components was demonstrated. Refractive structuring is presented in Figure 38a in the form of printable reflectors. For the prototype, reflective glass beads were mixed with CA prior to printing and after solvent evaporation the structure reflected light. The prototypes for flexible structuring in all-cellulose textiles (Figure 38b-c and Figure 38e-f) represented the application

potential to use 3D printable cellulosic materials in seams to replace stiches (Figure 38b, e). For example in children's clothes or sportswear, non-slip structuring (Figure 38c) and padding for knees or elbows (Figure 38f) could be utilized. A prototype for rigid structuring (Figure 38d) controls the stretch of the fabric. A thermoresponsive tag (Figure 38g) was made by mixing thermochromic material with APC solution and the same materials were used in an indicator for embedded conductive wiring in clothing (Figure 38h). The colour changes when heat is produced by the resistance of the current passing through. Cellulose also provides protection against direct skin contact.

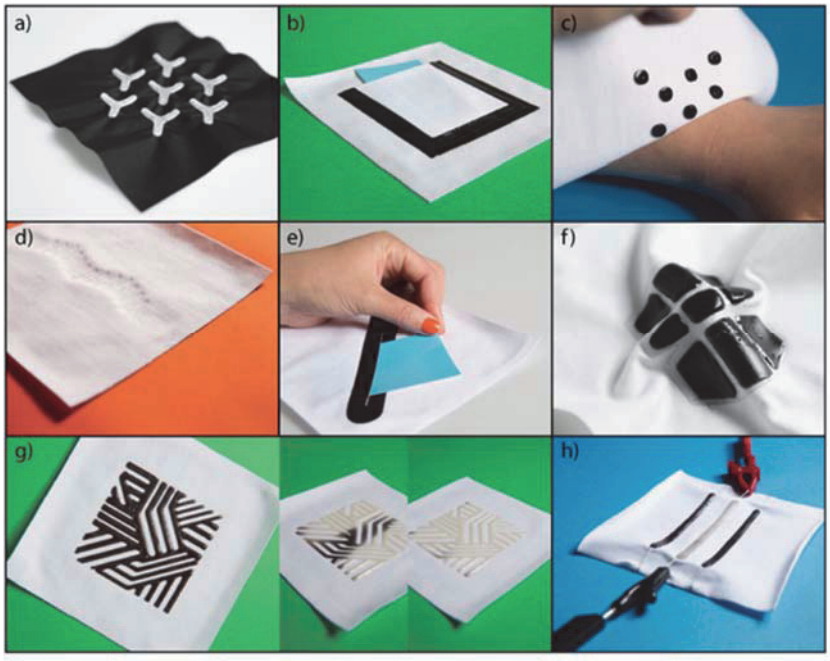

Figure 38 Functional prototypes developed were a) reflective beads mixed with CA to form reflective structures, b-c) soft printed structuring with coloured APC, d) CA on a controlled stretch structure, e-f) structures printed with pure and coloured APC, and g-h) thermoresponsive structures using APC (design: Pauliina Varis, photos: Eeva Suorlahti)

For the decorative set of prototypes cellulose dissolved in ionic liquid was used. 3D printing of the cellulose dissolved in IL has been previously published by Markstedt et al. (2014) and IL has been used for partial dissolution of cotton fabric by Shibata et al. (2013). Therefore, the assumption was that IL with dissolved cellulose would adhere well to cellulosic fabrics. According to Shibata et al. (2013) it can chemically

entangle with the filament surfaces of the fabric via partial surface dissolution. Due to the relatively low cellulose concentration (10 wt%) the material shrunk after regeneration during drying. This property enables the usage for novel textile design for smocking effects on fabrics as presented in Figure 39.

Figure 39 Decorative surface modification (smocking) using cellulose dissolved in ionic liquid (design: Pauliina Varis and Ilona Damski, photos: Eeva Suorlahti)

5. Concluding remarks

This thesis provides a thorough investigation of the versatility and utilization of three cellulosic building blocks: pulp fibres, CNF and polymeric cellulose, in the development of novel 1D-, 2D- and 3D-applications by exploiting the inherent properties of the materials. The work validates the use of complementary analytical methods to reveal the link between the surface interactions and the properties at a molecular level to the properties in macroscale applications.

A novel method for producing 1D fibre yarns directly from softwood pulp was developed utilizing DES as a dispersion agent and fibre spinning medium. Furthermore, the effect of the DES on pulp fibres was determined. It was concluded that negatively charged cellulose fibres can electrostatically bind positively charged DES molecules. The residuals of choline chloride are difficult to remove and affect the charge of the fibre yarn, which could affect the usability of the material. The applicability of the fibre yarn technology was demonstrated via knitted cloth and a composite structure. However, in order to make the product commercially viable development on the strength of the fibre yarn is required.

The approach in the manufacture of 2D CNF film was to determine the effect of xylan on molecular level stability and water uptake ability and associate it with the properties of the final product. CNF films exhibit promising characteristics for use as high performance biofilms due to recent developments in CNF production and the upscaling of the film manufacturing process. It was observed that xylan has an effect on molecular level stability and surface interactions, however, the effect diminished at macroscale, which encourages the removal and exploitation of xylan in other value-added applications without compromising the properties of large scale CNF films.

All-cellulose garments and functionalized textiles were developed using 3D printing. The variability of cellulosic derivatives was explored as adsorption and adhesion of soft and rigid cellulosic materials to cellulosic fabrics were studied. Additionally, several textile application prototypes were designed and demonstrated. The method has a high potential to be utilized in textile customization and functionalization. However, prior to commercialization there are challenges to overcome in relation to the prices of the biopolymers as well as the production speed, which is currently restricting the broader use of 3D printing technologies.

Overall, the findings in this thesis will provide new insight for the utilization of cellulosic building blocks in less conventional ways and offer an introduction for the development of new all-cellulose applications. The key to successful material design and development is a comprehensive understanding of the material properties and interactions both at a molecular level and in macroscale.

References

Abbott, A. P., Bell, T. J., Handa, S., and Stoddart, B. (2006). “Cationic functionalisation of cellulose using a choline based ionic liquid analogue,” *Green Chemistry*, 8(9), 784–786. DOI: 10.1039/B605258D

Abbott, A. P., Capper, G., Davies, D. L., Rasheed, R. K., and Tambyrajah, V. (2003). “Novel solvent properties of choline chloride/urea mixtures,” *Chemical Communications*, 99(1), 70–71. DOI: 10.1039/b210714g

Agarwal, U. P., Reiner, R. S., and Ralph, S. A. (2010). “Cellulose I crystallinity determination using FT-Raman spectroscopy: Univariate and multivariate methods,” *Cellulose*, 17(4), 721–733. DOI: 10.1007/s10570-010-9420-z

Ahola, S., Salmi, J., Johansson, L. S., Laine, J., and Österberg, M. (2008). “Model films from native cellulose nanofibrils. Preparation, swelling, and surface interactions,” *Biomacromolecules*, 9(4), 1273–1282. DOI: 10.1021/bm701317k

Akutsu, H. (1981). “Direct determination by Raman scattering of the conformation of the choline group in phospholipid bilayers.,” *Biochemistry*, 20(26), 7359–7366. DOI: 10.1021/bi00529a006

Ardenkjaer-Larsen, J. H., Fridlund, B., Gram, A., Hansson, G., Hansson, L., Lerche, M. H., Servin, R., Thaning, M., and Golman, K. (2003). “Increase in signal-to-noise ratio of > 10,000 times in liquid-state NMR.,” *Proceedings of the National Academy of Sciences of the United States of America*, 100(18), 10158–63. DOI: 10.1073/pnas.1733835100

Arola, S., Malho, J., Laaksonen, P., Lille, M., and Linder, M. B. (2013). “The role of hemicellulose in nanofibrillated cellulose networks,” *Soft Matter*, 9(4), 1319–1326. DOI: 10.1039/C2SM26932E

Atalla, R. H. (1999). “Celluloses,” in: *Comprehensive Natural Products Chemistry*, D. Barton, K. Nakanishi, and O. Meth-Cohn, eds., Elsevier, 529–598.

Atalla, R. H., and Vanderhart, D. L. (1984). “Native Cellulose: A Composite of Two Distinct Crystalline Forms,” *Science*, 223(4633), 283–285. DOI: 10.1126/science.223.4633.283

Aulin, C., Gällstedt, M., and Lindström, T. (2010). “Oxygen and oil barrier properties of microfibrillated cellulose films and coatings,” *Cellulose*, 17(3), 559–574. DOI: 10.1007/s10570-009-9393-y

Azizi, N., and Gholibeglo, E. (2012). “A highly efficient synthesis of dithiocarbamates in green reaction media,” *RSC Advances*, 2(19), 7413. DOI:

10.1039/c2ra20615c

Beamson, G., and Briggs, D. (1993). “Cellulose Spectra in High Resolution XPS of Organic Polymers: The Scienta ESCA300 database,” *J. Chem. Educ.*, 70(2), A25. DOI: 10.1021/ed070pA25.5

Belbekhouche, S., Bras, J., Siqueira, G., Chappey, C., Lebrun, L., Khelifi, B., Marais, S., and Dufresne, A. (2011). “Water sorption behavior and gas barrier properties of cellulose whiskers and microfibrils films,” *Carbohydrate Polymers*, Elsevier Ltd., 83(4), 1740–1748. DOI: 10.1016/j.carbpol.2010.10.036

Benítez, A. J., Torres-Rendon, J., Poutanen, M., and Walther, A. (2013). “Humidity and multiscale structure govern mechanical properties and deformation modes in films of native cellulose nanofibrils,” *Biomacromolecules*, 14(12), 4497–4506. DOI: 10.1021/bm401451m

Berman, B. (2012). “3-D printing: The new industrial revolution,” *Business Horizons*, “Kelley School of Business, Indiana University,” 55(2), 155–162. DOI: 10.1016/j.bushor.2011.11.003

Blackburn, R. S. (2009). *Sustainable Textiles: Life Cycle and Environmental Impact*, Woodhead Publishing.

Borrega, M., Tolonen, L. K., Bardot, F., Testova, L., and Sixta, H. (2013). “Potential of hot water extraction of birch wood to produce high-purity dissolving pulp after alkaline pulping,” *Bioresource Technology*, Elsevier Ltd, 135, 665–671. DOI: 10.1016/j.biortech.2012.11.107

Braconnot, H. (1833). “De la transformation de plusieurs substances vegetales en un principe nouveau,” *Ann. Chim. Phys.*, 52, 290–294.

Canejo, J. P., Borges, J. P., Godinho, M. H., Brogueira, P., Teixeira, P. I. C., and Terentjev, E. M. (2008). “Helical twisting of electrospun liquid crystalline cellulose micro- and nanofibers,” *Advanced Materials*, 20(24), 4821–4825. DOI: 10.1002/adma.200801008

Cao, Y., Li, H., Zhang, Y., Zhang, J., and He, J. (2010). “Structure and properties of novel regenerated cellulose films prepared from cornhusk cellulose in room temperature ionic liquids,” *Journal of Applied Polymer Science*, 116(1), 547–554. DOI: 10.1002/app.31273

Casdorff, K., Keplinger, T., and Burgert, I. (2017). “Nano-mechanical characterization of the wood cell wall by AFM studies: Comparison between AC- and QI™ mode,” *Plant Methods*, BioMed Central, 13(1), 1–9. DOI: 10.1186/s13007-017-0211-5

Chanzy, H. (1980). “Quellung und Lösen von Cellulose im Amin-oxid-Wasser-System,” *J. Polym. Sci., Polymer Phys. Ed.*, 18, 1137–1144.

Conte, P., Piccolo, A., van Lagen, B., Buurman, P., and de Jager, P. (1997). “Quantitative differences in evaluating soil humic substances by liquid- and solid-state 13C-NMR spectroscopy,” *Geoderma*, 80(3–4), 339–352. DOI: 10.1016/S0016-7061(97)00059-1

Cross, C. F., Nard, E., Bevan, J., Eadle, C. B., London, O. F., To, A., and Nichols, H. G. (1894). “Plastic compound of cellulose.”

Dorris, G., and Gray, D. (1978). “The surface analysis of paper and wood fibers by Esca - electron spectroscopy for chemical analysis - I. Applications to cellulose and lignin,” *Cellulose chemistry and technology*, 12, 9–23.

Duchemin, B. J. C., Mathew, A. P., and Oksman, K. (2009). “All-cellulose composites by partial dissolution in the ionic liquid 1-butyl-3-methylimidazolium chloride,” *Composites Part A: Applied Science and Manufacturing*, Elsevier Ltd, 40(12), 2031–2037. DOI: 10.1016/j.compositesa.2009.09.013

Duchesne, I., Hult, E., Molin, U., Daniel, G., Iversen, T., and Lennholm, H. (2001). “The influence of hemicellulose on fibril aggregation of kraft pulp fibres as revealed by FE-SEM and CP/MAS13C-NMR,” *Cellulose*, 8(2), 103–111. DOI: 10.1023/A:1016645809958

Dufresne, A. (2012). *Nanocellulose : From Nature to High Performance Tailored Materials*, De Gruyter.

Earl, W. L., and VanderHart, D. L. (1981). “Observations by high-resolution carbon-13 nuclear magnetic resonance of cellulose I related to morphology and crystal structure,” *Macromolecules*, 14(3), 570–574. DOI: 10.1021/ma50004a023

Edgar, K. J., Buchanan, C. M., Debenham, J. S., Rundquist, P. A., Seiler, B. D., Shelton, M. C., and Tindall, D. K. (2001). “Advances in cellulose ester performance and application,” *Prog. Polym. Sci.*, 26, 1605–1688.

Edwards, H. G., Farwell, D. W., and Webster, D. (1997). “FT Raman microscopy of untreated natural plant fibres.,” *Spectrochimica acta. Part A, Molecular and biomolecular spectroscopy*, 53A(13), 2383–2392. DOI: 10.1016/S1386-1425(97)00178-9

EFSA FEEDAP Panel. (2011). “Scientific Opinion on safety and efficacy of choline chloride as a feed additive for all animal species,” *EFSA Journal*, 9(9), 1–15. DOI: 10.2903/j.efsa.2011.2353.

Einstein, A. (1905). “Über einen die Erzeugung und Verwandlung des Lichtes betreffenden heuristischen Gesichtspunkt,” *Annalen Der Physik*, 322(6), 132–148.

Eronen, P., Österberg, M., Heikkinen, S., Tenkanen, M., and Laine, J. (2011). “Interactions of structurally different hemicelluloses with nanofibrillar cellulose,” *Carbohydrate Polymers*, Elsevier Ltd., 86(3), 1281–1290. DOI: 10.1016/j.carbpol.2011.06.031

Eronen, P., Österberg, M., and Jääskeläinen, A. S. (2009). “Effect of alkaline treatment on cellulose supramolecular structure studied with combined confocal Raman spectroscopy and atomic force microscopy,” *Cellulose*, 16(2), 167–178. DOI: 10.1007/s10570-008-9259-8

Fall, A. B., Lindstr, S. B., Sundman, O., Odberg, L., and Lars, W. (2011). “Colloidal Stability of Aqueous Nanofibrillated Cellulose Dispersions,” *Langmuir*, 27, 11332–11338.

Fan, M., Dai, D., and Huang, B. (2016). “Fourier Transform Infrared Spectroscopy for Natural Fibres,” in: *Fourier Transform – Materials Analysis*, S. Salih, ed., InTech.

Faulde, M., Albiez, G., and Nehring, O. (2012). “Novel long-lasting impregnation technique transferred from clothing to bednets: Extended efficacy and residual activity of different pyrethroids against Aedes aegypti as shown by EN ISO 6330-standardized machine laundering,” *Parasitology Research*, 110(6), 2341–2350. DOI: 10.1007/s00436-011-2769-6

Fengel, G., and Wegener, D. (1984). *Wood: chemistry, ultrastructure, reactions*, *Holzforschung*. DOI: 10.1515/hfsg.1984.38.6.U

Fernandes Diniz, J. M. B., Gil, M. H., and Castro, J. A. A. M. (2004). “Hornification - Its origin and interpretation in wood pulps,” *Wood Science and Technology*, 37(6), 489–494. DOI: 10.1007/s00226-003-0216-2

Ferraro, J. R., Nakamoto, K., and Brown, C. W. (2002). *Introductory Raman Spectroscopy*, Elsevier Science.

Filip, D., Costa, I., Figueirinhas, J. L., and Godinho, M. H. (2006). “Anisotropic cellulose-derived matrix for dispersed liquid crystals,” *Liquid Crystals*, 33(1), 109–114. DOI: 10.1080/02678290500450758

Fischer, S., Leipner, H., Thümmler, K., Brendler, E., and Peters, J. (2003). “Inorganic molten salts as solvents for cellulose,” *Cellulose*, 10(3), 227–236. DOI: 10.1023/A:1025128028462

Friese, M. A., and Banerjee, S. (1995). “FT-IR Spectroscopy,” in: *Surface analysis of paper*, T. E. Conners and S. Banerjee, eds., CRC Press LLC, 346.

Fu, J., Zhang, J., Song, X., Zarrin, H., Tian, X., Qiao, J., Rasen, L., Li, K., and Chen, Z. (2016). “A flexible solid-state electrolyte for wide-scale integration of rechargeable zinc–air batteries,” *Energy Environ. Sci.*, Royal Society of Chemistry, 9(2), 663–670. DOI: 10.1039/C5EE03404C

Ghasemi, S., Tajvidi, M., Bousfield, D. W., Gardner, D. J., and Gramlich, W. M. (2017). “Dry-spun neat cellulose nanofibril filaments: Influence of drying temperature and nanofibril structure on filament properties,” *Polymers*, 9(9), 1–14. DOI: 10.3390/polym9090392

Godinho, M. H., Filip, D., Costa, I., Carvalho, A. L., Figueirinhas, J. L., and Terentjev, E. M. (2009). “Liquid crystalline cellulose derivative elastomer films under uniaxial strain,” *Cellulose*, 16(2), 199–205. DOI: 10.1007/s10570-008-9258-9

Greenspan, L. (1977). “Humidity fixed points of binary saturated aqueous solutions,” *Journal of Research of the National Bureau of Standards Section A: Physics and Chemistry*, 81A(1), 89. DOI: 10.6028/jres.081A.011

Gross, A. S., and Chu, J. W. (2010). “On the molecular origins of biomass recalcitrance: The interaction network and solvation structures of cellulose microfibrils,” *Journal of Physical Chemistry B*, 114(42), 13333–13341. DOI: 10.1021/jp106452m

Gustafsson, E. (2012). “Tailoring adhesion and wetting properties of cellulose fibers and model surfaces,” KTH Royal Institute of Technology.

Hakalahti, M., Mautner, A., Johansson, L. S., Hänninen, T., Setälä, H., Kontturi, E., Bismarck, A., and Tammelin, T. (2016). “Direct Interfacial Modification of Nanocellulose Films for Thermoresponsive Membrane Templates,” *ACS Applied Materials and Interfaces*, 8(5), 2923–2927. DOI: 10.1021/acsami.5b12300

Hakalahti, M., Tenhunen, T. M., Hänninen, T., and Pere, J. (2015). “Process for producing shaped articles based on cellulose.”

Hannuksela, T., Holmbom, B., Mortha, G., Lachenal, D., Française, E., and Papeterie, D. (2004). “Effect of sorbed galactoglucomannans and galacto-mannans on pulp and paper handsheet properties ,” *Nordic Pulp and Paper Research Journal*, 19(2), 237–244.

Hassinen, T., Alastalo, A., Eiroma, K., Tenhunen, T.-M., Kunnari, V., Kaljunen, T., Forsström, U., and Tammelin, T. (2016). “All-Printed Transistors on Nano

Cellulose Substrate," *MRS Advances*, 1(10), 645–650. DOI: 10.1557/adv.2015.31

Hauru, L. K. J., Ma, Y., Hummel, M., Alekhina, M., King, A. W. T., Kilpeläinen, I., Penttilä, P. A., Serimaa, R., and Sixta, H. (2013). "Enhancement of ionic liquid-aided fractionation of birchwood. Part 1: autohydrolysis pretreatment," *RSC Advances*, 3(37), 16365. DOI: 10.1039/c3ra41529e

Hearle, J. W. S. (1958). "A fringed fibril theory of structure in crystalline polymers," *Journal of Polymer Science*, 28(117), 432–435. DOI: 10.1002/pol.1958.1202811722

Heinze, T. (2016). "Cellulose: Structure and Properties," in: *Cellulose Chemistry and Properties: Fibers, Nanocelluloses and Advanced Materials*, O. J. Rojas, ed., Springer International, 341. DOI: 10.1007/978-3-319-26015-0

Helmerius, J., von Walter, J. V., Rova, U., Berglund, K. A., and Hodge, D. B. (2010). "Impact of hemicellulose pre-extraction for bioconversion on birch Kraft pulp properties," *Bioresource Technology*, Elsevier Ltd, 101(15), 5996–6005. DOI: 10.1016/j.biortech.2010.03.029

Henke, K., and Treml, S. (2013). "Wood based bulk material in 3D printing processes for applications in construction," *European Journal of Wood and Wood Products*, 71(1), 139–141. DOI: 10.1007/s00107-012-0658-z

Hertz, H. (1887). "Über einen Einfluss des ultravioletten Lichtes auf die electrische Entladung," *Annalen Der Physik*, 267(8), 938–1000.

Hiltunen, J., Kemppainen, K., and Pere, J. (2015). "Process for producing fibrillated cellulose material. WO2015/092146 A1. Finnish Patent FI126698," Finnish Patent FI126698.

Ho, T. T. T., Zimmermann, T., Hauert, R., and Caseri, W. (2011). "Preparation and characterization of cationic nanofibrillated cellulose from etherification and high-shear disintegration processes," *Cellulose*, 18(6), 1391–1406. DOI: 10.1007/s10570-011-9591-2

Hoeger, I., Taajamaa, L., Kontturi, E., Laine, J., and Rojas, O. J. (2014). "Thin Film Deposition Techniques," in: *Handbook of Green Materials: Self- and direct-assembling of bionanomaterials*, K. Oksman, A. P. Mathew, O. J. Rojas, and M. Sain, eds., World Scientific Publishing Co. Pte. Ltd., 7–16.

Holdich, R. G. (2002). "Hindered systems and rheology," in: *Fundamentals of Particle Technology*, Information Technology and Publishing, Loughborough, UK, 55–66.

Holmberg, M., Berg, J., Stemme, S., and Ödberg, L. (1997). “Surface force studies of Langmuir-Blodgett cellulose films,” *Journal of Colloid and Interface Science*, 186, 369–381.

Hooshmand, S., Aitomäki, Y., Norberg, N., Mathew, A. P., and Oksman, K. (2015). “Dry-Spun Single-Filament Fibers Comprising Solely Cellulose Nanofibers from Bioresidue,” *ACS Applied Materials and Interfaces*, 7(23), 13022–13028. DOI: 10.1021/acsami.5b03091

Håkansson, K. M. O., Fall, A. B., Lundell, F., Yu, S., Krywka, C., Roth, S. V., Santoro, G., Kvick, M., Prahl Wittberg, L., Wågberg, L., and Söderberg, L. D. (2014). “Hydrodynamic alignment and assembly of nanofibrils resulting in strong cellulose filaments,” *Nature Communications*, 5. DOI: 10.1038/ncomms5018

Hämmerle, F. M. (2011). “the Cellulose Gap (the Future of Cellulose Fibres),” *Lenzinger Berichte*, 89, 12–21.

Häyrinen, E. (1973). *Kehruuteknologia*, Teknillisen Korkeakoulon Ylioppilaskunta, Otaniemi.

Höök, F., Rodahl, M., Brezezinski, P., and Kasemo, B. (1998). “Energy Dissipation Kinetics for Protein and Antibody - Antigen Adsorption under Shear Oscillation on a Quartz Crystal Microbalance,” *Langmuir*, 14(21), 729–734. DOI: 10.1021/la970815u

Isogai, A., and Atalla, R. H. (1998). “Dissolution of cellulose in aqueous NaOH solutions,” *Cellulose*, 5(4), 309–319. DOI: 10.1023/A:1009272632367

Iwamoto, S., Abe, K., and Yano, H. (2008). “The Effect of Hemicelluloses on Wood Pulp Nanofibrillation and Nanofiber Network Characteristics The Effect of Hemicelluloses on Wood Pulp Nanofibrillation and Nanofiber Network Characteristics,” *Scanning Electron Microscopy*, 1022–1026. DOI: 10.1021/bm701157n

Jacobsen, N. E. (2007). *NMR Spectroscopy Explained: Simplified Theory, Applications and Examples for Organic Chemistry and Structural Biology*, John Wiley & Sons.

Johansson, L. S., and Campbell, J. M. (2004). “Reproducible XPS on biopolymers: Cellulose studies,” *Surface and Interface Analysis*, 36(8), 1018–1022. DOI: 10.1002/sia.1827

Kang, H., Liu, R., and Huang, Y. (2013). “Cellulose derivatives and graft copolymers as blocks for functional materials,” *Polymer International*, 62(3), 338–344. DOI: 10.1002/pi.4455

Kangas, H. (2014). *Guide to cellulose nanomaterials - English summary*.

Kargarzadeh, H., Ioelovich, M., Ahmad, I., Thomas, S., and Dufresne, A. (2017). “Methods for Extraction of Nanocellulose from Various Sources,” in: *Handbook of Nanocellulose and Cellulose Nanocomposites*, H. Kargarzadeh, I. Ahmad, S. Thomas, and A. Dufresne, eds., Wiley-VCH Verlag GmbH & Co. KGaA, Weinheim, Germany, 1–49. DOI: 10.1002/9783527689972

Kargl, R., Mohan, T., Bračč, M., Kulterer, M., Doliška, A., Stana-Kleinschek, K., and Ribitsch, V. (2012). “Adsorption of carboxymethyl cellulose on polymer surfaces: Evidence of a specific interaction with cellulose,” *Langmuir*, 28(31), 11440–11447. DOI: 10.1021/la302110a

Karim, Z., Hakalahti, M., Tammelin, T., and Mathew, A. P. (2017). “In situ TEMPO surface functionalization of nanocellulose membranes for enhanced adsorption of metal ions from aqueous medium,” *RSC Adv.*, Royal Society of Chemistry, 7(9), 5232–5241. DOI: 10.1039/C6RA25707K

Klemm, D., Philipp, B., Heinze, T., Heinze, U., and Wagenknecht, W. (1998). *Comprehensive Cellulose Chemistry*, Wiley-VCH Verlag GmbH & Co. KGaA, Weinheim, FRG. DOI: 10.1002/3527601929

Kontturi, E., Tammelin, T., and Österberg, M. (2006). “Cellulose—model films and the fundamental approach,” *Chem. Soc. Rev.*, 35(12), 1287–1304. DOI: 10.1039/B601872F

Kosan, B., Michels, C., and Meister, F. (2008). “Dissolution and forming of cellulose with ionic liquids,” *Cellulose*, 15(1), 59–66. DOI: 10.1007/s10570-007-9160-x

Köhler, S., and Heinze, T. (2007). “New Solvents for Cellulose: Dimethyl Sulfoxide/Ammonium Fluorides,” *Macromolecular Bioscience*, 7(3), 307–314. DOI: 10.1002/mabi.200600197

Köhnke, T., Lund, K., Brelid, H., and Westman, G. (2010). “Kraft pulp hornification: A closer look at the preventive effect gained by glucuronoxylan adsorption,” *Carbohydrate Polymers*, 81(2), 226–233. DOI: 10.1016/j.carbpol.2010.02.023

Lahtinen, P., Liukkonen, S., Pere, J., Sneck, A., and Kangas, H. (2014). “A Comparative study of fibrillated fibers from different mechanical and chemical pulps,” *BioResources*, 9(2), 2115–2127.

Laivins, G. V., and Gray, D. G. (1985). “Characterization and chain stiffness of (Acetoxypropyl)cellulose,” *Macromolecules*, 18(9), 1746–1752. DOI: 10.1021/ma00151a018

Langmuir, I., and Schaefer, V. J. (1938). “Activities of Urease and Pepsin Monolayers,” *J. Am. Chem. Soc.*, 60(6), 1351–1360.

Leppiniemi, J., Lahtinen, P., Paajanen, A., Mahlberg, R., Metsä-Kortelainen, S., Pinomaa, T., Pajari, H., Vikholm-Lundin, I., Pursula, P., and Hytönen, V. P. (2017). “3D-Printable Bioactivated Nanocellulose-Alginate Hydrogels,” *ACS Applied Materials and Interfaces*, 9(26), 21959–21970. DOI: 10.1021/acsami.7b02756

Lewandowska, A. E., Soutis, C., Savage, L., and Eichhorn, S. J. (2015). “Carbon fibres with ordered graphitic-like aggregate structures from a regenerated cellulose fibre precursor,” *Composites Science and Technology*, Elsevier Ltd, 116, 50–57. DOI: 10.1016/j.compscitech.2015.05.009

Li, L., and Frey, M. (2010). “Preparation and characterization of cellulose nitrate-acetate mixed ester fibers,” *Polymer*, Elsevier Ltd, 51(16), 3774–3783. DOI: 10.1016/j.polymer.2010.06.013

Li, R., Zhang, L., and Xu, M. (2012). “Novel regenerated cellulose films prepared by coagulating with water: Structure and properties,” *Carbohydrate Polymers*, Elsevier Ltd., 87(1), 95–100. DOI: 10.1016/j.carbpol.2011.07.023

Lindström, T., Wågberg, L., and Larsson, T. (2005). “On the nature of joint strength in paper – a review of dry and wet strength resins used in paper manufacturing,” *13th Fundamental Research Symposium*, 32(May 2005), 457–562.

Lobo, H. R., Singh, B. S., and Shankarling, G. S. (2012). “Deep eutectic solvents and glycerol: a simple, environmentally benign and efficient catalyst/reaction media for synthesis of N- aryl phthalimide derivatives,” *Green Chemistry Letters and Reviews*, 5(4), 487–533. DOI: 10.1080/17518253.2012.669500

Lucenius, J., Parikka, K., and Österberg, M. (2014). “Nanocomposite films based on cellulose nanofibrils and water-soluble polysaccharides,” *Reactive and Functional Polymers*, Elsevier B.V., 85, 167–174. DOI: 10.1016/j.reactfunctpolym.2014.08.001

Lundahl, M. J., Cunha, A. G., Rojo, E., Papageorgiou, A. C., Rautkari, L., Arboleda, J. C., and Rojas, O. J. (2016). “Strength and Water Interactions of Cellulose i Filaments Wet-Spun from Cellulose Nanofibril Hydrogels,” *Scientific Reports*, Nature Publishing Group, 6(July), 1–13. DOI: 10.1038/srep30695

Lundahl, M. J., Klar, V., Wang, L., Ago, M., and Rojas, O. J. (2017). “Spinning of cellulose nanofibrils into filaments: A review,” *Industrial and Engineering Chemistry Research*, 56(1), 8–19. DOI: 10.1021/acs.iecr.6b04010

Lyytikäinen, K. (2017). “Removal of xylan from birch kraft pulps and the effect of its removal on fiber properties, colloidal interactions and retention in papermaking,” Lappeenranta University of Technology.

Maji, S., Kundu, S., Pinto, L. F. V., Godinho, M. H., Khan, A. H., and Acharya, S. (2013). “Improved mechanical stability of acetoxypropyl cellulose upon blending with ultranarrow pbs nanowires in langmuir monolayer matrix,” *Langmuir*, 29(49), 15231–15239. DOI: 10.1021/la402753n

Mariano, M., El Kissi, N., and Dufresne, A. (2014). “Cellulose nanocrystals and related nanocomposites: Review of some properties and challenges,” *Journal of Polymer Science, Part B: Polymer Physics*, 52(12), 791–806. DOI: 10.1002/polb.23490

Markstedt, K., Escalante, A., Toriz, G., and Gatenholm, P. (2017). “Biomimetic inks based on cellulose nanofibrils and crosslinkable xylans for 3D printing,” *ACS Applied Materials & Interfaces*, acsami.7b13400. DOI: 10.1021/acsami.7b13400

Markstedt, K., Mantas, A., Tournier, I., Martínez Ávila, H., Hägg, D., and Gatenholm, P. (2015). “3D Bioprinting Human Chondrocytes with Nanocellulose-Alginate Bioink for Cartilage Tissue Engineering Applications,” *Biomacromolecules*, 16(5), 1489–1496. DOI: 10.1021/acs.biomac.5b00188

Markstedt, K., Sundberg, J., and Gatenholm, P. (2014). “3D Bioprinting of Cellulose Structures from an Ionic Liquid,” *3D Printing and Additive Manufacturing*, 1(3), 115–121. DOI: 10.1089/3dp.2014.0004

Mautner, A., Hakalahti, M., Rissanen, V., and Tammelin, T. (2018). “Crucial interfacial features of nanocellulose materials,” in: *Nanocellulose and Sustainability Production, Properties, Applications, and Case Studies*, Koon-Yang Lee, ed., CRC Press, 314.

Mautner, A., Lee, K. Y., Tammelin, T., Mathew, A. P., Nedoma, A. J., Li, K., and Bismarck, A. (2015). “Cellulose nanopapers as tight aqueous ultra-filtration membranes,” *Reactive and Functional Polymers*, Elsevier B.V., 86, 209–214. DOI: 10.1016/j.reactfunctpolym.2014.09.014

McCormick, C. L., and Callais, P. A. (1987). “Derivatization of cellulose in lithium chloride and N-N-dimethylacetamide solutions,” *Polymer*, 28(13), 2317–2323. DOI: 10.1016/0032-3861(87)90393-4

Medronho, B., Romano, A., Miguel, M. G., Stigsson, L., and Lindman, B. (2012). “Rationalizing cellulose (in)solubility: Reviewing basic physicochemical aspects and role of hydrophobic interactions,” *Cellulose*, 19(3), 581–587. DOI: 10.1007/s10570-011-9644-6

Melnikova, R., Ehrmann, A., and Finsterbusch, K. (2014). “3D printing of textile-based structures by Fused Deposition Modelling (FDM) with different polymer materials,” *IOP Conference Series: Materials Science and Engineering*, 62. DOI: 10.1088/1757-899X/62/1/012018

Moon, R. J., Martini, A., Nairn, J., Simonsen, J., and Youngblood, J. (2011). *Cellulose nanomaterials review: structure, properties and nanocomposites*, *Chemical Society Reviews*. DOI: 10.1039/c0cs00108b

Moon, R. J., Pöhler, T., and Tammelin, T. (2014). “Microscopic Charachterization of Nanofibres and Nanocrystals,” in: *Handbook of green materials*, K. Oksman, ed., Singapore ; Hackensack, N.J. : World Scientific Pub. Co., 2014.

Myllytie, P., Salmi, J., and Laine, J. (2009). “The Influence of pH on the Adsorption and Interaction of Chitosan with Cellulose,” *BioResources*, 4(4), 1647–1662.

Newman, R. H. (2008). “Simulation of X-ray diffractograms relevant to the purported polymorphs cellulose IVI and IVII,” *Cellulose*, 15(6), 769–778. DOI: 10.1007/s10570-008-9225-5

Nigmatullin, R., Lovitt, R., Wright, C., Linder, M., Nakari-Set??l??, T., and Gama, M. (2004). “Atomic force microscopy study of cellulose surface interaction controlled by cellulose binding domains,” *Colloids and Surfaces B: Biointerfaces*, 35(2), 125–135. DOI: 10.1016/j.colsurfb.2004.02.013

Nippon Paper Group. (2017). “Cellulose nanofiber manufacturing technology and application development,” *http://www.nipponpapergroup.com/english/research/organize/cnf.html*.

Nishiyama, Y. (2014). “Structure and Physical Porperties of Cellulose: Micro- to Nanoscale,” in: *Handbook of Green Materials: Bionanomaterials: Separation processes, characterization and properties*, K. Oksman, A. P. Mathew, A. Bismarck, O. J. Rojas, and M. Sain, eds., World Scientific Publishing Co. Pte. Ltd., 5–15.

Nishiyama, Y., Kim, U. J., Kim, D. Y., Katsumata, K. S., May, R. P., and Langan, P. (2003a). “Periodic disorder along ramie cellulose microfibrils,” *Biomacromolecules*, 4(4), 1013–1017. DOI: 10.1021/bm025772x

Nishiyama, Y., Langan, P., and Chanzy, H. (2002). “Crystal structure and hydrogen-bonding system in cellulose Iβ from synchrotron X-ray and neutron fiber diffraction,” *Journal of the American Chemical Society*, 124(31), 9074–9082. DOI: 10.1021/ja0257319

Nishiyama, Y., Sugiyama, J., Chanzy, H., and Langan, P. (2003b). “Crystal Structure and Hydrogen Bonding System in Cellulose Iα from Synchrotron X-

ray and Neutron Fiber Diffraction," *Journal of the American Chemical Society*, 125(47), 14300–14306. DOI: 10.1021/ja037055w

Nockemann, P., Thijs, B., Driesen, K., Janssen, C. R., Van Hecke, K., Van Meervelt, L., Kossmann, S., Kirchner, B., and Binnemans, K. (2007). "Choline saccharinate and choline acesulfamate: Ionic liquids with low toxicities," *Journal of Physical Chemistry B*, 111(19), 5254–5263. DOI: 10.1021/jp068446a

Nogi, M., Iwamoto, S., Nakagaito, A. N., and Yano, H. (2009). "Optically Transparent Nanofiber Paper," *Advanced Materials*, 21(16), 1595–1598. DOI: 10.1002/adma.200803174

NREL Standard. (2008). *Determination of Structural Carbohydrates and Lignin in Biomass, Laboratory Analytical Procedure (LAP) Issue Date: 4/25/2008, Technical Report NREL/TP-510-42618, Revised April 2008.*

Oksanen, T., Buchert, J., and Viikari, L. (1997). "The role of hemiocelluloses in the hornification of bleached kraft pulps," *Holzforschung*, 51(4), 355–360.

Olsson, C., and Westman, G. (2013). "Direct Dissolution of Cellulose: Background, Means and Applications," in: *Cellulose - Fundamental Aspects*, L. Godbout and T. van de Ven, eds., InTech. DOI: 10.5772/52144

Orelma, H., Teerinen, T., Johansson, L. S., Holappa, S., and Laine, J. (2012). "CMC-modified cellulose biointerface for antibody conjugation," *Biomacromolecules*, 13(4), 1051–1058. DOI: 10.1021/bm201771m

Paananen, A., Österberg, M., Rutland, M., Tammelin, T., Saarinen, T., Tappura, K., and Stenius, P. (2003). "Interaction between Cellulose and Xylan: An Atomic Force Microscope and Quartz Crystal Microbalance Study," in: *Hemicelluloses: Science and Technology*, 269–290. DOI: 10.1021/bk-2004-0864.ch018

Palit, D., and Moulik, S. P. (2000). "Adsorption of methylene blue on cellulose from its own solution and its mixture with methyl orange," *Indian Journal of Chemistry - Section A Inorganic, Physical, Theoretical and Analytical Chemistry*, 39(6), 611–617.

Pandey, K. K. (1999). "A study of chemical structure of soft and harwood and wood polymers by FTIR spectrscopy," *Journal of Applied Polymer Science*, 71(May), 1969–1975. DOI: 10.1002/(sici)1097-4628(19990321)71:12<1969::aid-app6>3.3.co;2-4

Pattinson, S. W., and Hart, A. J. (2017). "Additive Manufacturing of Cellulosic Materials with Robust Mechanics and Antimicrobial Functionality," *Advanced*

Materials Technologies, 2(4). DOI: 10.1002/admt.201600084

Payen, A. (1838). “Mémoire sur la composition du tissu propre des plantes e du ligneux,” *C. R. Hebd. Seances Acad. Sci.*, 7, 1052–1056.

Pei, E., Shen, J., and Watling, J. (2015). “Direct 3D printing of polymers onto textiles: experimental studies and applications,” *Rapid Prototyping Journal*, 21(5), 556–571. DOI: 10.1108/RPJ-09-2014-0126

Peng, H., Mankoff, J., Hudson, S. E., and McCann, J. (2015). “A Layered Fabric 3D Printer for Soft Interactive Objects,” *Proceedings of the ACM CHI’15 Conference on Human Factors in Computing Systems*, 1, 1789–1798. DOI: 10.1145/2702123.2702327

Penttilä, P. A., Varnai, A., Pere, J., Tammelin, T., Salmen, L., Siika-aho, M., Viikari, L., and Serimaa, R. (2013). “Xylan as limiting factor in enzymatic hydrolysis of nanocellulose,” *Bioresource Technology*, 129, 135–141. DOI: 10.1016/j.biortech.2012.11.017

Peresin, M. S., Kammiovirta, K., Setälä, H., and Tammelin, T. (2012). “Structural Features and Water Interactions of Etherified Xylan Thin Films,” *Journal of Polymers and the Environment*, 20(4), 895–904. DOI: 10.1007/s10924-012-0469-7

Pfister, A., Landers, R., Laib, A., Hübner, U., Schmelzeisen, R., and Mülhaupt, R. (2004). “Biofunctional Rapid Prototyping for Tissue-Engineering Applications: 3D Bioplotting versus 3D Printing,” *Journal of Polymer Science, Part A: Polymer Chemistry*, 42(3), 624–638. DOI: 10.1002/pola.10807

Puls, J., Wilson, S. A., and Hölter, D. (2011). “Degradation of Cellulose Acetate-Based Materials: A Review,” *Journal of Polymers and the Environment*, 19(1), 152–165. DOI: 10.1007/s10924-010-0258-0

Pääkko, M., Ankerfors, M., Kosonen, H., Nykänen, A., Ahola, S., Österberg, M., Ruokolainen, J., Laine, J., Larsson, P. T., Ikkala, O., and Lindström, T. (2007). “Enzymatic hydrolysis combined with mechanical shearing and high-pressure homogenization for nanoscale cellulose fibrils and strong gels,” *Biomacromolecules*, 8(6), 1934–1941. DOI: 10.1021/bm061215p

Pääkkönen, T., Dimic-Misic, K., Orelma, H., Pönni, R., Vuorinen, T., and Maloney, T. (2016). “Effect of xylan in hardwood pulp on the reaction rate of TEMPO-mediated oxidation and the rheology of the final nanofibrillated cellulose gel,” *Cellulose*, 23(1), 277–293. DOI: 10.1007/s10570-015-0824-7

Radošević, K., Bubalo, M. C., Srček, V. G., Grgas, D., Dragičević, T. L., and Redovniković, I. R. (2015). “Evaluation of toxicity and biodegradability of

choline chloride based deep eutectic solvents," *Ecotoxicology and Environmental Safety*, 112, 46–53. DOI: 10.1016/j.ecoenv.2014.09.034

Ralph, J., Lundquist, K., Brunow, G., Lu, F., Kim, H., Schatz, P. F., Marita, J. M., Hatfield, R. D., Ralph, S. A., Christensen, J. H., and Boerjan, W. (2004). "Lignins: Natural polymers from oxidative coupling of 4-hydroxyphenyl-propanoids," *Phytochemistry Reviews*, 3(1–2), 29–60. DOI: 10.1023/B:PHYT.0000047809.65444.a4

Rauvanto, I., Pere, J., and Henricson, K. (2006). "Fibre damage in unbleached reinforcement pulp-The effect of hemicelluloses and lignin on the susceptibility of fibres to damage during oxygen delignification," *Nord.Pulp Pap Res J.*, 21(3), 328–335.

Reza, M., Ruokolainen, J., and Vuorinen, T. (2014). "Out-of-plane orientation of cellulose elementary fibrils on spruce tracheid wall based on imaging with high-resolution transmission electron microscopy," *Planta*, 240(3), 565–573. DOI: 10.1007/s00425-014-2107-1

Rodahl, M., Höök, F., Krozer, A., Brzezinski, P., and Kasemo, B. (1995). "Quartz crystal microbalance setup for frequency and Q -factor measurements in gaseous and liquid environments," *Review of Scientific Instruments*, 66(7), 3924–3930. DOI: 10.1063/1.1145396

Rodahl, M., and Kasemo, B. (1996). "A simple setup to simultaneously measure the resonant frequency and the absolute dissipation factor of a quartz crystal microbalance," *Review of Scientific Instruments*, 67(9), 3238–3241. DOI: 10.1063/1.1147494

Rohm, S., Hirn, U., Ganser, C., Teichert, C., and Schennach, R. (2014). "Thin cellulose films as a model system for paper fibre bonds," *Cellulose*, 21(1), 237–249. DOI: 10.1007/s10570-013-0098-x

Roman, M. (2009). "Model Cellulosic Surfaces: History and Recent Advances," *Model Cellulosic Surfaces*, 1019, 3–53. DOI: doi:10.1021/bk-2009-1019.ch001

Rosenau, T., Potthast, A., Sixta, H., and Kosma, P. (2001). "The chemistry of side reactions and byproduct formation in the system NMMO/cellulose," *Prog. Polym. Sci.*, 26, 1763–1837.

Rånby, B. G. (1951). "Fibrous macromolecular systems. Cellulose and muscle. The colloidal properties of cellulose micelles," *Discuss. Faraday Soc.*, 11, 158–164. DOI: 10.1039/DF9511100158

Saalwächter, K., Burchard, W., Klüfers, P., Kettenbach, G., Mayer, P., Klemm, D.,

and Dugarmaa, S. (2000). “Cellulose solutions in water containing metal complexes,” *Macromolecules*, 33(11), 4094–4107. DOI: 10.1021/ma991893m

Saito, T., Kimura, S., Nishiyama, Y., and Isogai, A. (2007). “Cellulose nanofibers prepared by TEMPO-mediated oxidation of native cellulose,” *Biomacromolecules*, 8(8), 2485–2491. DOI: 10.1021/bm0703970

Saito, T., Nishiyama, Y., Putaux, J. L., Vignon, M., and Isogai, A. (2006). “Homogeneous suspensions of individualized microfibrils from TEMPO-catalyzed oxidation of native cellulose,” *Biomacromolecules*, 7(6), 1687–1691. DOI: 10.1021/bm060154s

Salmela, J., Kiiskinen, H., and Oksanen, A. (2013). “Method for the manufacture of fibrous yarn, fibrous yarn and use of the fibrous yarn.”

Sappi. (2017). “Nanocellulose,” *https://www.sappi.com/nanocellulose*.

Sauerbrey, G. (1959). “The use of quartz oscillators for weighing thin layers and for microweighing,” *Zeitschrift für Physik*, 155(2), 206–222. DOI: 10.1007/BF01337937

Schönberg, C., Oksanen, T., Suurnäkki, A., Kettunen, H., and Buchert, J. (2001). “The importance of xylan for the strength properties of spruce kraft pulp fibres,” *Holzforschung*, 55(6), 639–644. DOI: 10.1515/HF.2001.104

Shen, Y., Orelma, H., Sneck, A., Kataja, K., Salmela, J., Qvintus, P., Suurnäkki, A., and Harlin, A. (2016). “High velocity dry spinning of nanofibrillated cellulose (CNF) filaments on an adhesion controlled surface with low friction,” *Cellulose*, 23(6), 3393–3398. DOI: 10.1007/s10570-016-1044-5

Shibata, M., Teramoto, N., Nakamura, T., and Saitoh, Y. (2013). “All-cellulose and all-wood composites by partial dissolution of cotton fabric and wood in ionic liquid,” *Carbohydrate Polymers*, Elsevier Ltd., 98(2), 1532–1539. DOI: 10.1016/j.carbpol.2013.07.062

Singh, B., Lobo, H., and Shankarling, G. (2011). “Selective N-alkylation of aromatic primary amines catalyzed by bio-catalyst or deep eutectic solvent,” *Catalysis Letters*, 141(1), 178–182. DOI: 10.1007/s10562-010-0479-9

Sirviö, J. A., Visanko, M., and Liimatainen, H. (2015). “Deep eutectic solvent system based on choline chloride-urea as a pre-treatment for nanofibrillation of wood cellulose,” *Green Chem.*, Royal Society of Chemistry, 17(6), 3401–3406. DOI: 10.1039/C5GC00398A

Sjöström, E. (1993). *Wood Chemistry: Fundamentals and Applications*, Academic

Press, London.

Sluiter, A., Hames, B., Ruiz, R., Scarlata, C., Sluiter, J., Templeton, D., and Crocker, D. (2012). “NREL/TP-510-42618 analytical procedure - Determination of structural carbohydrates and lignin in Biomass,” *Laboratory Analytical Procedure (LAP)*, (April 2008), 17. DOI: NREL/TP-510-42618

Smith, B. C. (2011). *Fundamentals of Fourier Transform Infrared Spectroscopy, Second Edition*, CRC Press.

Solala, I. (2015). “Mechanochemical reactions in lignocellulosic materials,” Aalto University, School of Chemical Technology.

Spoljaric, S., Auvinen, H., Orelma, H., Pere, J., and Seppälä, J. (2017). “Enzymatically fibrillated cellulose pulp-based monofilaments spun from water; enhancement of mechanical properties and water stability,” *Cellulose*, 24(2), 871–887. DOI: 10.1007/s10570-016-1133-5

Spoljaric, S., Salminen, A., Luong, N. D., and Seppälä, J. (2013). “Crosslinked nanofibrillated cellulose: Poly(acrylic acid) nanocomposite films; enhanced mechanical performance in aqueous environments,” *Cellulose*, 20(6), 2991–3005. DOI: 10.1007/s10570-013-0061-x

Stappers, P. J. (2006). “Designing as a Part of Research,” in: *Design and Growth of Knowledge: Best Practices and Ingredients for Successful Design Research*, R. V. D. Lugt and P. J. Stappers, eds., Delft: ID Studiolab Press, 12–17.

Suchy, M., Hakala, T., Kangas, H., Kontturi, E., Tammelin, T., Pursula, T., and Vuorinen, T. (2009). “Effects of commercial cellobiohydrolase treatment on fiber strength and morphology of bleached hardwood pulp,” *Holzforschung*, 63(6), 731–736. DOI: 10.1515/HF.2009.104

Suopajärvi, T., Sirviö, J. A., and Liimatainen, H. (2017). “Nanofibrillation of deep eutectic solvent-treated paper and board cellulose pulps,” *Carbohydrate Polymers*, Elsevier Ltd., 169, 167–175. DOI: 10.1016/j.carbpol.2017.04.009

Swatloski, R. P., Spear, S. K., Holbrey, J. D., and Rogers, R. D. (2002). “Dissolution of cellose with ionic liquids,” *Journal of the American Chemical Society*, 124(18), 4974–4975. DOI: 10.1021/ja025790m

Swerin, A., Odberg, L., Lindstrbm, T., and Pulp, S. (1990). “Deswelling of hardwood kraft pulp fibers by cationic polymers,” *Nordic Pulp and Paper Research Journal*, 5(4), 188–196.

Syverud, K., and Stenius, P. (2009). “Strength and barrier properties of MFC films,” *Cellulose*, 16(1), 75–85. DOI: 10.1007/s10570-008-9244-2

Tammelin, T., Abburi, R., Gestranius, M., Laine, C., Setälä, H., and Österberg, M. (2015). “Correlation between cellulose thin film supramolecular structures and interactions with water,” *Soft Matter*, Royal Society of Chemistry, 11(21), 4273–4282. DOI: 10.1039/C5SM00374A

Tammelin, T., Hippi, U., and Salminen, A. (2013). “Method for the preparation of NFC films on supports.”

Tammelin, T., Paananen, A., and Österberg, M. (2009). “Hemicelluloses at Interfaces: Some Aspects of the Interactions,” in: *The Nanoscience and Technology of Renewable Biomaterials*, L. A. Lucia and O. Rojas, eds., John Wiley & Sons.

Tammelin, T., Saarinen, T., Österberg, M., and Laine, J. (2006). “Preparation of Langmuir/Blodgett-cellulose surfaces by using horizontal dipping procedure. Application for polyelectrolyte adsorption studies performed with QCM-D,” *Cellulose*, 13(5), 519–535. DOI: 10.1007/s10570-005-9002-7

Tammelin, T., and Vartiainen, J. (2014). “Nanocellulose Films and Barriers,” in: *Handbook of green materials*, 213–229. DOI: 10.1142/9789814566469_0044

Tanaka, R., Saito, T., Hänninen, T., Ono, Y., Hakalahti, M., Tammelin, T., and Isogai, A. (2016). “Viscoelastic Properties of Core-Shell-Structured, Hemicellulose-Rich Nanofibrillated Cellulose in Dispersion and Wet-Film States,” *Biomacromolecules*, 17(6), 2104–2111. DOI: 10.1021/acs.biomac.6b00316

TAPPI. (2011). “TAPPI WI 3021: Standard Terms and Their Definition for Cellulose Nanomaterials, draft,” 1–6.

Tseng, S.-L., Valente, A., and Gray, D. G. (1981). “Cholesteric liquid crystalline phases based on (acetoxypropyl)cellulose,” *Macromolecules*, 14(3), 715–719. DOI: 10.1021/ma50004a049

Tsoumis, G. (1991). *Science and Technology of Wood - Structure, Properties, Utilization*, Van Nostrand Reinhold, New York.

Tunc, M. S., and Van Heiningen, A. R. P. (2008). “Hemicellulose extraction of mixed southern hardwood with water at 150 °C: Effect of time,” *Industrial and Engineering Chemistry Research*, 47(18), 7031–7037. DOI: 10.1021/ie8007105

Turbak, A. F., Snyder, F. W., and Sandberg, K. R. (1983). “Microfibrillated cellulose, a new cellulose product: properties, uses, and commercial potential,” in: *J. Appl. Polym. Sci.: Appl. Polym. Symp.*

Uetani, K., and Yano, H. (2012). “Zeta potential time dependence reveals the swelling dynamics of wood cellulose nanofibrils,” *Langmuir*, 28(1), 818–827. DOI: 10.1021/la203404g

Uhlin, K. I., Atalla, R. H., and Thompson, N. S. (1995). “Influence of hemicelluloses on the aggregation patterns of bacterial cellulose,” *Cellulose*, 2(2), 129–144. DOI: 10.1007/BF00816385

Ulbrich, M., Mühlsteff, J., Sipilä, A., Kamppi, M., Koskela, A., Myry, M., Wan, T., Leonhardt, S., and Walter, M. (2014). “The IMPACT shirt: textile integrated and portable impedance cardiography,” *Physiological Measurement*, 35(6), 1181–1196. DOI: 10.1088/0967-3334/35/6/1181

VanderHart, D. L., and Atalla, R. H. (1984). “Studies of microstructure in native celluloses using solid-state carbon-13 NMR,” *Macromolecules*, 17(8), 1465–1472. DOI: 10.1021/ma00138a009

Vartiainen, J., Kaljunen, T., Kunnari, V., Lahtinen, P., and Tammelin, T. (2013). “Large-Scale Production of CNF Films,” in: *Production and Applications of Cellulose Nanomaterials*, TAPPI, 239–240.

Wada, M., Heux, L., and Sugiyama, J. (2004). “Polymorphism of cellulose I family: Reinvestigation of cellulose IVI,” *Biomacromolecules*, 5(4), 1385–1391. DOI: 10.1021/bm0345357

Walther, A., Timonen, J. V. I., Díez, I., Laukkanen, A., and Ikkala, O. (2011). “Multifunctional high-performance biofibers based on wet-extrusion of renewable native cellulose nanofibrils,” *Advanced Materials*, 23(26), 2924–2928. DOI: 10.1002/adma.201100580

Wan, J., Wang, Y., and Xiao, Q. (2010). “Effects of hemicellulose removal on cellulose fiber structure and recycling characteristics of eucalyptus pulp,” *Bioresource Technology*, Elsevier Ltd, 101(12), 4577–4583. DOI: 10.1016/j.biortech.2010.01.026

Wen, Q., Chen, J. X., Tang, Y. L., Wang, J., and Yang, Z. (2015). “Assessing the toxicity and biodegradability of deep eutectic solvents,” *Chemosphere*, Elsevier Ltd, 132, 63–69. DOI: 10.1016/j.chemosphere.2015.02.061

Whitney, S. E. C., Brigham, J. E., Darke, A. H., Reid, J. S. G., and Gidley, M. J. (1998). “Structural aspects of the interaction of mannanbased polysaccharides with bacterial cellulose,” *Carbohydrate Research*, 307(3–4), 299–309. DOI: 10.1016/S0008-6215(98)00004-4

Wiley, J. H., and Atalla, R. (1987). “Band assignments in the Raman-spectra of celluloses,” *Carbohydrate Research*, 160, 113–129. DOI:

dx.doi.org/10.1016/0008-6215(87)80306-3

Willberg-Keyriläinen, P., Hiltunen, J., and Ropponen, J. (2017). “Production of cellulose carbamate using urea-based deep eutectic solvents,” *Cellulose*. DOI: 10.1007/s10570-017-1465-9

Willför, S., Pranovich, A., Tamminen, T., Puls, J., Laine, C., Suurnäkki, A., Saake, B., Uotila, K., Simolin, H., Hemming, J., and Holmbom, B. (2009). “Carbohydrate analysis of plant materials with uronic acid-containing polysaccharides-A comparison between different hydrolysis and subsequent chromatographic analytical techniques,” *Industrial Crops and Products*, 29(2–3), 571–580. DOI: 10.1016/j.indcrop.2008.11.003

Wilson, B. P., Paukkonen, N., Yliniemi, K., Hakalahti, M., Tammelin, T., Kontturi, E., and Lundström, M. (2017). “Deposition of Ultrathin Cellulose Nanofibers Films As Bio-Implant Corrosion Coatings,” in: *In Meeting Abstracts: The Electrochemical Society*, 930–930.

Woodings, C. (2001). *Regenerated cellulose fibres*, Woodhead Publishing Limited. DOI: 10.1533/9781855737587

Wågberg, L., Winter, L., Ödberg, L., and Lindström, T. (1987). “On the charge stoichiometry upon adsorption of a cationic polyelectrolyte on cellulosic materials,” *Colloids and Surfaces*, 27(4), 163–173. DOI: 10.1016/0166-6622(87)80140-3

Wågberg, L., Österberg, M., and Enarsson, J.-E. (2010). “Interactions at cellulose model surfaces,” in: *Encyclopedia of Surface and Colloid Science*, Taylor & Francis, London, UK, 1–19.

Yang, R., Aubrecht, K. B., Ma, H., Wang, R., Grubbs, R. B., Hsiao, B. S., and Chu, B. (2014). “Thiol-modified cellulose nanofibrous composite membranes for chromium (VI) and lead (II) adsorption,” *Polymer (United Kingdom)*, 55(5), 1167–1176. DOI: 10.1016/j.polymer.2014.01.043

Young, G. H., and Rowland, B. N. (1933). “The relation between hydration capacity and pentosan content of softwood pulps,” *Paper Trade Journal*, 97(15), 44–46.

Zhang, L. N., Ruan, D., and Zhou, J. P. (2001). “Structure and properties of regenerated cellulose films prepared from cotton linters in NaOH/Urea aqueous solution,” *Industrial & Engineering Chemistry Research*, 40(25), 5923–5928. DOI: Doi 10.1021/Ie0010417

Zhao, C., Zhang, H., Zeng, X., Li, H., and Sun, D. (2016). “Enhancing the inter-fiber bonding properties of cellulosic fibers by increasing different fiber charges,”

Cellulose, Springer Netherlands, 23(3), 1617–1628. DOI: 10.1007/s10570-016-0941-y

Österberg, M., and Claesson, P. M. (2000). “Interactions between cellulose surfaces: effect of solution pH,” *Journal of Adhesion Science and Technology*, 14(5), 603–618. DOI: 10.1163/156856100742771

Österberg, M., Laine, J., Stenius, P., Kumpulainen, A., and Claesson, P. M. (2001). “Forces between Xylan-Coated Surfaces: Effect of Polymer Charge Density and Background Electrolyte,” *Journal of Colloid and Interface Science*, 242(1), 59–66. DOI: 10.1006/jcis.2001.7752

Österberg, M., and Valle-Delgado, J. J. (2017). “Surface forces in lignocellulosic systems,” *Current Opinion in Colloid and Interface Science*, Elsevier Ltd, 27, 33–42. DOI: 10.1016/j.cocis.2016.09.005

Österberg, M., Vartiainen, J., Lucenius, J., Hippi, U., Seppälä, J., Serimaa, R., and Laine, J. (2013). “A fast method to produce strong NFC films as a platform for barrier and functional materials,” *ACS Applied Materials and Interfaces*, 5(11), 4640–4647. DOI: 10.1021/am401046x

Paper I

Tenhunen Tiia-Maria; Hakalahti Minna; Kouko Jarmo; Salminen Arto; Härkäsalmi Tiina; Pere Jaakko; Harlin Ali; Hänninen Tuomas (2016). Method for Forming Pulp Fibre Yarns Developed by a Design-driven Process, BioResources 11(1), 2492-2503

Method for Forming Pulp Fibre Yarns Developed by a Design-driven Process

Tiia-Maria Tenhunen,[a] Minna Hakalahti,[a] Jarmo Kouko,[a] Arto Salminen,[b] Tiina Härkäsalmi,[c] Jaakko Pere,[a] Ali Harlin,[a] and Tuomas Hänninen [a, d,]*

A simple and inexpensive method for producing water-stable pulp fibre yarns using a deep eutectic mixture composed of choline chloride and urea (ChCl/urea) was developed in this work. Deep eutectic solvents (DESs) are eutectic mixtures consisting of two or more components that together have a lower melting point than the individual components. DESs have been previously studied with respect to cellulose dissolution, functionalisation, and pre-treatment. This new method uses a mixture of choline chloride and urea, which is used as a swelling and dispersing agent for the pulp fibres in the yarn-forming process. Although the pulp seemed to form a gel when dispersed in ChCl/urea, the ultrastructure of the pulp was not affected. To enable water stability, pulp fibres were crosslinked by esterification using polyacrylic acid. ChCl/urea could be easily recycled and reused by distillation. The novel process described in this study enables utilisation of pulp fibres in textile production without modification or dissolution and shortening of the textile value chain. An interdisciplinary approach was used, where potential applications were explored simultaneously with material development from process development to the early phase prototyping.

Keywords: Softwood pulp; Fibre yarn; Deep eutectic solvent; Polyacrylic acid

*Contact information: a: VTT Technical Research Centre of Finland Ltd, P. O. Box 1000, FI-02044 VTT, Finland; b: Aalto University School of Chemical Technology, Polymer Technology, Department of Biotechnology and Chemical Technology, P.O. Box 16100, 00076 Aalto, Finland; c: Aalto University School of Arts, Design and Architecture, P.O. Box 31000, 00076 Aalto, Finland; d: Lumir Oy, Valimotie 22, 01510 Vantaa, Finland; *Corresponding author: tuomas.hanninen@lumir.fi*

INTRODUCTION

To add value to materials, a material-oriented design approach is often employed, focusing on a multidimensional perspective of the material properties. In addition to technical parameters, perceptual qualities are also considered, *e.g.*, tactility and visual appearance (Ashby *et al.* 2009; Ashby and Johnson 2010). A design-driven approach can positively contribute to every step of the research process and steer the material development in a more user-oriented direction to enhance its future potential in novel applications. A sustainable design-driven approach in the development of new materials requires a holistic life cycle perspective.

Wood-based pulp is commonly used to produce two-dimensional web structures such as paper and paperboard. However, in this study, it was utilised to produce a one-dimensional structure: fibre yarn. Utilisation of pulp fibres without dissolution would decrease the number of processing steps needed to produce the fibre yarns and enable the exploitation of natural wood fibre properties.

Forming fibre yarn from wood pulp is not as simple as it is with other fibrous materials. The long fibres of flax or staple fibres of cotton naturally form strong yarns, whereas short, wood-based cellulose fibres cannot be spun using current methods and have a tendency to disintegrate in water. Therefore, wood fibres are commonly used to form yarn through dissolution and regeneration processes. These processes result in man-made cellulosic textile fibres, *e.g.*, viscose, modal, and lyocell (Woodings 2001). Fibre yarn preparation without the dissolution of cellulose has been demonstrated using normal pulps (Salmela *et al.* 2014) and cellulose nanofibrils (CNF) (Iwamoto *et al.* 2011; Walther *et al.* 2011; Håkansson *et al.* 2014).

Environmental concerns are important when designing a new process or product. Fibre yarns prepared from wood pulp are considered to be more environmentally friendly than cotton, for example, which can consume up to 11 m^3 water/kg during production. It has also been predicted that by 2030, one-third of textile fibres must be produced with cellulose fibres, and cotton production cannot be increased because of the limited availability of arable land (Hämmerle 2011). Therefore, infrastructure for wood-based cellulose fibre yarns in applications that traditionally use cotton is needed.

This method for fibre yarn production was designed to use an environmentally friendly and easily recyclable choline chloride and urea mixture (ChCl/urea) as a solvent. ChCl/urea is a deep eutectic solvent (DES): a eutectic mixture with a melting point lower than that of its individual components. DESs have comparable physicochemical qualities to ionic liquids, but are much cheaper and more environmentally friendly (Abbott *et al.* 2004; Jhong *et al.* 2009; Zhang *et al.* 2012a). Recyclability of the ChCl/urea was evaluated by studying the recycled solvent after fibre yarn production.

In the method described in this paper, fibre yarns were prepared from dope, where ChCl/urea acted as a rheology modifier. The suspension of ChCl/urea and pulp became gel-like and could be extruded into a solvent bath. Rheology could be further modified with a small addition of polyacrylic acid (PAA), which also functioned as a crosslinking agent that provided water stability to the fibre yarns. The effects of PAA addition on morphology and mechanical properties were analysed.

In design-driven development of materials, the final product is not considered the driving force of research. Possible applications are determined by the intrinsic properties of the developed material. The novel pulp fibre yarns demonstrated in this study can be used not only in textiles but also in composite applications.

EXPERIMENTAL

Materials

Never-dried, bleached softwood pulp was supplied by a mill in central Finland. Polyacrylic acid (PAA) (M_v ~450 000 mol/g), urea, and ChCl were purchased from Sigma-Aldrich, USA. All chemicals and solvents were of analytical grade and used as received.

Preparation of Dope

ChCl/urea was prepared using a modified procedure according to Abbott *et al.* (2003). ChCl and urea were mixed together in a molar ratio of 1:2, respectively, and heated at 100 °C with constant stirring (in a closed system) until a clear homogenous liquid was formed.

The pulp was washed with excess acetone and dried before preparation of the dope. Washed pulp, PAA, and ChCl/urea were dried at 40 °C overnight in vacuum and stored in a desiccator.

Dopes were prepared by dispersing pulp in ChCl/urea overnight at 100 °C with constant stirring. Dispersions were then cooled to room temperature and mixed in a SpeedMixer (FlackTek Inc., UK) in a vacuum (800 rpm for 2 min and 1500 rpm for 8 min). PAA was added to the suspension and mixed with the SpeedMixer. Dopes with a dry matter content of 4.5 wt% were prepared with varying PAA concentrations (0%, 5%, 10%, and 25%). Dopes were stored in a desiccator until use.

Capillary viscometry

Viscosity average molecular weights of the untreated pulp sample and pulp sample after ChCl/urea and were determined by capillary viscometry according to ISO 5351 (2004). Prior to measurement, samples were washed and filtrated (1 µm) using distilled water and dried in a vacuum at 40 °C.

^{13}C CP MAS NMR spectroscopy

^{13}C cross polarisation magic angle spinning (CP MAS) NMR spectrometer (Bruker AVANCE-III 400 MHz, Bruker BioSpin, Germany) was used to measure spectra from the untreated reference sample and a pulp sample kept in ChCl/urea overnight (~16 h) at 100 °C. Both samples were washed thoroughly with acetone and dried in a vacuum oven (40 °C, overnight) prior to measurements.

CP MAS NMR spectroscopy was used to characterise the solid-state structures of the untreated pulp and pulp sample after dispersing and washing procedures. For each sample, 10,000 scans were collected using 8 kHz spinning frequency, 2 ms contact time, and 5 s delay between pulses.

Formation of Pulp Fibre Yarn

Pulp fibre yarns were produced using a laboratory-scale device (assembled at VTT). Dope was extruded at a constant speed (~1.4 mL/min) into ethanol from a 5-mL syringe through a tapered tip with a 0.63-mm diameter nozzle. Fibre yarns were washed in ethanol in order to remove DES for at least 10 min and dried in ambient conditions. Subsequently, fibre yarns were dipped in room temperature distilled water for 5 s and placed in an oven at 140 °C for 30 min. The process is illustrated in Fig. 1.

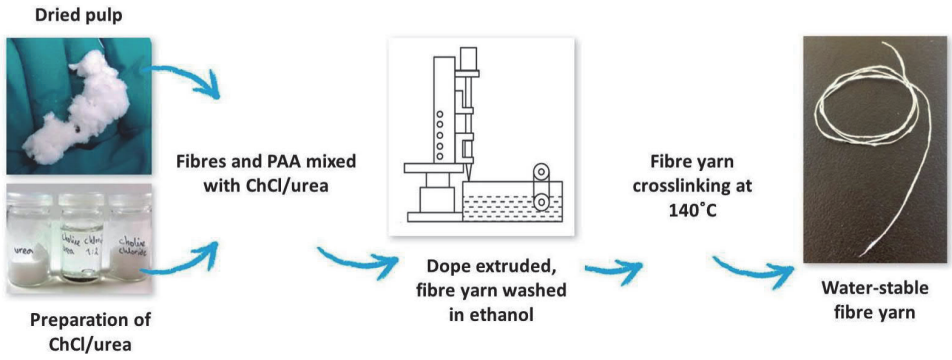

Fig. 1. Process chart for producing the fibre yarn

Tensile testing of fibre yarns

A C-Impact fast strain rate tensile tester (assembled at VTT) was used for the tensile testing. The span length of the sample was 50 mm. The strain rate was 1 mm/s (2 %/s). The accuracy of displacement and force measurements were better than 6 µm and 15 mN, respectively.

Prior to tensile testing the dry fibre yarn, samples were stored at 23 °C in 50% relative humidity (RH) for at least 24 h. Some of the fibre yarns were immersed in water for 24 h to analyse the wet strength. Tenacity (cN/tex) values were calculated dividing ultimate breaking force of the fibre yarns by the linear density, tex (g/km). The weight of all the fibre yarns were measured at 50% RH and 23 °C temperature.

SEM

Scanning electron microscopy (SEM) (Merlin® FE-SEM, Carl Zeiss NTS GmbH, Germany) was used to study the morphology of the fibre yarns with various pulp:PAA ratios. Samples were prepared on double-sided carbon adhesive discs attached to aluminium specimen stubs. Prior to imaging, the samples were sputter-coated (Agar™ Auto Sputter Coater, England) with platinum (Pt) to improve specimen conductivity. The imaging was conducted using 3.0 keV electron energy and 30 pA probe current. The pixel resolution was 2048 × 1536.

FT-IR

An FT-IR spectrometer with ATR diamond (Thermo Scientific™ Nicolet™ iS™50 FT-IR Spectrometer, United States) was used to study the chemical structure of crosslinked and non-crosslinked fibre yarns with 10% PAA. Spectra of pure cellulose and DES were acquired for references. The spectrum for PAA was acquired from Aldrich FT-IR collection edition II. All spectra were obtained from 32 scans with a resolution of 4 cm^{-1} and transmission mode from 350 to 4000 cm^{-1}.

Recycling ChCl/urea

Four millilitres of dope (ChCl/urea 95.5%, pulp 4.05%, PAA 0.45%) was extruded in ethanol (50 mL) that was evaporated in ambient conditions overnight to study the recycling of ChCl/urea; the remaining liquid fraction was studied using FT-IR and compared to the measured pure ChCl/urea.

RESULTS AND DISCUSSION

Effect of ChCl/Urea on Pulp Properties

The fibre yarn preparation process that utilises cellulose has a tendency to form a highly viscose gel-like suspension with ChCl/urea. The formation of cellulose gel is commonly associated with swelling and dissolution. It has been proposed that ChCl/urea interacts with cellulose; however, there are no studies on how ChCl/urea affects the structure of cellulose (Abbott *et al.* 2006; Sirviö *et al.* 2015).

Changes in the cellulosic structure caused by ChCl/urea treatment were analysed using capillary viscometry and ^{13}C CP MAS NMR, which can be used to distinguish different crystalline allomorphs of cellulose. The ^{13}C CP MAS NMR spectrum of the pulp did not change after being dispersed in ChCl/urea overnight at 100 °C (Fig. 2). Spectra of both samples resembled the spectrum of native form cellulose I reported in the literature

(Atalla and Vanderhart 1984). This indicates that the crystalline structure and chemical composition remained mostly unchanged by the ChCl/urea, which is in the agreement with previous studies (Zhang *et al*. 2012b; de Olivieira Vigier and Jerome 2014). In addition, no new peaks were observed, which indicates a lack of degradation products.

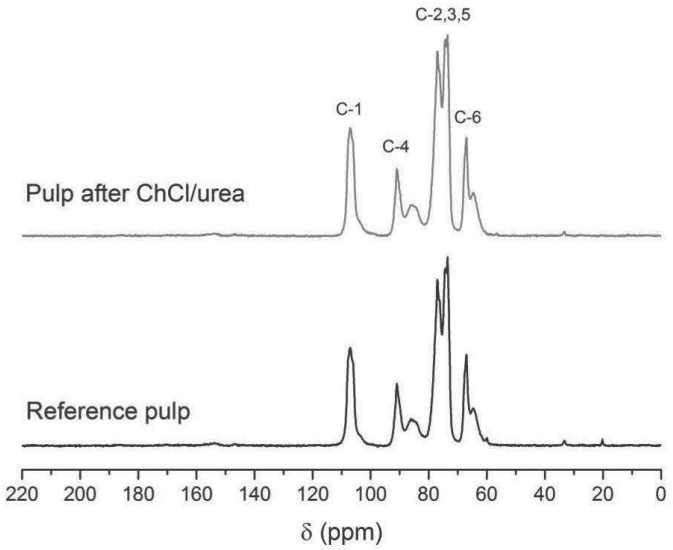

Fig. 2. ^{13}C CP MAS NMR spectrum of bleached softwood pulp before (bottom) and after (top) dispersing in ChCl/urea at 100 °C overnight

The degree of polymerisation (DP) of cellulose was approximated from the intrinsic viscosity of cellulose dissolved in cupriehylenediamine measured with a capillary viscometer (da Silva Perez and van Heiningen 2002; ISO 5351 2004). According to the measurements, the DP of cellulose decreased only slightly after being dispersed in ChCl/urea overnight at 100 °C, from 1226 (± 0.5%) to 1194 (± 0.8%). Such a difference could be the result of mechanical damage caused by stirring, for example.

Fibre Yarn Morphology and Chemical Crosslinking

SEM micrographs of the fibre yarns (Fig. 3) show that most of the pulp fibres became well aligned along the fibre yarn axis. Good fibre orientation can be assumed to have a positive effect on the strength properties of fibre yarn. The structure of fibre yarns, according to SEM micrographs, appears to be porous. Fibres had not been packed tightly together and voids can be seen between them. Such a structure is likely to be caused by the solvent used to wash the ChCl/urea. The polarity of the solvent has a significant effect on shrinkage and formation of hydrogen bonds during cellulose drying (Klemm *et al.* 1998).

The PAA concentration of the dope does not seem to have affected the morphology of the fibre yarns. Even up to the addition of 25 wt% of PAA, pulp fibres can be clearly distinguished. The PAA content did not affect the linear densities of the fibre yarns, which were between 21 and 24 tex.

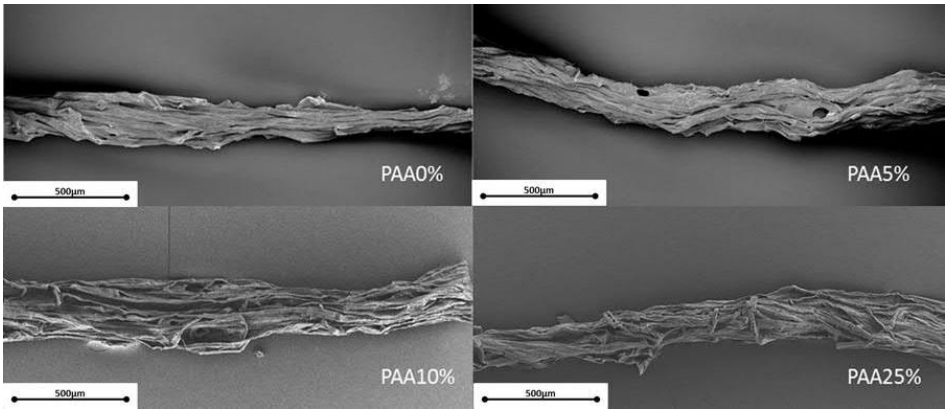

Fig. 3. SEM micrographs of pulp-PAA fibre yarns

Pulp fibres were crosslinked with different amounts of PAA using heat-initiated esterification (Fig. 4a), where carboxyl groups of PAA form ester bonds with hydroxyl groups of cellulose (Spoljaric *et al.* 2013; Hakalahti *et al.* 2015) to provide water stability to fibre yarns and increase tensile strength. This process was enhanced by quickly immersing the dried fibre yarns into water prior to crosslinking at 140 °C.

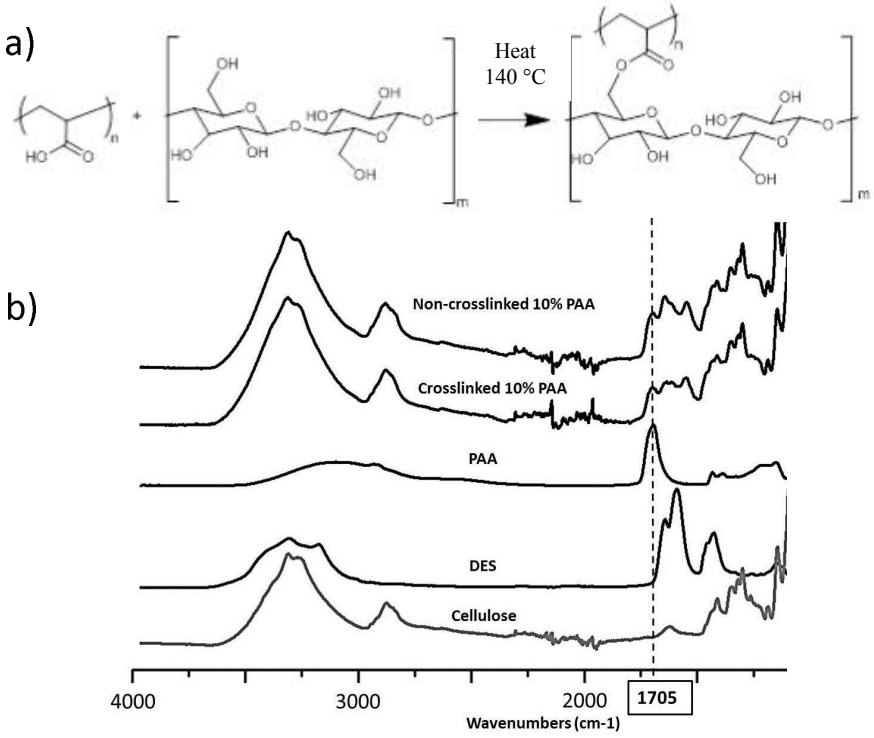

Fig. 4. (a) Crosslinking pulp fibres with PAA by heat initiated esterification and (b) IR spectra measured from untreated and crosslinked fibre yarns with 10% PAA

An FT-IR spectrometer was used to analyse the bonding between cellulose and PAA. However, crosslinking could not be distinguished from IR spectra (Fig. 4b). In dense CNF films, structural crosslinking has been seen as a shift of the carbonyl band in the 1705 cm^{-1} region (Spoljaric *et al.* 2013). The amount of linkages formed in the studied fibre yarns is likely to be so low that it cannot be seen from the spectra, but sufficient enough to provide water stability.

Mechanical Properties of Fibre Yarns

The mechanical properties of the fibre yarns (Fig. 5) were analysed in a dry (RH 50%) and wet state. The reinforcing effect of PAA can be seen from the tenacities of the dry fibre yarns. Tenacity seemed to reach its maximum near 10% PAA content. The declining tenacity curve indicates that above 10%, PAA is left unbound or crosslinked with a single fibre and is not contributing to bridging. Tenacities of cotton and viscose measured using our tensile tester were 16.2 cN/tex and 15 cN/tex, respectively.

A similar trend could also be seen with water-soaked fibre yarns. However, the differences between fibre yarns with different PAA contents were less prominent in this case. Wet fibre yarn without any PAA could not be mounted in the tensile tester. In fibre yarns without PAA, only hydrogen bonds hold the fibres together and they are cleaved upon immersion in water. The wet strengths of the PAA-containing fibre yarns were roughly 1/3 of the dry strengths, which indicates that in addition to crosslinking by PAA, hydrogen bonding between fibres also played an important role in a dry state.

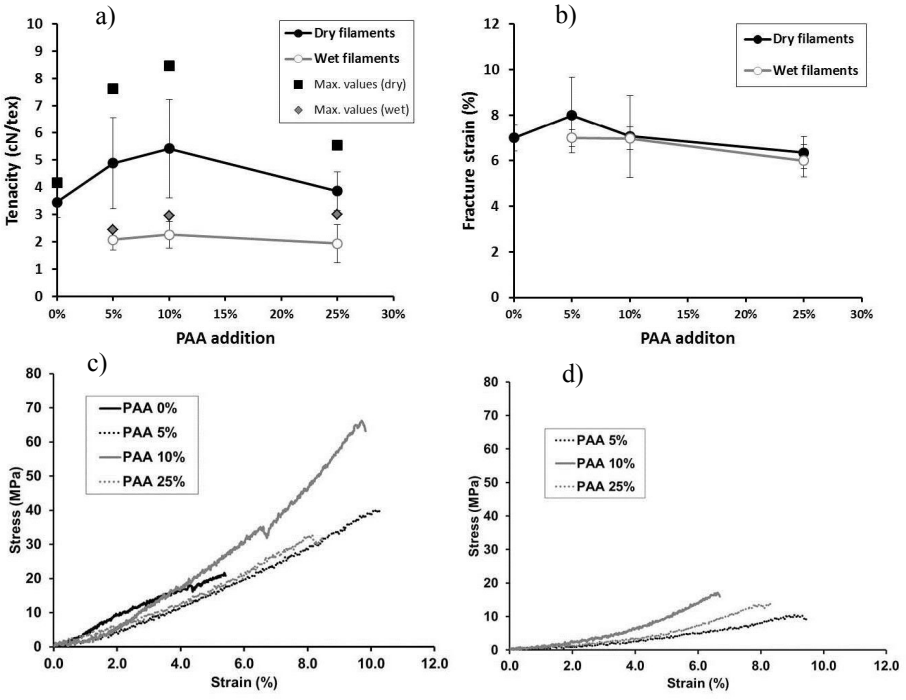

Fig. 5. Average tenacities and measured maximum tenacity values (a) and fracture strain (b) measured from dry and wet samples. Stress-strain curves from dry (c) and wet (d) from most presentable fibre yarns

The fracture strain of the fibre yarns seemed to decrease with increasing PAA content, which could be an indication of decreasing PAA bridging between fibres. The fracture strain values for the fibre yarns were at a similar level as cotton (8.5%) and approximately half the value of viscose (16.4%). Imperfect shape and defects in the fibre yarn affected the mechanical strength values negatively, which can be observed from the long error bars. No marked differences could be seen between the fracture strains of the dry and wet samples. This could indicate that PAA plays an important role in tensile load bearing.

Stress strain curves of the most presentable fibre yarns (no weak spots) were chosen to Fig. 5c (dry) and 5d (wet). The stress-strain behaviour of the studied yarns was non-linear and strain hardening phenomenon was clearly detectable in the stress-strain curves of the yarns with addition of PAA. This can be considered as an indirect implication that crosslinking is improving the strength after hydrogen bonding. In wet fibre yarns, where interfibre hydrogen bonding plays a minor role, the strength is provided by PAA-cellulose bonds. Average tensile strengths are presented in Table 1.

Table 1. Average Tensile Strengths and Standard Deviations

	Tensile strength, MPa	Tensile strength SD, MPa
PAA 0%	13.35	3.78
PAA 5%	23.81	8.80
PAA 10%	33.55	15.60
PAA 25%	20.35	7.17
PAA 5% WET	9.49	1.73
PAA 10% WET	13.13	2.87
PAA 25% WET	8.61	3.12

Because the tensile strength values of fibre yarns were noticeably lower than values of individual pulp fibres (~1 000 MPa) (Faruk and Sain 2013), it seems that inter-fibre bonding dominated in the mechanical properties of the fibre yarns. Using more fibrillated fibres or enhancing the fibre-fibre bonding area by other means, the mechanical properties of fibre yarns could be improved significantly. According to the literature (Häyrinen 1973), twisting even a single filament improves tenacity values, and plying and cabling several filaments improves those values even more. Improving the mechanical properties of the fibre yarns will be in the scope of following studies.

Recycling the Chemicals

Recyclability of the process chemicals is an important factor in designing a new process. Recycling the process chemicals not only decreases the environmental impact of the process, but also makes it economically more attractive.

FT-IR spectra (Fig. 6) of freshly prepared and recycled ChCl/urea collected from ethanol used for washing DES from fibre yarns were identical, and no bands arising from PAA or pulp could be observed. This indicates that recycling ChCl/urea can easily be done by evaporating the ethanol used for regeneration. There are also studies where ChCl/urea has been successfully recycled in different processes (Singh *et al*. 2011; Azizi and Gholibegloa 2012; Lobo *et al.* 2012). The ethanol can also be reused using fractional distillation.

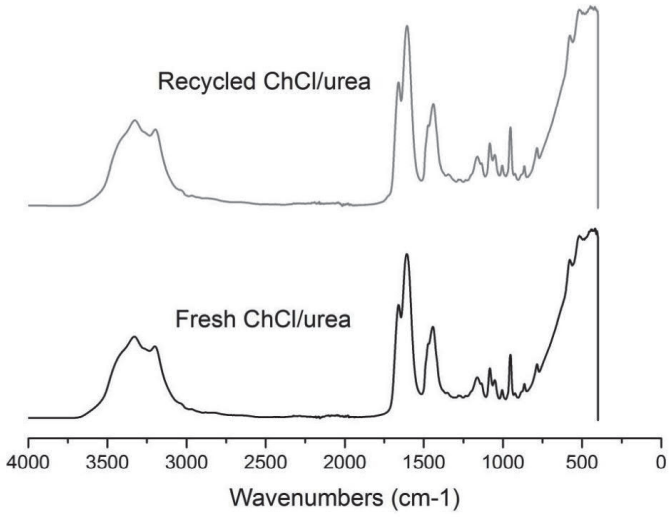

Fig. 6. FT-IR spectra of recycled and fresh ChCl/urea

In the sustainable design approach, the whole life cycle of the fibre yarn from manufacturing to recycling is taken into consideration. Cellulose, which is the main component of the fibre yarns, is easily recyclable. However, PAA, with a molecular weight over ~700 Mw is not biodegradable. Despite this fact, PAA has been used for decades in cleaning products and detergents and can be efficiently removed during wastewater treatment. Additionally, its toxicity to aquatic and terrestrial organisms is low (Freeman and Bender 1993; Larson *et al*. 1997). Replacing PAA with bio-based crosslinkers will be in the scope of future studies.

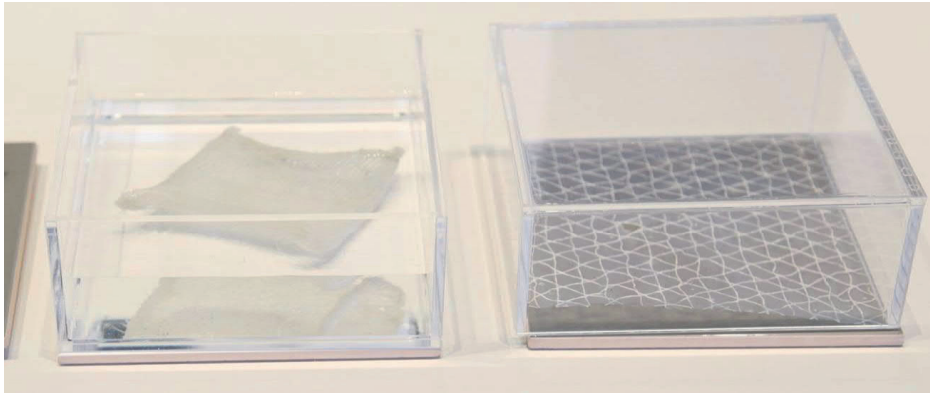

Fig. 7. Early phase prototyping: knitted sample in water (left), composite structure: fibre yarn embedded into a nanocellulose film (right), photo: Eeva Suorlahti

Novel pulp fibre yarn has applications in textiles as well as composites. From a design-driven perspective, the inherent properties of the materials should be well utilised in its intended applications. As cellulose has good affinity to itself, fibre yarns can be used

as reinforcement in all-cellulose composites (Fig. 7). By embedding a textile structure prepared from the fibre yarn into a nanocellulose film structure, the inherently brittle nanocellulose films could be made easier to handle.

CONCLUSIONS

1. A new, simple, and inexpensive method for producing water-stable pulp fibre yarns using a DES composed of choline chloride and urea was developed.
2. ChCl/urea can be used as a dispersion medium for fibre yarn formation without affecting the pulp ultrastructure. The method allows the cellulose I crystalline structure to remain in the fibre yarn.
3. All of the process chemicals are recyclable and reusable.
4. The novel process enables shortening of the textile value chain.

ACKNOWLEDGMENTS

This work was done in TEKES-funded Design Driven Value Chains in the World of Cellulose– project cooperation with Aalto University School of Arts, Design and Architecture and School of Chemical Technology. This work made use of Joint Aalto University and VTT Bioeconomy Infrastructure.

REFERENCES CITED

Abbott, A., Capper, G., Davies, D., Rasheed, R., and Tambyrajah, V. (2003). "Novel solvent properties of choline chloride/urea mixtures," *Chem. Commun*. 1(1), 70-71. DOI: 10.1039/b210714g

Abbott, A., Boothby, D., Capper, G., Davies, D., and Rasheed, R. (2004). "Deep eutectic solvents formed between choline chloride and carboxylic acids: Versatile alternatives to ionic liquids," *J. Am. Chem. Soc.* 126(29), 9124-9147. DOI: 10.1021/ja048266

Abbott, A., Bell, T., Handa, S., and Stoddart, B. (2006). "Cationic functionalization of cellulose using a choline chloride based ionic liquid analogue," *Green Chem.* 8(1), 784-786. DOI: 10.1039/B605258D

Ashby, M. F., and Johnson, K. (2010). *Materials and Design: The Art and Science of Material Selection in Product Design* (2nd Ed.), Elsevier, Oxford, UK.

Ashby, M. F., Ferreira, P. J., and Schodek, D. L. (2009). *Nanomaterials, Nanotechnologies and Design: An Introduction for Engineers and Architects*, Elsevier, Oxford, UK.

Atalla, R., and Vanderhart, D. (1984). "Native cellulose: A composite of two distinct crystalline forms," *Science* 223(4633), 283-285. DOI: 10.1126/science.223.4633.283

Azizi, N., and Gholibegloa, E. (2012). "A highly efficient synthesis of dithiocarbamates in green reaction media," *RSC Adv*. 2(1), 7413-7416. DOI: 10.1039/C2RA20615C

Faruk, O., and Sain, M. (2013). *Developments in Fiber-reinforced Polymer (FRP) Composites for Civil Engineering*, Uddin, N. (ed.), Woodhead Publishing Limited, Cambridge, UK.

Freeman, M. B., and Bender, T. M. (1993). "An environmental fate and safety assessment for a low molecular weight polyacrylate detergent additive," *Environ. Technol.* 14(2), 101-112. DOI: 10.1080/09593339309385269

Hämmerle, F. (2011). "Cellulose gap (The future of cellulose fibres)," *Lenzinger Berichte* 89(1), 12-21.

Hakalahti, M., Salminen, A., Seppälä, J., Tammelin, T., and Hänninen, T. (2015). "Effect of interfibrillar PVA bridging on water stability and mechanical properties of TEMPO/$NaClO_2$ oxidized cellulosic nanofibril films," *Carbohydr. Polym.* 126, 78-82. DOI: 10.1016/j.carbpol.2015.03.007

Håkansson, K. M. O., Fall, A. B., Lundell, F., Yu, S., Krywka, C., Roth, S. V., Santoro, G., Kvick, M., Prahl Wittberg, L., Wågberg, L., and Söderberg, L. D. (2014). "Hydrodynamic alignment and assembly of nanofibrils resulting in strong cellulose fibre yarns," *Nature Commun.* 5(1), 1-10. DOI: 10.1038/ncomms5018

Häyrinen, E. (1973). *Kehruuteknologia,* Otaniemi, Teknillisen Korkeakoulun Ylioppilaskunta.

ISO 5351 (2004). Pulps, "Determination of limiting viscosity number in cupri-ethylenediamine (CED) solution"

Iwamoto, S., Isogai, A., and Iwata, T. (2011). "Structure and mechanical properties of wet-spun fibers made from natural cellulose nanofibers," *Biomacromolecules* 12(3), 831-836. DOI: 10.1021/bm101510r

Jhong, H. R., Wong, D., Wan, C. C., Wang, Y. Y., and Wei, T. C. (2009). "A novel deep eutectic solvent-based ionic liquid used as electrolyte for dye-sensitized solar cells," *Electrochem. Commun.* 11(1), 209-211. DOI: 10.1016/j.elecom.2008.11.001

Klemm, D., Philipp, B., Heinze, T., Heinze, U., and Wagenknecht, W. (1998). *Comprehensive Cellulose Chemistry, Volume l, Fundamentals and Analytical Method*, Viley-VHC, New York.

Larson, R. J., Bookland, E. A., Williams, R. T., Yocom, K. M., Saucy, D. A., Freeman, M. B., and Swift, G. (1997). "Biodegradation of acrylic acid polymers and oligomers by mixed microbial communities in activated sludge," *J. Environ. Polym. Degrad.* 5(1), 41-48. DOI: 10.1007/BF02763567

Lobo, H., Singh, B., and Shankarling, G. (2012). "Deep eutectic solvents and glycerol: A simple, environmentally benign and efficient catalyst/reaction media for synthesis of N-aryl phthalimide derivatives," *Green Chem. Lett. Rev.* 5(4), 487-533. DOI: 10.1080/17518253.2012.669500

de Oliveira Vigier, K., and Jérôme, F. (2014). *Biofuels and Biorefineries 1: Production of Biofuels and Chemicals with Ionic Liquids*, Fang, Z., Smith, R. Jr., and Qi, X. (eds.), Springer Science+Business Media, Dordrecht, Netherlands.

Salmela, J., Kiiskinen, H., and Oksanen, A. (2014). "Method for the manufacture of fibrous yarn," *US Patent 20140331893 A1*.

da Silva Perez, D., and van Heiningen, A. R. P. (2002). "Determination of cellulose degree of polymerization in chemical pulps by viscosimetry," *Seventh European Workshop on Lignocellulosics and Pulp proceedings*, Turku, Finland, pp. 393-396.

Singh, B., Lobo, H., and Shankarling, G. (2011). "Selective N-alkylation of aromatic primary amines catalyzed by bio-catalyst or deep eutectic solvent," *Catal. Lett.* 141(1), 178-182. DOI: 10.1007/s10562-010-0479-9

Sirviö, J. A., Visanko, M., and Liimatainen, H. (2015). "Deep eutectic solvent system based on choline chloride-urea as a pre-treatment for nanofibrillation of wood cellulose," *Green Chem.* 17(1), 3401-3406. DOI: 10.1039/C5GC00398A

Spoljaric, S., Salminen, S., Luong, N. D., and Seppälä, J. (2013). "Crosslinked nanofibrillated cellulose: Polyacrylic acid nanocomposite films; Enhanced mechanical performance in aqueous environment," *Cellulose* 20(6), 2991-3005. DOI: 10.1007/s10570-013-0061-x

Walther, A., Timonen, J. V. I., Diez, I., Laukkanen, A., and Ikkala, O. (2011). "Multifunctional high-performance biofibers based on wet-extrusion of renewable native cellulose nanofibrils," *Adv. Mat.* 23(26), 2924-2928. DOI: 10.1002/adma.201100580

Woodings, C. (2001). "A brief history of regenerated cellulose fibres," in: *Regenerated Cellulose Fibres*, Woodings, C (eds.) Textile Institute, Manchester, UK, pp. 1-20

Zhang, Q., de Oliveira Vigier, K., Royer, S., and Jérôme, F. (2012a). "Deep eutectic solvents: Syntheses, properties and applications," *Chem. Soc. Rev.* 41(21), 7108-7146. DOI: 10.1039/C2CS35178A

Zhang, Q., Benoit, M., de Olivieira Vigier, K., Barrault, J., and Jérôme, F. (2012b). "Green and inexpensive choline-derived solvents for cellulose decrystallization," *Chem. Eur. J.* 18(4), 1043-1046. DOI: 10.1002/chem.201103271

Article submitted: August 17, 2015; Peer review completed: October 16, 2015; Revised version received and accepted: November 23, 2015; Published: January 26, 2016.
DOI: 10.15376/biores.11.1.2492-2503

Paper II

Tenhunen Tiia-Maria; Lewandowska Anna E.; Orelma Hannes; Johansson Leena-Sisko; Virtanen Tommi; Harlin Ali; Österberg Monika; Eichhorn Stephen J.; Tammelin Tekla (2018) Understanding the interactions of cellulose fibres and deep eutectic solvent of choline chloride and urea. Cellulose 25,137-150

Cellulose (2018) 25:137–150
https://doi.org/10.1007/s10570-017-1587-0

ORIGINAL PAPER

Understanding the interactions of cellulose fibres and deep eutectic solvent of choline chloride and urea

Tiia-Maria Tenhunen · Anna E. Lewandowska · Hannes Orelma · Leena-Sisko Johansson · Tommi Virtanen · Ali Harlin · Monika Österberg · Stephen J. Eichhorn · Tekla Tammelin

Received: 21 June 2017 / Accepted: 17 November 2017 / Published online: 5 December 2017

Abstract A deep eutectic solvent composed of choline chloride (ChCl) and urea has been recently introduced as a promising cellulose compatible medium that enables e.g. fibre spinning. This paper clarifies the influence of such a solvent system on the structure and chemical composition of the cellulosic pulp fibres. Special emphasis was placed on the probable alterations of the chemical composition due to the dissolution of the fibre components and/or due to the chemical derivatisation taking place during the DES treatment. Possible changes in fibre morphology were studied with atomic force microscopy and scanning electron microscopy. Chemical compositions of pulp fibres were determined from the carbohydrate content, and by analysing the elemental content. Detailed structural characterisation of the fibres was carried out using spectroscopic methods; namely X-Ray Photoelectron Spectroscopy, solid state Nuclear Magnetic Resonance and Raman Spectroscopy. No changes with respect to fibre morphology were revealed and negligible changes in the carbohydrate composition were noted. The most significant change was related to the nitrogen content of the pulp after the DES treatment. Comprehensive examination using spectroscopic methods revealed that the nitrogen originated from strongly bound ChCl residuals that could not be removed with a mild ethanol washing procedure. According to Raman spectroscopic data and methylene blue adsorption tests, the cationic groups of ChCl seems to be attached to the anionic groups of pulp by electrostatic forces. These findings will facilitate the efficient utilisation of DES as a cellulose compatible medium without significantly affecting the native fibre structure.

Keywords Deep eutectic solvent · Urea · Choline chloride · DES · Pulp

Electronic supplementary material The online version of this article (https://doi.org/10.1007/s10570-017-1587-0) contains supplementary material, which is available to authorized users.

T.-M. Tenhunen · H. Orelma · T. Virtanen · A. Harlin · T. Tammelin (✉)
VTT Technical Research Centre of Finland Ltd, P.O. Box 1000, 02044 VTT Espoo, Finland
e-mail: tekla.tammelin@vtt.fi

A. E. Lewandowska · S. J. Eichhorn
College of Engineering, Mathematics and Physical Sciences, University of Exeter, North Park Road, Exeter EX4 4QF, UK

L.-S. Johansson · M. Österberg
Department of Forest Products Technology, Aalto University School of Chemical Technology, P.O. Box 16300, 00076 Aalto, Finland

Present Address:
S. J. Eichhorn
Bristol Composites Institute (ACCIS), University of Bristol, Queen's Building, University Walk, Bristol BS8 1TR, UK

Introduction

Interest in deep eutectic solvents (DES) for utilisation as cellulose compatible solvent system has increased in recent years. A number of applications of this solvent system, varying from its use as a fibre spinning medium to a pre-treatment prior to nanofibrillation, have been proposed (Zhang et al. 2012; Sirviö et al. 2015; Tenhunen et al. 2016). The physicochemical properties of DES solvents are comparable to ionic liquids. They are however composed of two or three chemicals that consist of a hydrogen bond donor and a hydrogen bond acceptor. These components form a eutectic mixture with a lower melting point than the individual components. Compared to ionic liquids, DESs are generally considered to be easier to prepare, less expensive and less toxic (Abbott et al. 2006; Zhang et al. 2012; Wen et al. 2015).

Choline chloride (ChCl) and urea has been the most popular DES system probably due to the availability of these chemicals and their low melting point ($\sim$ 12 °C) (Abbott et al. 2003). Even though this solvent system does not dissolve cellulose, it has been investigated for several applications with promising results (Abbott et al. 2006; Park et al. 2013; Sirviö et al. 2015; Wang et al. 2015; Tenhunen et al. 2016; Xu et al. 2016; Suopajärvi et al. 2017; Willberg-Keyriläinen et al. 2017). Abbott et al. (2006) have utilised a eutectic mixture of a choline chloride derivative (Chlorcholine chloride-based (ClChCl;$ClCH_2CH_2N(Me)_3Cl$)) and urea to cationise cotton. Successful cationisation was detected via an increased hydrophilicity and by a repulsion of a cationic dye. According to their study, cationic functionalisation occurred when choline chloride reacted with the available OH-groups of cellulose. Sirviö et al. (2015) and Suopajärvi et al. (2017) utilised a DES system composed of ChCl and urea as a pre-treatment to promote nanofibrillation of bleached pulp or secondary fibre sources. They suggested that some of the hemicelluloses might dissolve during the treatment. They also suggested that a small number of cellulose hydroxyl groups are possibly converted to carbamates, leading to the distortion of the hydrogen bonding of the fibres. Carbamate conversion was observed by Willberg-Keyriläinen et al. (2017) when they treated wet pulp with a urea based DES system; this was found to occur most readily at 120 °C. Xu et al. (2016) tested ChCl-urea as a pre-treatment in order to remove hemicelluloses and lignin from corn stover prior to butanol fermentation. However, that particular DES system did not have any significant effect on the removal of these components. Park et al. (2013) used a mixture of 3,3′4,4′-benzophenone tetracarboxylic dianhydride (BPTCD) and ChCl-urea as a treatment medium in order to introduce antibacterial properties to cotton. Wang et al. (2015) used ChCl-urea as a plasticizer in regenerated cellulose films. They concluded that the ChCl-urea DES disrupted the inter- and intra-hydrogen bonds of cellulose, but there was no chemical reaction between these components and the regenerated cellulose.

Choline chloride itself has been used to cationise cotton. The method was originally developed by Harper Jr. and Stone (1986). Since then there have been several reported studies of this process, where choline-based substances have been used for cationic functionalisation by introducing quaternary ammonium groups to cellulose (Abbott et al. 2006; Ho et al. 2011; Kim and Choi 2014; Samanta et al. 2015). Urea is known to interact with cellulose. Several authors have reported on the formation of cellulose carbamate due to a reaction between the OH-groups of cellulose and urea (Segal and Eggerton 1961; Ekman et al. 1984; Fu et al. 2015). Dissolution becomes possible in solvents such as aqueous NaOH by first converting cellulose to cellulose carbamate. Urea has also been extensively used with alkaline solvents for the direct dissolution of cellulose (Cai and Zhang 2005). Ershova et al. (2012) presented the possibility of decreasing cellulose degradation (peeling) under alkaline conditions by using urea as a co-solvent.

Previously we have shown that a DES system comprising choline chloride (ChCl) and urea was a suitable medium for pulp fibre yarn manufacturing (Tenhunen et al. 2016). This eutectic mixture was able to disperse pulp fibres and dissolve the crosslinking polymer (polyacrylic acid). Furthermore, this solvent system was shown to form a gel-like suspension, which was then spun into fibre yarns using an extrusion method. Since no dissolution of cellulose took place in the process, and the cellulose I structure remained intact without regeneration to cellulose II, the method could enable the production of wood-based textiles. This was achieved without the use of harsh chemicals or excessive consumption of water, bringing new options to the textile industry.

Despite several promising new applications and research efforts, the interactions between cellulose fibres and ChCl-urea based DES systems are still mostly unknown. In the present work, the aim was to clarify the interactions between bleached pine pulp and mentioned choline chloride/urea DES system. Since both choline chloride and urea have been used together and separately to functionalise cellulose and also as a reaction medium, it raises a number of questions. Does DES have an influence on fibre morphology or does it act as an inert medium for cellulosic fibres? Does DES chemically modify pulp fibres? Our approach is an extensive and systematic characterisation of wood pulp materials treated with a DES system.

Experimental

Materials

Never-dried bleached, sodium washed pine pulp from a Finnish pulp mill was used as the starting material for the DES treatment. Pulp was ion-exchanged to a sodium form based on a slightly modified version of a method originally described by Swerin et al. (1990). Modifications have been described by Lahtinen et al. (2014). In brief, the method includes washing the metal counter ions from the pulp at low pH (0.01 M HCl, $pH < 3$). After filtration and washing with deionized water, conversion of the carboxyl groups into their sodium form was achieved by mixing the pulp with 0.005 M $NaHCO_3$ solution. The pH was set to slightly alkaline with 1 M NaOH and held constant for 15 min while stirring the suspension. Finally, the pulp was rinsed with deionized water until the conductivity of the filtrate was below 20 µS/cm. Sodium washed pulp was diluted and mixed using Diaf's Minibatch Type 20 (Pilvad Diaf A/S, Denmark) for 30 min at 2000 rpm. The excess water was then removed by filtration using a Buchner funnel and a double filter cloth. Pulp samples were stored at 4 °C before they were used.

The DES system was prepared using a modified procedure according to Abbott et al. (2003). Choline chloride (Sigma-Aldrich, USA) and urea (Sigma-Aldrich, USA) (used as purchased without further purification) were mixed in a closed system using a molar ratio of 1:2 at 100 °C until a homogenous and transparent liquid was formed. DES was used immediately once prepared.

Ethanol and acetone were both analytical grades and supplied by Sigma-Aldrich, USA. Methylene blue (3,7-Bis(dimethylamino)phenothiazinium chloride, C. I. 52015, Reag. PhEur, Merck) was used as received.

Methods

Preparation of samples

Figure 1 presents the sample preparation protocol. Sample preparation was carried out according to the procedure by Tenhunen et al. (2016), with some modifications. Preparation commenced with water removal by acetone exchange. 100 g of wet (8 wt%) sodium washed pine pulp (1. Pulp) was mixed with 1 kg of acetone with constant stirring for 1 h. The mixture was then filtered using a Buchner funnel and a filter cloth. This acetone exchange procedure was repeated 3 times. Final filtering was conducted using a Buchner funnel and filter paper (mesh size 0.45 µm). Finally, the pulp was dried in a vacuum oven (at 40 °C) overnight (2. Acetone exchanged). Part of the dried pulp was washed in an excess of ethanol for 2 h, vacuum filtrated and dried. The resultant sample was an ethanol treatment reference for DES pulp (3. Ethanol reference). For the DES treatment, dried pulp was placed in a closed glass reactor (Radleys, UK) with the clear DES solution and mixed for 16 h at 100 °C with constant stirring. The pulp consistency was 1%. Subsequently, the mixture was washed twice with an excess of ethanol for 1 h and vacuum filtrated in between each washing step. After the final filtration using filter paper (mesh 0.45 µm) the sample was dried (4. DES pulp). However, due to a rather high variation in nitrogen content after conventional washing, an extra washing step was added to the procedure. Extensive washing was done for dried DES treated pulp using an extraction method in boiling ethanol (80 °C) in a soxhlet for 4 h (5. Extracted DES pulp). Prior to analysis, all the pulp samples were dried between pulp blotting board sheets at room temperature and stored in desiccator until further use.

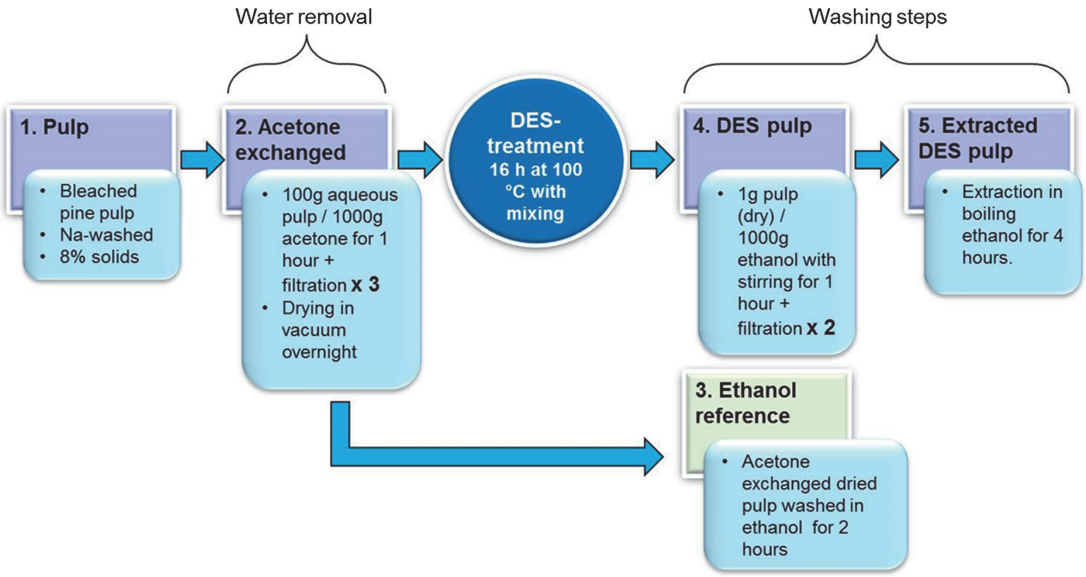

Fig. 1 Scheme of the sample preparation protocol including the water removal phase, treatment with deep eutectic solvent and the mild washing step with ethanol as well as a more efficient washing step including extraction with boiling ethanol. Ethanol reference pulp is a reference test point only for the mild ethanol-washing step

Fibre morphology studied by SEM and AFM

Scanning electron microscopy (SEM) (Merlin® FE-SEM, Carl Zeiss NTS GmbH, Germany) was used to investigate the changes in pulp morphology taking place during water removal, DES treatment and the washing steps. Pulp samples were attached on double-sided carbon adhesive discs on aluminium specimen stubs and sputter coated with platinum to improve the sample conductivity using an Agar Automatic Sputter Coater (Agar Scientific Ltd, UK). Imaging with the magnifications of × 100, × 500 and × 5000 was done using an electron beam energy of 3.0 keV and a 30 pA probe current with a pixel resolution of 2048 × 1536.

Atomic force microscopy (AFM) (Nanoscope IIIa multimode AFM, Digital Instrument, Santa Barbara, CA) was used to characterise the changes in the morphology of the surface of the pulp. Images were scanned in tapping mode in air using a 10279EVLR scanner and silicon cantilevers (NCHV-A, Bruker, Camarillo, CA) with a spring constant of 42 N/m and a resonant frequency of 320 kHz. Three different areas were scanned and no image processing, other than flattening, was performed.

Overall chemical composition of fibres

Carbohydrate composition (rhamnose, arabinose, galactose, glucose, xylose, and mannose) of the pulps was determined by hydrolysis. The resulting monosaccharides' contents were determined by HPAEC with pulse amperometric detection (Dionex ICS-5000 equipped with a CarboPac PA20 column) according to an NREL method (Willför et al. 2009; Sluiter et al. 2012).

Elemental analysis (C, H, N, S) of the pulp samples was carried out by using a FLASH 2000 series analyser (Thermo Scientific, USA). The samples were dried at 105 °C overnight to remove excess moisture. The elemental compositions of the pulp samples were calculated based on the carbon, hydrogen, and oxygen composition of an anhydroglucose unit ($C_6H_{10}O_6$).

Structural characteristics of fibres by spectroscopy

X-Ray photoelectron spectroscopy (XPS) was used to analyse the surface elemental compositions and chemical states. The equipment used was an AXIS Ultra electron spectrometer (Kratos Analytical Ltd, UK.) with monochromatic A1 Kα irradiation at

100 W and effective charge neutralisation with slow thermal electrons. The set-up and acquisition parameters have been previously reported by Johansson and Campbell (2004). Prior to the measurements, the samples were evacuated in a pre-chamber overnight. Low-resolution wide spectra in addition to high resolution spectra of the carbon (C 1s) region were collected. Three measurements from each sample were recorded. A sample of ash free 100% cellulose filter paper, stored under dust free ambient conditions, was analysed as an in situ reference (Johansson and Campbell 2004). No degradation of the samples due to ultrahigh vacuum or X-rays was observed during the measurements.

Liquid state ^{13}C NMR spectroscopy was carried out using a Bruker Avance III 500 NMR spectrometer with a magnetic flux density of 11.7 T. 30 mg of ChCl or urea was dissolved in DMSO-d_6, and transferred into a regular 5 mm NMR tube. A ^{13}C spectrum was acquired with a BB(F)O double resonance probe head at 22 °C, using a 30-degree pulse and a waltz 16 proton decoupling sequence. A total of 1200 scans were collected with a 1.5 s relaxation delay between successive scans. Referencing was carried out using the lock frequency, and the spectrum was processed using Bruker TopSpin 3.5 software.

Solid state ^{13}C cross polarisation (CP) magic angle spinning (MAS) NMR measurements were taken in order to detect DES system residuals from dried pulp samples. The measurements were performed using an Agilent 600 NMR spectrometer with a magnetic flux density of 14.1 T, using a 3.2 mm triple-resonance MAS NMR probe in a double resonance mode. 20,000 scans were accumulated using a 1.1 ms contact time and a 3.0 s relaxation delay between successive scans, with a MAS rate of 10 kHz. In all experiments a SPINAL-64 proton decoupling of 80 kHz was used. 90-degree pulse durations and Hartmann-Hahn matches for cross polarisation were calibrated using α-glycine. The chemical shifts were externally referenced via adamantine by setting the low field signal to $\sim$ 38.5 ppm.

Raman spectroscopy was used to study the structural properties of pulp fibres. The measurements were performed using a Renishaw RM-1000 System equipped with a thermoelectrically cooled CCD detector. The laser was focused on the samples using a 50 × objective lens attached to a Leica microscope. A 785 nm wavelength laser was used to record spectra using an exposure time of 10 s and ten accumulations. The power of the laser was kept at 100% of the source power. The pulp fibres were oriented parallel and perpendicular to the polarisation configuration of the laser used to excite and record the Raman scattering. Raman spectra of pulp fibres were normalised with respect to the intensity of a band located at $\sim$ 897 cm^{-1} (Agarwal et al. 2010).

Fibre charge determination by methylene blue adsorption

Methylene blue adsorption was used to study the changes in the pulp charge due to the DES treatment. The method is based on the adsorption of the cationic dye to the anionic sites of cellulose via electrostatic interactions, and the changes in the intensity level of the supernatant is monitored (Palit and Moulik 2000). The dye adsorptions were carried out according to a protocol described by Ho et al. (2011) with some modifications. Briefly, cationic methylene blue dye solution was prepared by mixing 0.0161 g of methylene blue (Fig. 2) with 100 ml MilliQ-water at room temperature. 0.016 g of dry pulp was mixed with 1 ml of dye solution and 39 g of MilliQ-water. This mixture was continuously shaken for 24 h at room temperature (speed 160 rpm) using a Stuart orbital shaker (SSL1, UK). The dispersion was then centrifuged for 30 min at 10,000 rpm and a few millilitres of supernatant was collected and the absorbance was measured using a UV–vis spectrophotometer (UV/VIS/NIR Lambda 900, Perkin Elmer, USA) with a 1 cm polystyrene cuvette. The position of the maximum absorbance (λ_{max}) for methylene blue was 664 nm.

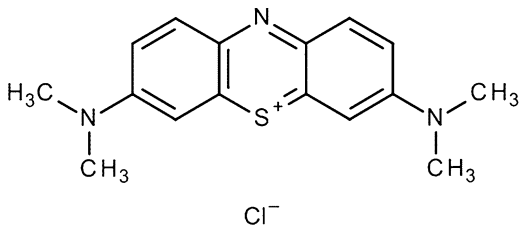

Fig. 2 Chemical structure of methylene blue

Results and discussion

Changes in fibre morphology

SEM imaging was used to visually assess any possible changes that may have occurred to the morphology of the pulp fibre during the DES treatment protocol (see Fig. 1). Representative SEM images of samples undergoing this treatment, at different levels of magnification, are shown in Fig. 3. Similar structural details are seen for samples that underwent a solvent exchange step in acetone or ethanol, compared to pulp fibres after the DES treatment step. Minor increase in fibrillation and possible cracking of the fibres can be attributed to pulp drying, as previously demonstrated by Suchy et al. (2009), rather than just the DES treatment.

AFM was used to more closely analyse possible changes in the surface morphology of the fibres, and to determine if mercerisation of cellulose was taking place. In Fig. 4 the 4. DES pulp sample is compared to the reference 1. Pulp sample. The surfaces of both pulp fibres appear to be identical, and additionally did not indicate that mercerisation had taken place. Eronen et al. (2009) showed that during mercerisation, the pulp fibre surface morphology clearly changes resulting in a formation of an irregular layer on the fibre surface. In the present sample, the microfibrils and cell wall layers are still visible indicating that the cell wall structure remains unchanged. This result is in accordance with the finding that the crystalline structure of cellulose I remains intact during a DES treatment (Sirviö et al. 2015; Tenhunen et al. 2016).

Overall changes in chemical composition

Carbohydrate composition

Carbohydrate analysis was used to determine the possible dissolution of hemicelluloses. The monosaccharide compositions of the pulp samples are presented in Table 1. The changes in carbohydrate contents are negligible, and they fall below the measuring accuracy of the method (internal standard), which varies within the range 6–8%. In addition, it has been shown that the degree of polymerisation (DP) does not change with the DES system treatment; this would have been expected to be affected by the dissolution of hemicelluloses (Sirviö et al. 2015; Tenhunen et al. 2016). The DES treatment does not appear to dissolve glucose or galactose, but minor dissolution of xylose, mannose and arabinose cannot be completely excluded.

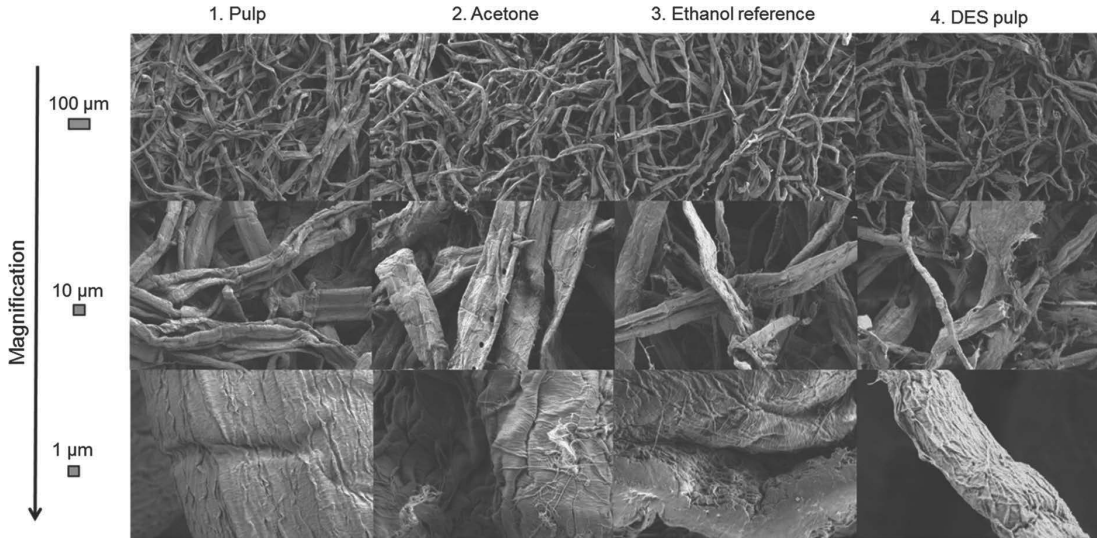

Fig. 3 SEM images with the magnifications of× 100, × 500 and × 5000 for bleached pine pulp samples when exposed to different treatment stages. Scale bars are given on the left hand side of the images

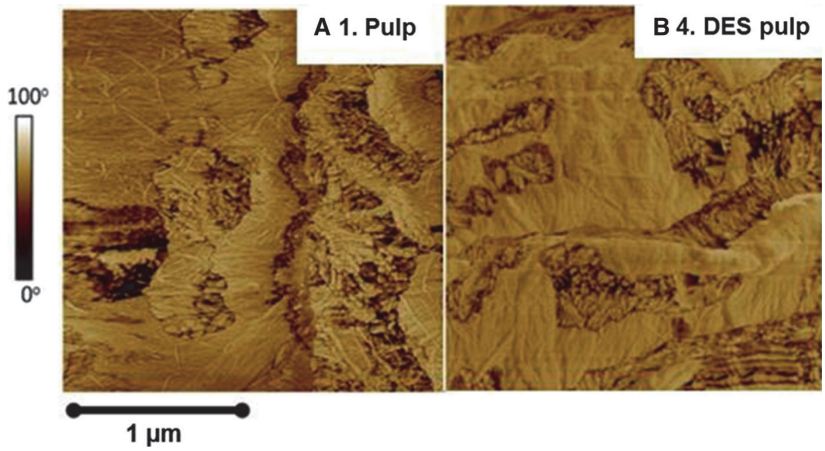

Fig. 4 Typical phase contrast AFM images of A 1. Pulp and B 4. DES pulp sample

Table 1 The composition of neutral sugars of pulp samples after treatment with a DES system

Pulp sample	Monosaccharides (mg/100 mg)					
	Rhamnose	Arabinose	Galactose	Glucose	Xylose	Mannose
1. Pulp	< 0.1 ± 0.00	0.63 ± 0.03	0.22 ± 0.01	85.07 ± 0.73	7.50 ± 0.12	6.23 ± 0.15
2. Acetone	< 0.1 ± 0.00	0.63 ± 0.02	0.22 ± 0.01	83.68 ± 0.41	7.40 ± 0.13	6.21 ± 0.12
3. Ethanol reference	< 0.1 ± 0.00	0.63 ± 0.02	0.22 ± 0.01	85.28 ± 0.91	7.47 ± 0.07	6.28 ± 0.09
4. DES pulp	< 0.1 ± 0.00	0.54 ± 0.04	0.20 ± 0.01	83.19 ± 0.11	6.96 ± 0.12	5.86 ± 0.13

Values are quoted standard deviations from the mean as errors

Elemental analysis

Elemental analysis was carried out to determine changes in chemical composition during the pulp sample processing steps (Table 2). There was no change in carbon, hydrogen or sulphur contents (no sulphur was detected); the analysis however revealed changes in nitrogen content of the DES treated pulp sample. The nitrogen content was also found to vary substantially between two different batches, despite using similar washing procedures.

The elemental nitrogen content varied in the range 0.5–1.6% which indicates that the mild ethanol washing procedure was not efficient enough to remove the DES derived nitrogen. Therefore, the washing procedure was improved by implementing an ethanol extraction step. Pulp was extensively washed in boiling ethanol at 80 °C for 4 h. As a result of this treatment the elemental nitrogen content was decreased to 0.2%. This final nitrogen fraction is thought to be relatively tightly bound to the pulp fibres. In order to further clarify the binding mechanism, spectroscopic methods were employed.

Revealing structural characteristics by spectroscopy

XPS: chemical composition of the fibre surface

XPS was used to study the elemental composition of the fibre surface before and after DES-treatment. Figure 5 presents XPS spectra of samples 1. Pulp and 4. DES pulp, as well as, the XPS reference sample of pure cellulose (Johansson and Campbell 2004), with high resolution carbon C 1s. Both samples were remarkably similar to the reference sample, with a typical cellulose C 1s signature consisting of carbons with one or two bonds to oxygen; namely peaks

Table 2 Elemental composition of pulp samples

Pulp sample	Carbon (%) ± SD	Hydrogen (%) ± SD	Nitrogen (%) ± SD
1. Pulp	43.6 ± 0.1	6.3 (0.01)	0.0 (0.0)
2. Acetone	44.0 (0.0)	6.3 (0.0)	0.0 (0.0)
3. Ethanol reference	43.5 (0.0)	6.3 (0.0)	0.0 (0.0)
4. DES pulp	42.9 ± 0.1	6.4 ± 0.1	1.6 ± 0.1
	43.1 ± 0.2	6.2 (0.03)	0.5 (0.0)
5. Extracted DES pulp	43.2 (0.0)	6.3 ± 0.1	0.2 (0.0)

Errors are shown as standard deviations (SD) from the mean. If the error is less than 0.1 then it is given in brackets

located at 286.7 and 288.1 eV (Beamson and Briggs 1993). Apart from the presence of these peaks, a non-cellulosic component originating from carbon atoms without oxygen neighbors was located at 285.0 eV, as is typically the case for all experimental XPS data from cellulose (Johansson et al. 2011). However, this signal is not more intense than what it is found for the pure cellulose reference sample. Therefore, the XPS data confirmed that the DES treatment process did not contaminate or chemically change the sample surfaces. The only difference observed was a barely detectable amount of nitrogen (0.3 at.%) in the DES modified pulp sample (sample no 4). Data are presented in Table 3, and the nitrogen N 1s peak located at ~ 400 eV is shown in the inset of Fig. 5. Nitrogen seems to originate from ChCl since further examination of the chloride region (Cl 2p at 199 eV) revealed minor traces of this substance; however, the signal was below the quantification limit (not shown, less than 0.1 at % for Cl 2p with the instrumental setup used).

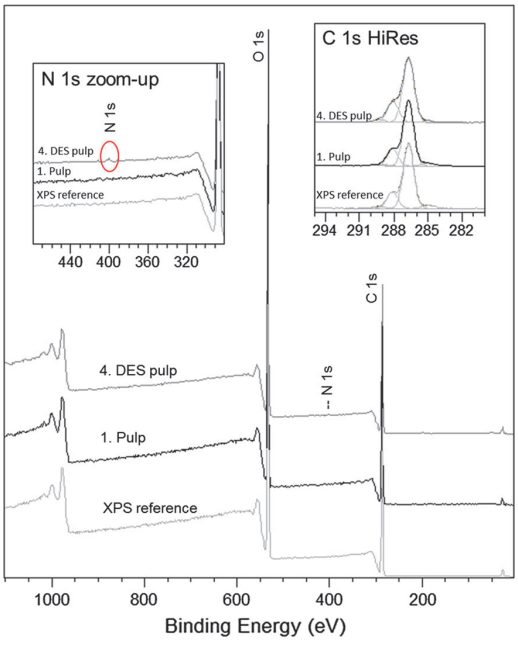

Fig. 5 Typical low resolution wide spectra of in situ XPS reference for cellulose, 1. Pulp and 4. DES pulp showing signals due to emission of O 1s, N 1s and C 1s. Insets show the magnification of N 1s region and the C 1s HiRes regions

NMR: chemical composition in bulk

Both solid state and liquid state NMR techniques were used to determine the origin of the nitrogen observed using XPS and elemental analyses, and to reveal the possible derivatisation of the DES treated pulp. Figure 6 reports solid-state NMR spectra of the reference pine pulp sample. Also reported in this figure are samples of DES treated pulp with a high nitrogen content (4. DES pulp with 1.6% nitrogen) after mild washing, and DES treated pulp with a low nitrogen content (5. Extracted DES pulp with 0.2% nitrogen) after extensive washing with boiling ethanol. Liquid state NMR was used for the assignment of signals for pure ChCl and urea (Online Resource Fig. S1). The signal for urea was observed to be located at 161.1 ppm, and resonances for ChCl were determined from signals corresponding to HO–CH_2–CH_2–N– (67.2 ppm) (triplet), HO–CH_2– (55.2 ppm) (singlet) and –CH_2–N–$(CH_3)_3$ (53.5 ppm) (triplet) moieties. The signals are comparable to previously published data (Ardenkjaer-Larsen et al. 2003; Lobo et al. 2012). Spectra acquired for the reference sample 1. Pulp are typical for cellulose I obtained from

Table 3 Elemental surface concentrations and relative abundance of carbon bonds for the fibre samples

Sample	Elemental surface concentration (at.%)			Relative abundance of carbon bonds (at.%)			
	C 1s	O 1s	N 1s	C–C	C–O	O–C–O	C=O
1. Pulp	59.3	40.7	0.0	3.9	72.6	20.7	2.7
2. Acetone	60.0	39.9	0.0	3.6	66.8	24.3	5.2
3. Ethanol reference	58.6	41.4	0.0	3.0	69.1	23.7	4.2
4. DES pulp	58.7	41.0	0.3	2.7	70.4	23.2	3.7
XPS reference	59.1	40.9	0.0	4.1	75.2	18.9	1.9

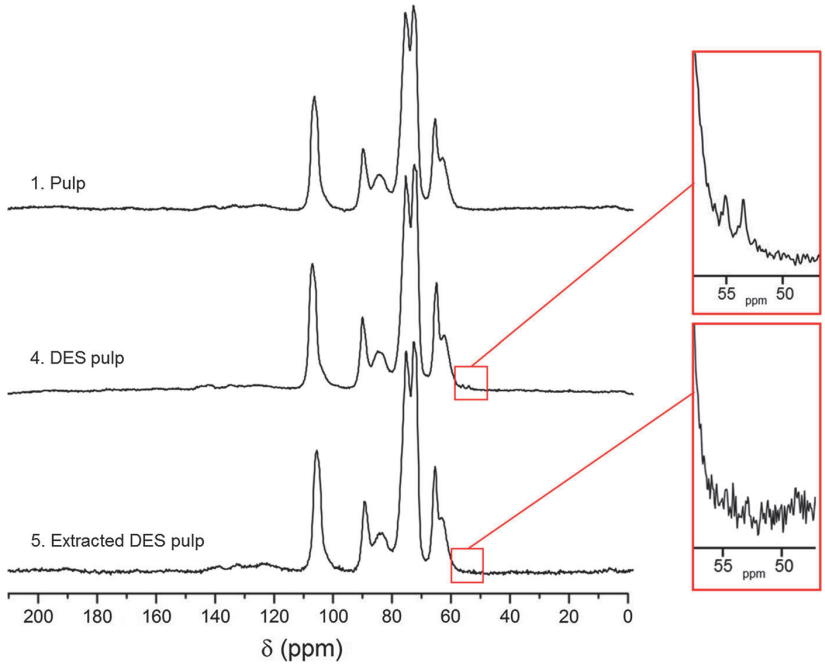

Fig. 6 Typical solid-state NMR spectra of 1. Pulp (bleached pine pulp reference), 4. DES pulp (after DES treatment and conventional washing) and 5. Extracted DES pulp (after extensive washing). Insets in the figure show details of peaks close to the shoulder of peak located in the range 60–70 ppm

softwood pulp (Larsson et al. 1999), without the presence of any additional signals. Spectra of sample 4. DES pulp and 5. Extracted DES pulp were also similar to the spectra obtained from the reference sample. Careful examination of these spectra identified two additional signals located at 55.0 and 53.0 ppm. This region of the spectra is comparable to the ChCl moieties containing nitrogen. Additional signals in the region of urea (161.1 ppm) were not detected, and therefore, the formation of carbamate bonds discussed by Sirviö et al. (2015) were thought to not occur. Spectra measured after extensive washing steps (5. Extracted DES pulp) were identical to the reference spectra without any additional signals. This result was expected due to the lesser amount of nitrogen observed from XPS data. These results also agree with the findings of Yin et al. (2007), who showed that it is difficult for urea to impregnate into cellulose without a solvent such as water.

Raman: structural properties of bulk materials

Raman spectroscopy was used to study the structural properties of the pulp fibres. Figure 7 shows typical Raman spectra of pulp fibres after different stages of treatment. Raman bands emanating from the

vibrational modes of atoms in cellulose chains are sensitive to the orientation of the fibres with respect to the polarisation configuration of the laser light (Wiley and Atalla 1987; Lewandowska et al. 2015). Typical Raman spectra of pulp fibres illustrate the changes in the intensity of the Raman bands as a function of the orientation of the fibres; namely parallel (Fig. 7A) and perpendicular (Fig. 7B), to the polarisation configuration of the laser light. The bands found in the region 250–600 cm^{-1} are assigned to skeletal-bending modes involving the CCC, COC, OCC and OCO internal coordinates (Wiley and Atalla 1987). Additionally, the bending (CCH and OCH) and skeletal stretching modes (CC and CO) are thought to also contribute to peaks within this region (Wiley and Atalla 1987). The well-resolved Raman bands located at $\sim$ 897 and $\sim$ 1095 cm^{-1} are assigned to the main chain segmental stretching modes (Wiley and Atalla 1987). The band located at $\sim$ 897 cm^{-1} is assigned to the C–O–C in plane stretching (Edwards et al. 1997), while the band centred at $\sim$ 1095 cm^{-1} corresponds to C–O ring stretching modes and the β-1,4 glycosidic linkage (C–O–C) stretching modes between the glucose rings of the cellulose chains (Edwards et al. 1997; Gierlinger et al. 2006). Finally, heavy atom stretching (CC, CO) and the HCC, HCO, HOC and HCH bending modes contribute to the bands shown in the range 1200–1500 cm^{-1} (Wiley and Atalla 1987). Raman spectra of pulp fibres washed with acetone (2. Acetone) and ethanol (3. Ethanol reference) solvents are similar to those obtained from the initial 1.Pulp material (curves b, c and d in Fig. 7). The absence of differences between the Raman spectra of 1. Pulp, 2. Acetone and 3. Ethanol reference materials suggests that the pulp fibres maintain their chemical and structural properties after washing with the solvents. Additionally, a Raman band located at $\sim$ 715 cm^{-1} appears in the spectrum obtained from 4. DES pulp fibres treated with the DES solvent (curve e in Fig. 7). The origin of this band seems to result from the moieties of DES in the fibre structure, since the region of 700–850 cm^{-1} is devoid of any significant features corresponding to cellulose structures. Fig. S2 in Online Resource reports the Raman spectra of pure choline chloride (ChCl) and urea, two principal components of the DES system. The most intense Raman band from ChCl is centred at $\sim$ 719 cm^{-1}, and is assigned to the "totally" symmetric stretching vibration of four C–N bonds (ν_1) in the choline group (Fig. S2 A, Online Resource (Akutsu 1981). The medium intensity Raman bands located at $\sim$ 865 and $\sim$ 954 cm^{-1} are attributed to the symmetric (ν_2) and asymmetric (ν_3 and ν_4) stretching vibrations of the C–N bonds (Akutsu 1981). The position of Raman bands corresponding to the symmetric stretching vibrations (ν_1 and ν_2) of the C–N bonds indicates that most of the O–C–C–N^+ backbones in the choline group are in the gauche conformation (Akutsu 1981). A weak Raman band centred at $\sim$ 768 cm^{-1} is assigned to the "totally" symmetric stretching vibration of four C–N bonds (ν_1) in the trans conformation of the O–C–C–N^+ backbone in the choline group

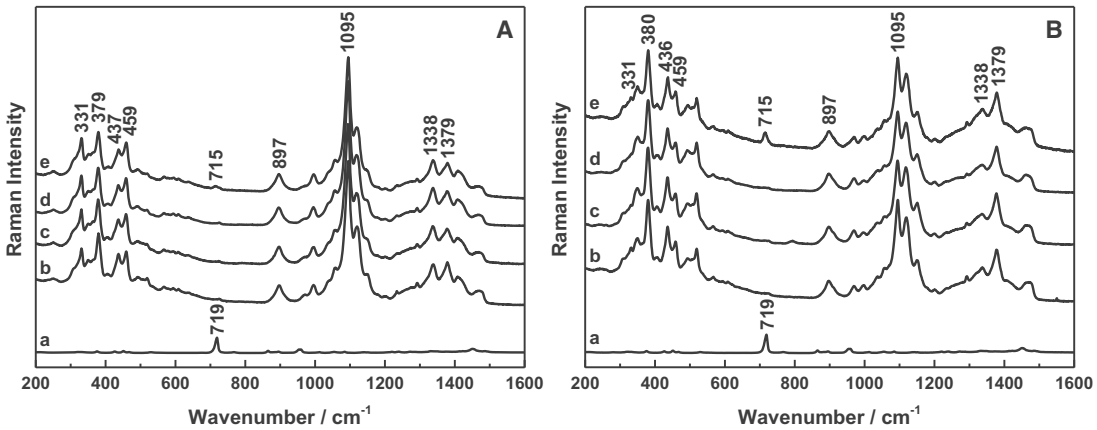

Fig. 7 Typical Raman spectra of (*a*) ChCl, (*b*) 1. Pulp, (*c*) 2. Acetone, (*d*) 3. Ethanol reference and (*e*) 4. DES pulp recorded in **A** parallel and **B** perpendicular orientation of the fibres to the polarisation configuration of the laser light

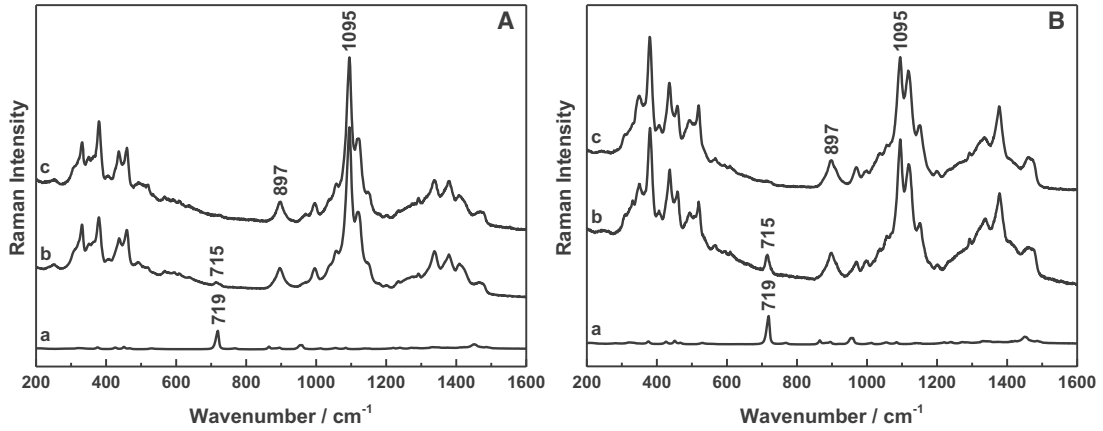

Fig. 8 Typical Raman spectra of (*a*) ChCl, (*b*) 4. DES pulp and (*c*) 5. Extracted DES pulp recorded in **A** parallel and **B** perpendicular orientation of the fibres to the polarisation configuration of the laser light

(Akutsu 1981). The strongest Raman band of urea located at $\sim$ 1010 cm^{-1} is assigned to the symmetric stretching vibration of the C–N bonds (Fig. S2 B, Online Resource). The asymmetric stretching vibration of the C–N bonds in the solid state urea appears at $\sim$ 1463 cm^{-1} (Keuleers et al. 1999). This suggests that the Raman band located at $\sim$ 715 cm^{-1} in the spectrum of 4. DES pulp corresponds to the initial choline group, but excluding the possibility of a chemical reaction between the –OH groups of cellulose and the components of DES during processing. Furthermore, the intensity of this band is sensitive to the orientation of the fibre with respect to the polarisation configuration of the laser, showing a higher intensity when the 4. DES pulp fibre is oriented perpendicular to the polarisation direction (curve b in Fig. 7). This suggests that the choline groups (positive charge) interact electrostatically with the anionic groups of cellulose (negative charge) and their $^{+}$N–C–C–O backbones 'poke out' perpendicularly from the cellulose chain. A shift of Raman band of 4. DES pulp (715 cm^{-1}) to a lower wavelength compared to ChCl ($\sim$ 719 cm^{-1}) indicates a slight decrease in the symmetry of the choline group. The relative intensity of the Raman band located at $\sim$ 715 cm^{-1} varies between the studied fibres in the perpendicular orientation (Fig. S3 B, Online Resource). The choline groups remain in the 4. DES pulp fibres after mild washing of the material with an excess of ethanol. Figure 8 shows the changes in the Raman spectra of 4. DES pulp before and after the extraction of the fibres in boiling ethanol (5. Extracted DES pulp). The intensity of the Raman bands assigned to the bond vibrations corresponding to the main chain segmental stretching and bending modes are similar for 4. DES pulp and 5. Extracted DES pulp spectra. This similarity suggests the preservation of chemical and structural properties of cellulose chains. Whereas, the process of boiling the 4. DES pulp in ethanol leads to the substantial removal of the choline groups from the pulp fibres. This is confirmed by the disappearance of the Raman band located at $\sim$ 715 cm^{-1} in the 5. Extracted DES pulp spectrum (curve c in Fig. 8).

Assessment of the binding of nitrogen

Methylene blue adsorption experiments on the pulp fibres were carried out to clarify the binding mechanism of choline chloride groups to cellulose fibres. Changes in the anionic charge of the DES treated pulp fibres were studied after the mild washing step with ethanol, and after the extensive washing step with boiling ethanol (4. DES pulp and 5. Extracted DES pulp) (see Fig. 9). The results were compared to the ethanol reference pulp (3. Ethanol reference), and furthermore a sample without pulp was measured as an internal reference of the method.

Significant differences in absorbance of visible light of wavelength of $\lambda_{max} = 664$ nm can be observed between the pulp samples. The higher the absorbance, the higher the dye concentration is in the supernatant indicating that the anionic sites of pulp are

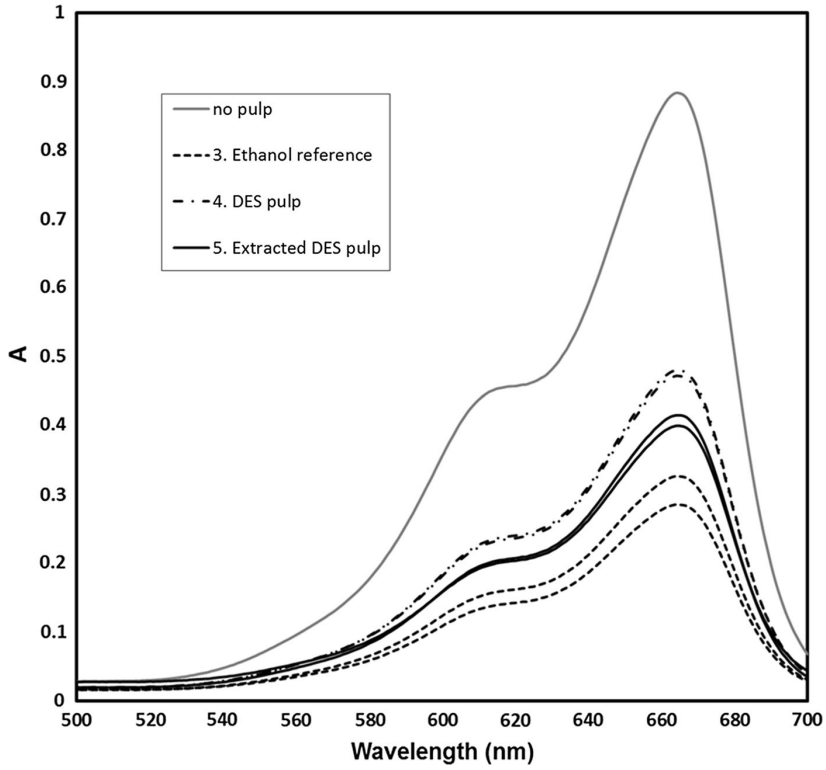

Fig. 9 Typical absorption spectra for 3. Ethanol reference pulp, 4. DES pulp and 5. Extracted DES pulp sample, and a measurement without pulp. Two parallel measurements of each pulp sample are shown

no longer available for the cationic dye particles to adsorb. This also suggests that the sites are occupied with other cationic substances, in this case choline ions. Therefore, the increase in the intensity of supernatant can be considered to be proportional to the decrease in the negative charge of the pulp, which is related to adsorption taking place via electrostatic interactions. The absorbance of visible light for the ethanol reference sample (no DES treatment) with a nitrogen content of 0% was lower compared to both the DES treated pulp samples. After DES treatment, a higher amount of methylene blue was found in the supernatant as observed from the higher intensity recorded. Extensive washing with boiling ethanol again lowered the intensity indicating the partial removal of the choline groups from the pulp surface. These results support the Raman spectroscopy results that a small amount of choline groups are tightly bound to the pulp fibres, and they seem to be attached via electrostatic forces which directly affects the charge state of the fibres. The strength of the interactions is thought to be relatively strong since choline residuals could not be completely removed even by extensive washing.

Conclusions

The influence of a cellulose compatible DES system based on choline chloride and urea on bleached pine pulp fibres was revealed using a systematic approach with complementary research methods. DES treatment carried out for 16 h at 100 °C has been found to have no influence on pulp fibre morphology. In addition, no evidence on the derivatisation of cellulose was observed during the DES treatment. Negligible changes were observed in the xylose, mannose and arabinose content and thus, minor dissolution of some of the hemicelluloses cannot be excluded. Elemental analysis and XPS surface elemental analysis suggested that nitrogen containing residuals remained even after the extensive pulp washing stage. Thorough examination by NMR and Raman spectroscopy revealed that the nitrogen residuals originate from tightly bound

choline chloride. In addition, Raman spectroscopy data suggest that cationic choline ions are interacting with the anionic groups of cellulose fibres via electrostatic interactions. This result was also supported by the cationic methylene blue adsorption results. These findings should facilitate the efficient utilisation of a green solvent system when developing advanced materials solutions from lignocellulosic-based sources.

Acknowledgments The authors acknowledge the Finnish Funding Agency for Innovation (TEKES) for funding the work via Design Driven Value Chains in the World of Cellulose 2.0 project. The Academy of Finland (Project ID 300367) is acknowledged for enabling the research mobility of T.T. to the University of Exeter, UK. Unto Tapper (VTT) is thanked for the SEM imaging, Atte Mikkelson, Ritva Heinonen and Marita Ikonen (VTT) for the chemical analysis and Robertus Nugroho (Aalto University) for the AFM imaging.

References

Abbott AP, Capper G, Davies DL et al (2003) Novel solvent properties of choline chloride/urea mixtures. Chem Commun 99:70–71. https://doi.org/10.1039/b210714g

Abbott AP, Bell TJ, Handa S, Stoddart B (2006) Cationic functionalisation of cellulose using a choline based ionic liquid analogue. Green Chem 8:784–786. https://doi.org/10.1039/B605258D

Agarwal UP, Reiner RS, Ralph SA (2010) Cellulose I crystallinity determination using FT-Raman spectroscopy: univariate and multivariate methods. Cellulose 17:721–733. https://doi.org/10.1007/s10570-010-9420-z

Akutsu H (1981) Direct determination by Raman scattering of the conformation of the choline group in phospholipid bilayers. Biochemistry 20:7359–7366. https://doi.org/10.1021/bi00529a006

Ardenkjaer-Larsen JH, Fridlund B, Gram A et al (2003) Increase in signal-to-noise ratio of > 10,000 times in liquid-state NMR. Proc Natl Acad Sci U S A 100:10158–10163. https://doi.org/10.1073/pnas.1733835100

Beamson G, Briggs D (1993) Cellulose spectra in high resolution XPS of organic polymers: the scienta ESCA300 database. J Chem Educ 70:A25. https://doi.org/10.1021/ed070pA25.5

Cai J, Zhang L (2005) Rapid dissolution of cellulose in LiOH/urea and NaOH/urea aqueous solutions. Macromol Biosci 5:539–548. https://doi.org/10.1002/mabi.200400222

Edwards HG, Farwell DW, Webster D (1997) FT Raman microscopy of untreated natural plant fibres. Spectrochim Acta A Mol Biomol Spectrosc 53A:2383–2392. https://doi.org/10.1016/S1386-1425(97)00178-9

Ekman K, Eklund V, Fors J et al (1984) Regenerated cellulose fibers from cellulose carbamate solutions. Lenzing Ber 57:38–40

Eronen P, Österberg M, Jääskeläinen A-S (2009) Effect of alkaline treatment on cellulose supramolecular structure studied with combined confocal Raman spectroscopy and atomic force microscopy. Cellulose 16:167–178. https://doi.org/10.1007/s10570-008-9259-8

Ershova O, da Costa EV, Fernandes AJS et al (2012) Effect of urea on cellulose degradation under conditions of alkaline pulping. Cellulose 19:2195–2204. https://doi.org/10.1007/s10570-012-9791-4

Fu F, Xu M, Wang H et al (2015) Improved synthesis of cellulose carbamates with minimum urea based on an easy scale-up method. ACS Sustain Chem Eng 3:1510–1517. https://doi.org/10.1021/acssuschemeng.5b00219

Gierlinger N, Schwanninger M, Reinecke A, Burgert I (2006) Molecular changes during tensile deformation of single wood fibers followed by Raman microscopy. Biomacromolecules 7:2077–2081. https://doi.org/10.1021/bm060236g

Harper RJ Jr, Stone RL (1986) Cationic cotton plus easy care. Text Chem Color 18:33–35

Ho TTT, Zimmermann T, Hauert R, Caseri W (2011) Preparation and characterization of cationic nanofibrillated cellulose from etherification and high-shear disintegration processes. Cellulose 18:1391–1406. https://doi.org/10.1007/s10570-011-9591-2

Johansson LS, Campbell JM (2004) Reproducible XPS on biopolymers: cellulose studies. Surf Interface Anal 36:1018–1022. https://doi.org/10.1002/sia.1827

Johansson L, Tammelin T, Campbell JM et al (2011) Experimental evidence on medium driven cellulose surface adaptation demonstrated using nanofibrillated cellulose. Soft Matter 7:10917. https://doi.org/10.1039/c1sm06073b

Keuleers R, Desseyn HO, Rousseau B, Van Alsenoy C (1999) Vibrational analysis of urea. J Phys Chem A 103:4621. https://doi.org/10.1021/jp984180z

Kim JY, Choi H-M (2014) Cationization of periodate-oxidized cotton cellulose with choline chloride. Cellul Chem Technol 48:25–32

Lahtinen P, Liukkonen S, Pere J et al (2014) A Comparative study of fibrillated fibers from different mechanical and chemical pulps. BioResources 9:2115–2127

Larsson PT, Hult E, Wickholm K et al (1999) CPrMAS 13 C-NMR spectroscopy applied to structure and interaction studies on cellulose I. Solid State Nucl Magn Reson 15:31–40. https://doi.org/10.1016/S0926-2040(99)00044-2

Lewandowska AE, Soutis C, Savage L, Eichhorn SJ (2015) Carbon fibres with ordered graphitic-like aggregate structures from a regenerated cellulose fibre precursor. Compos Sci Technol 116:50–57. https://doi.org/10.1016/j.compscitech.2015.05.009

Lobo HR, Singh BS, Shankarling GS (2012) Deep eutectic solvents and glycerol: a simple, environmentally benign and efficient catalyst/reaction media for synthesis of N-aryl phthalimide derivatives. Green Chem Lett Rev 5:487–533. https://doi.org/10.1080/17518253.2012.669500

Palit D, Moulik SP (2000) Adsorption of methylene blue on cellulose from its own solution and its mixture with methyl orange. Indian J Chem Sect A Inorg Phys Theor Anal Chem 39:611–617

Park JH, Oh KW, Choi HM (2013) Preparation and characterization of cotton fabrics with antibacterial properties treated by crosslinkable benzophenone derivative in choline chloride-based deep eutectic solvents. Cellulose 20:2101–2114. https://doi.org/10.1007/s10570-013-9957-8

Samanta AK, Kar TR, Mukhopadhyay A et al (2015) Studies on dyeing process variables for salt free reactive dyeing of glycine modified cationized cotton muslin fabric. J Inst Eng Ser E 96:31–44. https://doi.org/10.1007/s40034-015-0062-4

Segal L, Eggerton FV (1961) Some aspects of the reaction between urea and cellulose. Text Res J 31:460–471

Sirviö JA, Visanko M, Liimatainen H (2015) Deep eutectic solvent system based on choline chloride-urea as a pretreatment for nanofibrillation of wood cellulose. Green Chem 17:3401–3406. https://doi.org/10.1039/C5GC00398A

Sluiter A, Hames B, Ruiz R et al (2012) NREL/TP-510-42618 analytical procedure—determination of structural carbohydrates and lignin in Biomass. Lab Anal Proced 17

Suchy M, Hakala T, Kangas H et al (2009) Effects of commercial cellobiohydrolase treatment on fiber strength and morphology of bleached hardwood pulp. Holzforschung 63:731–736. https://doi.org/10.1515/HF.2009.104

Suopajärvi T, Sirviö JA, Liimatainen H (2017) Nanofibrillation of deep eutectic solvent-treated paper and board cellulose pulps. Carbohydr Polym 169:167–175. https://doi.org/10.1016/j.carbpol.2017.04.009

Swerin A, Odberg L, Lindstrbm T, Pulp S (1990) Deswelling of hardwood kraft pulp fibers by cationic polymers. Nord Pulp Pap Res J 5:188–196

Tenhunen T, Hakalahti M, Kouko J et al (2016) Method for forming pulp fiber yarns developed by a design driven process. BioResources 11:2492–2503. https://doi.org/10.15376/biores.11.1.2492-2503

Wang S, Peng X, Zhong L et al (2015) Choline chloride/urea as an effective plasticizer for production of cellulose films. Carbohydr Polym 117:133–139. https://doi.org/10.1016/j.carbpol.2014.08.113

Wen Q, Chen JX, Tang YL et al (2015) Assessing the toxicity and biodegradability of deep eutectic solvents. Chemosphere 132:63–69. https://doi.org/10.1016/j.chemosphere.2015.02.061

Wiley JH, Atalla R (1987) Band assignments in the Raman-spectra of celluloses. Carbohydr Res 160:113–129. https://doi.org/10.1016/0008-6215(87)80306-3

Willberg-Keyriläinen P, Hiltunen J, Ropponen J (2017) Production of cellulose carbamate using urea-based deep eutectic solvents. Cellulose. https://doi.org/10.1007/s10570-017-1465-9

Willför S, Pranovich A, Tamminen T et al (2009) Carbohydrate analysis of plant materials with uronic acid-containing polysaccharides-A comparison between different hydrolysis and subsequent chromatographic analytical techniques. Ind Crops Prod 29:571–580. https://doi.org/10.1016/j.indcrop.2008.11.003

Xu GC, Ding JC, Han RZ et al (2016) Enhancing cellulose accessibility of corn stover by deep eutectic solvent pretreatment for butanol fermentation. Bioresour Technol 203:364–369. https://doi.org/10.1016/j.biortech.2015.11.002

Yin C, Li J, Xu Q et al (2007) Chemical modification of cotton cellulose in supercritical carbon dioxide: synthesis and characterization of cellulose carbamate. Carbohydr Polym 67:147–154. https://doi.org/10.1016/j.carbpol.2006.05.010

Zhang Q, De Oliveira Vigier K, Royer S, Jerome F (2012) Deep eutectic solvents: syntheses, properties and applications. Chem Soc Rev 41:7108–7146. https://doi.org/10.1039/c2cs35178a

Supplementary Material

Cellulose

Understanding the interactions of cellulose fibres and deep eutectic solvents of choline chloride and urea

Tiia-Maria Tenhunen[a], Anna E. Lewandowska[b], Hannes Orelma[a], Leena-Sisko Johansson[c], Tommi Virtanen[a], Ali Harlin[a], Monika Österberg[c], Stephen J. Eichhorn[b], Tekla Tammelin[a*]

[a] *VTT Technical Research Centre of Finland Ltd, P.O. Box 1000, 02044 VTT, Finland, tekla.tammelin@vtt.fi, +358 020 722 4632*

[b] *University of Exeter, College of Engineering, Mathematics and Physical Sciences, North Park Road, Exeter, EX4 4QF, United Kingdom*

[c] *Aalto University School of Chemical Technology, Department of Forest Products Technology, P.O. Box 16300, 00076 Aalto, Finland*

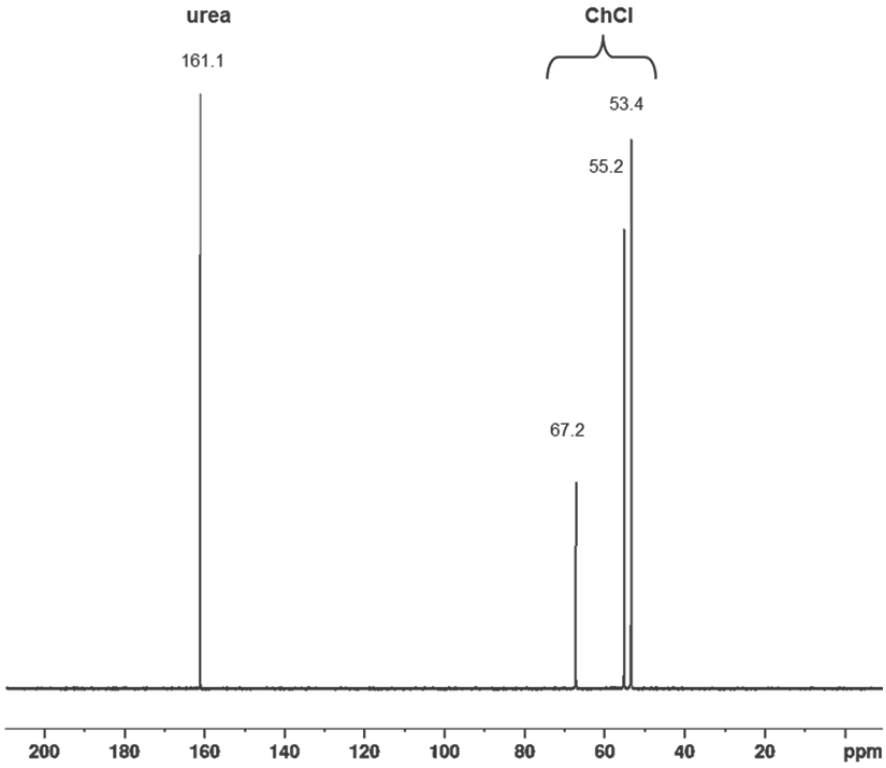

Fig. S1 A typical liquid state NMR spectrum of urea and ChCl

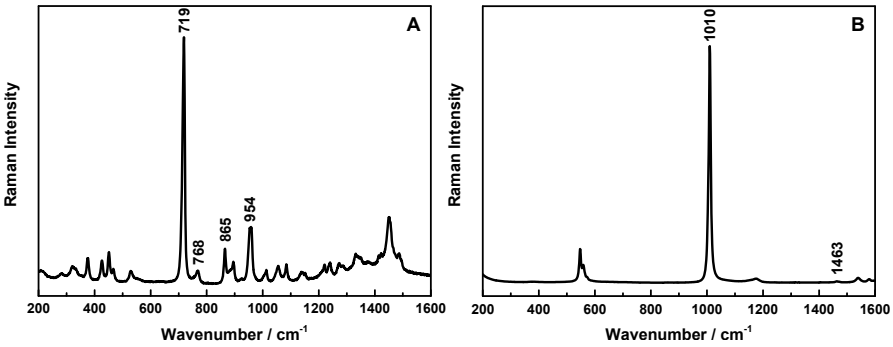

Fig. S2 Typical Raman spectra for (A) choline chloride (ChCl) and (B) urea.

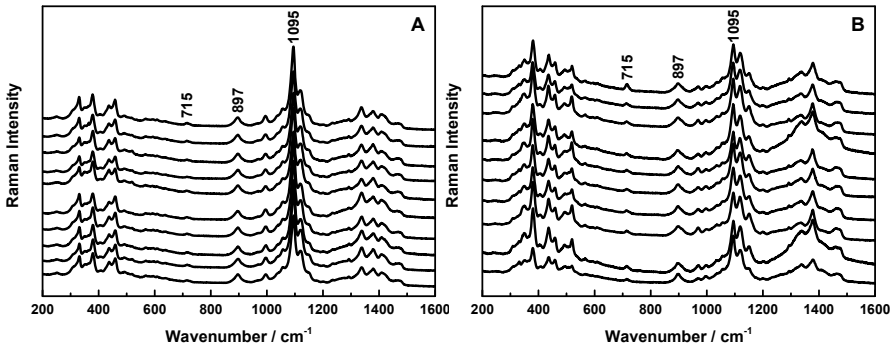

Fig. S3 Typical Raman spectra of 4. DES pulp recorded at different pulp fibres in (A) parallel and (B) perpendicular orientation of the fibres to the polarisation configuration of the laser light.

Paper III

Tenhunen Tiia-Maria; Peresin, Maria Soledad; Penttilä Paavo A.; Pere Jaakko; Serimaa, Ritva; Tammelin Tekla (2014) Significance of xylan on the stability and water interactions of cellulosic nanofibrils. Reactive and Functional Polymers 85, 157-166

Reactive & Functional Polymers 85 (2014) 157–166

Contents lists available at ScienceDirect

Reactive & Functional Polymers

journal homepage: www.elsevier.com/locate/react

Significance of xylan on the stability and water interactions of cellulosic nanofibrils

Tiia-Maria Tenhunen [a], Maria Soledad Peresin [a], Paavo A. Penttilä [b], Jaakko Pere [a], Ritva Serimaa [b], Tekla Tammelin [a,*]

[a] VTT – Technical Research Centre of Finland, P.O. Box 1000, FI-02044 Espoo, Finland
[b] University of Helsinki, Department of Physics, P.O. Box 64, FI-00014 Helsinki, Finland

ARTICLE INFO

Article history:
Received 5 July 2014
Received in revised form 26 August 2014
Accepted 28 August 2014
Available online 6 September 2014

Keywords:
Cellulose nanofibrils
Xylan
Electrosteric stability
Oxygen barrier
Films
Water interactions

ABSTRACT

In this paper, the significance of xylan on the behaviour of kraft birch pulp based nanofibrillated cellulose (CNF) is discussed. The influence of CNF xylan content on fibril morphology, charge and stability as well as on the film formation ability was investigated, and the features detected on nanoscale and on macroscale are compared. In addition to this, the ability of fibrils to uptake water molecules were investigated by bulk and surface sensitive methods which are dynamic water sorption analysis (DVS) and quartz crystal microbalance with dissipation monitoring (QCM-D) equipped with the humidity module, respectively. Surface xylan plays a significant role as an electrosteric stabilizer in dilute CNF dispersions when the surface forces are dominant whereas the removal of xylan drastically changes the CNF dispersion properties. The settling of the unstable CNF dispersions displays behaviour which is typical for hindered sedimentation. When considering thin nanoscale layers of CNF, nanofibrillated cellulosic materials with high content of surface xylan has somewhat higher ability to bind water molecules. However, it seems that in more concentrated CNF dispersions where the fibrillar network itself plays also a decisive role, especially with respect to film formation ability, the impact of xylan diminishes. Solvent cast macroscale CNF films are still enough dense to maintain good oxygen barrier performance at higher humid conditions although agglomeration tendency of fibrils is higher due to the excessive xylan removal. These findings are of high relevance when considering nanocellulosic materials, especially in the form of gels and films, as templates for high added value material solutions.

1. Introduction

Due to the unique physical features, e.g. high strength and stiffness of nanoscaled cellulosic materials (cellulose nanofibrils (CNF), microfibrillated cellulose (MFC) or cellulose nanocrystals (CNC)), there is a growing interest for seeking novel application areas [1–5]. The main reasons for the growing interest in CNF and MFC are the development of energy efficient and up-scalable production methods [6–8] and the extraordinary properties of this renewable material [9,10]. High aspect ratio and large interfacial area with an enhanced hydrogen bonding capability compared to native fibres enable the inherent gel formation [6] which makes it suitable to be incorporated in applications such as thickeners and emulsifiers for e.g. food, cosmetics and paints. Besides, the inherent film formation tendency of fibrils upon drying together with the facile and up-scalable film production methods [11–13], should open up numerous new opportunities for highly functional (nano)materials to be utilized e.g. as packaging materials [14], in electronics [15] and in diagnostics [16].

The main drivers to utilize nanoscaled lignocellulosic materials have been the sustainability trend, increasing prices of petroleum and possibility to gain additional functionalities which biobased building blocks may offer. In order to significantly improve and develop functional (nano)material structures using biomass derived building blocks, the understanding of the interfacial interactions becomes of high relevance. Nanocellulosic materials rarely exist as pure cellulose, on the contrary, plant derived cellulose nanofibrils contain hemicelluloses, lignin and wood extractives depending on the pulp source and processing. For example, birch kraft pulp based cellulosic nanofibrils utilized in this study contain approximately 23 wt% of glucuronoxylan, major hemicellulose present in hardwood [17]. Especially the accessible xylan located on fibril surface has a decisive role when dealing with interfacial interactions, physical properties and performance of new, advanced biomaterials [18–20]. On the other hand, the removal

* Corresponding author. Tel.: +358 20 722 4632.
E-mail address: tekla.tammelin@vtt.fi (T. Tammelin).

http://dx.doi.org/10.1016/j.reactfunctpolym.2014.08.011
1381-5148/

of xylan when processing of cellulosic biomass to green biorefineries have also been an active subject and several biomass pre-treatments have been developed, in order to recover hemicelluloses and use them in a more profitable pathway [21]. The potential of xylan has been seen for example in new bio-derived films and coatings, where it can be used in packaging applications as well as edible coatings and medical applications [22–26].

However, the impact of xylan removal on the properties of remaining cellulosic material is not trivial and the association of cellulose and xylan within biomass has been discussed in several studies. Cellulose fibrils are coated with hemicelluloses, which then form larger units that are embedded in a lignin–hemicellulose matrix [17]. In several studies, hemicelluloses have been noticed to have an impact in the aggregation behaviour of the cellulose by affecting the crystalline structure and changing the dimensions of the cellulose microfibrils [27–30]. Xylan has affinity towards fibres [31] and it also re-adsorbs onto fibres at the end of pulp cooking process with an impact on final properties of such fibres [32,33]. Few studies suggest that the presence of xylan on pulp fibres improves paper strength [34,35] since the presence of hemicelluloses promotes the formation of bond within cellulosic fibres. Thus, low hemicellulose content pulps are not desired for manufacture of high-quality paper and board, but they are a requisite for the production of dissolving-grades pulps [36]. With the increase in the current industrial interest on utilization of nanocelluloses for different applications, those pulps destined to the production of nanocellulose have a potential to be integrated in the biorefinery concept, as an alternative of hemicellulose source. To this end, deeper understanding on the effect of the removal of xylans on the final properties of these nanocelluloses is needed.

In this work the significance of glucuronoxylan on molecular level and macroscale level behaviour of cellulosic nanofibrils (CNF) is elucidated. The influence of xylan content on nanocellulosic fibril morphology, charge, colloidal stability as well as on film formation tendency and their oxygen barrier performance has been systematically investigated using a series of CNF grades with variable xylan content. In addition, the water interactions of CNF with respect to xylan content were revealed using bulk approach (dynamic vapour sorption, DVS, analysis) and surface sensitive approach (QCM-D equipped with humidity chamber).

2. Experimental

2.1. Materials

2.1.1. Pulp

Elemental chlorine free (ECF) never-dried bleached birch kraft pulp (UPM-Kymmene Oyj, Pietarsaari) was used as a raw material for the production of nanofibrillated cellulose grades (CNF) with variable xylan content. In order to control the fibre swelling and to enhance the fibrillation, the carboxyl groups of the pulp were converted to the sodium form prior to the fibrillation according to the method described previously [37]. Briefly, the method includes washing out the metal counterions from the pulp at low pH (0.01 M HCl, pH < 3). After filtration and washing with deionized water, conversion of the carboxyl groups into their sodium form is achieved by mixing the pulp with a discrete amount of 0.005 M $NaHCO_3$ solution. Finally, pH was set to slightly alkaline and rinsing with deionized water was performed in order to remove excess salt.

2.2. Methods

2.2.1. Preparation of pulps with variable xylan content

Birch kraft pulps of decreasing xylan content were prepared by selective and targeted xylan hydrolysis using purified *Trichoderma reesei* Xyl II (pI9) xylanase [38]. Hydrolysis was performed in deionized water at 45 °C for variable times (3, 24 and 68 h) and enzymatic action was terminated by soaking the pulps in a hot water bath (90 °C, 15 min). Carbohydrate composition of the pulps were analysed by HPLC after the enzymatic total hydrolysis to monosaccharides was achieved [39]. Charge of the pulps was measured using the standard titration method SCAN CM 65:02.

2.2.2. Preparation of nanofibrillated cellulose

Pre-refining of the pulp was carried out with a Voith laboratory scale refiner (LR-1, Voith) to ease feeding and to avoid clogging during fibrillation. Fibrillation was performed using a high-pressure fluidizer (Microfluidizer EH110, Microfluidicies Corp.) after diluting pulps to a consistency of 1.8% with deionized water and pre-dispersing using Dispermat (VMA Getsman Gmbh) at 3400 rpm for 60 min. Several successive passes through two differently sized chamber pairs were performed in order to induce efficient fibrillation. First, the pulps passed a chamber pair with diameters of 400 μm and 200 μm at a pressure of 1350 bars, followed by 17 passes through a chamber pair with diameters of 400 μm and 100 μm at a pressure of 1850 bars. Final material appearance was that of a viscous, gel-like material. Samples were then stored at +4 °C until further used.

2.2.3. Microscopic analysis of CNF with variable xylan content by AFM and SEM

The size of nanofibrillated cellulose grades with different xylan content was analysed using Atomic Force Microscopy (AFM) and Scanning Electron Microscopy (SEM). AFM imaging was performed using a Nanoscope IIa Multimode scanning probe microscope (Digital Instruments Inc., Santa Barbara, CA USA). The nanofibril samples were prepared by spincoating a dilute CNF dispersion on silica surface as described in Ahola et al. [40]. The images were scanned in tapping mode, in air using silicon cantilevers (IMasch, Tallinn, Estonia) with nominal resonance frequencies of 320–360 kHz. No image processing except flattening was made and at least 5 areas on each sample were measured.

SEM imaging was performed using LEO DSM 982 Gemini FEG-SEM (Noran Instruments Inc. Middleton, USA). The nanofibril samples were first solvent exchanged to acetone and the removal of acetone was carried out by critical point drying method (CPD, Bal-Tec CPD 030 Critical Point Dryer) using CO_2 as the transition liquid. Prior to the SEM analysis the CNF samples were sputter coated (Agar Automatic Sputter Coater, Stansted, UK) with platinum to improve specimen conductivity and examination was performed using an acceleration voltage of 2.0 keV.

2.2.4. Crystallinity analysis of pulp and CNF with variable xylan content by WAXS

Freeze-dried pulp and CNF samples were pressed into metal rings of thickness of 1 mm and wide-angle X-ray scattering (WAXS) was measured under perpendicular transmission geometry. The used setup consisted of a Seifert ID 3003 X-ray generator equipped with an X-ray tube producing Cu Kα radiation (wavelength 1.54 Å). The X-ray beam was monochromatized with a Montel multilayer and the scattering pattern was recorded by a two-dimensional image plate detector (MAR345, Marresearch). The measured intensity was corrected for measurement geometry, angle-dependent absorption and backgrounds due to air-scattering and noise from to the image reading of the detector. Crystallinity and crystal width in the [200] direction of cellulose Iβ were obtained from the corrected WAXS intensities by applying the fitting procedures described in Penttilä et al. [41].

2.2.5. Stability of CNF dispersions

The stability of the dilute CNF dispersions with variable xylan content was measured using turbidity analyser Turbiscan LAB (Formulaction SA, L'Union, France) in which transmission, light and backscattering were measured. 0.05 wt% CNF dispersions with varying electrolyte concentrations (0.1 M, 0.01 M and 0.001 M NaCl) were prepared using homogenizer (Heidolph, SilentCrusher M, Typ 18 F/M, Germany) during 1 min at 12,000 rpm. The dispersions were analysed in a cylindrical glass cell, in scanning mode, where the optical reading head scanned the length of the sample cell (up to 55 mm), acquiring transmission and backscattering data every 40 μm. Data was collected every 5 min during 2 h. The measurements were plotted into curves where transmitted and backscattered light flux are provided in percentages relative to standards (suspension of monodisperse spheres and silicone oil) as a function of the sample height, measured on millimetres.

2.2.6. Water vapour uptake and release of CNF with variable xylan content by DVS and QCM-D

Dynamic gravimetric water vapour sorption instrument (DVS, Surface Measurement Systems, UK) was applied to determine water vapour sorption isotherms for the freeze-dried CNF powders with different xylan content at 20 °C. The results were expressed as total water content versus relative humidity. The curve was calculated from the mass change of dry CNF at different relative humidity and from initial water content of one sample (three replicates) in RH 54% which was determined by Karl Fischer titration using a method reported earlier by Partanen et al. [42]. Extraction was performed with methanol–formamide mixture (1:1).

Quartz crystal microbalance with dissipation monitoring (QCM-D E4, Q-sense AB, Göteborg) equipped with humidity module (QHM401) was used to monitor the water vapour uptake and release ability of thin films of CNF with different xylan content. The QCM-D technique enables the *in situ* studies of mass changes taking place at solid/liquid and solid/gas interface. The interpretation of the QCM-D data is described in detailed elsewhere [43,44]. Briefly, the piezoelectric quartz crystal oscillates at a resonance frequency f_o which is lowered or increased when mass changes are sensed on the surface of the crystal. The resonant frequency of the crystal depends on the total oscillating mass, including the water coupled to the oscillation. By measuring simultaneously several overtones of frequency and dissipation responses, it becomes possible to determine whether the layer on the sensor surface is fully elastic or viscoelastic which is not possible by looking only at the frequency response. If the film on the sensor surface is not fully elastic (rigidly adhered), frictional losses occur that lead to damping of the oscillation with a decay rate of amplitude which is dependent on the viscoelastic properties of the material. With the QCM-D the change in dissipation ($\Delta D = D - D_0$) is measured and the energy dissipation, D, is defined by Eq. (1).

$$D = \frac{E_{\text{diss}}}{2\pi E_{\text{stor}}} \tag{1}$$

where E_{diss} is the total dissipated energy during one oscillation cycle, E_{stor} is the total energy stored in the oscillation. The change in dissipation (ΔD), measures qualitatively the rigidity and softness of the film adhered on the sensor surface. The film can be considered fully elastic and rigid when $\Delta D \leqslant 1 \times 10^{-6}$. If the layer is evenly distributed, rigidly attached, fully elastic and small compared to the mass of the crystal, the change in frequency is directly proportional to the mass change per unit surface by the Sauerbrey equation [45].

$$\Delta m = -\frac{C\Delta f}{n} \tag{2}$$

where Δm is the mass change per unit surface, C is a constant that describes the sensitivity of the device to changes in mass, Δf is the frequency shift and n is the overtone number ($n = 1, 3, 5, 7$).

CNF thin layers with constant areal mass of 11–15 mg/m^2 were prepared by spin coating (at 3000 rpm for 10 min) 50 μl of dilute (~0.05–0.1 wt.%) and ultrasonic treated (ultrasonic microtip, Branson Digital Sonifier) CNF dispersions on the QCM-D sensors (AT-cut quartz crystals coated with silica, supplied by Q-sense with the thickness of 0.3 mm, fundamental frequency (f_0) of ≈ 5 MHz and sensitivity constant (C) of ≈ 0.177 mg m^{-2} Hz^{-1}). Prior to the spin coating of the CNF suspension, the sensors were cleaned with UV/ozone treatment for 15 min and immersed to polyvinyl amine (PVAm) solution when necessary to improve the adhesion within sensor surface and nanofibrils as described in Ahola et al. [40]. In case of high xylan content CNF the anchoring layer of PVAm was needed whereas the adhesion within fibrils and sensor surface was sufficient without premodification.

The constant areal mass (11–15 mg/m^2) of the spin coated CNF layers was determined using a QCM-D humidity module by measuring the difference in frequency response of the sensor, before and after CNF deposition in air upon stabilization of the signal at 23 °C with an air flow of 0.1 ml/min for 25 min. After spin coating, the CNF layer was rinsed with Milli-Q water, dried with N_2 (g) and heat-treated in oven for 30 min at 80 °C to evaporate the remaining water and enhance the adhesion. Finally, the collected frequency data before and after CNF deposition was stitched together using QTools-software, and the areal mass of the CNF films was calculated using the Eq. (2) as described in Peresin et al. [46]. High xylan content CNF layer yielded the areal mass of 11 mg/m^2 and low xylan content CNF layer yielded the areal mass of 14.5 mg/m^2.

Prior to the humidity uptake measurements, CNF coated sensors were stored in desiccator, in dark and were allowed to stabilize inside the QCM-D humidity module at RH 11% overnight. Finally water vapour uptake and changes in viscoelastic properties of the CNF layers were followed by monitoring the frequency and dissipation changes as a function of time when exposed to different relative humidities. This was done by circulating different saturated salt solutions (Table 1) through the humidity chamber using a peristaltic pump (High Precision Multichannel Dispenser, Ismatec, Germany) at a flow rate of 100 ml/min for 30 min at 23 °C.

2.2.7. Oxygen permeability

The oxygen transmission rate (OTR) through the CNF films with variable xylan content was determined according to the standard ASTM F1927 using Ox-Tran 2/20 Oxygen transmission rate tester (Mocon, Modern Controls Inc., USA). CNF films of 30 μm thickness were prepared by solvent casting 0.4 wt% CNF dispersions on petri dish, targeting test area of 8 cm^2. The tests were carried out at 23 °C and at varying relative humidity between 0% RH and 90% RH using 100% oxygen as test gas.

Table 1
Different saturated salt solutions and respective relative humidity used in water vapour uptake monitored with QCM-D [47].

Salt solution	Relative humidity (%)
LiCl	11
MgCl2	33
$Mg(NO_3)2$	53
NaCl	75
K_2SO_4	97
Pure milliQ H_2O	100

3. Results and discussion

3.1. Chemical composition, charge and morphology of pulp and CNF samples

In order to clarify the role of glucuronoxylan on the molecular level and on the macroscale level behaviour of nanofibrillated cellulose, a series of pulps with different xylan content was prepared using bleached kraft birch pulp as starting material, see Table 2. These pulps were further fibrillated using high shear and high pressure fluidizer to achieve nanofibrillated cellulose grades with similar and comparable fibrillar dimensions with four different xylan contents. Besides xylan, the reference pulp contains only traces of non-cellulosic residuals, 0.2% lignin and 0.09% extractives [48], and thus, the chemical composition of pulps and CNFs is well known.

Birch pulps with varying xylan content were produced by enzymatic hydrolysis using purified *Trichoderma reesei* xylanase II, which has previously shown to be a specific method to extract/hydrolyse xylan without any hydrolytic action on other pulp components [49]. The carbohydrate composition of the pulps with four levels of glucuronoxylan as monosaccharides and acidic oligomers is summarised in Table 2.

As shown by Table 2, the bleached birch pulp used as a starting material contains approximately 23% xylan. The acidic side groups, glucuronic and hexenuronic acid groups, contribute to the anionic charge of the fibres and fibrils. With extending xylanase treatment times (3 h, 24 h and 68 h), a set of pulps with decreasing glucuronoxylan content was obtained (~21%, ~17% and ~13% of xylan, respectively). The most severe xylanase treatment (68 h) removed approximately 43% of the original xylan. As previously shown, the hydrolysable xylan fraction in bleached birch pulp is amorphous and loosely bound on cellulose surface whereas the residual fraction is more tightly associated to cellulose and cannot be removed by xylanase [18,50].

As expected, the charge of the fibres determined by the conductometric titration was correspondingly decreased as a function of pulp xylan content (Table 2). It is worthwhile to notice that the sensitivity of the conductometric titration seems to be rather low, especially when considering the medium and low xylan content pulps with low amount of charged side groups (only minor pulp charge changes detected by titration). However, the decreasing amount of acidic oligomers gives additional evidence on the decreasing anionic character of the fibres. The pH of pulps and the produced CNF was within 6–7 and the conductivity of the CNF suspension was ~5 μS/cm. Therefore, all the investigated changes in CNF stability, water sensitivity and film formation ability discussed in this paper can be expected to take place only due to the changes in CNF xylan content.

Extensive high shear and high pressure fibrillation of the pulps with variable xylan content through the microfluidizer resulted in gel-like nanocellulosic materials with solid content of ~1.8%. The SEM and AFM images of the carefully dried nanofibrils show that the dimensions of the fibrils were similar despite of the different xylan content. The fibril width, which is roughly estimated to be approximately 10 nm, is fully independent from the carbohydrate composition and furthermore, the size distribution of the fibrils seems to be uniform, whilst large fibre-like structures were not detected.

The effects of xylan removal and nanofibrillation on the crystal structure of cellulose were studied with WAXS (Fig. 2, Table 3). During the xylanase hydrolysis, cellulose crystal size in the [200] direction (crystal width) did not change systematically, remaining between 4.3 and 4.4 nm, whereas the removal of xylan resulted in a slightly increasing trend in sample crystallinity which can be due to a removal of loosely bound and more disordered xylan from the sample. A more obvious increase in sample crystallinity (from 43% to 50%) was detected in the CNF samples, which was accompanied by an increase in the width of cellulose crystallites from 4.0 to 4.2 nm. As an overall trend, however, both the sample crystallinity as well as the crystal width decreased during nanofibrillation, which can be accounted to the high mechanical shearing forces present during the fibrillation. The decrease in sample crystallinity during the fibrillation was more pronounced with the samples containing high amount of xylan (from 49% to 43%). The presence on anionic xylan facilitates the liberation of fibrils similarly as carboxymethylation [7] and TEMPO-oxidation [8] of pulp by generating repulsion between fibrils. Thus, the impact of shearing on CNF morphology seems to be higher leading to less ordered fine structure of the fibrillar material. Fibrillar dimensions, especially the fibril width, however, remained unaltered as seen in Fig 1.

3.2. Assessment of CNF dispersion stability

According to the results shown above, the most significant distinctions within the samples can be achieved by selecting the CNF samples containing the highest and lowest amounts of xylan (~23% and ~13% xylan, respectively) Therefore, the meaningful comparisons can be carried out by selecting these two CNF grades in order to explain the role of xylan, as well as the mechanisms when dealing with the CNF dispersion stability. The aim of the stability investigations here was to clarify the interactions within the individual nanofibrils, whilst avoiding the contribution of the CNF network on stability. Thus, the dilute CNF dispersions with the solid content as low as 0.05 wt.% were used for Turbiscan measurements.

Fig. 3 shows the measured light transmission curves of the CNF dispersions analysed along the sample cell. The achieved results can be simply interpreted as follows: the higher the light transmission (transparency of the sample), the more stable the CNF dispersion (clear dispersion). In addition, variations detected in transmission curves along the sample cell indicate disturbances in stability i.e. agglomeration and/or sedimentation occurs. As shown in Fig. 3, a dispersion prepared using high amount of xylan containing CNF is highly stable, since no variations take place in the transmission curve along the whole cell height. It can be clearly seen that the removal of xylan deteriorates the stability of the CNF dispersion. After 20 min clear variations in the transmission curve can be detected. This indicates that the CNF dispersion flocculates and larger agglomerates gradually settle.

To further investigate the mechanisms contributing to the stability within the cellulosic nanofibrils, the effect of electrolyte

Table 2
Carbohydrate composition and charge of the birch pulps used for production of nanocellulose samples.

Pulp sample	Neutral sugars and acidic oligomers (mg/100 mg)				Anionic charge (mmol/kg)
	Glucose	Xylose	Methyl glucuronic acid	HexA oligomers	
High xylan	73.0	23.0	0.154	0.086	39
Medium xylan 1	79.1	21.0	0.126	0.064	19
Medium xylan 2	80.7	16.8	0.092	0.041	15
Low xylan	88.5	13.3	0.078	0.020	13

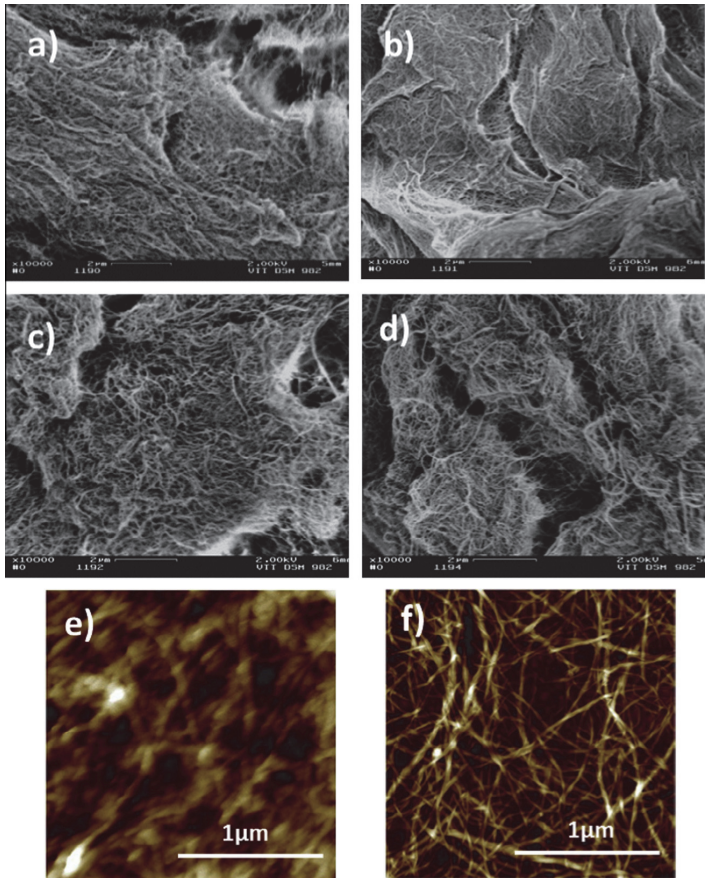

Fig. 1. SEM images (×10,000) (a–d) and AFM topography images (e–f) of nanofibrillated cellulose with variable xylan content. (a) CNF with high xylan content, (b) CNF with intermediate xylan content (level 1), (c) CNF with intermediate xylan content (level 2), (d) CNF with low xylan xylan content, (e) CNF with high xylan content and (f) CNF with low xylan content. The AFM image size is 4 μm^2 and the height scale 60 nm and 35 nm, respectively.

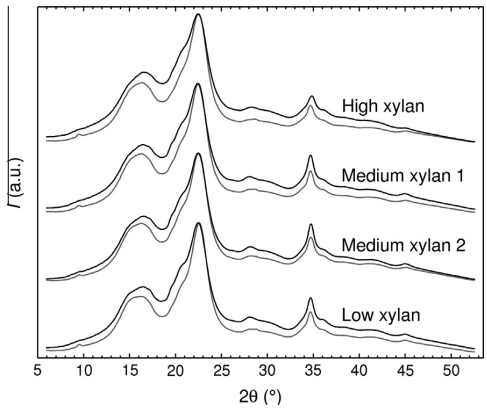

Fig. 2. WAXS intensities of pulp and CNF samples with different xylan content (pulps with grey line, CNFs with black line) normalized with the mean intensity between $2\theta = 46°$ and 48° and shifted vertically for clarity.

concentration on CNF dispersion stability with respect to CNF xylan content was analysed. Table 4 shows the NaCl concentrations and the effect of electrolyte addition on conductivity and pH of the CNF dispersions. The pH of the dispersions remained more or less stable and therefore only the amount of xylan and the electrolyte addition is considered to have influence on CNF dispersion stability.

As shown by Fig. 4a, despite of the gradual increase in ionic strength, after two hours the shape of light transmission curves remains unaltered when considering high xylan content CNF dispersion. However, the level of the curve is somewhat decreased whilst the noise of the curve is increased. These changes indicate minor disturbances in the dispersion stability but electrolyte addition did not lead to any local concentration variations originating from the migration of the cellulosic nanofibrils.

It seems that although the stability is affected by the addition of simple electrolyte, the interactions within the fibrils are dominated by steric contributions, not only by double-layer repulsion. Loosely bound charged glucuronoxylan located on the nanocellulose fibril surface seems to effectively stabilise the CNF dispersion through the electrosteric interactions. In the system, electrostatic contribution derives from the repulsion within the charged acidic groups whereas the steric contribution is derived from loosely bound and more mobile xylan molecules located on the fibril surface. Electrolyte addition has been shown to affect the conformation

Table 3
Crystal width corresponding to the (200) reflection of cellulose and crystallinity (CrI) of whole sample and their cellulose fractions determined from WAXS intensities.

Sample	Crystal width (nm)	Sample crystallinity (%)[a]	Cellulose crystallinity (%)[b]	Cellulose content (wt.%)[c]
High xylan pulp	4.3 ± 0.1	49 ± 3	60	66
Medium xylan 1 pulp	4.4 ± 0.1	52 ± 3	59	71
Medium xylan 2 pulp	4.3 ± 0.1	53 ± 3	59	73
Low xylan pulp	4.4 ± 0.1	52 ± 3	53	80
High xylan CNF	4.0 ± 0.1	43 ± 3	53	66
Medium xylan 1 CNF	4.0 ± 0.1	45 ± 3	51	71
Medium xylan 2 CNF	4.1 ± 0.1	50 ± 3	56	73
Low xylan CNF	4.2 ± 0.1	50 ± 3	51	80

[a] Proportion (wt.%) of crystalline cellulose (I_β) in whole sample.
[b] Calculated based on cellulose content.
[c] Cellulose content as anhydrosugars.

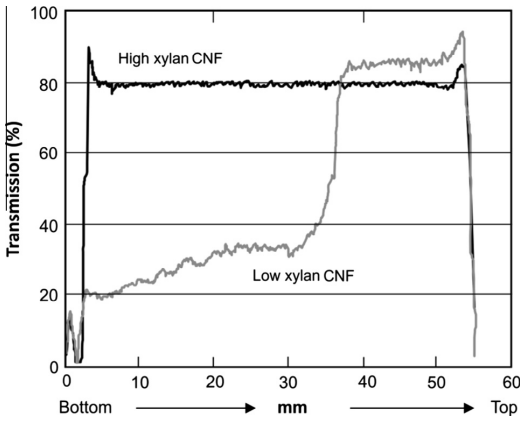

Fig. 3. Transmission profiles of high xylan content CNF and low xylan content CNF. Samples are scanned from bottom to top $t = 20$ min.

Table 4
The effect of electrolyte addition on conductivity and pH.

Sample	NaCl (M)	Conductivity (μS/cm)	pH
High xylan CNF	0	5.2	6.6
	0.001	125.5	6.6
	0.01	1135	6.3
	0.1	9895	6.2
Low xylan CNF	0	4.9	6.3
	0.001	125	6.4
	0.01	1145	5.7
	0.1	9890	6.0

of the xylan located on the cellulose surface via electrostatic interactions [51] although the overall effect of electrostatics on xylan behaviour was shown to be relatively weak [52]. At high electrolyte concentration the mobile xylan layer on the cellulosic fibril surface probably takes rather compact conformation (electrostatic repulsion between anionic charges are screened in the presence of NaCl) which can be expected to lower the steric repulsion within the fibrils. The lowered steric repulsion and screened electrostatic interactions can be seen as minor changes in CNF dispersion stability (Fig 4a). However, high amount of xylan located on the fibril surface although being in a more compact conformation is still a source for steric interaction since severe agglomeration and sedimentation do not occur.

Fig. 4b gives supplementary evidence on the interactions dominating within the fibrils in the presence of surface xylan. If more loosely bound and charged surface xylan is removed, the stability of the fibrils is completely deteriorated. The dilute CNF dispersion with 13% of xylan rapidly agglomerates even without the electrolyte addition (see light transmission curves after 20 min in Fig 3 and after 2 h in Fig 4b). Fibrils with low xylan content are weakly charged (see Table 2) but the charge state is not high enough to create an effective electrostatic repulsion within the fibrils in order to prevent the agglomeration of the CNF dispersion. According to Fall et al. [53] approximately three times higher CNF surface charge is needed to stabilise the fibrils via electrostatic repulsion at neutral pH and at low ionic strength, and still severe agglomeration took place upon salt addition. Simultaneously the xylan removal leads to the elimination of the steric hindrance and the fibrils instantaneously agglomerate upon the electrolyte addition. The absence of thermodynamic repulsive forces results in agglomeration of individual fibrils leading to the formation of fibrillar entanglements arranged as a network structure with higher viscosity. It is well known that CNF dispersions form entangled, gel-like network structures already at low solid content [6]. In such system the sedimentation behaviour corresponds to a hindered sedimentation or hindered settling regime where the interface between settling suspension and supernatant is clear, sharp and slowly moving [54]. CNF dispersion with low xylan content behaves exactly this way, see Fig. 5. As time proceeds loosely bound CNF flocks interact, and the dispersion settling leads to formation of compacting sediment, which can be seen as decreasing transparency values as the function of time at the bottom of the sample cell. Simultaneously the length of the clear supernatant boundary falls with time indicating hindered sedimentation regime in which the formation of stronger network and collective compaction occur. Therefore, the CNF network contributes to the stability behaviour of CNF dispersions already at low concentrations mainly due to the formation of viscous gel, and rather than single CNF fibril or flock migration, the collective compaction of entangled fibrillar flocks takes place during the agglomeration of CNF dispersion.

3.3. The influence of CNF xylan content on the interactions with water molecules

High surface area of nanofibrillated cellulose results in large amount of available hydroxyl groups located on the fibril surface. Additionally, the presence of glucuronoxylan introduces carboxylic acid groups on the fibril surface. Both of this groups are highly susceptible towards water and, therefore, the influence of CNF glucuronoxylan content on the interactions with water molecules were systematically investigated using bulk approach (dynamic vapour sorption, DVS, analysis) and surface sensitive approach (QCM-D equipped with humidity chamber).

Fig. 6 shows a typical sigmoidal shape profile for the water uptake behaviour when plotted versus relative humidity content obtained for cellulosic and many other hydrophilic materials

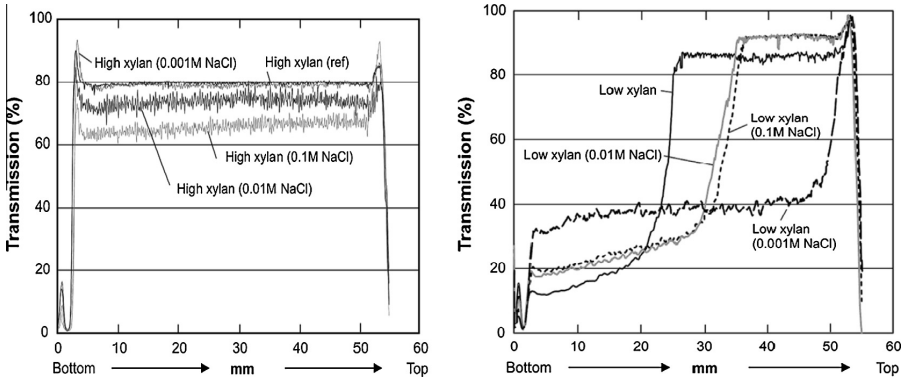

Fig. 4. Transmission profiles of high xylan content CNF and low xylan content CNF. Samples are scanned from bottom to top $t = 2$ h.

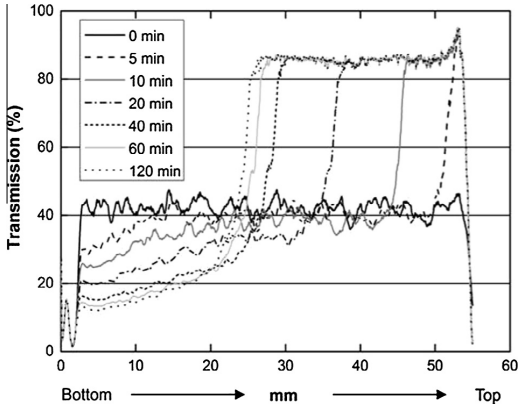

Fig. 5. Time dependence of transmission profiles of low xylan content CNF. Samples are scanned from bottom to top.

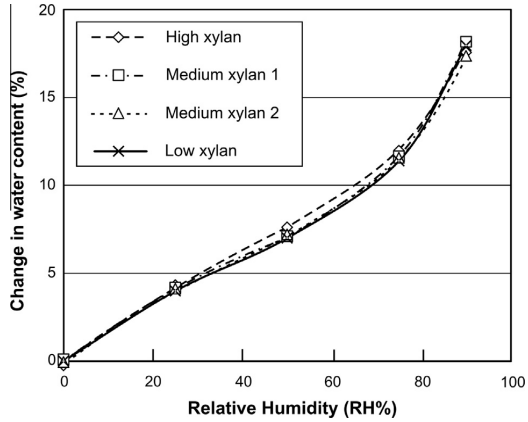

Fig. 6. Change in water content vs. relative humidity for nanofibrillated cellulose samples with variable xylan content at 20 °C determined by DVS analysis.

[55]. The behaviour of cellulose nanofibrils when exposed to different relative humidity levels is more or less similar regardless on the xylan content or fibril morphology. The similar behaviour is also reported by Arola et al. [19] for the xylanase treated CNF grades as well as by Belbekchouche et al. [56] for the nanoscaled cellulosic materials with different morphologies from sisal.

In order to gain deeper understanding how chemical composition, especially the xylan content of nanofibrillated cellulose is influencing on the water uptake ability of the nanocellulosic materials, the water vapour uptake was followed using highly surface sensitive QCM-D (quartz crystal microbalance with dissipation monitoring) method equipped with the humidity module. Thin layers of nanocellulose (11–15 mg/m^2) with different xylan content were deposited on quartz crystal by spin coating, and the layers were then exposed to gradually increasing relative humidity levels. The mass uptake as a change in frequency due to water vapour was monitored simultaneously with the change in dissipation which enables the qualitative assessment of the rigidity and softness of the CNF layers when exposed to different levels of humidity. This information is highly essential when considering the material behaviour in the presence of water especially when e.g. permeability of molecules is relevant.

As previously shown in this study, the most meaningful comparison of the CNF samples can be carried out when selecting nanofibrillated cellulose grades with the lowest and highest amount of xylan. Prior to the vapour uptake measurements, the spin coated nanocellulosic layers were allowed to stabilize in the relative humidity of 11% overnight (~16 h). Fig. 7 shows the behaviour of the CNF layers with high amount of xylan (~23% xylan) and the lowest amount of xylan (~13% xylan) at RH 11%. Increasing changes in frequency indicate that the CNF layers, although stored in dry conditions in desiccator are still releasing some moisture. The frequency change curves level off, and the equilibrium with the surrounding humidity can be considered to be achieved after 13 h when the frequency change is less than the typical instrumental drift (<0.5 Hz/h). Changes in dissipation remained close to zero during the entire stabilisation step, indicating that the CNF layers are rigidly attached on the sensor surface. Rapid minor changes in dissipation factor seen in Fig. 6 cannot be interpreted as true changes in rheological behaviour of CNF layers due to the moisture release.

Fig. 8 shows the most informative part of the QCM-D water vapour uptake analysis for high xylan content CNF and low xylan content CNF in which the changes in frequency and dissipation are followed as a function of gradually increasing relative humidity (RH 11%–RH 97%). The lowest level of relative humidity (RH 11%) is set as a baseline for the measurement.

At first glance both thin layers of CNF have very similar response towards gradually increasing moisture content. CNF

layers are very sensitive towards moisture since clear negative changes in frequency (positive mass change) can be instantaneously detected with increasing levels of relative humidity. Changes in dissipation remained zero indicating that the fibrils are rigidly attached on the sensor surface. Minor changes in dissipation seem to take place when the humidity level reached the RH 97% indicating slight changes in CNF layer properties. CNF layers become slightly less rigid which may originate from swelling of the fibrils. However, these layers with the areal mass of ~15 mg/m^2 are exceedingly thin and therefore the attained responses are probably due to the behaviour of individual fibrils and their submonolayers not due to the response of the entire evenly distributed fibrillar network upon exposure to different levels of humid air. Previously we have shown that thicker layers (areal mass of ~170 mg/m^2) of CNF deposited on the QCM-D sensor surface have shown higher changes in dissipation (up to 4.5×10^{-6}) with increasing relative humidity [57] and therefore these previously reported responses may originate also from softening of the entire CNF network. Based on these findings, the swellability of surface xylan could not be observed as has been recently shown by Uetani and Yano [20] since here both CNF layers, independently from the surface xylan content, showed similar water molecule induced changes in rheological properties, see right hand side of Fig. 8.

Fig. 9 summarises the water vapour uptake data as milligrams of water bound by milligrams of CNF calculated using Sauerbrey equation from data collected using the 3rd overtone.

CNF with high xylan content (~23 wt.%) seems to be able to uptake to some extent higher amount of water molecules compared to CNF with low xylan content (13 wt.%). This trend is even more pronounced at higher levels of humidity (75% and 97%). The deviation of the water vapour uptake analysis is < 0.004 mg H_2O/mg deposited cellulosic material at relative humidity levels of 11–75% and ~0.03 mg H_2O/mg deposited cellulosic material at RH 97% [58]. The differences are however rather minor and they become merely significant only when the surface behaviour is dictating the material performance in the presence of water molecules.

3.4. Oxygen barrier performance of CNF films with variable xylan content

Highly hydrophilic CNF films have shown significantly retarded oxygen permeability values also at higher humid conditions (RH% 50–75) [14], see also Fig. 10. The oxygen barrier performance of CNF films is not lost completely until above relative humidity level of 80%.

The substantial difference of CNF films when compared to films from other natural polymeric sources is that the original fibrillar substructure of cellulose I with tightly packed crystalline regions which are impermeable in water are present in the film structure. Together with the crystalline regions, nanoscaled fibrils with high aspect ratio create orientation and therefore more tortuous diffusion path [59] for molecules to permeate through film. In

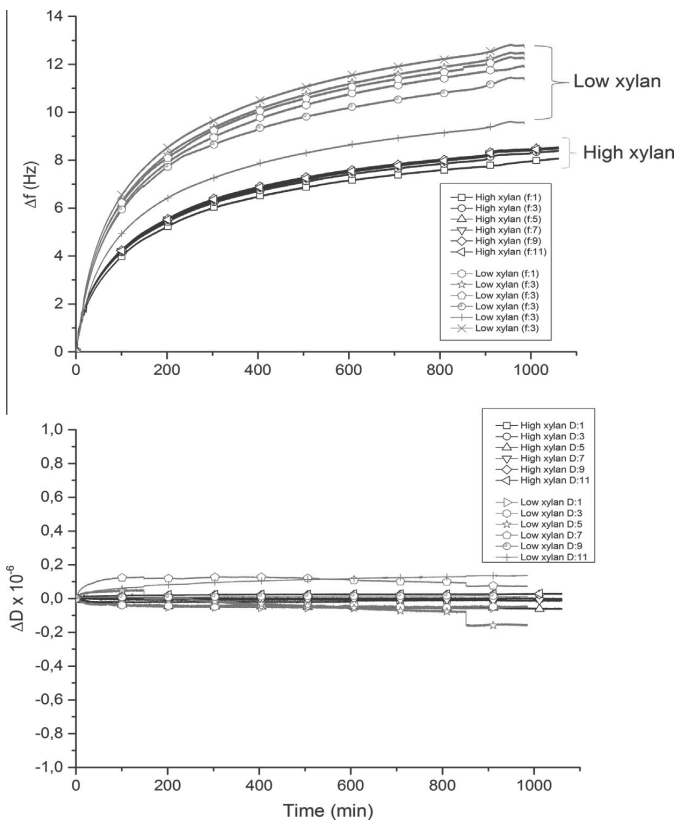

Fig. 7. Changes in frequency (top) and changes in dissipation (bottom) as a function of time recorded for spin coated CNF thin layers with low and high xylan content as stabilisation steps at RH11%. The constant areal mass of the CNF layers deposited on QCM-D sensor is ~15 mg/m^2 (f_0 = MHz, n = 1, 3, 5, 7, 9, 11).

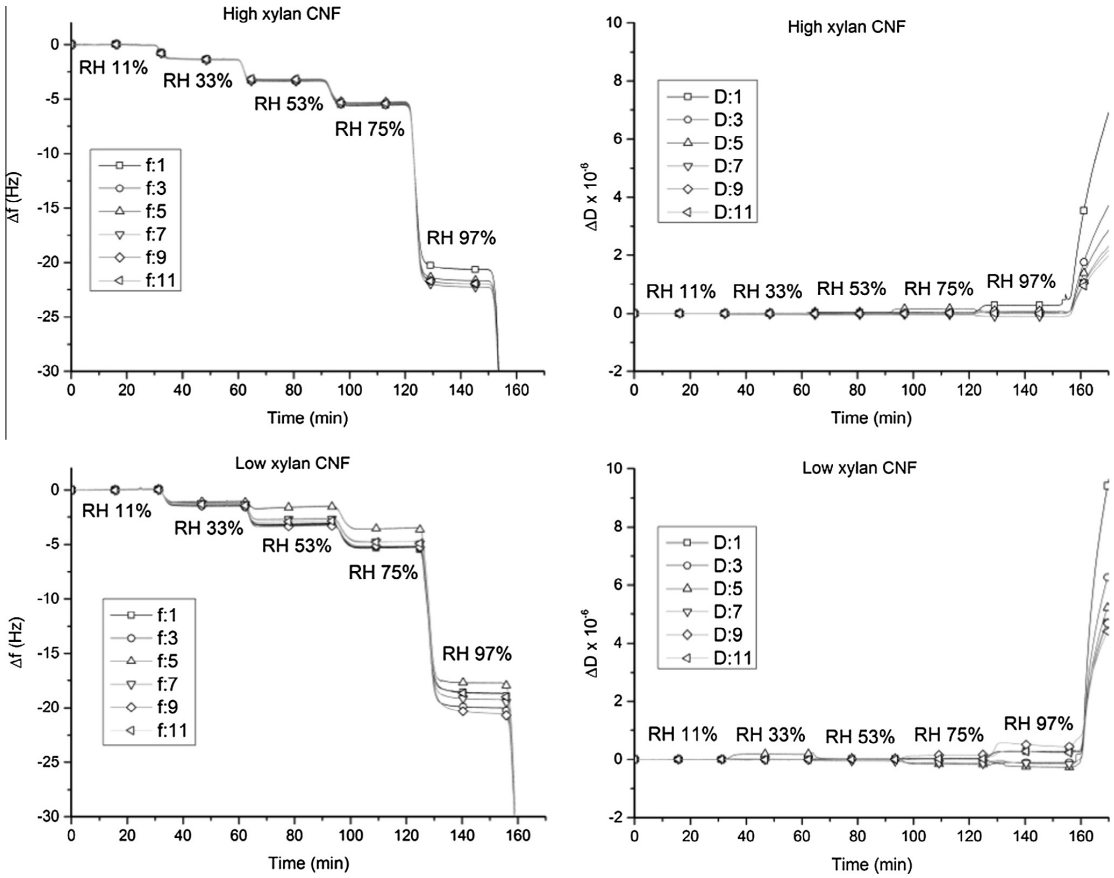

Fig. 8. Change in frequency (left) and dissipation (right) as a function of time for high xylan CNF with the areal mass of 11 mg/m^2 (top) and low xylan CNF with the areal mass of 14.5 mg/m^2 (bottom) at different levels of humidity (f_0 = MHz, n = 1, 3, 5, 7, 9, 11).

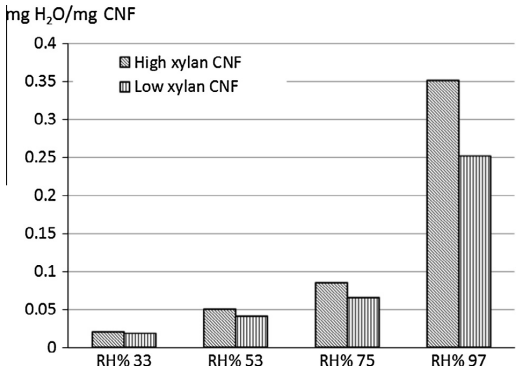

Fig. 9. Water vapour uptake ability of CNF thin layers calculated using Eq. (2). based on data shown in Fig. 8.

addition, strong inter-fibrillar interactions via hydrogen bonding lead to the formation of dense and strong film structures. Since CNF films possess such crucial features (polarity, crystallinity, orientation, close packing and high aspect ratio) which have a positive influence on lowered oxygen permeation rates as a function of

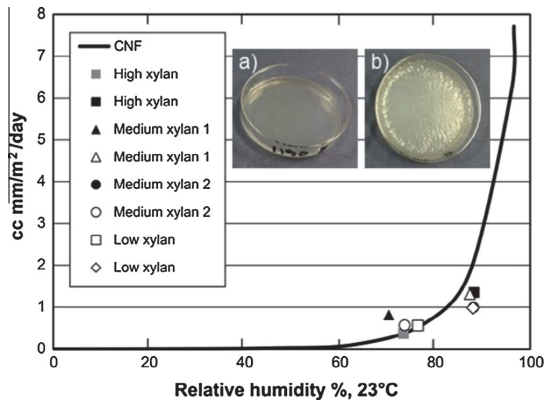

Fig. 10. Oxygen transmission rates as a function of relative humidity for CNF films with variable xylan content. Photographs indicate visually the agglomeration tendency of low xylan content CNF upon drying (b) when compared to stable high xylan containing CNF dispersion (a). Trendline is added as a visual guide but is based on the true oxygen barrier behaviour of CNF films prepared using unmodified birch kraft pulp derived fibrils.

relative humidity, the oxygen permeability can be low even at higher humid conditions. As shown by the QCM-D investigations in Fig. 8, the cellulosic nanofibrils are capable to uptake 3–4 times more water vapour when the relative humidity is increased from 75% up to 97%. Simultaneously fibrils show softening (increase in change in dissipation) and this explains why the material properties are significantly altered at this high level of humidity and why plain CNF films are poor water vapour barriers and poor oxygen barriers at high humidity.

Increased agglomeration tendency of nanofibrils due to disturbed stability of low xylan content CNF dispersion can be visually observed also during the film formation upon drying as seen in photographs in Fig. 10. Surprisingly the flocculation tendency did not affect the oxygen barrier performance of the films. The formed films are enough even and dense in order to maintain the low oxygen transmission rates despite of the agglomeration tendency of fibrils due to the xylan removal.

4. Conclusions

In dilute colloidal CNF dispersions glucuronoxylan located on the fibril surface has a significant role as an electrosteric stabilizer. The presence of surface xylan prevents the agglomeration of CNF dispersions also at high electrolyte concentrations. Thus, in molecular level the benefits of xylan are evident and this is when the surface forces are dominating and dictating the behaviour of the system. However, from the practical point of view, it is worth noting that CNF with reduced xylan content did not represent a major problem for the manufacture of macroscale films since for example oxygen barrier performance of the films were still on the acceptable range. When considering the water interactions with respect to presence of surface xylan investigated using surface sensitive methods, CNF submonolayers with high xylan content seems to be able to some extent uptake higher amount of water compared to CNF layers with low xylan content. The similar trend could not be observed using bulk approach and again in macroscale the significance of xylan diminishes and the fibrillar network plays the prevailing role.

Acknowledgements

Finnish Funding Agency for Technology and Innovation, Tekes, and companies within the Naseva II project are acknowledged for financial support. The CNF sample was received from UPM Kymmene Corporation. Vuokko Liukkonen, Katja Pettersson, Heljä Heikkinen and Teija Jokila are thanked for their valuable laboratory assistance.

References

[1] Y. Habibi, L.A. Lucia, O.J. Rojas, Chem. Rev. 110 (2010) 3479–3500.
[2] S.J. Eichhorn, Soft. Matter. 7 (2011) 303–315.
[3] D. Klemm, F. Kramer, S. Moritz, T. Lindström, M. Ankerfors, D. Gray, A. Dorris, Angew. Chem. Int. Ed. 50 (2011) 5438–5466.
[4] A. Dufresne, Nanocellulose From Nature to High Performance Tailored Materials, Walter De Gruyter, Berlin/Boston, 2012.
[5] I. Siró, D. Plackett, Cellulose 17 (2010) 459–494.
[6] M. Pääkkö, M. Ankerfors, H. Kosonen, A. Nykänen, S. Ahola, M. Österberg, J. Ruokolainen, J. Laine, P.T. Larsson, O. Ikkala, T. Lindström, Biomacromolecules 8 (2007) 1934–1941.
[7] L. Wågberg, G. Decher, M. Norgren, T. Lindström, M. Ankerfors, K. Axnas, Langmuir 24 (2008) 784–795.
[8] T. Saito, S. Kimura, Y. Nishiyama, A. Isogai, Biomacromolecules 8 (2007) 2485–2491.
[9] A. Walther, I. Bjurhager, J.-M. Malho, J. Pere, J. Ruokolainen, L.A. Berglund, O. Ikkala, Nano Lett. 10 (2010) 2742–2748.
[10] S.J. Eichhorn, A. Dufresne, M. Aranguren, N.E. Marcovich, J.R. Capadona, S.J. Rowan, C. Weder, W. Thielemans, M. Toman, S. Renneckar, W. Gindl, S. Veigel, J. Keckes, H. Yano, K. Abe, M. Nogi, A.N. Nakagaito, A. Mangalam, J. Simonsen, A.S. Benight, A. Bismarck, L.A. Berglund, T.J. Peijs, J. Mater. Sci. 45 (2010) 1–33.
[11] T. Tammelin, A. Salminen, U. Hippi, PCT Int. Appl. (2013). WO 2013060934 A2 20130502.
[12] M.S. Peresin, J. Vartiainen, V. Kunnari, T. Kaljunen, T. Tammelin, P. Qvintus, Large-scale nanofibrillated cellulose film: an overview on its production, properties, and potential applications, in: the 4th International Conference on Pulping, Papermaking and Biotechnology (ICPPB'12), Nanjing, China, 2012, pp. 891–895.
[13] M. Österberg, J. Vartiainen, J. Lucenius, U. Hippi, J. Seppälä, R. Serimaa, J. Laine, ACS Appl. Mater. Interf. 5 (2013) 4640–4647.
[14] N. Lavoine, I. Desloges, A. Dufresne, J. Bras, Carbohydr. polym. 90 (2012) 735–764.
[15] G. Chinga-Carrasco, D. Tobjörk, R. Österbacka, J. Nanopart. Res. 14 (2012) 1213–1223.
[16] H. Orelma, I. Filpponen, L.-S. Johansson, M. Österberg, O. Rojas, J. Laine, Biointerphases 7 (2012) 1–12.
[17] D. Fengel, G. Wegener, Wood: Chemistry, Ultrastructure, Reactions, de Gruyter, Berlin, 1984.
[18] P. Penttilä, A. Várnai, J. Pere, T. Tammelin, L. Salmén, M. Siika-aho, L. Viikari, R. Serimaa, Bioresour. Technol. 129 (2013) 135–141.
[19] S. Arola, J.-M. Malho, P. Laaksonen, M. Lille, M. Linder, Soft Matter. 9 (2013) 1319–1326.
[20] K. Uetani, H. Yano, Langmuir 28 (2012) 818–827.
[21] M.S. Tunc, A.R.P. van Heiningen, Ind. Eng. Chem. Res. 47 (2008) 7031–7037.
[22] N. Hansen N, T. Blomfeldt, M. Hedenqvist, D. Plackett, Cellulose 19 (2012). 2015-2013.
[23] A. Ebringerova, T. Heinze, Macromol. Rapid Commun. 21 (2000) 542–556.
[24] B.S. Kayserilioglu, U. Bakir, L. Yilmaz, N. Akkas, Bioresour. Technol. 87 (2003) 239–246.
[25] K.S. Mikkonen, M. Tenkanen, Trends Food Sci. Technol. 28 (2012) 90–102.
[26] C. Laine, A. Harlin, J. Hartman, S. Hyvärinen, K. Kammiovirta, B. Krogerus, H. Pajari, H. Rautkoski, H. Setälä, J. Sievänen, J. Uotila, M. Vähä-Nissi, Ind. Crop. Prod. 44 (2013) 692–704.
[27] J. Hackney, R. Atalla, D. VanderHart, Int. J. Biol. Macromol. 16 (1994) 215–218.
[28] K. Uhlin, R. Atalla, N. Thompson, Cellulose 2 (1995) 129–144.
[29] T. Iwata, L. Indrarti, J.-I. Azuma, J-I. Cellulose 5 (1998) 215–228.
[30] M. Fujita, H. Harada, Ultrastructure and formation of wood cell wall, in: D. Hon, N. Shiraishi (Eds.), Wood and Cellulosic Chemistry, second ed., Marcel Dekker, New York, NY, 2001.
[31] S. Yllner, B. Enström, Svensk Papperstidn. 59 (1956) 229–232.
[32] M. Mitikka-Eklund, Sorption of Xylans on Cellulose Fibres. Licenciate Thesis, University of Jyväskylä, Department of Chemistry, Laboratory of Applied Chemistry, Jyväskylä, Finland, 1996.
[33] F. Mora, K. Ruel, J. Comtat, J.-P. Joseleau, Holzforschung 40 (1986) 85–91.
[34] J. Buchert, A. Teleman, V. Harjunpää, M. Tenkanen, L. Viikari, L.T. Vuorinen, T. Tappi J. 78 (1995) 125–130.
[35] C. Schönberg, T. Oksanen, A. Suurnäkki, H. Kettunen, J. Buchert, Holzforschung 55 (2001) 639–644.
[36] M. Borrega, L.K. Tolonen, F. Bardot, L. Testova, H. Sixta, Bioresour. Technol. 135 (2013) 665–671.
[37] A. Swerin, L. Ödberg, T. Lindström, Nord. Pulp Pap. Res. J. 5 (1990) 188–196.
[38] M. Tenkanen, J. Puls, K. Poutanen, Enzyme Microb. Technol. 14 (1992) 566–574.
[39] M. Tenkanen, M. Siika-aho, J. Biotechnol. 78 (2000) 149–161.
[40] S. Ahola, J. Salmi, L.-S. Johansson, J. Laine, M. Österberg, Biomacromolecules 9 (2008) 1273.
[41] P.A. Penttilä, P. Kilpeläinen, L. Tolonen, J.-P. Suuronen, H. Sixta, S. Willför, R. Serimaa, Cellulose 20 (2013) 2335–2347.
[42] R. Partanen, P. Hakala, O. Sjövall, H. Kallio, P. Forssell, J. Food Sci. 70 (2005) E37–E43.
[43] M. Rodahl, F. Höök, A. Krozer, P. Brzezinski, B. Kasemo, Rev. Sci. Instrum. 66 (1995) 3924–3930.
[44] F. Höök, M. Rodahl, P. Brzezinski, B. Kasemo, Langmuir 14 (1998) 729–734.
[45] G. Sauerbrey, Z. Phys 155 (1959) 206–222.
[46] M.S. Peresin, K. Kammiovirta, H. Setälä, T. Tammelin, J. Polym. Environ. 20 (2012) 895–904.
[47] L. Greenspan, J. Res. Natl. Bureau Stand 81 (1977) 89.
[48] S. Asikainen, A. Fuhrmann, L. Robertsen, Nord. Pulp Pap. Res. J. 25 (2010) 269–276.
[49] I. Rauvanto, J. Pere, K. Henricson, K. Nordic Pulp Pap Res J 21 (2006) 328–335.
[50] A. Teleman, P.T. Larsson, T. Iversen, Cellulose 8 (2001) 209–215.
[51] M. Österberg, J. Laine, P. Stenius, A. Kumpulainen, P.M. Claesson, J. Colloid Interf. Sci. 242 (2001) 59–66.
[52] T. Tammelin, A. Paananen, M. Österberg, Hemicelluloses at interfaces: some aspects on the interactions, in: A.L. Lucia, O.J. Rojas (Eds.), The Nanoscience and Technology of Renewable Biomaterials, Wiley- Blackwell Publishing Ltd, West Sussex, UK, 2009. pp. 149–172.
[53] A.B. Fall, S.B. Lindström, O. Sundman, L. Ödberg, L. Wågberg, Langmuir 27 (2011) 11332–11338.
[54] R.G. Holdich, Hindered systems and rheology, in: Fundamentals of Particle Technology, Midland Information Technology and Publishing, Loughborough, UK, 2002. pp. 55–66.
[55] A.R. Urquhardt, A.M. Williams, J. Text. Inst. Trans. (Manchester) 75 (1924) 559.
[56] S. Belbekhouche, J. Bras, G. Siqueira, C. Chappey, L. Lebrun, B. Khelifi, S. Marais, A. Dufresne, Carbohydr. polym. 83 (2011) 1740–1748.
[57] T. Tammelin, J. Vartiainen, Nanocellulose films and barriers, in: K. Oksman, A.P. Mathew, A. Bismarck, O. Rojas, M. Sain (Eds.), Handbook of Green Materials, Self- and Directed Assembling of Bionanomaterials, vol. 3, World Scientific Publishing Co., Pte. Ltd., Singapore, 2014. pp. 213–229.
[58] T. Tammelin, A. Ramarao, M. Gestratnius, C. Laine, H. Setälä, M. Österberg, Manuscript (2014).
[59] D.R. Paul, L.M. Robeson, Polymer 49 (2008) 3187–3204.

Paper IV

Tenhunen Tiia-Maria; Moslemian Oldouz; Kammiovirta Kari; Harlin Ali; Kääriäinen Pirjo; Österberg Monika; Tammelin Tekla; Orelma Hannes (2018) Surface tailoring and design-driven prototyping of fabrics with 3D-printing: An all-cellulose approach, Materials & Design 140, 409-419

Materials and Design 140 (2018) 409–419

Contents lists available at ScienceDirect

Materials and Design

journal homepage: www.elsevier.com/locate/matdes

Surface tailoring and design-driven prototyping of fabrics with 3D-printing: An all-cellulose approach

Tiia-Maria Tenhunen [a,*], Oldouz Moslemian [b], Kari Kammiovirta [a], Ali Harlin [a], Pirjo Kääriäinen [b], Monika Österberg [c], Tekla Tammelin [a], Hannes Orelma [a]

[a] VTT Technical Research Centre of Finland Ltd, P.O. Box 1000, 02044 VTT, Finland
[b] Aalto University School of Arts, Design and Architecture, P.O. Box 31000, 00076 Aalto, Finland
[c] Aalto University School of Chemical Technology, Department of Forest Products Technology, P.O. Box 16300, 00076 Aalto, Finland

HIGHLIGHTS

- A method for modifying cellulose fabrics using direct-write 3D-printing is presented.
- A combination of surface sensitive approach and physical methods reveals the compatibility of all-cellulose structures.
- Cellulose derivatives can be used to attach functionalities such as refractive and thermoresponsive elements on textiles.
- Excellent mechanical durability was achieved with 3D-printed cellulose acetate on cellulose fabrics.

GRAPHICAL ABSTRACT

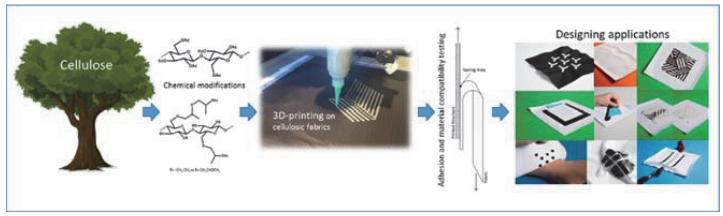

ARTICLE INFO

Article history:
Received 20 October 2017
Received in revised form 5 December 2017
Accepted 6 December 2017
Available online 06 December 2017

Keywords:
3D-printing
Cellulose derivatives
Cellulose acetate
Acetoxypropyl cellulose
Design-driven
Prototyping

ABSTRACT

In this work, we present a new all-cellulose approach for modifying and functionalizing textiles. The use of 3D-printing and two acetylated cellulose derivatives, rigid cellulose acetate (CA) and flexible acetoxypropyl cellulose (APC), on cellulosic fabrics were studied. In addition, prototypes were generated using a design-driven approach. The interactions of cellulose derivatives with cellulose were assessed by quartz crystal microbalance with dissipation monitoring (QCM-D). 3D-printing of cellulosic materials on cellulosic fabrics was performed using a direct-write method by printing cellulose derivatives on woven and knitted cotton and woven viscose fabrics. The adhesion of the printed structures was evaluated via peeling and washability tests. The results indicated that although both cellulose derivatives had a positive attraction towards the cellulose substrate, CA had higher affinity and good adhesion properties, whereas the more branched molecular structure of APC was less firmly attached to cellulosic material. The applicability of 3D-printing cellulosic materials for textile modification and functionalization was assessed through iterative prototyping. Visual effects and functional surface structures were demonstrated. Utilization of 3D-printing of cellulosic materials for surface tailoring of cellulosic textiles, eliminates labour intensive processing or external glues and may enable new and simple customization processes with minimized material usage.

* Corresponding author.
E-mail address: tiia-maria.tenhunen@vtt.fi (T.-M. Tenhunen).

https://doi.org/10.1016/j.matdes.2017.12.012
0264-1275/

1. Introduction

Investigation and development of biobased materials has increased extensively due to the awareness of ecological issues related to traditional petroleum-based polymers [1,2]. New additive manufacturing technologies present high potential for processing these biomaterials. 3D-printing technology, which falls under the vast group of additive manufacturing methods, has an immense potential for developing new application areas in manufacturing industries, but is currently only implemented in incremental number of practical applications [3]. 3D-printing could enable mass customization of products on-demand and in-store by minimizing the material usage [4]. Currently, the most prominent interest in developing 3D-printable biomaterials has been in medical applications, due to their high value potential and demand for biocompatibility [5–7]. However, the increased use of biomaterials could be beneficial in various industries such as textiles and fashion. The substantial utilization of petroleum based materials in textile productions, as well as the add-ons on garments and footwear such as buttons, prints, and labelling in fashion, impede the recycling processes [8]. Cellulose, as the most abundant biopolymer in the world that is fully renewable, non-toxic, and encompasses extremely versatile properties, could be a suitable candidate for replacing these polymeric materials in textiles. Also, due to the high internal affinity of cellulosic materials, by using cellulosic fabrics such as cotton or viscose, the structural bonding could form in the interface without glues or additives that further facilitates the all-cellulose approach [9]. Printable cellulosic materials have the potential to be utilized as printed structuring and topographical modifications, enabling printing of functionalities such as stimuli-responsive materials.

In textile applications, 3D-printing technology is mostly used for creating textile-based structures [10], and in some cases for post-surface modifications using fused deposition modelling (FDM) with thermoplastic polymers (ABS, PLA and Nylon) [11–13]. Although FDM is suitable for many applications, there exist issues surrounding the thermoplastics processing and the narrow selection of materials that are pre-moulded into filaments. Paste extrusion (direct-write or direct ink writing) is a widely used method in biomedical or ceramic applications that utilize paste or gel-like materials [14,15]. Drying or solidifying of the printed material is usually based on evaporation. Direct-write could also be used with cellulosic materials that do not possess the thermoplastic properties required in the FDM method [16]. Moreover, paste extrusions techniques could be adopted for simple post modifications made in shops or at the point of sale [17].

Despite the interest in developing new biomaterials for 3D-printing, limited literature surrounding the 3D-printing of cellulose based materials exists. The previous reports include studies on cellulose dissolved in an ionic liquid and nanocellulose based ink for biomedical applications [18,19]. Printing of cellulosic objects using cellulose acetate and cellulose nanofibrils has also been recently reported [19,20]. Moreover, research on using wood chips with gypsum as a binder to manufacture 3D objects has been conducted [21]. The printing materials chosen for the study were cellulose derivatives with different properties. Cellulose acetate, which is commercially available and widely used, and acetoxypropyl cellulose (APC), which was synthetized from hydroxypropyl cellulose (HPC) by acetylation. APC has been previously studied mainly due to its ability to form cholesteric liquid crystalline solutions [22,23]. CA and APC materials are chemically similar as both are acetylated, but due to the more branched structure of APC, a difference in material and adhesion properties was expected. 100% APC forms flexible (amorphous solid) structures and the more linear structure of CA led to the formation of rigid structures.

The key factor in new 3D-printed textile applications is the compatibility of the printed material, the fabric and the 3D-printing system, which requires comprehensive research into existing and new materials, polymer-textile adhesion, and deposition techniques [13]. However, successful utilization of the system requires a multidisciplinary approach in which the possible end-users are taken into consideration. Fusing the disciplines of science and design, this integrative and experimental approach would allow for further strategic realization of prospective trends, contexts of use, and consumer needs, which results in higher impact generation in research [24,25]. Modification and customization of textiles using 3D-printing with bio-based materials could lead to the establishment of new application areas and generate novel design and business concepts.

The aim of this work was to study direct-write 3D-printing of cellulosic materials on cellulosic fabrics and to investigate potential end-use design applications through textile modification and functionalization. Material compatibility of two acetylated cellulose derivatives (CA and APC) on three cellulosic fabrics (woven cotton, knitted cotton, woven viscose) was examined in detail. Interactions between cellulosic materials were studied via adsorption test using quartz crystal microbalance with dissipation monitoring (QCM-D), and via adhesion experiments using peeling and washability tests. The investigation into the versatility of cellulose derivatives in 3D-printing and their suitability for functional textile applications was carried out through experimental and explorative design research approaches [26,27]. Several prototypes were generated by utilizing the experimental findings, portraying the potential end-use design applications and future material development possibilities. Therefore, this work is of high importance in contributing to the generation of new knowledge in the field of utilizing bio-based materials in 3D-printing, while providing valuable trajectories in product design by combining 3D-printing and textiles through functional (rigid and flexible structuring, refractive, thermoresponsive) and decorative (smocking), end-use applications.

2. Materials and methods

2.1. Materials

Cellulose fabrics (Fig. 1) used in the 3D-printing studies were uncoated and undyed woven cotton (plain weave, 100% cotton, 150 g/m^2, Iisalmen kangastukku, Finland), knitted cotton (single knit, 100% cotton, 155 g/m^2, Orneule, Finland) and woven viscose (Bamboo Plain Ivory (BB12), 100% viscose, 140 g/m^2, Whaleys Bradford Ltd., UK). The woven cotton fabric was relatively stiff and had a rough feel, whereas the stretchy knitted cotton was softer (evaluated by hand). The woven viscose fabric was soft and smooth without clear stretching. Knit textiles are stretchy since they are produced by looping yarns continuously in rows. Woven fabrics are tighter due to multiple yarns that are interlaced at right angles during the production [11]. Chemical composition of the fabrics was investigated with Fourier Transform Infrared Spectroscopy (FTIR). The fabrics exhibited cellulosic structure that can be observed from the FTIR spectra typical for cellulose I (cotton) and II (viscose) (Fig. S1, Supporting information). The measured FTIR peak patterns were comparable to the data reported earlier for regenerated cellulose and cotton [28,29]. Altogether, we can conclude that the fabrics used in the study had highly cellulosic internal structures.

Cellulose derivatives used in this study were cellulose acetate (CA, DS_{Ac} of 3, M_w ~ 60,000) (Fig. 2a) and hydroxypropyl cellulose (HPC80, DS_{HP} of 4–5, M_w ~ 80,000, average M_n ~ 10,000, powder, 20 mesh particle size) (Fig. 2b), both obtained from Sigma Aldrich (USA). Trimethylsilyl cellulose (TMSC), used in adsorption investigations, was produced from high purity cellulose powder from spruce (Sigma Aldrich, USA) and synthesized by using a previously reported method [30]. Chemicals used in the synthesis of APC (*N*,*N*-dimethylacetamide, pyridine and acetic anhydride) were obtained from Sigma Aldrich (USA).

The QCM-D sensor crystals were Au coated-crystals (GSX301, from Q-Sense, Gothenburg, Sweden) with a fundamental resonance frequency of (f_0) 5 MHz and a sensitivity constant of $C \approx 0.177$ mg m^{-2} Hz^{-1}.

Prototype materials for tailoring fabric surfaces were cellulose dissolved in ionic liquid (IL), 1-ethyl-3-methylimidazolium acetate

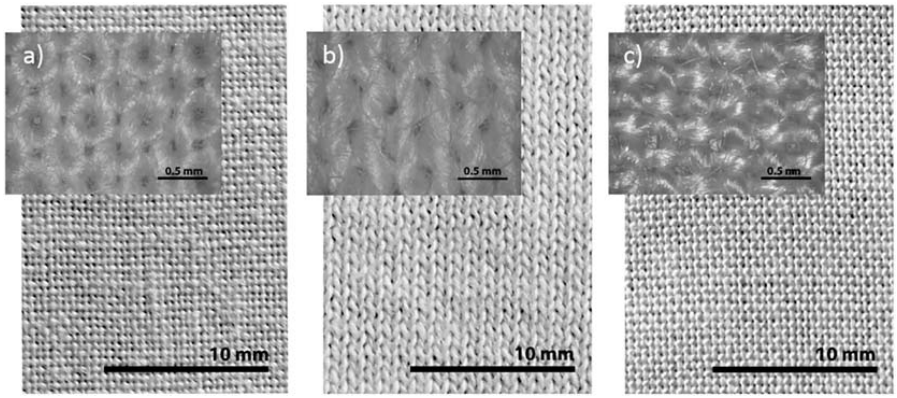

Fig. 1. Photographs of cellulose fabrics used as the substrates for printed structures. a) Woven cotton, b) knitted cotton and c) woven viscose fabric. Insets show microscopy images of the yarn looping of the textiles used.

([EMIM][OAc]), which was obtained from IoLiTec (Germany) and cellulose cotton linters from Milouban (Israel). Thermochromic pigment paste used in the prototypes was a commercial product that was acquired from Zenit (Sweden). Reflective beads (commercial high index standard beads, particle size of 180–600 μm, white/clear) were obtained from Cole Safety International (USA). The black colourant used was a commercial food grade paste colourant. Conductive yarn was BEKAERT's Bekinox VN12/1 * 275/100Z steel yarn (Belgium). Water used in this study was MilliQ-water. All other chemicals used were analytical grade.

2.2. Methods

2.2.1. Synthesis of acetoxypropyl cellulose (APC)

Synthesis of APC from HPC via esterification was conducted as described by Tseng et al. [22], with slight modifications. 100 g of HPC (0.62 mol) was first dissolved in *N*,*N*-dimethylacetamide (HPC consistency of 25%) at 35 °C. The acetylation was performed by adding 100 ml of pyridine and 100 ml (1.23 mol) of acetic anhydride to the reaction medium (Fig. 3). The solution was then allowed to react under stirring overnight at 35 °C and precipitated with deionized water. The precipitated APC was collected and further purified twice with acetone dissolution and water precipitation cycles. The prepared APC was finally dried in a vacuum oven at 40 °C and stored at room temperature until use.

2.2.2. Characterization of materials

A **Fourier Transform Infrared Spectroscopy (FTIR)** spectrometer with ATR diamond (Thermo Scientific™ Nicolet™ iS™50 FTIR Spectrometer, United States) was used to determine the chemical composition of the fabrics, synthetized APC, and the purity of the regenerated cellulose from ionic liquid. All spectra were obtained from 32 scans with a resolution of 4 cm^{-1} in transmission mode from 350 to 4000 cm^{-1}.

A **liquid state ^{13}C Nuclear Magnetic Resonance (NMR) spectrometer** (Bruker Avance III 500, Germany) was used to characterize synthetized APC by determining the molar substitution of hydroxypropyl cellulose (HPC) and the degree of acetylation of HPC. APC was dissolved in acetone d_6 with a concentration of 100 mg ml^{-1} and 8 mg ml^{-1} and $Cr(acac)_3$ was added for enhanced relaxation. A BB(F)O double resonance probe head was used at 22 °C to acquire a ^{13}C spectrum. 20,000 scans were collected with a 1.5 s relaxation delay. Referencing was carried out using the lock frequency, and the spectrum was processed using Bruker TopSpin 3.5 software.

A **Differential Scanning Calorimeter (DSC)**, Mettler Toledo Differential Scanning Calorimeter model DSC2 (Mettler Toledo GmbH, Switzerland), was used to characterize synthetized APC by determining the glass transition temperature. The DSC measures the temperature and heat flow associated with the thermal transition of a material. The calorimeter was equipped with an intra-cooler (TC100MT, Huber, Germany) allowing a minimum starting temperature of −90 °C. N_2 flow used was 80 ml min^{-1} in order to purge the measurement cell

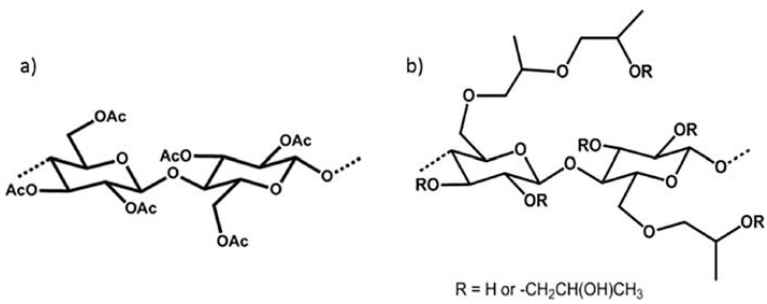

Fig. 2. Chemical structures of a) cellulose acetate and b) hydroxypropyl cellulose.

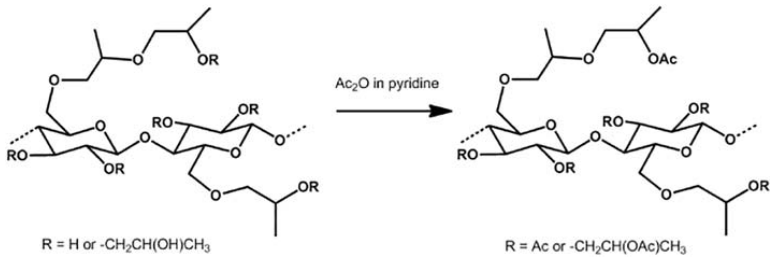

Fig. 3. Acetylation of hydroxypropyl cellulose with pyridine and acetic anhydride to acetoxypropyl cellulose.

and prevent water condensation. For the measurement, 40 μl sealed aluminium crucibles were used.

2.2.3. Assessment of the interactions via adsorption investigations using QCM-D

A Quartz crystal microbalance with dissipation monitoring (QCM-D E4, Q-sense AB, Gothenburg, Sweden) was used to investigate the adsorption of CA and APC on a pure cellulose surface. The QCM-D technique is an acoustic method that is sensitive to the mass changes on the crystal surface [31,32]. The QCM-D technique simultaneously measures the frequency and dissipation changes on the crystal surface at a fundamental resonance frequency and its overtones. The piezoelectric quartz crystal oscillates at a resonance frequency, f_0. Frequency depends on the total oscillating mass (including the solvent) and it increases or decreases with mass changes on the crystal surface. The amount of adsorbed material can be calculated using the Sauerbrey equation [33] if the mass of adsorbed materials is evenly distributed, rigid and small (compared to the mass of the crystal). In this case, the shift in frequency $\Delta f = f - f_0$ is related to the adsorbed mass, Δm, per unit surface.

$$\Delta m = -\frac{C\Delta f}{n} \tag{2}$$

where C is a constant that describes the sensitivity of the device to changes in mass and n is the overtone number ($n = 1, 3, 5, 7$). When the material is coated onto a crystal surface, the adsorption of studied material onto substrate can be monitored on-line [34].

If the film on the sensor surface is not fully elastic or rigidly attached, frictional losses occur that lead to damping of oscillation with a decay rate of amplitude, which is dependent on the viscoelastic properties of the material. The change in dissipation ($\Delta D = D - D_0$) measures qualitatively the softness and rigidity of the film on the sensor surface and is calculated using dissipation, D, defined by Eq. (1).

$$D = \frac{E_{diss}}{2\pi E_{stor}} \tag{1}$$

where E_{diss} is the total dissipated energy during one oscillation cycle and E_{stor} is the total energy stored in oscillation. The film can be considered fully elastic and rigid when $\Delta D \le 1 \times 10^{-1}$, and there is no spreading of the overtones.

Prior to the QCM-D measurements, the bare crystal surfaces were deposited with TMSC using a spin coating procedure and regenerated to cellulose [35]. The gold coated QCM-D crystals were first cleaned by UV/ozone treatment for 30 min. Subsequently, the crystal was wetted with toluene, following spinning at a speed of 3000 rpm for 15 s to purify the crystal surface. 10 mg ml^{-1} of TMSC in toluene was then spin coated onto the crystal surface with a speed of 4000 rpm for 60 s. Finally, the coated crystals were dried in an oven (60 °C) for at least 10 min to ensure sufficient adhesion. Desilylation was carried out in 10% HCl vapor in vacuum for 5 min. After regeneration of TMSC to cellulose, the cellulose surfaces were kept in MilliQ-water overnight before conducting the measurements with the QCM-D. Just before the measurement, the cellulose surfaces were gently dried with nitrogen gas and placed in the QCM-D chamber. Acetone was pumped through the chamber until a plateau frequency signal was achieved. Then, CA or APC dissolved into acetone was allowed to flow over the cellulose surface. Acetone was used as a solvent for both materials, due to the hazardous nature and distinctive smell of 100% acetic acid, which would have been difficult to remove and could have damaged the sensitive system. Adsorption studies were performed with dilute dispersions (0.5 mg ml^{-1}) in acetone at a flow rate of 0.1 ml min^{-1} with a constant temperature of 22 °C. All measurements were replicated twice.

2.2.4. Preparation of printing pastes

The printable CA solution was prepared by dissolving commercial CA in acetic acid (concentration 30 wt%). The APC solution was produced by dissolving APC in acetone in a concentration of 80 wt% using rotating vials.

For prototyping purposes, cellulose cotton linters were dissolved in [emim]OAc in 10% concentration. Dissolution of cotton linters was done in a vertical kneader system following the previously reported procedure [36]. The dissolved cellulose in ionic liquid was stored in a sealed bottle at room temperature prior to 3D-printing.

2.2.5. 3D-printing of cellulosic materials on fabrics

The modification of fabric surfaces was carried out using a commercial direct-write 3D-printer (3Dn-300, nScrypt Inc., USA). The 3D-printer system used is based on an extrusion technique for paste-like materials with a wide range of suitable viscosities. The system utilizes a simple syringe pump system with disposable 2.5 ml syringes and tapered tips. The nozzle size of the tip used was 0.84 mm (Nordson EFD, USA). Printing speed used for materials was 5 mm/s. The printing pressure was set at 41.5 psi for CA and at 20.5 psi for APC, due to its lower viscosity. Fabrics were attached onto plastic films using adhesive tape during printing and drying.

Moreover, an in-house built 3D-printer was used for prototyping purposes. This 3D-printer functioned exactly the same way as nScrypt by utilizing the extrusion technique and tapered tips.

2.2.6. Adhesion of printed materials via peeling test

The adhesion of printed structures to cellulose fabrics was investigated utilizing a Lloyd materials testing machine LS5 (Lloyd Instruments Ltd., UK) with a 100 N load cell. The system measures the tensile force as a function of material extension that correlates with the load needed to peel the printed structure from a fabric (Fig. 4c). Preload of the experiment was 0.5 N (preload speed 1 mm/min) and the separation speed was kept at a constant of 5 mm/min. All measurements were carried out in standard conditions at 23 °C with 65% humidity. All samples were stored for 24 h in standard conditions prior to mechanical testing. Three measurements were taken from each sample point.

Printed structures for the peeling resistance measurements were prepared by printing half of the structure on fabric and the other half of the structure on a tape on the fabric with two successive layers (Fig. 4a). The tape prevented adhesion to the fabric, and the other end

of the structure could be mounted between jaws of the material tester. The dimension of the test strip was 10 mm × 40 mm and the adhered print on the fabric was 20 mm long.

2.2.7. Washability testing of 3D-printed structures

The washability test was utilized to investigate the durability of the printed structures on cellulose fabrics. The test was carried out using standard ISO 6330 (Domestic washing and drying procedures for textile testing) with standard washing powder (IEC-A Reference Detergent 60456 without phosphate) at 40 °C for 48 min. Two layered structures with 10 mm × 10 mm dimensions were printed for washability tests (Fig. 4c). The solvents in the printed CA and APC structures were evaporated in vacuum hood conditions. Five washing cycles were conducted and after each wash cycle, the printed structures were dried on a flat surface in air and were observed with both the naked eye and a microscope. The dried structures were evaluated with the following criteria: +++ = no change, ++ = print has peeled-off at its corners, + = only small amount left, − = nothing left.

2.2.8. Design-driven prototyping for 3D-printing

Five types of prototypes (refractive, thermoresponsive, rigid structuring, flexible structuring and smocking) were printed using the studied materials, and cellulose dissolved in IL. ACP (pure and coloured) in acetone was used for flexible printed fabric structures and CA in acetic acid for rigid structuring. The refractive printing material was prepared by mixing reflective beads in CA and acetic acid. The thermochromic pigment paste was mixed with the APC dissolved in acetone. The smocking of the fabric was carried out using the ionic liquid dissolved cellulose. The smocking patterns were specifically designed to experiment visual effects and the samples were regenerated in a water bath overnight and dried in air, which caused the formation of the pattern by shrinkage in the fabric. The printed structures were allowed to set for approximately 1 h prior to regeneration in a water bath. All mixing was done using a SpeedMixer™ DAC 150 SP (FlackTek Inc., UK).

3. Results and discussion

In this work, the potential of utilizing 3D-printable cellulosic materials for surface tailoring and functionalizing cellulosic fabrics was studied. Prior to printing, the prepared materials were characterized and the material interactions were studied via adsorption tests, and after printing, via peeling and washability tests. Finally, the materials were utilized in prototypes.

3.1. Characterization of acetoxypropyl cellulose (APC)

Acetoxypropyl cellulose (APC) was synthetized by esterification of hydroxypropyl cellulose (Fig. 3). Structural analysis and grafting density of synthetized APC were determined of using FTIR and liquid state ^{13}C NMR spectroscopy. In FTIR spectra (Fig. S2, Supporting information), acetylation of HPC can be observed from the appearance of a C═O ester band at around 1740 cm^{-1}, an asymmetric C—O—C stretching peak of an acetate ester centered at 1240 cm^{-1}, and the reduction of the wide hydroxyl stretching band in 3200–3700 cm^{-1} [22,23]. From quantitative ^{13}C NMR spectra, the molar substitution of hydroxypropyl cellulose is determined by the peak area of —CH_3 signals of the hydroxypropyl substituents (~15 ppm) and the degree of substitution for acetylation at the peak area of acetyl substituents (~170 ppm). According to the spectra (Fig. S3, Supporting information), the molar substitution of hydroxypropyl cellulose was MS_{HP} 4.3 and the degree of substitution for acetylation was DS_{Ac} 3.0, which implies that all free hydroxyl groups were acetylated.

In DSC measurement, a glass transition temperature of T_g −8 °C (Fig. S4, Supporting information) was acquired, which is comparable to the previously reported value for APC by Rusig et al. [37].

3.2. Interactions of cellulose derivatives with cellulose revealed with QCM-D

In order to elucidate the cellulose-cellulose derivative interactions and to further understand the processes taking place during 3D-printing, the adsorption studies were carried out on pure cellulose thin films deposited on a QCM-D sensor surface. The compatibility as well as the strength of interactions between either CA or APC with cellulose can be qualitatively monitored by following their time dependent adsorption behaviour. Fig. 5a–b shows the change in frequency and the change in dissipation as a function of time for the adsorption experiments of 0.5 mg ml^{-1} CA and APC dispersions dissolved in acetone.

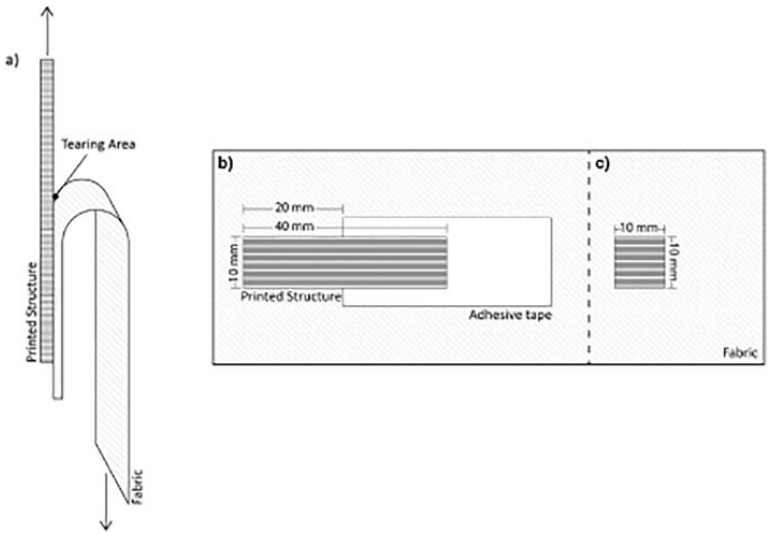

Fig. 4. a) Schematic image of peeling test: printed structure and fabric are attached between clamps and pulled apart at an angle of 180° and fabric samples for printed structures for b) peeling resistance and c) washing tests.

Prior to the introduction of the dilute dispersions of either CA or APC, the cellulose surface was allowed to stabilise in acetone for approximately 10 min. After the replacement of acetone in the QCM-D chamber with an acetone solution of cellulose derivative, the adsorption was monitored for 60 min followed by the gentle washing step of the system with pure acetone. As shown by Fig. 5a, both cellulose derivatives induced clear negative frequency changes with a simultaneous increase in dissipation factor (Fig. 5b) corresponding to a mass increase taking place on the cellulose coated sensor surface. CA instantaneously adsorbs on cellulose yielding a frequency and dissipation change of −39 Hz and 6.5×10^{-6}, respectively. The frequency change of APC was significantly smaller (−10 Hz) with a simultaneously recorded dissipation change of 3×10^{-6}. In addition, in the case of APC, the adsorption equilibrium was not completely reached within 60 min. Gentle acetone washing did not significantly remove either of the adsorbed cellulose derivatives. Minor changes in frequency and dissipation responses indicate that changes in adlayer conformation are more likely than remarkable ongoing desorption. Qualitative interpretation of the QCM-D data suggests that both cellulose derivatives indeed possess a positive attraction towards cellulose. When looking at the rate of adsorption as well as the amount of adsorbed material at the end of the process, it seems that APC was less prone to adsorb on cellulose compared to AC, which indicates its lower affinity towards cellulose. However, the rinsing with pure acetone resulted in only a minor increase in the frequency of oscillation. This indicates either negligible removal of material or reorganization of the adsorbed layer [38], which points towards relatively strongly attached polymers on the cellulose sensor surface.

There were no previous QCM data in the literature for adsorption of CA or APC or for adsorption of materials in acetone on pure cellulose model film. Hence, the adsorption data was compared to changes in frequencies made in water. Previous studies of the adsorption of chitosan on a pure cellulose surface in water reflected a −9 Hz change in frequency [39] and anionic CMC adsorption on cellulose in water reflected a −40 Hz change in frequency [40]. Therefore, it can be concluded that acetone acts relatively well as an adsorption medium for acetylated cellulose derivatives in a similar fashion to water for water-soluble cellulose derivatives.

In order to compare the viscoelastic properties of the adsorbed layers of cellulose derivatives, the QCM-D data was plotted as change in dissipation versus change in frequency (Fig. 5c). This approach allows the determination of the ability of the adsorbed layer to bind energy, i.e. the steeper the ΔD/Δf curve, the more dissipative the layer is and the more energy is bound per frequency change unit [41]. Both cellulose derivatives display a perfectly linear relationship and the ΔD/Δf ratio at the end of the adsorption is equal, which suggests that a similar amount of energy is bound and exhibits layers with similar viscoelastic properties. When compared to the linear structure of CA. we can speculate that the branched structure of APC does not have a significant influence on the physical properties of the adsorbed layer. However, CA seems to have higher affinity towards cellulose, as shown in Fig. 5a, due to a significantly higher adsorption rate and the absorbed amount of CA compared to APC. In order to attain further clarification on true adhesion after drying, a more detailed analysis of cellulose derivatives on cellulose substrate will be investigated by means of practical peeling and washability tests.

3.3. 3D-printing of cellulose acetate and acetoxypropyl cellulose

As CA and APC are soluble in both acetone and acetic acid, these two solvents could be, in principle, used to form printable solutions of the materials suitable for direct-write printing on commercial cellulosic fabrics. Acetone evaporates faster compared to acetic acid. However, for CA, it was observed that the slower evaporation rate was more expedient in 3D-printing. Thus, acetic acid was used as a solvent for CA. This improved the processability, enabled printing of several layers, and prevented clogging of the printer nozzle. The printing was conducted with a 30 wt% of CA content, which was considered a good compromise to achieve the required printing quality. High viscosity or a high solids content is usually desired in direct-write 3D-printing method and results in better 3D-formation and smaller shrinkage. However, if the viscosity is too high the material does not extrude or attach to the

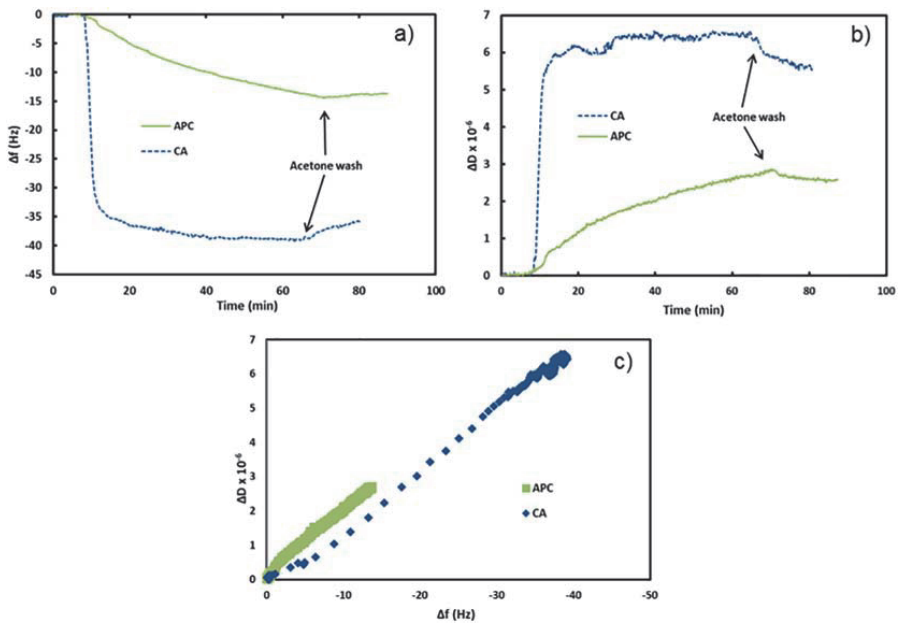

Fig. 5. a) The change in the frequency and b) dissipation on the adsorption of dilute CA and APC dispersions on pure cellulose surfaces followed by rinsing with acetone. c) Change in dissipation factor as a function of the change in frequency for adsorption. $f_0 = 5$ MHz, $n = 5$.

substrate. Therefore, the 3D-printing process requires optimization between the printability, shrinkage, and adhesion properties. According to visual observation, the printed CA on the fabric formed a transparent layer and the two successive layers fused evenly together. It was perceived that during solvent evaporation, shrinkage of the printed CA structure caused mild creasing of the fabric consequent of the relatively high solvent content of the printing dope. However, minor shrinkage can be prevented by stretching the textile while drying.

In case of APC, acetone was used as a solvent. The faster evaporation rate of acetone, did not induce similar limitations as in the case of CA, therefore, it seemed more practical choice for solvent. Visually, APC forms a white layer, which after drying, is soft, flexible, and slightly tacky without any fabric shrinkage. It was observed that the 3D-printer could process APC in much higher concentrations (~80 wt%) compared to CA due to the lower viscosity of the material. No significant changes to the quality of the print were noticed between tested fabrics.

3.4. Adhesion of the printed structures

3.4.1. Peeling test

Adhesion of the fabric and printed material is largely affected by the contact area, which is closely related to material compatibility and the textile structure [11,42]. In order to achieve firm adhesion, the polymer should be compatible with the fabric and penetrate and spread evenly on the yarn surfaces [10]. The adhesion of printed CA and APC on cellulose fabrics was investigated by using a tensile testing approach with the T-peel test. The force required to peel the printed structure off the fabric was measured from a 10 mm wide strip with a separation speed of 5 mm/min, which gave an indication of the mechanical durability of the print when used in textile applications. The results were converted to N/100 mm width by dividing the average load by the width of the specimen and then multiplying by 100 [43]. The average peeling forces are presented in the force-extension curves in Fig. 6 and Table 1.

In Fig. 6, the first slope in the force-extension curve comprises the physical elongation of the fabric. Thereafter, the peeling of the print from the fabric or tearing of the fabric starts to dominate. It was observed that the type of fabric (woven or knitted) significantly altered the shape of curves, e.g. the knitted fabric stretched significantly more than the woven fabrics (Fig. S5, Supporting information). Due to the fragility of the viscose fabric, the strength of adhesion of the printed CA structure could not be measured and the result for CA on viscose in Fig. 6 and in Table 1 represent the force required to tear the fabric. Therefore, in this case the strength of adhesion overpowered the strength of the fabric. The average peeling forces from three parallel measurements for CA on woven and knitted cotton fabrics were within a similar range. However, CA on knitted cotton required slightly higher peeling strength. This could be due to the more complex structure of the knit in z-direction that enables more surface area for adhesion.

The maximum peeling forces of APC on all tested fabrics were approximately 1/10 of peeling forces of CA (10–20 N/100 mm versus 150–250 N/100 mm, respectively) (Fig. 6). Significantly less force was needed to peel the printed APC from the surface of the fabric compared to CA. It can be speculated that the longer substituents of APC lead to the lower adhesion with the cellulose surfaces of the fabrics, which may explain the peeling results. Moreover, the high solids content (80 wt%) and the use of fast drying acetone as a solvent might prevent the material from passing into the fabric structure and lower the contact area between the print and the fabric.

Table 1
Average peeling force converted to N/100 mm width (speed 5 mm/min) with standard deviations. 3 parallel measurements.

Average peeling force (N/100 mm width)	Woven cotton	Knitted cotton	Woven viscose
CA	124.8 ± 2.0	193.0 ± 19.2	(90.8[a] ± 1.7)
APC	12.2 ± 1.7	15.1 ± 10.0	15.0 ± 4.3

[a] Viscose fabric tore instead of peeling.

Sanatgar et al. [13] have previously measured the average peeling force values for printed nylon on polyamide (PA) (40–120 N/100 mm width) and for printed polylactic acid (PLA) on PA (5–70 N/100 mm). Due to differences in measurement conditions (25 mm wide testing strip and 100 mm/min peeling rate in their case), the average peeling forces could only be qualitatively compared. In comparison, the average peeling force of CA with tested cotton fabrics can be considered at the very least as high. Whereas, the peeling results of APC suggest a relatively poor adhesion to the tested fabrics. However, in our case, a slower peeling rate that requires less energy to peel was used. Therefore, the values should be in fact greater than those presented in Table 1 [44,45]. It is conceivable that CA is very compatible with the cellulose textile materials and diffused into the fabric structure, increasing the contact area between the print and the fabric.

The adhesion of synthetic FDM 3D-printable polymers (ABS and PLA) on fabrics (polyester, polypropylene, wool, polywool, knit soy and woven cotton) has also been studied by Pei et al. [11]. In their study, woven cotton fabric presented the best results in adhesion properties and good compatibility with non-cellulosic polymers. In general, natural fabrics or natural fabric blends were better suited for 3D-printing purposes.

3.4.2. Washability test

The mechanical durability of printed cellulose structures was investigated with a standard washing test. Samples were washed 5 times with detergent according to standard ISO 6330, which is the most widely used method to determine visible changes in the appearance of the textile after a number of washing cycles [46,47]. Results presented in Table 2 demonstrate how well the textile would last in domestic washing [48]. Printed CA came only slightly off from its corners during the first wash, but endured all 5 washing cycles without significant changes.

APC did not endure any of the washing cycles. As shown in peeling tests, adhesion between APC and cellulose fabrics was significantly

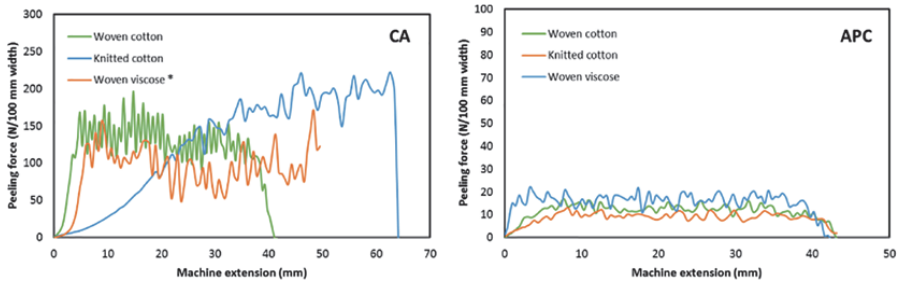

Fig. 6. The peeling force as a function of machine extension for CA (left) and the peeling force as a function of machine extension for APC (right). *Fabric tore instead of peeling.

Table 2
Washability tests of the CA and APC printed fabrics during five washing cycles.

Sample	Fabric	1. wash	2. wash	3. wash	4. wash	5. wash
CA	Woven cotton	++	++	++	++	++
	Knitted cotton	++	++	++	++	++
	Woven viscose	++	++	++	++	++
APC	Woven cotton	−	n.a.	n.a.	n.a.	n.a.
	Knitted cotton	−	n.a.	n.a.	n.a.	n.a.
	Woven viscose	−	n.a.	n.a.	n.a.	n.a.

− = nothing left.
+ = only partially left.
++ = print has come off its corners.
+++ = no change after washing.

lower compared to CA and fabrics. In addition, acetylation of HPC alters the solubility behaviour of the polymer while pure HPC is soluble in cold water when MS_{HP} is approximately 4 [16,22]. Based on this, it seems that poor adhesion plays the main role, although, the contribution of surface active components of detergents cannot be completely ruled out. The choice of fabric did not affect the results.

The washability results support the interaction and peeling data. 3D-printed CA could be used in textile applications where mechanical durability and wash resistance are needed. Whereas, the strength of the bonding between the APC and fabric requires improvement or alternatively, different types of textile applications should be considered.

3.5. Design-driven prototyping - 3D printing of functional and decorative structures

The material and design experimentations described in this section demonstrate the potential of using cellulosic materials in 3D-printing on cellulosic textiles, utilizing the knowledge generated in the first section of the study. In this design-driven development, the integrative and nonlinear design approach provided insight into the identification of potential challenges and opportunities in the utilization of new materials and technologies [49,50]. In this study, the examples were developed through iterative prototyping methods [51], in which the qualities and capacities of the materials were explored. Prototyping is used as a tool to broaden the possibilities of development and to concretize ideas from different angles. Additionally, it enhances communication and understanding through tangible and visual representations [52,53]. Direct-write printing was utilized to study the usability of the materials in textile modifications. In addition to CA and APC, we also demonstrated the utilization of cellulose dissolved in ionic liquid (IL), [emim]OAc.

3.5.1. Functional prototypes

In many textile applications, good adhesion and the ability to wash are crucial properties (e.g. seams). However, there are also applications where these properties are not needed and in some cases, such as disposable textiles, the possibility to remove the material by washing could be advantageous. 3D-printing of structures or patterns on textiles enables personalization of the material or product. Textiles can be mass manufactured through traditional methods and post-customized by printing according to the intended application or to the individuals' needs. There are several advantages in using wood-based materials for textile modifications. In general, cellulose-based materials are from renewable resources and environmentally safe and are often also hypoallergenic [54,55]. By using chemically similar materials, the post-consumer textile recycling could be simplified.

To validate the usability of cellulosic materials for integration of functionalities onto cellulosic fabrics five types of prototypes were

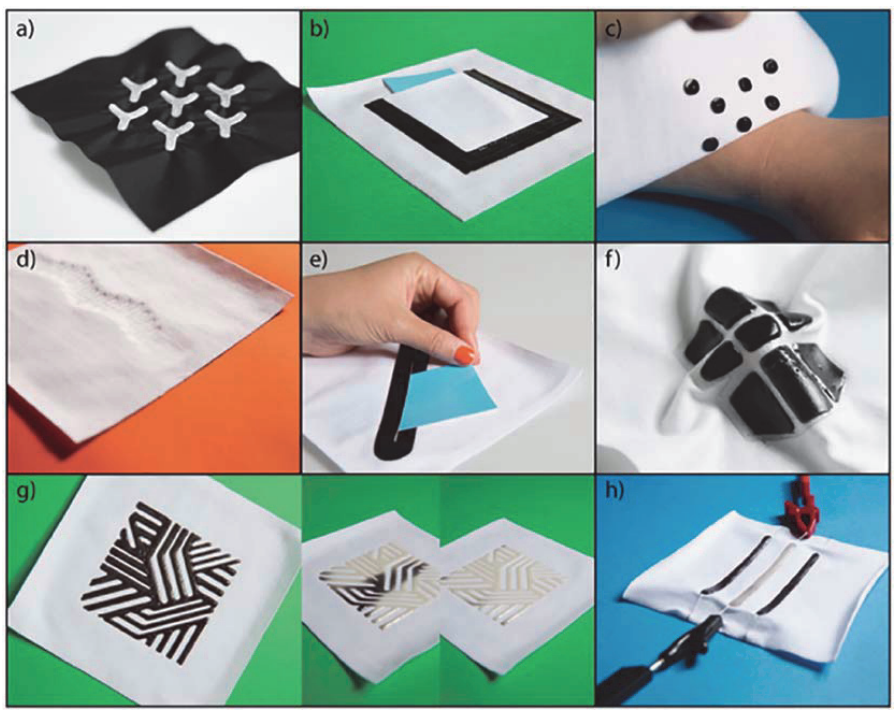

Fig. 7. a) Reflective beads mixed with CA to form reflective structures. b–c) Structures printed with coloured APC. d) CA on a controlled stretch structure. e–f) Structures printed with pure and coloured APC. g) APC mixed with thermochromic pigment paste to form thermoresponsive structures. h) Thermochromic structures with APC (design: Pauliina Varis, photos: Eeva Suorlahti).

developed (refractive, flexible structuring, rigid structuring, thermoresponsive, and smocking). In refractive prototypes, reflective glass beads were mixed in CA caused the material reflect light and printable reflectors could be produced. This prototype verifies the ability to attach active components on cellulose fabrics by using CA as a binder. The prototypes of flexible structuring were made to demonstrate the 3D-printing of all-cellulosic textiles (Fig. 7b–c and e–f) using pure and coloured APC. These prototypes showcase application potential for implementation of printed seam materials replacing stitches (Fig. 7b, e), printed non-slip structures (Fig. 7c), and printed pads for knees or elbows (Fig. 7f). The third prototype was rigid structuring that can be used to control the stretch of the textile (Fig. 7d). The thermoresponsive prototypes utilized thermochromic powder, mixed into the APC solution, resulting in a printable thermoresponsive cellulose tag (Fig. 7g). The same technology can be used for indicator purposes and in Fig. 7h a conductive metal yarn was embedded into the print. When current was passed through the wire, the heat produced by the resistance of the wire changed the colour of the printed tag on the fabric. Cellulose acted as an indicator, while providing protection against direct skin contact with the wire.

3.5.2. Decorative prototypes

Ionic liquid (IL) has been previously used in 3D-printing of dissolved cellulose [19] and for partial dissolution of cotton fabric [56]. These approaches led to a hypothesis that ILs could be utilized to permanently bind printed structures to cellulosic fabrics, as the printed IL dissolved cellulose can chemically entangle with the filament surfaces of the fabric via partial surface dissolution [56]. The cellulose content in the IL was 10% and the material itself was very viscous requiring high pressure for extrusion in 3D-printing. During printing, the adjacent lines and layers were completely fused together since the IL dissolved cellulose requires regeneration with water for precipitation into a solid form. The high viscosity of the cellulose solution created challenges for forming sharp corners. Another challenge in this process was to produce high structures, due to the collapse of the printed material before regeneration. Similar behaviour has been reported in previous literature [19]. The cellulose concentration of IL dissolved printing dope could be potentially increased up to 16% in [emim]OAc or even higher if microwave heating is used [57,58].

Subsequent to printing, the samples were placed in excess water, acting as an anti-solvent, in order to regenerate the cellulose and remove the remaining ionic liquid. After regeneration, the print presented a swollen hydrogel structure (Fig. S6, Supporting information). It is reported that in thin structures, such as in filaments, the cellulose coagulation is faster compared to the behaviour in thick structures, as the diffusion to the inner structures is decreased by the dense gel surface [59]. Therefore, the printed structures were kept in water overnight to ensure that all IL was removed from the printed cellulose. This was confirmed by FTIR (Fig. S7, Supporting information). The hydrogel structures were dried in air, which caused significant shrinking and hardening of the printed material (Fig. S6, Supporting information). It was observed that the cellulose printed from IL was strongly attached on the fabric.

The strong shrinking property of cellulose dissolved in IL was utilized to induce smocking of the fabric for novel textile design (Fig. 8). The smocking effect achieved by the 3D-printing of IL dissolved cellulose makes the structuring process of fabric fast, easy, and affordable. In addition, it can be applied according to need, thus allowing more freedom throughout the design process. The IL structure was also proven (results not shown) to be washable and retained its form.

4. Conclusions

In this paper, a multidisciplinary all-cellulose approach for surface tailoring and functionalizing textiles was presented. We have investigated the use of 3D-printing and two cellulose derivatives, rigid CA and flexible APC, for the modification of cellulosic fabrics. Detailed studies of the adsorption of the cellulose derivatives to cellulose and durability tests were combined with prototyping of 3D-printable cellulosic textile applications using a design-driven approach. It was determined

Fig. 8. Structures printed using cellulose dissolved in ionic liquid could be used for smocking effects (design: Pauliina Varis and Ilona Damski, photos: Eeva Suorlahti).

that due to its more branched molecular structure, APC was less firmly attached to cellulosic materials as indicated by the QCM-D, peel tests, and washing tests. Meanwhile, the linear structure of CA enabled the material to align well with cellulose molecules in the substrate, resulting in good adsorption and excellent adhesion properties for the printed structures. However, both materials could be considered suitable for use in textile applications and the application potentials were successfully presented via different functional and visual textile demonstration models. Utilization of 3D-printing of cellulosic materials on cellulose fabrics opens new perspectives in developing all-cellulose textile customization without labour intensive processing. Moreover, by using renewable and recyclable materials, the development of new products and services could be implemented in an environment friendly fashion.

Acknowledgments

This work has been funded by Tekes (Finnish Funding Agency for Innovation) through a strategic opening entitled Design Driven Value Chains in the World of Cellulose 2.0. We acknowledge the contributions of Pauliina Varis and Ilona Damski from Aalto University School of Arts, Design and Architecture for textile designs, Harri Setälä for cellulose derivative chemistry, Arja Puolakka from Tampere University of Technology for the washability tests, and Hanna Iitti (VTT) (623/31/2015) and Ville Klar (Aalto University) for the 3D-printing.

Appendix A. Supplementary data

Supplementary data to this article can be found online at https://doi.org/10.1016/j.matdes.2017.12.012.

References

[1] T. Willke, K.-D. Vorlop, Industrial bioconversion of renewable resources as an alternative to conventional chemistry, Appl. Microbiol. Biotechnol. 66 (2004) 131–142, https://doi.org/10.1007/s00253-004-1733-0.
[2] UNEP, Biodegradable Plastics and Marine Litter, Misconceptions, Concerns and Impacts on Marine Environments, United Nations Environment Programme (UNEP), Nairobi, 2015.
[3] F. Liravi, E. Toyserkani, A hybrid additive manufacturing method for the fabrication of silicone bio-structures: 3D printing optimization and surface characterization, Mater. Des. 138 (2017) 46–61, https://doi.org/10.1016/j.matdes.2017.10.051.
[4] B. Berman, 3-D printing: the new industrial revolution, Bus. Horiz. 55 (2012) 155–162, https://doi.org/10.1016/j.bushor.2011.11.003.
[5] D. Ozdil, H.M. Aydin, Polymers for medical and tissue engineering applications, J. Chem. Technol. Biotechnol. 89 (2014) 1793–1810, https://doi.org/10.1002/jctb.4505.
[6] H.N. Chia, B.M. Wu, Recent advances in 3D printing of biomaterials, J. Biol. Eng. 9 (2015) 1–14, https://doi.org/10.1186/s13036-015-0001-4.
[7] L. Bedian, A.M. Villalba-Rodriguez, G. Hernandez-Vargas, R. Parra-Saldivar, H.M.N. Iqbal, Bio-based materials with novel characteristics for tissue engineering applications - a review, Int. J. Biol. Macromol. 98 (2017) 837–846, https://doi.org/10.1016/j.ijbiomac.2017.02.048.
[8] R.S. Blackburn, Sustainable Textiles: Life Cycle and Environmental Impact, Woodhead Publishing, 2009.
[9] T. Huber, J. Müssig, O. Curnow, S. Pang, S. Bickerton, M.P. Staiger, A critical review of all-cellulose composites, J. Mater. Sci. 47 (2012) 1171–1186, https://doi.org/10.1007/s10853-011-5774-3.
[10] R. Melnikova, A. Ehrmann, K. Finsterbusch, 3D printing of textile-based structures by Fused Deposition Modelling (FDM) with different polymer materials, IOP Conf. Ser. Mater. Sci. Eng. 62 (2014)https://doi.org/10.1088/1757-899X/62/1/012018.
[11] E. Pei, J. Shen, J. Watling, Direct 3D printing of polymers onto textiles: experimental studies and applications, Rapid Prototyp. J. 21 (2015) 556–571, https://doi.org/10.1108/RPJ-09-2014-0126.
[12] L. Sabantina, F. Kinzel, A. Ehrmann, K. Finsterbusch, Combining 3D printed forms with textile structures - mechanical and geometrical properties of multi-material systems, IOP Conf. Ser. Mater. Sci. Eng. 87 (2015)https://doi.org/10.1088/1757-899X/87/1/012005.
[13] R.H. Sanatgar, C. Campagne, V. Nierstrasz, Investigation of the adhesion properties of direct 3D printing of polymers and nanocomposites on textiles: effect of FDM printing process parameters, Appl. Surf. Sci. 403 (2017) 551–563, https://doi.org/10.1016/j.apsusc.2017.01.112.
[14] J.A. Lewis, J.E. Smay, J. Stuecker, J. Cesarano, Direct ink writing of three-dimensional ceramic structures, J. Am. Ceram. Soc. 89 (2006) 3599–3609, https://doi.org/10.1111/j.1551-2916.2006.01382.x.
[15] M. Guvendiren, J. Molde, R.M.D. Soares, J. Kohn, Designing biomaterials for 3D printing, ACS Biomater Sci. Eng. 2 (2016) 1679–1693, https://doi.org/10.1021/acsbiomaterials.6b00121.
[16] D. Klemm, B. Philipp, T. Heinze, U. Heinze, W. Wagenknecht, Comprehensive Cellulose Chemistry, Wiley-VCH Verlag GmbH & Co. KGaA, Weinheim, FRG, 1998https://doi.org/10.1002/3527601929.
[17] A. van Wijk, I. van Wijk, 3D Printing With Biomaterials: Towards a Sustainable and Circular Economy, 2015https://doi.org/10.3233/978-1-61499-486-2-i.
[18] K. Markstedt, A. Mantas, I. Tournier, H. Martínez Ávila, D. Hägg, P. Gatenholm, 3D bioprinting human chondrocytes with nanocellulose-alginate bioink for cartilage tissue engineering applications, Biomacromolecules 16 (2015) 1489–1496, https://doi.org/10.1021/acs.biomac.5b00188.
[19] K. Markstedt, J. Sundberg, P. Gatenholm, 3D bioprinting of cellulose structures from an ionic liquid, 3D print, Addit. Manuf. 1 (2014) 115–121, https://doi.org/10.1089/3dp.2014.0004.
[20] S.W. Pattinson, A.J. Hart, Additive manufacturing of cellulosic materials with robust mechanics and antimicrobial functionality, Adv. Mater. Technol. 2 (2017)https://doi.org/10.1002/admt.201600084.
[21] K. Henke, S. Treml, Wood based bulk material in 3D printing processes for applications in construction, Eur. J. Wood Wood Prod. 71 (2013) 139–141, https://doi.org/10.1007/s00107-012-0658-z.
[22] S.-L. Tseng, A. Valente, D.G. Gray, Cholesteric liquid crystalline phases based on (acetoxypropyl)cellulose, Macromolecules 14 (1981) 715–719, https://doi.org/10.1021/ma50004a049.
[23] G.V. Laivins, D.G. Gray, Characterization and chain stiffness of (acetoxypropyl)cellulose, Macromolecules 18 (1985) 1746–1752, https://doi.org/10.1021/ma00151a018.
[24] R. Buchanan, Design research and the new learning, Des. Issues 17 (2001) 3–23, https://doi.org/10.1162/07479360152681056.
[25] H. Nowotny, P.B. Scott, M.T. Gibbons, Re-thinking Science: Knowledge and the Public in an Age of Uncertainty, Polity, Cambridge, 2001.
[26] C. Frayling, Research in art and design, R. Coll. Art Res. Pap. 1 1993, pp. 1–5http://www.opengrey.eu/handle/10068/492065.
[27] N. Cross, Designerly ways of knowing: design discipline versus design science, Des. Issues 17 (2001) 49–55, https://doi.org/10.1162/074793601750357196.
[28] F. Carrillo, X. Colom, J.J. Suñol, J. Saurina, Structural FTIR analysis and thermal characterisation of lyocell and viscose-type fibres, Eur. Polym. J. 40 (2004) 2229–2234, https://doi.org/10.1016/j.eurpolymj.2004.05.003.
[29] C. Chung, M. Lee, E.K. Choe, Characterization of cotton fabric scouring by FT-IR ATR spectroscopy, Carbohydr. Polym. 58 (2004) 417–420, https://doi.org/10.1016/j.carbpol.2004.08.005.
[30] M. Österberg, P.M. Claesson, Interactions between cellulose surfaces: effect of solution pH, J. Adhes. Sci. Technol. 14 (2000) 603–618, https://doi.org/10.1163/156856100742771.
[31] M. Rodahl, B. Kasemo, A simple setup to simultaneously measure the resonant frequency and the absolute dissipation factor of a quartz crystal microbalance, Rev. Sci. Instrum. 67 (1996) 3238–3241, https://doi.org/10.1063/1.1147494.
[32] F. Höök, M. Rodahl, P. Brezezinski, B. Kasemo, Energy dissipation kinetics for protein and antibody - antigen adsorption under shear oscillation on a quartz crystal microbalance, Langmuir 14 (1998) 729–734, https://doi.org/10.1021/la970815u.
[33] G. Sauerbrey, The use of quartz oscillators for weighing thin layers and for microweighing, Zeitschrift Für Phys. 155 (1959) 206–222, https://doi.org/10.1007/BF01337937.
[34] M. Rodahl, F. Höök, A. Krozer, P. Brzezinski, B. Kasemo, Quartz crystal microbalance setup for frequency and Q-factor measurements in gaseous and liquid environments, Rev. Sci. Instrum. 66 (1995) 3924–3930, https://doi.org/10.1063/1.1145396.
[35] E. Kontturi, P.C. Thüne, J.W. Niemantsverdriet, Cellulose model surfaces-simplified preparation by spin coating and characterization by X-ray photoelectron spectroscopy, infrared spectroscopy, and atomic force microscopy, Langmuir 19 (2003) 5735–5741, https://doi.org/10.1021/la0340394.
[36] B. Kosan, C. Michels, F. Meister, Dissolution and forming of cellulose with ionic liquids, Cellulose 15 (2008) 59–66, https://doi.org/10.1007/s10570-007-9160-x.
[37] I. Rusig, M.H. Godinho, L. Varichon, P. Sixou, J. Dedier, C. Filliatre, A.F. Martins, Optical properties of cholesteric (2-hydroxypropyl) cellulose (HPC) esters, J. Polym. Sci. B Polym. Phys. 32 (1994) 1907–1914, https://doi.org/10.1002/polb.1994.090321108.
[38] R. Kargl, T. Mohan, M. Bračč, M. Kulterer, A. Doliška, K. Stana-Kleinschek, V. Ribitsch, Adsorption of carboxymethyl cellulose on polymer surfaces: evidence of a specific interaction with cellulose, Langmuir 28 (2012) 11440–11447, https://doi.org/10.1021/la302110a.
[39] P. Myllytie, J. Salmi, J. Laine, The influence of pH on the adsorption and interaction of chitosan with cellulose, Bioresources 4 (2009) 1647–1662.
[40] H. Orelma, T. Teerinen, L.S. Johansson, S. Holappa, J. Laine, CMC-modified cellulose biointerface for antibody conjugation, Biomacromolecules 13 (2012) 1051–1058, https://doi.org/10.1021/bm201771m.
[41] T. Tammelin, T. Saarinen, M. Österberg, J. Laine, Preparation of Langmuir/Blodgett-cellulose surfaces by using horizontal dipping procedure. Application for polyelectrolyte adsorption studies performed with QCM-D, Cellulose 13 (2006) 519–535, https://doi.org/10.1007/s10570-005-9002-7.
[42] E. Gustafsson, Tailoring Adhesion and Wetting Properties of Cellulose Fibers and Model Surfaces, KTH Royal Institute of Technology, 2012.
[43] S.L. Schaeffer, J. Slusarski, V. Vantiem, M.L. Johnson, Tensile strength comparison of athletic tapes: assessed using ASTM D3759M-96, standard test method for tensile strength and elongation of pressure-sensitive tapes, J. Ind. Technol. 16 (2000) 1–6.
[44] D.H. Kaelble, Theory and analysis of peel adhesion: mechanisms and mechanics, Trans. Soc. Rheol. 3 (1959) 161–180, https://doi.org/10.1122/1.548850.

[45] M.D. Gower, R.A. Shanks, The effect of chain transfer agent level on adhesive performance and peel master-curves for acrylic pressure sensitive adhesives, Macromol. Chem. Phys. 205 (2004) 2139–2150, https://doi.org/10.1002/macp.200400177.
[46] M. Ulbrich, J. Mühlsteff, A. Sipilä, M. Kamppi, A. Koskela, M. Myry, T. Wan, S. Leonhardt, M. Walter, The IMPACT shirt: textile integrated and portable impedance cardiography, Physiol. Meas. 35 (2014) 1181–1196, https://doi.org/10.1088/0967-3334/35/6/1181.
[47] M. Faulde, G. Albiez, O. Nehring, Novel long-lasting impregnation technique transferred from clothing to bednets: extended efficacy and residual activity of different pyrethroids against *Aedes aegypti* as shown by EN ISO 6330-standardized machine laundering, Parasitol. Res. 110 (2012) 2341–2350, https://doi.org/10.1007/s00436-011-2769-6.
[48] M.L. Scarpello, I. Kazani, C. Hertleer, H. Rogier, D. Vande Ginste, Stability and efficiency of screen-printed wearable and washable antennas, IEEE Antennas Wirel. Propag. Lett. 11 (2012) 838–841, https://doi.org/10.1109/LAWP.2012.2207941.
[49] V. Kumar, 101 Design Methods: A Structured Approach for Driving Innovation in Your Organization, John Wiley & Sons, Inc., 2012
[50] D.A. Norman, R. Verganti, Incremental and radical innovation: design research vs. technology and meaning change, Des. Issues 30 (2014) 78–96, https://doi.org/10.1162/DESI_a_00250.
[51] P.J. Stappers, Designing as a part of research, in: R.V.D. Lugt, P.J. Stappers (Eds.), Des. Growth Knowl. Best Pract. Ingredients Success. Des. Res. ID Studiolab Press, Delft 2006, pp. 12–17.
[52] K.T. Ulrich, S.D. Eppinger, Product Design and Development, McGraw-Hill, 1995.
[53] P.J. Stappers, Doing design as a part of doing research, in: R. Michel (Ed.), Des. Res. Now, Birkhäuser Basel, Basel 2007, pp. 81–91, https://doi.org/10.1007/978-3-7643-8472-2_6.
[54] L. Li, M. Frey, Preparation and characterization of cellulose nitrate-acetate mixed ester fibers, Polymer (Guildf) 51 (2010) 3774–3783, https://doi.org/10.1016/j.polymer.2010.06.013.
[55] B.J.C. Duchemin, A.P. Mathew, K. Oksman, All-cellulose composites by partial dissolution in the ionic liquid 1-butyl-3-methylimidazolium chloride, Compos. A: Appl. Sci. Manuf. 40 (2009) 2031–2037, https://doi.org/10.1016/j.compositesa.2009.09.013.
[56] M. Shibata, N. Teramoto, T. Nakamura, Y. Saitoh, All-cellulose and all-wood composites by partial dissolution of cotton fabric and wood in ionic liquid, Carbohydr. Polym. 98 (2013) 1532–1539, https://doi.org/10.1016/j.carbpol.2013.07.062.
[57] M. Zavrel, D. Bross, M. Funke, J. Büchs, A.C. Spiess, High-throughput screening for ionic liquids dissolving (ligno-)cellulose, Bioresour. Technol. 100 (2009) 2580–2587, https://doi.org/10.1016/j.biortech.2008.11.052.
[58] M. Isik, H. Sardon, D. Mecerreyes, Ionic liquids and cellulose: dissolution, chemical modification and preparation of new cellulosic materials, Int. J. Mol. Sci. 15 (2014) 11922–11940, https://doi.org/10.3390/ijms150711922.
[59] C. Olsson, Cellulose Processing in Ionic Liquid Based Solvents, Chalmers University of Technology, 2014.

Supporting information

Surface tailoring and design-driven prototyping of fabrics with 3D-printing: an all-cellulose approach

Tiia-Maria Tenhunen[a*], Oldouz Moslemian[b], Kari Kammiovirta[a], Ali Harlin[a], Pirjo Kääriäinen[b], Monika Österberg[c], Tekla Tammelin[a], Hannes Orelma[a]

[a] VTT Technical Research Centre of Finland Ltd, P.O. Box 1000, 02044 VTT, Finland

[b] Aalto University School of Arts, Design and Architecture, P.O. Box 31000, 00076 Aalto, Finland

[c] Aalto University School of Chemical Technology, Department of Forest Products Technology, P.O. Box 16300, 00076 Aalto, Finland

*Corresponding author: e-mail address: tiia-maria.tenhunen@vtt.fi

Supplementary Figure Captions:

Figure S1 FTIR-ATR spectrum of woven cotton (cellulose I), knitted cotton (cellulose I) and woven viscose (cellulose II)

Figure S2 FTIR-ATR spectrum of HPC (before acetylation) and APC (after acetylation)

Figure S3 Liquid state 13C NMR spectrum of APC

Figure S4 DSC curve of APC

Figure S5 Peeling test with woven cotton and CA

Figure S6 Photographs of the behaviour of dissolved cellulose in an ionic liquid a) after printing b) after regeneration c) after drying

Figure S7 FTIR-ATR spectrum of regenerated cellulose after dissolution to ionic liquid.

1. FTIR-ATR spectra for fabrics

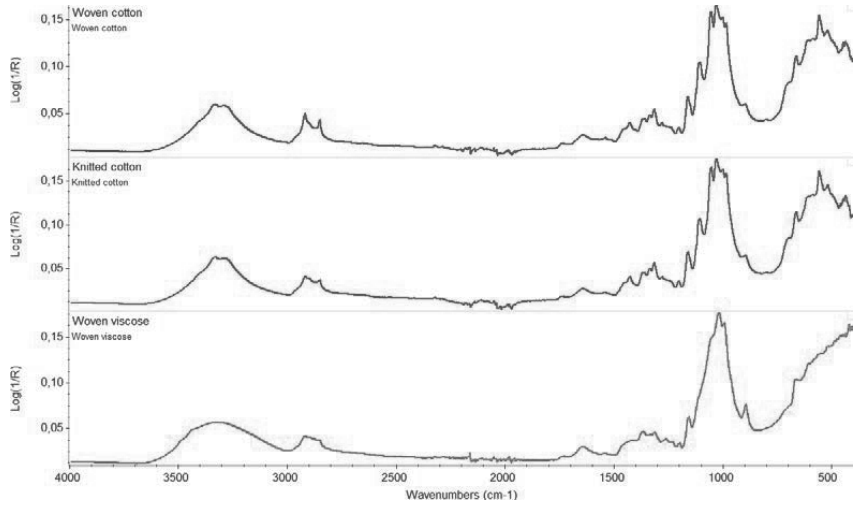

Figure S1 FTIR-ATR spectrum of woven cotton (cellulose I), knitted cotton (cellulose I) and woven viscose (cellulose II)

2. Characterization of APC

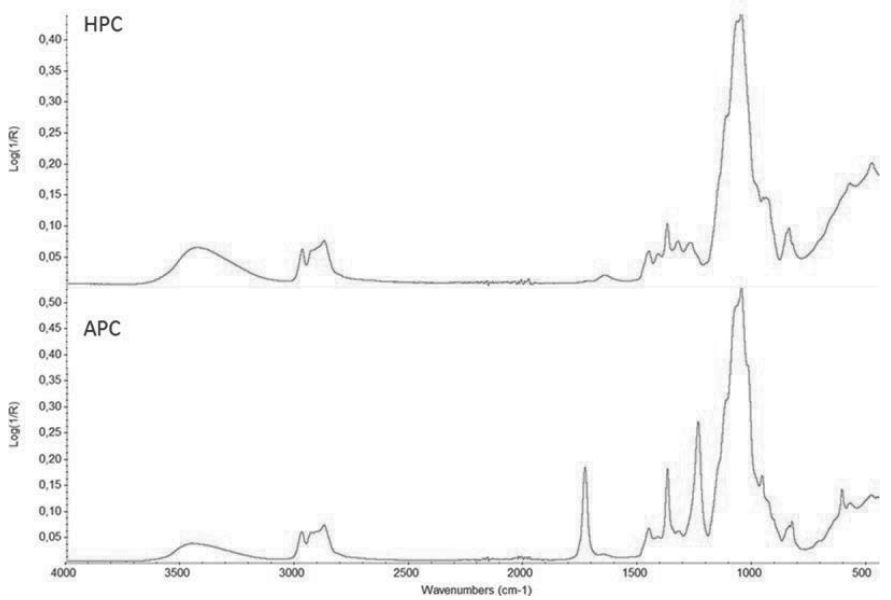

Figure S2 FTIR-ATR spectrum of HPC (before acetylation) and APC (after acetylation)

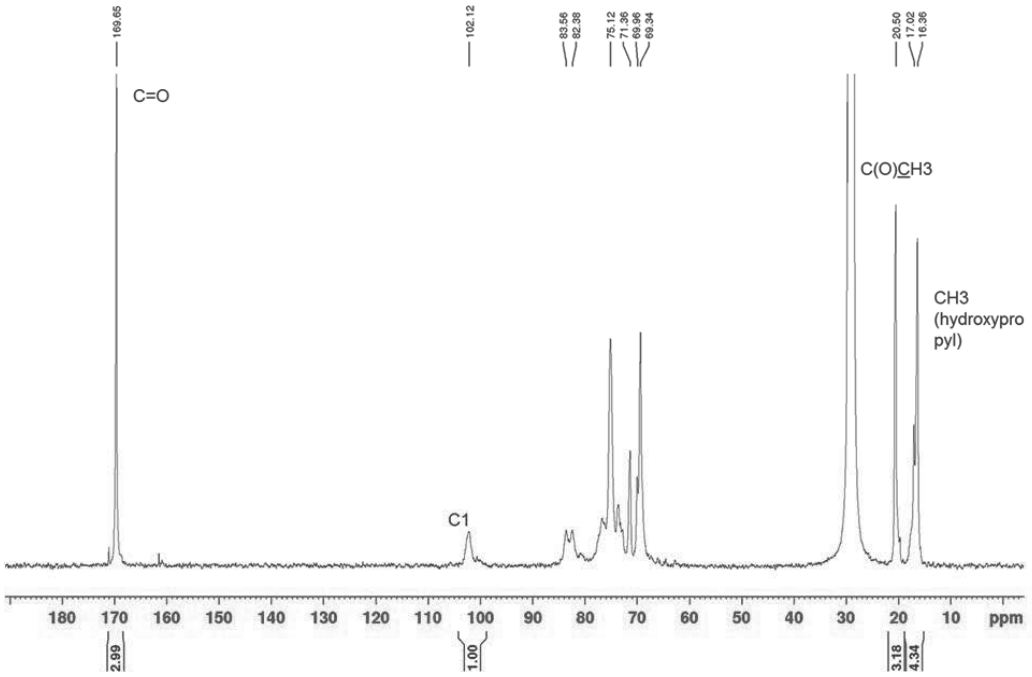

Figure S3 Liquid state ^{13}C NMR spectrum of APC

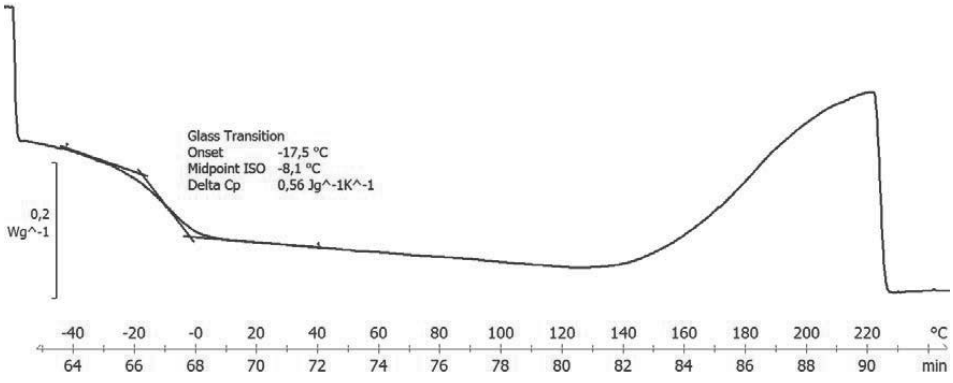

Figure S4 DSC curve of APC

3. Adhesion of the printed structures

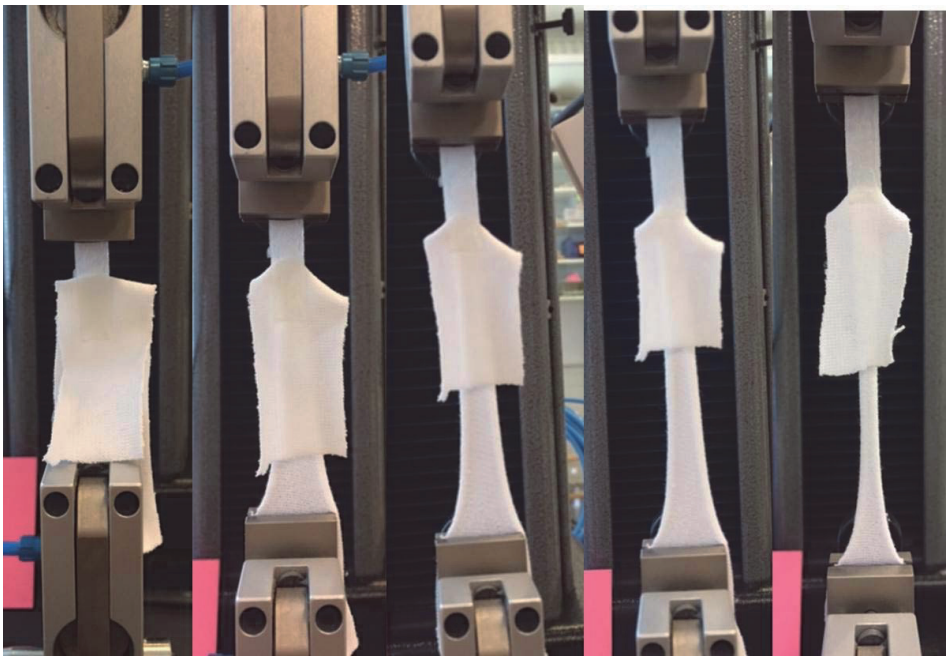

Figure S5 Peeling test with woven cotton and CA

4. IL dissolved cellulose

Figure S6 Photographs of the behaviour of dissolved cellulose in an ionic liquid a) after printing b) after regeneration c) after drying

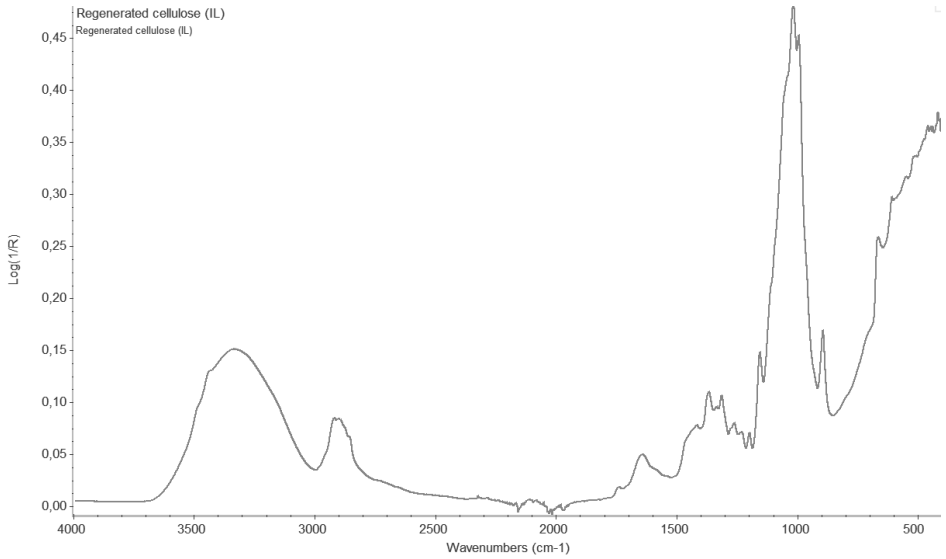

Figure S7 FTIR-ATR spectrum of regenerated cellulose after dissolution to ionic liquid.

Aalto-DD 94/2018
VTT SCIENCE 175

ISBN 978-952-60-7994-3 (printed)
ISBN 978-952-60-7995-0 (pdf)
ISSN 1799-4934 (printed)
ISSN 1799-4942 (pdf)

978-951-38-8636-3 (printed)
978-951-38-8635-6 (pdf)
2242-119X (printed)
2242-1203 (pdf)

Aalto University
School of Chemical Engineering
Department of Bioproducts and Biosystems
www.aalto.fi

BUSINESS + ECONOMY

ART + DESIGN + ARCHITECTURE

SCIENCE + TECHNOLOGY

CROSSOVER

DOCTORAL DISSERTATIONS